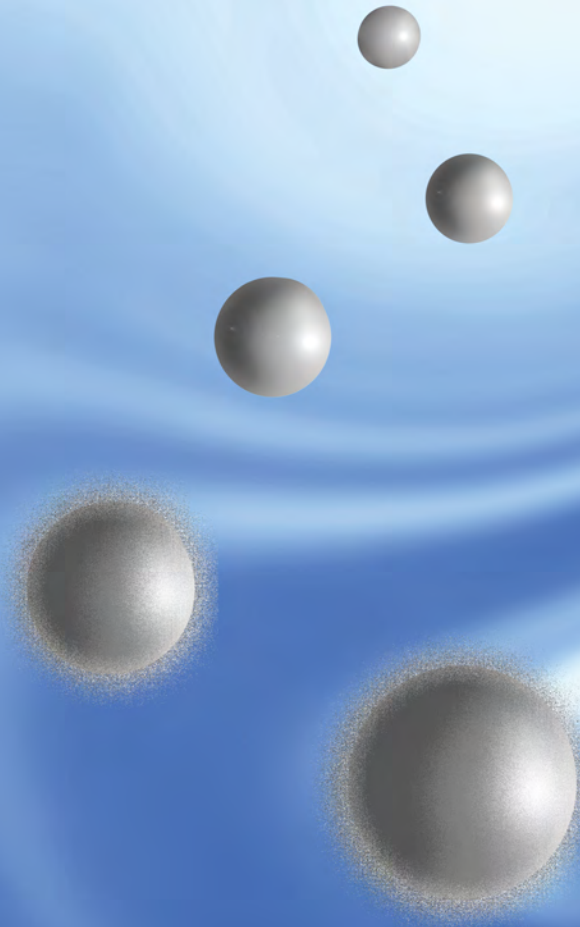


# Effects of silver nanoparticles and ions and interaction with first line of defense

Anastasia Georgantzopoulou

A. Georgantzopoulou

Effects of silver nanoparticles and ions and interaction with first line of defense



Effects of silver nanoparticles and ions  
and interaction with first line of defense

Anastasia Georgantzopoulou

## **Thesis committee**

### **Promotor**

Prof. Dr A.J. Murk

Personal chair at the sub-department of Environmental Technology  
Wageningen University

### **Co-promotor**

Dr A.C. Gutleb

Luxembourg Institute of Science and Technology (LIST), Belvaux, Luxembourg

### **Other members**

Prof. Dr A.A. Koelmans, Wageningen University

Prof. Dr W.J.G.M. Peijnenburg, RIVM, Bilthoven/ Leiden University

Prof. Dr A.P. van Wezel, Utrecht University

Dr M.V.D.Z. Park, RIVM, Bilthoven

This research was conducted under the auspices of the Graduate School for Socio-Economic and Natural Sciences of the Environment (SENSE).

# Effects of silver nanoparticles and ions and interaction with first line of defense

Anastasia Georgantzopoulou

## **Thesis**

submitted in fulfilment of the requirements for the degree of doctor  
at Wageningen University  
by the authority of the Rector Magnificus  
Prof. Dr M.J. Kropff,  
in the presence of the  
Thesis Committee appointed by the Academic Board  
to be defended in public  
on Friday 6 February 2015  
at 11 a.m. in the Aula.

Anastasia Georgantzopoulou

Effects of silver nanoparticles and ions and interaction with first line of defense  
186 pages.

PhD thesis, Wageningen University, Wageningen, NL (2015)

With references, with summaries in Dutch and English

ISBN 978-94-6257-249-2

Στους γονείς μου Σωκράτη και Λεμονιά

*“Thoroughly conscious ignorance is the prelude to every real advance in science”*

James Clerk Maxwell

# Table of Contents

<b>Chapter 1</b>	<b>7</b>
General introduction and thesis outline	
<b>Chapter 2</b>	<b>23</b>
Effects of silver nanoparticles and ions on a co-culture model for the gastrointestinal epithelium	
<b>Chapter 3</b>	<b>61</b>
Ag nanoparticles: size- and surface-dependent effects on model aquatic organisms and uptake evaluation with NanoSIMS	
<b>Chapter 4</b>	<b>89</b>
P-gp efflux pump inhibition potential of common environmental contaminants determined <i>in vitro</i>	
<b>Chapter 5</b>	<b>115</b>
Inhibition of multidrug resistance (MDR) transporters by silver nanoparticles and -ions <i>in vitro</i> and <i>in vivo</i>	
<b>Chapter 6</b>	<b>147</b>
General discussion and future perspectives	
<b>Chapter 7</b>	<b>163</b>
Summary	
<b>Chapter 8</b>	<b>169</b>
Nederlandse samenvatting	
<b>Appendix</b>	<b>175</b>
Acknowledgements	
About the author	
List of publications	
Conferences and proceedings	
SENSE diploma	

# Chapter 1

General introduction and thesis outline



## **Silver nanoparticles and environmental concerns**

Lately there is a lot of discussion about the benefits and risks of nanotechnology, a novel scientific, technological and economic growth area that uses material in the nanometer scale providing them with unique properties that can differ from the same material in a larger form (McNeil 2005; Nel et al. 2006). The use of nanomaterials (materials with at least one dimension below 100 nm) is rapidly and continuously expanding and they are applied in diverse areas such as electronics, medicine, environmental technology and remediation among others (Handy et al. 2008; McNeil 2005; National Nanotechnology Initiative; Oberdörster et al. 2007). Among the different classes of nanoparticles, (particles with all dimensions <100 nm), silver nanoparticles (Ag NPs) are very promising for future applications and therefore of high commercial interest. They are increasingly produced and applied, for example for water disinfection and filters for drinking water purification, food packaging and medical equipment due their broad spectrum antimicrobial activity. Ag NPs have been incorporated in a variety of consumer products such as textiles and plastics, personal health care products (cosmetics, toothpaste, toothbrushes, soaps), food supplements, food storage containers, wound dressings etc. (Wijnhoven et al. 2009; Woodrow Wilson International Center for Scholars 2014). These are 'open applications' resulting in release of the Ag NPs into the environment.

The application of silver (Ag) is not new, as it has been known for its antimicrobial activities since antiquity. However, the use of Ag nano forms brings new challenges for toxicology, risk assessment and regulation. Silver is enlisted among the priority hazardous pollutants in natural waters by the US EPA due to its persistence and high toxicity to aquatic organisms and is therefore regulated (Luoma 2008). The question now is whether a unique identifier should be added to the nano form of silver or whether the existing regulatory framework for silver is adequate for the nano form as well (Luoma 2008; Nowack et al. 2011).

Nanoparticles can enter the environment during the whole life cycle of the NP from production to use in a NP-containing product, recycling and disposal. Especially the open applications will result in emission to the environment during the use in a consumer product (Gottschalk and Nowack 2011). In addition, occupational exposure as well as consumer exposure are possible through food packaging and food supplements, cosmetics and textiles (Nowack et al. 2013). Ag has been shown to be released, both in nano and ionic form, from Ag-containing textiles such as socks (Benn and Westerhoff 2008) and t-shirts (Lorenz et al.

2012). Furthermore, Ag can be released directly into the environment from Ag NP-containing paint from building facades under normal weather conditions (Kaegi et al. 2010).

However, there is little data on both the actual release of NPs as well as the potential exposure. Currently no data are available on the environmental Ag NP concentrations due to measurement- and instrument limitations that do not allow the detection and quantification of nano-sized materials in the environment at ng/L concentrations (Luoma 2008). Environmental concentrations are, however, estimated using material flow analysis. The estimated emission concentrations for nano Ag for Switzerland were between 30 and 80 ng/L (realistic and high emission scenario, respectively) (Mueller and Nowack 2008). Furthermore, it has been calculated that the amount of Ag entering the environment from Ag-containing plastics and textiles is 40 and 140 ng/L for a minimum and intermediate scenario, respectively (Blaser et al. 2008).

The increase in use of Ag NP-containing products together with their predicted release in the environment, the yet not fully understood unique properties of NPs as well as the inherent toxicity of silver itself, have raised concern over their human and environmental safety and health. A better understanding is needed of the factors that govern the toxicity of Ag NPs among which the extent of Ag ion release from NPs and the size and surface properties of the NPs. Furthermore realistic *in vitro* and *in vivo* tools for Ag NP toxicity testing are urgently needed.

### **Silver ions possibly released from Ag NPs**

Ag NPs are suggested to exert toxicity through dissolution and release of Ag ions (Auffan et al. 2009, Lowry et al. 2012). This is expected to occur during the use but also during the fate of the Ag NPs the environment. Silver ions are toxic to aquatic organisms through dietary exposure at concentrations as low as 50-100 ng/L as measured by a decrease in reproductive success (Luoma 2008). Dissolution is media (pH, ionic strength) and time-dependent as well as surface coating and NP size-dependent (Jung et al. 2014; Zhao and Wang 2012). Ag NPs may act as vehicles for cell membrane penetration and delivery of Ag ions into the cell that would otherwise not occur. This so called “Trojan horse type mechanism” would increase the Ag bioavailability and therefore lead to potentiation of effects compared to the Ag ions present as such (Gliga et al. 2014; Park et al. 2010). Due to all these uncertainties, it is still not known whether Ag NPs pose a hazard mainly due to their nano-

size and related qualities or whether the effects are mainly governed by Ag released from the NPs in the exposure medium or whether it is the combination of both.

### **Influence of NP size and surface on cellular uptake and effects**

Ag NPs have been shown to penetrate cellular membranes (Cronholm et al. 2013; Kim et al. 2009; Samberg et al. 2010) and the size, surface characteristics and agglomeration affect the degree of uptake and intracellular distribution (Ahamed et al. 2008). Smaller sized particles are supposed to have higher chances of entering the cell via vesicles or endosomes although non-endocytic mechanisms are also possible (Brain et al. 2009). In addition, particle size seems to affect the dissolution rate with smaller particles showing a faster dissolution rate (Brain et al. 2009). Particle size as well as surface properties and charge affect the formation of the so-called corona on the surface of the NP consisting of proteins and other molecules present in the biological media that will subsequently also affect potential uptake and interference with biological membranes as well as fate in the cell and organism.

Capping agents, very often organic materials used to stabilize the NPs in aqueous media and facilitate their dispersion, may affect the dissolution of Ag NPs in media (Kwok et al. 2012). Surface charge and coatings can also affect uptake, biodistribution and toxicity (Suresh et al. 2012) e.g. positively charged CeO<sub>2</sub> NPs were more toxic and bio accumulated to a higher degree in *Caenorhabditis elegans* than negatively charged or neutral NPs (Collin et al. 2014) while negatively charged quantum dots (carboxyl-modified) were taken up to a greater extent by *D. magna* (Feswick et al. 2013). Therefore all these factors that potentially influence the uptake and effect and should be taken into account when assessing the (eco) toxicological risk of NPs.

### **Potential uptake routes of NPs**

All barriers between the body and the outside world are potential route of uptake of NPs. The gastrointestinal tract (GIT) is a barrier that controls the entry of xenobiotics after oral exposure. This site for uptake and exchange of food, nutrients, water and foreign substances is the first port of entry for Ag NPs due to environmental exposure or ingestion of Ag NP-containing food or supplements, personal care products or drinking water (Hoet et al. 2004). Particles that are inhaled are cleared from the respiratory tract *via* the mucociliary escalator and also may end up in the GI tract (Oberdörster et al. 2005). In aquatic organisms,

direct uptake via the gills are of major importance in addition to oral uptake (Kahru and Dubourguier 2010; Moore 2006).

After uptake via the gut NPs can be translocated to other organs and tissues in the body (Feswick et al. 2013; Klaine et al. 2008; Rosenkranz et al. 2009). In fish, such indirect target organs may include the gut, gills, liver and brain. (Kwok et al. 2012; Wu and Zhou 2013). For invertebrate species detailed information on localization within the organisms is hardly available (Feswick et al. 2013; García-Alonso et al. 2011; Rosenkranz et al. 2009; van der Ploeg et al. 2014).

### *In vitro models for the gastrointestinal epithelium*

The most used gastrointestinal epithelium *in vitro* model is the human colon cancer cell line, Caco-2. It has been extensively used and well characterized to study intestinal absorption and endogenous transport systems for transport of drugs and uptake of nutrients and compounds (Bailey et al. 1996; Balimane et al. 2001; Kahru and Dubourguier 2010; Le Ferrec et al. 2001). Once the cell layer is confluent the cells spontaneously differentiate into polarized enterocyte-like cells exhibiting tight junctions and microvilli (Le Ferrec et al. 2001). However, in contrast to the *in vivo* situation, the mucus layer that clearly affects absorption is absent (Le Ferrec et al. 2001). In addition to the enterocytes (absorptive cells) the gastrointestinal epithelium is comprised of a heterogeneous population of cells (Balimane et al. 2001) with the mucus secreting cells (e.g. goblet cells) being the second major cell type (Behrens et al. 2001; Meaney and O'Driscoll 1999). The mucus layer is a semipermeable barrier that allows the exchange of nutrients etc. but traps most bacteria and pathogens. Mucus is continuously secreted and therefore pathogens and particles such as NPs have to move against this stream in order to reach the epithelium (Cone 2009). The mucus layer can trap NPs dependent on NP size and surface charge. Positively charged particles are entrapped in the negatively charged mucus glycoproteins while negatively charged NPs are better able to pass the mucus layer (Hoet et al. 2004).

The Caco-2 cell model is often used to study *in vitro* transport, uptake and toxicity of different groups of NPs (Abbott Chalew and Schwab 2013; Bhattacharjee et al. 2013; Böhmert et al. 2012; Fisichella et al. 2012; Gaiser et al. 2012; Gerloff et al. 2009; He et al. 2013). The absence of the mucus layer, though, can potentially lead to over/under estimation of effects,

especially when the impact of the surface charge of NPs is evaluated making the need for use of more physiologically relevant models evident.

### **Aquatic ecotoxicity testing with organisms from different trophic levels**

The generally accepted standard ecotoxicity tests may not necessarily be applicable as such for the evaluation of nanoparticle toxicity, although using existing methods allow comparison of results between pure compounds and NPs of the same composition. To be able to test a wide range of NPs produced with different sizes, surface modifications etc. there is a need for assays that are also fast, high-throughput, inexpensive and limiting the use of especially vertebrate animals. Although the ecosystem can never be fully represented in the laboratory, a combination of different bioassays is expected to represent different sensitivities. For ecotoxicological hazard assessment a battery of bioassays is applied using species representing different trophic levels especially bacteria, algae, crustaceans and fish.

Bacteria are of great importance for the functioning of organisms and ecosystem, among others because they play an important role in decomposition providing primary producers with recycled nutrients (Klaine et al. 2008). They grow fast and are easy and inexpensive to maintain in the lab. The marine bacteria *V. fischeri* are used on a fast and small scale test (Hamers et al. 2001; Macova et al. 2010) for the evaluation of toxicity of compounds and environmental samples (water, soil, sediment). This potentially makes the *V. fischeri* inhibition of luminescence assay a good candidate for a fast pre-screening of nanomaterials (International Organisation for Standardization (ISO 11348-1) 1999; Velzeboer et al. 2008).

Algae are primary producers providing with nutrient availability and used in ecotoxicity testing as adverse effects will impact higher different trophic levels (Baker et al. 2014). Algae are commonly used to assess toxic effects on plant growth and photosynthesis (International Organisation for Standardization (ISO 8692) 2004; Organisation for Economic Co-operation and Development (OECD) 1984).

Daphnids hold an important position in the food web and because of their small size respond fast to toxic exposures. They are not only used in ecotoxicity testing, but also effect bio-monitoring. Daphnids can be exposed to contaminants and NPs via their diet as filter feeders that sieve suspended particles from the water (Gillis et al. 2005). In addition to oral exposure through the water column exposure can also occur via the gills (Henry et al. 2012) because of their direct contact with the water. Also for NPs the main tissues of concern would

be the gills and the gut, but NPs could be translocated internally to other tissues as is the case with vertebrates. A great advantage of especially the juvenile daphnids is that they are transparent allowing visualization of NP uptake (Feswick et al. 2013).

### **Toxic potential of Ag NPs**

The toxicity of different Ag NPs depends on their ability to reach cells, be taken up by them, their subcellular localization and the extent of interaction with biological receptors. Depending on their chemical composition, size and surface properties but also on cell type, NPs can be taken up via energy-dependent endocytosis (such as pinocytosis, clathrin or caveolae-mediated endocytosis) as well as via passive processes (diffusion or adhesive interactions) (Unfried et al. 2007).

#### *Responses in vitro*

One of the proposed mechanisms for NP toxicity is through the formation of reactive oxygen species (ROS) leading to oxidative damage, especially if the cellular antioxidant defenses are compromised (Unfried et al. 2007). The *in vitro* responses differ in type and severity depending on the cell type, suggesting that different mechanisms take place in different cell types (Ahamed et al. 2008; Hsin et al. 2008; Kruszewski et al. 2013; Lankoff et al. 2012; Suresh et al. 2012). Several studies using various *in vitro* models such as colon cancer cells, hepatocytes, fibroblasts, revealed that oxidative stress plays an important role in NP toxicity (Arora et al. 2008; Hsin et al. 2008). In addition, indications have been found for pro-inflammatory responses (Greulich et al. 2009), cell cycle arrest (AshaRani et al. 2009), apoptosis (Ahamed et al. 2008; Hsin et al. 2008), DNA damage (Ahamed et al. 2008; AshaRani et al. 2009; Kruszewski et al. 2013) and stem cell differentiation inhibition (Park et al. 2011).

#### *Effects of silver nanoparticles in aquatic organisms*

Ag NPs have been reported to cause growth retardation, absence or malformations of eyes, axis and heart chambers defects and a decrease in touch stimuli in developing zebrafish embryos, although at very high concentrations (above 25 mg/L) (Asharani et al. 2011). Growth retardation of medaka (*Oryzias latipes*) embryos and eye and vertebral abnormalities have been reported upon exposure to slightly lower Ag NP levels (above 0.4 mg/L) (Wu et al. 2010). Delayed development, deformed larvae and skeletal malformations were seen in Ag NP

and ionic Ag-exposed sea urchins, although a lower percentage of animals showing defects was observed upon ionic Ag treatment compared to Ag NPs (Siller et al. 2013). Chronic exposure to 50 µg/L Ag NPs affected reproduction of *D. magna* resulting in less offspring with smaller body size (Zhao and Wang 2011). Ag NPs exposure also compromised the ability of *D. magna* to avoid predators at a concentration of 2 µg/L that had a slight impact on survival (Pokhrel and Dubey 2012).

The novel and unique properties of NP make it important that new biological activities, interactions with subcellular structures and mechanisms of action be considered (Oberdörster et al. 2005). In addition, novel techniques e.g. for visualization of NP uptake and elucidation of modes of NP toxicity, such as proteomics and genomics, could help the identification of subtle changes in cell functions at low, more realistic, concentrations. Particle-specific responses can be unraveled, toxicity pathways identified and biomarkers for mechanisms of action developed. Genomic studies already revealed differences in gene expression patterns in the liver of for AgNO<sub>3</sub> or Ag NPs-exposed Japanese medaka (*Oryzias latipes*). Animals exposed to AgNO<sub>3</sub> exhibited lower stress responses compared to the Ag NPs (Chae et al. 2009). Also, polyvinylpyrrolidone coated (PVP) Ag NPs and AgNO<sub>3</sub> clearly affected different pathways in liver and brain of fathead minnow (*Pimephales promelas*) (Garcia-Reyero et al. 2014) and showed distinct expression profiles in *D. magna* total body samples (Poynton et al. 2012).

#### *Indications for interaction of NPs with multi xenobiotic resistance (MXR) efflux pumps*

Cellular efflux pumps are membrane-bound energy dependent proteins that recognize and actively drive environmental compounds out of the cell (Bolhuis et al. 1997; Endicott and Ling 1989; Higgins 2007; Loo et al. 2004). They act as a first line of defense against toxic compounds and they lead to lower internal concentrations. They have a broad substrate specificity transporting structurally and chemically unrelated groups of chemicals (Epel et al. 2008). P-glycoprotein (P-gp) and multidrug resistance associated protein 1 (MRP1) are important members of this defense mechanism and they are responsible for the phenomenon of multixenobiotic or multidrug resistance (MXR/MDR) (Ambudkar et al. 1999; Kurelec 1992; van Tellingen 2001). These efflux transporters have been observed in all organisms studied so far from bacteria, mussels and sea urchins to humans (Bard 2000). They are localized in tissues with barrier or secretory function such as intestine, placenta, ovaries, liver,

kidney etc. (Brand et al. 2006; Chan et al. 2004; Schinkel and Jonker 2003). In aquatic organisms they are found at the interface between the inside world and the environment as well as special tissues with excretory function (gills, gut, liver, hepatopancreas etc.) (Smital et al. 2004). These also are the locations where NPs enter the bodies.

Organisms are exposed to mixtures of environmental pollutants, many of which can be excreted out of the cell (Epel et al. 2008). It also has been shown, though, that some of these chemicals can compromise the MXR defense mechanism leading to decreased transporter activity (Bain and LeBlanc 1996; Luckenbach and Epel 2004; Smital et al. 2004). With inhibited MXR activity, compounds that would normally be excreted can now accumulate in the cell. Recently also pluronic P-85 NPs have been shown to inhibit MXR activity in sea urchin larvae (Anselmo et al. 2012). Therefore it is very important to study further the potential interaction of Ag NPs inhibition.

### **Thesis outline**

Previous research with Ag NPs suggests that toxicity depends on particle size and dissolving ions, although the mechanisms of toxicity leading to observed effects still need to be further elucidated. Further evaluation in *in vitro* and *in vivo* systems is especially relevant for the aquatic organisms and oral exposure of humans.

This study aims at the evaluation of potential hazards of Ag NPs and identification of key factors that determine the toxicity of Ag NPs for aquatic organisms and intestinal toxicity.

For this evaluation the following research questions have been defined:

- How do particle size and synthesis method or ion dissolution contribute to toxicity and effects of Ag NPs?
- To what extent does a more realistic intestinal co-culture model with mucus producing cells alter the uptake and toxic effects of Ag NPs?
- What are the effects of Ag NPs on the standard ecotoxicological model organisms from different trophic levels: the marine bacteria *Vibrio fischeri*, the algae *Desmodesmus subspicatus* and the crustacean *Daphnia magna*? Are these bioassays suitable to study Ag NPs?

- Can differences in effects between Ag NPs and AgNO<sub>3</sub> be elucidated with a proteomic approach, can still unknown mechanisms of action be revealed and could this be a useful tool to explore novel biomarkers for Ag NP effects?
- Do Ag NPs have the potential to interfere with the multi xenobiotic mechanism (MXR) *in vitro* and *in vivo* (*D. magna*)?

These research questions are addressed in the following chapters:

**Chapter 2** describes the establishment and application of an intestinal co-culture model with mucus producing cells in order to evaluate the effects of different-sized Ag NPs. The potential uptake in cells in co-culture is assessed and a proteomic methodology is applied in order to evaluate subtle changes in cellular functions.

In **Chapter 3** the effects of Ag NPs of different sizes and synthesis method are studied with eco-toxicological model aquatic organisms from different trophic levels (bacteria, algae and daphnids). The internal distribution of Ag NPs in daphnids is discussed.

**Chapter 4** deals with the optimization of an *in vitro* assay for a fast assessment of the interference of common environmental contaminants with the multixenobiotic/multidrug resistance (MXR/MDR) mechanism.

**Chapter 5** provides evidence for interference of Ag NPs and soluble Ag ions with cellular efflux transporters involved in MXR *in vitro* and *in vivo*. The establishment of the *in vivo* assay using juvenile *D. magna* as a model organism is described.

**Chapter 6** discusses the knowledge acquired in this thesis and the relevance and implications of these findings. Conclusions and future perspectives are presented and issues of concern and gaps to be filled in future research are addressed.

**Chapter 7** summarizes the content of the PhD thesis

## References

- Abbott Chalew TE, Schwab KJ. 2013. Toxicity of commercially available engineered nanoparticles to Caco-2 and SW480 human intestinal epithelial cells. *Cell Biol. Toxicol.* 29:101–16.
- Ahamed M, Karns M, Goodson M, Rowe J, Hussain SM, Schlager JJ, et al. 2008. DNA damage response to different surface chemistry of silver nanoparticles in mammalian cells. *Toxicol. Appl. Pharmacol.* 233:404–410.
- Ambudkar SV, Dey S, Hrycyna CA, Ramachandra M, Pastan I, Gottesman MM. 1999. Biochemical, cellular, and pharmacological aspects of the multidrug transporter. *Annu. Rev. Pharmacol. Toxicol.* 39:361–98.

- Anselmo HMR, van den Berg JHJ, Rietjens IMCM, Murk AJ. 2012. Inhibition of cellular efflux pumps involved in multi xenobiotic resistance (MXR) in echinoid larvae as a possible mode of action for increased ecotoxicological risk of mixtures. *Ecotoxicology* 21:2276–87.
- Arora S, Jain J, Rajwade JM, Paknikar KM. 2008. Cellular responses induced by silver nanoparticles: *In vitro* studies. *Toxicol. Lett.* 179:93–100.
- Asharani P V, Lianwu Y, Gong Z, Valiyaveetil S. 2011. Comparison of the toxicity of silver, gold and platinum nanoparticles in developing zebrafish embryos. *Nanotoxicology* 5:43–54.
- AshaRani P V, Low Kah Mun G, Prakash Hande M, Valiyaveetil S. 2009. Cytotoxicity and genotoxicity of silver nanoparticles in human cells. *ACS Nano* 3: 279–290.
- Bailey CA, Bryla P, Malick AW. 1996. The use of the intestinal epithelial cell culture model, Caco-2, in pharmaceutical development. *Adv. Drug Deliv. Rev.* 22:85–103.
- Bain LJ, LeBlanc GA. 1996. Interaction of structurally diverse pesticides with the human MDR1 gene product P-glycoprotein. *Toxicol. Appl. Pharmacol.* 141:288–98.
- Baker TJ, Tyler CR, Galloway TS. 2014. Impacts of metal and metal oxide nanoparticles on marine organisms. *Environ. Pollut.* 186:257–71.
- Balimane P V, Chong S, Morrison RA. 2001. Current methodologies used for evaluation of intestinal permeability and absorption. *J. Pharmacol. Toxicol. Methods* 44: 301–12.
- Bard S. 2000. Multixenobiotic resistance as a cellular defense mechanism in aquatic organisms. *Aquat. Toxicol.* 48: 357–389.
- Behrens I, Stenberg P, Artursson P, Kissel T. 2001. Transport of lipophilic drug molecules in a new mucus-secreting cell culture model based on HT29-MTX cells. *Pharm. Res.* 18: 1138–45.
- Benn TM, Westerhoff P. 2008. Nanoparticle silver released into water from commercially available sock fabrics. *Environ. Sci. Technol.* 42: 4133–4139.
- Bhattacharjee S, Ershov D, Gucht J Van Der, Alink GM, Rietjens IMCM, Zuilhof H, et al. 2013. Surface charge-specific cytotoxicity and cellular uptake of tri-block copolymer nanoparticles. *Nanotoxicology* 7:71–84.
- Blaser SA, Scheringer M, Macleod M, Hungerbühler K. 2008. Estimation of cumulative aquatic exposure and risk due to silver: contribution of nano-functionalized plastics and textiles. *Sci. Total Environ.* 390:396–409.
- Böhmert L, Niemann B, Thünemann AF, Lampen A. 2012. Cytotoxicity of peptide-coated silver nanoparticles on the human intestinal cell line Caco-2. *Arch. Toxicol.* 86:1107–15.
- Bolhuis H, van Veen HW, Poolman B, Driessen a J, Konings WN. 1997. Mechanisms of multidrug transporters. *FEMS Microbiol. Rev.* 21: 55–84.
- Brain JD, Curran MA, Donaghey T, Molina RM. 2009. Biologic responses to nanomaterials depend on exposure, clearance, and material characteristics. *Nanotoxicology* 3:174–180.
- Brand W, Schutte ME, Williamson G, van Zanden JJ, Cnubben NHP, Groten JP, et al. 2006. Flavonoid-mediated inhibition of intestinal ABC transporters may affect the oral bioavailability of drugs, food-borne toxic compounds and bioactive ingredients. *Biomed. Pharmacother.* 60:508–19.
- Chae YJ, Pham CH, Lee J, Bae E, Yi J, Gu MB. 2009. Evaluation of the toxic impact of silver nanoparticles on Japanese medaka (*Oryzias latipes*). *Aquat. Toxicol.* 94:320–7.
- Chan LM., Lowes S, Hirst BH. 2004. The ABCs of drug transport in intestine and liver: efflux proteins limiting drug absorption and bioavailability. *Eur. J. Pharm. Sci.* 21:25–51.
- Collin B, Oostveen E, Tsyusko OV, Unrine JM. 2014. Influence of natural organic matter and surface charge on the toxicity and bioaccumulation of functionalized ceria nanoparticles in *Caenorhabditis elegans*. *Environ. Sci. Technol.* 48:1280–9.

- Cone RA. 2009. Barrier properties of mucus. *Adv. Drug Deliv. Rev.* 61:75–85.
- Cronholm P, Karlsson HL, Hedberg J, Lowe TA, Winnberg L, Elihn K, et al. 2013. Intracellular uptake and toxicity of Ag and CuO nanoparticles: a comparison between nanoparticles and their corresponding metal ions. *Small* 9:970–82.
- Endicott JA, Ling V. 1989. The biochemistry of P-glycoprotein-mediated multidrug resistance. *Annu. Rev. Biochem.* 58:137–171.
- Epel D, Luckenbach T, Stevenson CN, Macmanus-Spencer L a, Hamdoun A, Smital T. 2008. Efflux transporters: newly appreciated roles in protection against pollutants. *Environ. Sci. Technol.* 42: 3914–20.
- Feswick A, Griffitt RJ, Siebein K, Barber DS. 2013. Uptake , retention and internalization of quantum dots in *Daphnia* is influenced by particle surface functionalization. *Aquat. Toxicol.* 130-131:210–218.
- Fisichella M, Berenguer F, Steinmetz G, Auffan M, Rose J, Prat O. 2012. Intestinal toxicity evaluation of TiO<sub>2</sub> degraded surface-treated nanoparticles: a combined physico-chemical and toxicogenomics approach in Caco-2 cells. *Part. Fibre Toxicol.* 9:18.
- Gaiser BK, Fernandes TF, Jepson MA, Lead JR, Tyler CR, Baalousha M, et al. 2012. Interspecies comparisons on the uptake and toxicity of silver and cerium dioxide nanoparticles. *Environ. Toxicol. Chem.* 31:144–54.
- García-Alonso J, Khan FR, Misra SK, Turmaine M, Smith BD, Rainbow PS, et al. 2011. Cellular internalization of silver nanoparticles in gut epithelia of the estuarine polychaete *Nereis diversicolor*. *Environ. Sci. Technol.* 45:4630–6.
- Garcia-Reyero N, Kennedy AJ, Escalon BL, Habib T, Laird JG, Rawat A, et al. 2014. Differential effects and potential adverse outcomes of ionic silver and silver nanoparticles *in vivo* and *in vitro*. *Environ. Sci. Technol.* 48: 4546–4555.
- Gerloff K, Albrecht C, Boots AW, Förster I, Schins RPF. 2009. Cytotoxicity and oxidative DNA damage by nanoparticles in human intestinal Caco-2 cells. *Nanotoxicology* 3:355–364.
- Gillis PL, Chow-Fraser P, Ranville JF, Ross PE, Wood CM. 2005. *Daphnia* need to be gut-cleared too: the effect of exposure to and ingestion of metal-contaminated sediment on the gut-clearance patterns of *D. magna*. *Aquat. Toxicol.* 71:143–154.
- Gliga AR, Skoglund S, Wallinder IO, Fadeel B, Karlsson HL. 2014. Size-dependent cytotoxicity of silver nanoparticles in human lung cells: the role of cellular uptake, agglomeration and Ag release. *Part. Fibre Toxicol.* 11:11.
- Gottschalk F, Nowack B. 2011. The release of engineered nanomaterials to the environment. *J. Environ. Monit.* 13:1145–55.
- Greulich C, Kittler S, Epple M, Muhr G, Köller M. 2009. Studies on the biocompatibility and the interaction of silver nanoparticles with human mesenchymal stem cells ( hMSCs ). 495–502.
- Hamers T, Smit MGD, Murk AJ, Koeman JH. 2001. Biological and chemical analysis of the toxic potency of pesticides in rainwater. *Chemosphere* 45: 609–624.
- Handy RD, Owen R, Valsami-Jones E. 2008. The ecotoxicology of nanoparticles and nanomaterials: current status, knowledge gaps, challenges, and future needs. *Ecotoxicology* 17:315–25.
- He B, Lin P, Jia Z, Du W, Qu W, Yuan L, et al. 2013. The transport mechanisms of polymer nanoparticles in Caco-2 epithelial cells. *Biomaterials* 34:6082–98.
- Henry RP, Lucu C, Onken H, Weihrauch D. 2012. Multiple functions of the crustacean gill: osmotic/ionic regulation, acid-base balance, ammonia excretion, and bioaccumulation of toxic metals. *Front. Physiol.* 3:431.
- Higgins CF. 2007. Multiple molecular mechanisms for multidrug resistance transporters. *Nature* 446: 749–757.

- Hoet PH, Brüske-Hohlfeld I, Salata OV. 2004. Nanoparticles - known and unknown health risks. *J. Nanobiotechnology* 2:12.
- Hsin Y, Chen C, Huang S, Shih T, Lai P, Ju Chueh P. 2008. The apoptotic effect of nanosilver is mediated by a ROS- and JNK-dependent mechanism involving the mitochondrial pathway in NIH3T3 cells. *Toxicol. Lett.* 179:130–139.
- International Organisation for Standardization (ISO 11348-1). 1999. Water quality-Determination of the inhibitory effect of water samples on the light emission of *Vibrio fischeri* (Luminescent bacteria test).
- International Organisation for Standardization (ISO 8692). 2004. Water quality- freshwater algal growth inhibition test with unicellular green algae.
- Jung Y-J, Kim K-T, Kim JY, Yang S-Y, Lee B-G, Kim SD. 2014. Bioconcentration and distribution of silver nanoparticles in Japanese medaka (*Oryzias latipes*). *J. Hazard. Mater.* 267:206–213.
- Kaegi R, Sinnet B, Zuleeg S, Hagendorfer H, Mueller E, Vonbank R, et al. 2010. Release of silver nanoparticles from outdoor facades. *Environ. Pollut.* 158:2900–5.
- Kahru A, Dubourguier H-C. 2010. From ecotoxicology to nanoecotoxicology. *Toxicology* 269:105–19.
- Kim S, Eun Choi J, Choi J, Chung K, Park K, Yi J, et al. 2009. Oxidative stress-dependent toxicity of silver nanoparticles in human hepatoma cells. *Toxicol. Vitro.* 23:1076–1084.
- Klaine SJ, Alvarez PJJ, Batley G, Fernandes TF, Handy RD, Lyon D, et al. 2008. Nanomaterials in the environment: Behaviour, fate, bioavailability, and effects. *Environ. Toxicol. Chem.* 27: 1825–1851.
- Kruszewski M, Grądzka I, Bartłomiejczyk T, Chwastowska J, Sommer S, Grzelak A, et al. 2013. Oxidative DNA damage corresponds to the long term survival of human cells treated with silver nanoparticles. *Toxicol. Lett.* 219:151–9.
- Kurelec B. 1992. The multixenobiotic resistance mechanism in aquatic organisms. *Crit. Rev. Toxicol.* 22:23–43.
- Kwok KWH, Auffan M, Badireddy AR, Nelson CM, Wiesner MR, Chilkoti A, et al. 2012. Uptake of silver nanoparticles and toxicity to early life stages of Japanese medaka (*Oryzias latipes*): effect of coating materials. *Aquat. Toxicol.* 120-121:59–66.
- Lankoff A, Sandberg WJ, Wegierek-Ciuk A, Lisowska H, Refsnes M, Schwarze PE, et al. 2012. The effect of agglomeration state of silver and titanium dioxide nanoparticles on cellular response of HepG2, A549 and THP-1 cells. *Toxicol. Lett.* 208:197–213.
- Le Ferrec E, Chesne C, Artusson P, Brayden D, Fabre G, Gires P, et al. 2001. *In vitro* models of the intestinal barrier. *ATLA* 29: 649–668.
- Loo TW, Bartlett MC, Clarke DM. 2004. The drug-binding pocket of the human multidrug resistance P-glycoprotein is accessible to the aqueous medium. *Biochemistry* 43:12081–9.
- Lorenz C, Windler L, von Goetz N, Lehmann RP, Schuppler M, Hungerbühler K, et al. 2012. Characterization of silver release from commercially available functional (nano)textiles. *Chemosphere* 89:817–24.
- Lowry G V, Gregory KB, Apte SC, Lead JR. 2012. Transformations of nanomaterials in the environment. *Environ. Sci. Technol.* 46:6893–9.
- Luckenbach T, Epel D. 2004. Nitromusk and polycyclic musk compounds as long-term inhibitors of cellular xenobiotic defense systems mediated by multidrug transporters. *Environ. Health Perspect.* 113:17–24.
- Luoma SN. 2008. Silver nanotechnologies and the environment: old problems or new challenges? Project on Emerging Nanotechnologies (PEN). 1–66. Available: [www.nanotechproject.org](http://www.nanotechproject.org) [accessed 2 September 2014].
- Macova M, Escher BI, Reungoat J, Carswell S, Lee Chue K, Keller J, et al. 2010. Monitoring the biological activity of micropollutants during advanced wastewater treatment with ozonation and activated carbon filtration. *Water Res.* 44:477–92.

- McNeil SE. 2005. Nanotechnology for the biologist. *J. Leukoc. Biol.* 78:585–594.
- Meaney C, O’Driscoll C. 1999. Mucus as a barrier to the permeability of hydrophilic and lipophilic compounds in the absence and presence of sodium taurocholate micellar systems using cell culture models. *Eur. J. Pharm. Sci.* 8: 167–75.
- Moore MN. 2006. Do nanoparticles present ecotoxicological risks for the health of the aquatic environment? *Environ. Int.* 32:967–76.
- Mueller NC, Nowack B. 2008. Exposure modeling of engineered nanoparticles in the environment. *Environ. Sci. Technol.* 42: 4447–53.
- National Nanotechnology Initiative. Benefits and applications.  
Available: <http://www.nano.gov/you/nanotechnology-benefits>.
- Nel A, Xia T, Mädler L, Li N. 2006. Toxic potential of materials at the nanolevel. *Science* 311:622–7.
- Nowack B, Brouwer C, Geertsma RE, Heugens EHW, Ross BL, Toufektsian M-C, et al. 2013. Analysis of the occupational, consumer and environmental exposure to engineered nanomaterials used in 10 technology sectors. *Nanotoxicology* 7:1152–6.
- Nowack B, Krug HF, Height M. 2011. 120 years of nanosilver history: Implications for policy makers. *Environ. Sci. Technol.* 45:1177–83.
- Oberdörster G, Oberdörster E, Oberdörster J. 2005. Nanotoxicology: an emerging discipline evolving from studies of ultrafine particles. *Environ. Health Perspect.* 113:823–839.
- Oberdörster G, Stone V, Donaldson K. 2007. Toxicology of nanoparticles: A historical perspective. *Nanotoxicology* 1:2–25.
- Organisation for Economic Co-operation and Development (OECD). 1984. OECD Guidelines for the testing of chemicals/Test 201: Alga, growth inhibition test.
- Park E, Yi J, Kim Y, Choi K, Park K. 2010. Silver nanoparticles induce cytotoxicity by a Trojan-horse type mechanism. *Toxicol. Vitro.* 24:872–878.
- Park MVDZ, Neigh AM, Vermeulen JP, de la Fonteyne LJJ, Verharen HW, Briedé JJ, et al. 2011. The effect of particle size on the cytotoxicity, inflammation, developmental toxicity and genotoxicity of silver nanoparticles. *Biomaterials* 32:9810–9817.
- Pokhrel LR, Dubey B. 2012. Potential impact of low-concentration silver nanoparticles on predator-prey interactions between predatory dragonfly nymphs and *Daphnia magna* as a prey. *Environ. Sci. Technol.* 46: 7755–7762.
- Poynton H, Lazorchak J, Impellitteri CA, Blalock BJ, Rogers K, Allen HJ, et al. 2012. Toxicogenomic responses of nanotoxicity in *Daphnia magna* exposed to silver nitrate and coated silver nanoparticles. *Environ. Sci. Technol.* 46: 6288–6296.
- Rosenkranz P, Chaudhry Q, Stone V, Fernandes TF. 2009. A comparison of nanoparticle and fine particle uptake by *Daphnia magna*. *Environ. Toxicol. Chem.* 28:2142–9.
- Samberg ME, Oldenburg SJ, Monteiro-Riviere NA. 2010. Evaluation of silver nanoparticle toxicity in skin *in vivo* and keratinocytes *in vitro*. *Environ. Health Perspect.* 118:407–413.
- Schinkel AH, Jonker JW. 2003. Mammalian drug efflux transporters of the ATP binding cassette (ABC) family: an overview. *Adv. Drug Deliv. Rev.* 55: 3–29.
- Siller L, Lemloh M-L, Piticharoenphun S, Mendis BG, Horrocks BR, Brümmer F, et al. 2013. Silver nanoparticle toxicity in sea urchin *Paracentrotus lividus*. *Environ. Pollut.* 178:498–502.
- Smital T, Luckenbach T, Sauerborn R, Hamdoun AM, Vega RL, Epel D. 2004. Emerging contaminants-pesticides, PPCPs, microbial degradation products and natural substances as inhibitors of multixenobiotic defense in aquatic organisms. *Mutat. Res.* 552:101–17.

- Suresh AK, Pelletier DA, Wang W, Morrell-Falvey JL, Gu B, Doktycz MJ. 2012. Cytotoxicity induced by engineered silver nanocrystallites is dependent on surface coatings and cell types. *Langmuir* 28:2727–2735.
- Unfried K, Albrecht C, Klotz L-O, Von Mikecz A, Grether-Beck S, Schins RPF. 2007. Cellular responses to nanoparticles: Target structures and mechanisms. *Nanotoxicology* 1:52–71.
- Van der Ploeg MJC, Handy RD, Waalewijn-Kool PL, van den Berg JHJ, Herrera Rivera ZE, Bovenschen J, et al. 2014. Effects of silver nanoparticles (NM-300K) on *Lumbricus rubellus* earthworms and particle characterization in relevant test matrices including soil. *Environ. Toxicol. Chem.* 33:743–52.
- Van Tellingen O. 2001. The importance of drug-transporting P-glycoproteins in toxicology. *Toxicol. Lett.* 120: 31–41.
- Velzeboer I, Hendriks JA, Ragas AM, Van de Meent D. 2008. Aquatic ecotoxicity tests of some nanomaterials. *Environ. Toxicol. Chem.* 27: 1942–1947.
- Wijnhoven SWP, Peijnenburg WJGM, Herberts CA, Hagens WI, Oomen AG, Heugens EHW, et al. 2009. Nano-silver a review of available data and knowledge gaps in human and environmental risk assessment. *Nanotoxicology* 3:109–138.
- Woodrow Wilson International Center for Scholars. 2014. Project on emerging nanotechnologies. Available: <http://www.nanotechproject.org/> [accessed 15 August 2014].
- Wu Y, Zhou Q. 2013. Silver nanoparticles cause oxidative damage and histological changes in medaka (*Oryzias latipes*) after 14 days of exposure. *Environ. Toxicol. Chem.* 32:165–73.
- Wu Y, Zhou Q, Li H, Liu W, Wang T, Jiang G. 2010. Effects of silver nanoparticles on the development and histopathology biomarkers of Japanese medaka (*Oryzias latipes*) using the partial-life test. *Aquat. Toxicol.* 100:160–167.
- Zhao C-M, Wang W-X. 2011. Comparison of acute and chronic toxicity of silver nanoparticles and silver nitrate to *Daphnia magna*. *Environ. Toxicol. Chem.* 30:885–892.
- Zhao C-M, Wang W-X. 2012. Importance of surface coatings and soluble silver in silver nanoparticles toxicity to *Daphnia magna*. *Nanotoxicology* 6:361–370.

# Chapter 2

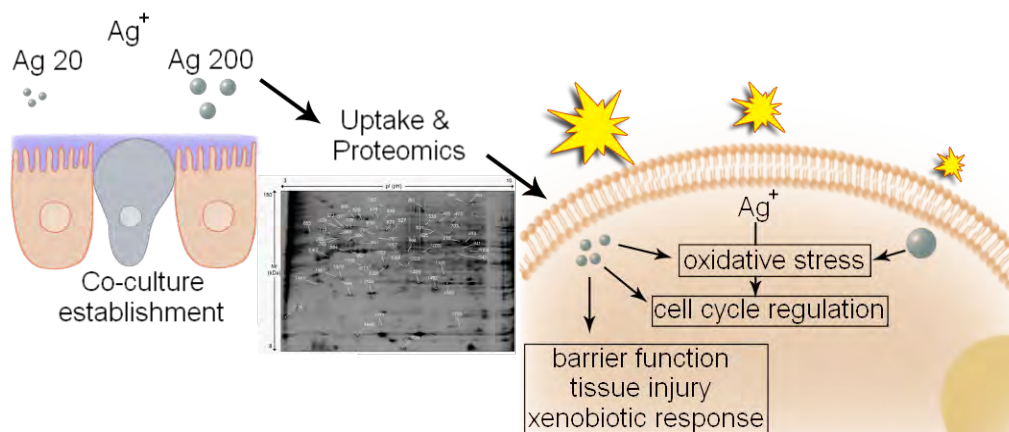
## Effects of silver nanoparticles and ions on a co-culture model for the gastrointestinal epithelium

Anastasia Georgantzopoulou, Tommaso Serchi, Céline C. Leclercq, Jenny Renaut, Jia Shao, Anna Lankoff, Marcin Kruszewski, Esther Lentzen, Patrick Grysan, Jean-Nicolas Audinot, Servane Contal, Johanna Ziebel, Cédric Guignard, Lucien Hoffmann, AlberTinka J. Murk, Arno C. Gutleb

*Tox. Sci.* (Submitted)

## Abstract

The increased incorporation of silver nanoparticles (Ag NPs) into consumer products makes the characterization of potential risk for humans and organisms essential. The oral route is an important uptake route for NPs, therefore the study of the gastrointestinal tract in respect to NP uptake and toxicity is very timely. In the present study a Caco-2/TC7:HT29-MTX intestinal co-culture model is established with mucus secretion, which constitutes an important protective barrier to exogenous agents *in vivo* and may strongly influence particle uptake. Particle size (Ag 20 and 200 nm) is taken into account for the assessment of uptake and toxic and inflammatory potential of Ag NPs. Both Ag 20 and 200 nm NPs are taken up by the cells and Ag NPs 20 nm are mainly localized in organelles with high sulfur content. A dose- and size-dependent increase in Interleukin-8 (IL-8) release is observed with a lack of cytotoxicity and oxidative stress. Sixty one differentially abundant proteins are identified involved in cytoskeleton arrangement and cell cycle, oxidative stress, apoptosis, metabolism/detoxification and stress. The low level of overlap between differentially abundant proteins observed in both Ag NPs and AgNO<sub>3</sub> treated co-culture suggests size-dependent responses that cannot only be attributed to soluble Ag.



## Introduction

Nanotechnology has brought about many advances in various fields from medicine and consumer products to environmental remediation. Nanotechnology has also raised many concerns due to the continuous increase in use and application of nanoparticles (NPs, all three dimensions in the order of 100 nm or less). Silver nanoparticles (Ag NPs) are commonly used in consumer products and numerous studies have shown size dependent effects, that differ from ionic Ag, in both animal models as well as *in vitro* cell culture models (Kruszewski et al. 2011). Among the reported effects are increased reactive oxygen species (ROS) levels, DNA damage and cell cycle arrest (AshaRani et al. 2009).

There is still a lack of knowledge about the fate and effects of Ag NPs on the gastrointestinal tract after oral exposure. This uptake route is possible via accidental ingestion during the production or due to their presence in water and in the food chain (due to their increased use in food preservation, food packaging material and water disinfection) (Piret et al. 2012). Caco-2 cells are widely used as a model for the intestinal epithelium in studies for drug permeability or nutrients and xenobiotics absorption and transport (Bailey et al. 1996). Caco-2 cells were also used in several studies to evaluate the effects of engineered NPs including Ag NPs (Abbott Chalew and Schwab 2013; Böhmert et al. 2012; Gaiser et al. 2012; Gerloff et al. 2009, 2013; Piret et al. 2012). However, the intestinal epithelium, apart from absorptive cells, also contains mucus-secreting cells (goblet cells) among others (Walter et al. 1996). The mucus is a selective and dynamic barrier protecting against toxic agents, particulate matter and pathogens (Colorado State University; Pontier et al. 2001), while facilitating the exchange of nutrients, metabolites, water etc. Mucus is continuously secreted, therefore particles etc. will have to move upstream to reach the epithelial cells (Cone 2009). Mucus is composed of a complex mixture of mucin molecules, lipids, proteins and other components that affect drug transport (Larhed et al. 1998). It has been suggested that the mucus layer has effects on Fe bioavailability and absorption (Jin et al. 2006) and it represents an additional barrier to the transport of ions (Pontier et al. 2001). However, there are only a few studies dealing with adverse effects of NPs on the gastrointestinal epithelium (Abbott Chalew and Schwab 2013; Böhmert et al. 2012; Bouwmeester et al. 2011; Gaiser et al. 2012; Gerloff et al. 2009, 2013; Piret et al. 2012; Verano-Braga et al. 2014).

The aim of the present study was to study the effects of different-sized Ag NPs (Ag 20 and 200 nm) as well as AgNO<sub>3</sub> as a source of ionic silver on an intestinal co-culture model which incorporates mucus for a more realistic simulation of the intestinal epithelium *in vitro*.

The hypothesis is that the mucus layer provides a protective barrier against NPs and ions, and that mucin-NPs complexes modify the reactive surface and lead to a different uptake pattern of the NPs. The human colon cancer cells Caco-2/TC7 (Grès et al. 1998) as well as the human adenocarcinoma mucus-secreting cells HT29-MTX (Lesuffleur et al. 1990) were used in the presented intestinal model. These two cell lines represent the two major cell types (absorptive and mucus secreting cells) that are present in the intestinal epithelium *in vivo*. This model has been described before for iron bioavailability prediction studies (Mahler et al. 2009) and drug absorption (Hilgendorf et al. 2000) including the evaluation of the efficiency of nanocarriers (Yuan et al. 2013). The metabolic activity of the cells was studied as a measure of cytotoxicity, reactive oxygen species generation and pro-inflammatory effects were studied on Caco-2/TC7, HT29-MTX cells alone and their co-culture. The effect of the Ag NPs and AgNO<sub>3</sub> on cells in co-culture was studied at proteome level by applying two-dimensional difference in gel electrophoresis (2D-DIGE) followed by Matrix Assisted Laser Desorption Ionization - Time Of Flight/ Time Of Flight (MALDI-TOF/TOF) mass spectrometry (MS) technique. This proteomic research can reveal key proteins and pathways that could be altered upon exposure to Ag NPs and AgNO<sub>3</sub> and elucidate whether the observed changes can be related to the different sizes or ion release. In addition, NanoSIMS analysis was carried out to study potential NP uptake and intracellular localization in relation to NP properties.

## **Materials and Methods**

### *Ag NPs and chemicals*

Ag NPs (20 and 200 nm) were obtained from PlasmaChem GmbH (Berlin, Germany). Silver nitrate (AgNO<sub>3</sub>) was purchased from VWR (Leuven, Belgium) and Alcian blue, H<sub>2</sub>O<sub>2</sub>, Toluidine blue, 2',7'-dichlorofluorescein diacetate (DCFH-DA), osmium tetroxide (OsO<sub>4</sub>), glutaraldehyde, resazurin sodium salt and the epoxy resin embedding kit from Sigma Aldrich (Bornem, Belgium). IL-8 kit was obtained from ENZO Life Sciences BVBA (Zandhoven, Belgium).

### *Ag NPs dispersion protocols*

Ag NP stock solutions were prepared as previously described (Georgantzopoulou et al. 2013; Lankoff et al. 2012). Briefly, the Ag NPs were suspended in 5% DMSO in sterile Milli-Q water (Millipak Express, Millipore) at a concentration of 2 mg/mL and sonicated on

ice for 3 minutes using a UP200S probe ultra sonicator (0.5 cycle, 30% amplitude, Hielscher, Germany). Stocks were always prepared fresh prior to each experiment. The characteristics of the NPs in different culture media can be found in previous studies (Georgantzopoulou et al. 2013; Kruszewski et al. 2013; Lankoff et al. 2012).

#### *Ag NPs characterization in medium*

Dynamic light scattering and zeta ( $\zeta$ ) potential measurements of NPs in solution were carried out with a nanoZetasizer (Malvern Instruments Ltd, UK). The stocks were added to the full cell culture medium containing 10% FBS in order to achieve the highest concentration at which the cells were exposed (100 mg/L).

#### *Cell culture*

The human colon cancer Caco-2 cell line sub-clone TC7 (Caco-2/TC7) was a generous gift from Monique Rousset (Nancy University, France). HT29-MTX cells were kindly provided by T. Lesuffleur (INSERM UMR S 938, Paris, France). Phosphate Buffer Saline (PBS) and heat-inactivated Fetal Bovine Serum (FBS) were all obtained from Invitrogen (Merelbeke, Belgium).

Both cell lines were maintained in Dulbecco's Modified Eagle Medium-Glutamax (DMEM-Glutamax, Invitrogen) supplemented with 10% fetal bovine serum, 1% non-essential amino acids and 1% penicillin/streptomycin solution (at 37 °C in a 10% CO<sub>2</sub> humidified incubator). The medium was replaced every other day and cells were split upon confluency with Trypsin-EDTA. In order to ensure full differentiation of cells, experiments were carried out 14 days post seeding.

#### *Co-culture system characterization*

*Alcian Blue staining (mucus localization).* Caco-2/TC7:HT29-MTX in co-culture at increasing ratios (100:0, 90:10, 50:50 and 0:100) were seeded in 6-well plates at an initial total cell concentration of  $1.2 \times 10^5$  cells/mL and cultured for 14 days as required for cell differentiation and formation of tight junctions. The culture medium was removed after the 14-day period, the monolayers were washed once with PBS and fixed with 6% formaldehyde in 0.27 M CaCl<sub>2</sub>, pH 4.0 at 4 °C for 1 hour as previously described (Mahler et al. 2009). Cell monolayers were washed with PBS and then stained with Alcian blue (pH 2.5), that stains the

acid muco-substances attached to HT29-MTX cells blue. Cells were observed under a microscope and pictures of the stained cells were acquired.

*Toluidine Blue staining- (mucus coverage):* Caco-2/TC7:HT29-MTX in co-culture at increasing ratios were seeded onto polycarbonate 0.4  $\mu\text{M}$  pore size trans-well inserts at an initial concentration of  $1.2 \times 10^5$  cells/mL and cultured for 14 days. The membranes were cut into strips and stained with 0.25% toluidine blue in PBS for 5 minutes and placed transversally in multiwell chambered coverslips (Sigma-Aldrich) for observation under a microscope (the cell monolayer is stained blue whereas the mucus layer is light purple) as previously described (Wikman et al. 1993). At the 90:10 Caco-2/TC7:HT29-MTX ratio the mucus layer covered the whole area of the monolayer and the presence of goblet cells in a healthy gastrointestinal epithelium is around 10%, therefore further studies were performed with this ratio.

#### *Metabolic activity assay (Alamar Blue) as a measure of cytotoxicity*

The single cell cultures of Caco-2/TC7, HT29-MTX and their co-culture at a 90:10 ratio were seeded at a concentration of  $1.2 \times 10^5$  cells/mL in 12-well plates and were grown for 14 days at 37 °C in a 10% CO<sub>2</sub> humidified incubator. After 14 days the medium was discarded and new medium containing increasing concentrations of the Ag NPs (0-100 mg/L) or AgNO<sub>3</sub> (0-60 mg/L) was added (serially diluted in complete medium). Due to higher toxicity of AgNO<sub>3</sub>, 60 mg/L was chosen as a maximum concentration according to preliminary experiments. After 24 hours of exposure, the medium containing the Ag NPs or AgNO<sub>3</sub> was discarded and replaced with 1 mL of 500  $\mu\text{M}$  resazurin per well. Resazurin is a cell permeable, non-fluorescent compound that is reduced by metabolically active cells into the fluorescent resorufin. After 1.5 hours of incubation at 37 °C in a 10% CO<sub>2</sub> humidified incubator in the dark, fluorescence was measured at an excitation wavelength of 530 nm and emission wavelength of 590 nm (Synergy 2, BioTek Instruments, Inc.). The reported metabolic activity is expressed relative to the untreated group, which was set at 100%.

#### *Measurement of intracellular reactive oxygen species formation*

The levels of reactive oxygen species (ROS) were evaluated with the use of a non-fluorescent probe (DCFH-DA) that once inside the cell it is deacetylated by cellular esterases into the non-fluorescent DCFH. When ROS are present DCFH is oxidized into the highly

fluorescent DCF. Single cell culture of Caco-2/TC7 and HT29-MTX and their co-culture at a 90:10 ratio were seeded at a concentration of  $1.2 \times 10^5$  cells/mL in 12-well plates and were grown for 14 days at 37 °C in a 10% CO<sub>2</sub> humidified incubator. After 14 days the medium was discarded and replaced with 1 mL of 150 µM DCFH-DA per well. After 1 hour of incubation at 37 °C in a 10% CO<sub>2</sub> humidified incubator in the dark, the dye was removed, the monolayers were washed with PBS and increasing concentrations of NPs or AgNO<sub>3</sub> were added in the wells (serially diluted in cell culture medium). After 2 hours, fluorescence was measured at an excitation wavelength of 480 nm and emission wavelength of 530 nm (Synergy 2, BioTek Instruments, Inc.). As a positive control, 0.01 % of H<sub>2</sub>O<sub>2</sub> was included in every plate and results were expressed relative to the maximal H<sub>2</sub>O<sub>2</sub> response.

#### *Measurement of IL-8 release*

Caco-2/TC7, HT29-MTX cells or cells in co-culture at a 90:10 ratio were seeded at a concentration of  $1.2 \times 10^5$  cells/mL in 12-well plates and were grown for 14 days at 37 °C in a 10% CO<sub>2</sub> humidified incubator. The medium was renewed every other day and after 14 days the medium was discarded and new medium containing increasing concentrations of the Ag NPs (0-100 mg/L) or AgNO<sub>3</sub> (0-20 mg/L) was added (serially diluted in complete medium). The highest concentration used for AgNO<sub>3</sub> was 20 mg/L due to increased cytotoxicity. At the end of the exposure period the supernatants were collected and stored at -80 °C until analysis. The amount of IL-8 released upon exposure to Ag 20, Ag 200 nm or AgNO<sub>3</sub> for 24 hours was evaluated with an enzyme-linked immunosorbent assay (ELISA) kit (Assay Designs/ENZO Life Sciences, Zandhoven, Belgium) according to the manufacturer's instruction protocol.

#### *Total soluble Ag release over time (Ultrafiltration and ICP-MS)*

The total amount of soluble Ag ionic species released from the Ag 20 and 200 nm particles in the cell culture medium was evaluated as previously described (Georgantzopoulou et al. 2013). Briefly, 2 mL of exposure medium (medium + Ag NPs at the highest working concentration of 100 mg/L or only medium in the absence of cells) were taken after 6 and 24 hours of incubation at 37 °C in a 10% CO<sub>2</sub> humidified incubator in the dark and were centrifuged for 40 min at 4000 g using centrifugal filter devices with 3 kDa cut-off (Amicon ultra-4, Millipore, Ireland). The ultra-filtrates were evaluated for the total soluble Ag content by Inductively Coupled Plasma Mass Spectrometry (ICP-MS) (Elan DRC-e, Perkin Elmer,

Waltham, MA, USA) as previously described (Boscher et al. 2010; Georgantzopoulou et al. 2013).

#### *Ag NP uptake evaluation in the co-culture (NanoSIMS50)*

The co-culture of Caco-2/TC7 and HT29-MTX at a 90:10 ratio was seeded in 12-well plates and after 14 days in culture the cells were exposed to 50 mg/L Ag 20 and 200 nm and 20 mg/L AgNO<sub>3</sub> for 24 hours. The cells were washed with PBS, detached with a cell scraper and transferred into eppendorf tubes. The settled cell pellets were fixed with 5% glutaraldehyde in PBS overnight. Glutaraldehyde was removed and cells were washed with PBS. They were then post fixed with 1% OsO<sub>4</sub> in milliQ water for 2 hours. After an additional washing step with PBS the cell pellets were placed in agar blocks (1% agar), they were dehydrated with increasing acetone concentrations (30%, 50%, 70%, 90% and 100% acetone), and they were finally embedded in epoxy resin (Epon 812 substitute) in molds (easy molds, Ted Pella, Inc). Samples were cut to 300 nm semi-thin sections (Leica Ultracut UCT, Le Pecq Cedex, France) and deposited on silicon wafers (Siltronix, Archamps, France) for SIMS analysis. The NanoSIMS 50 (Audinot et al. 2008; Georgantzopoulou et al. 2013; Gutleb et al. 2012) (Cameca, Courbevoie, France) analyses were performed by scanning of the surface (40 x 40 μm<sup>2</sup> and 20 x 20 μm<sup>2</sup>) with a primary Cs<sup>+</sup> ion. The impact of the primary beam was 16 keV with an intensity range of 1.0–0.8 pA. Images were recorded in a pixel format of 256 x 256 image points with a counting time of 20 ms per pixel. The probe-working diameter was estimated in the range of 80–100 nm (Georgantzopoulou et al. 2013). The secondary negative ions recorded simultaneously were: <sup>12</sup>C<sup>14</sup>N<sup>-</sup> (m = 26.00307 amu), <sup>31</sup>P<sup>-</sup> (m = 30.97376 amu), <sup>34</sup>S<sup>-</sup> (m = 33.96786 amu) and <sup>107</sup>Ag<sup>-</sup> (m = 106.90486 amu).

#### *Proteomic approach*

The co-culture of Caco-2/TC7 and HT29-MTX cells at a 90:10 ratio was seeded in cell culture flasks (Nunclon, 175cm<sup>2</sup>) at a concentration of 2.9x10<sup>5</sup> cells/mL (30 mL/flask) and were grown for 14 days at 37 °C in a 10% CO<sub>2</sub> humidified incubator with a medium change every other day. After 14 days the medium was discarded and replaced by new medium containing 1 mg/L Ag 20, Ag 200 nm or AgNO<sub>3</sub> for 24 hours. This dose was selected in order to ensure that cytotoxicity would not affect the results. Four replicates per treatment were used including untreated/solvent control (0.25% DMSO). At the end of the exposure period,

the medium was removed and the monolayers were washed twice with 7 mL ice-cold PBS. Five mL of ice-cold PBS were added and the cell monolayers were detached using a cell scraper and transferred in a 15 mL falcon tube. After centrifugation for 5 min at 1500 rpm at 4 °C (Beckman TM Allegra 64R Beckman Coulter, CA, U.S.) the supernatant was removed and the cells were stored at -20 °C until protein extraction.

*Protein extraction.* The cells were re-suspended in a lysis buffer (100 mM PIPES, 70mM NaCl) supplemented with a protease inhibitor cocktail (Protease inhibitor mix, GE Healthcare, Little Chalfont, UK). The cellular pellets were disrupted by the use of the French Press cell disruptor (Thermo Electron Corporation, MA, U.S.) at a pressure of 200 psi. Total cellular lysates were collected and stored on ice. Subsequently, the lysate was pelleted at 2,100 rpm for 15 min at 4 °C using the Beckman TM Allegra 64R centrifuge on a F1010 rotor (Beckman Coulter, CA, U.S.) in order to remove nuclei from the supernatant.

The supernatant (containing all cellular fractions excluding the nuclei) was centrifuged at 20,000 rpm during 20 min at 4 °C in Beckman TM Optima TM L90K ultracentrifuge on a 45Ti rotor (Beckman Coulter, CA, U.S.). This pellet consisted mainly of mitochondria and nucleus fragments. The supernatant was again centrifuged at 45,000 rpm for 80 min at 4 °C using a Beckman TM Optima TM L90K ultracentrifuge on a 45Ti rotor. The proteins in this supernatant, consisting of soluble cytosolic proteins, were precipitated overnight with ice-cold acetone at -20 °C. After centrifugation for 10 min at 7,500 rpm (4 °C) (Beckman TM Allegra 64R centrifuge on a F1010 rotor), the pellet of cytosolic proteins was dried under vacuum (SpeedVac, Thermo Fischer Scientific) and stored at -20 °C until further analysis.

The cytosolic proteins were then solubilized in labeling buffer (7M urea, 2M thiourea, 30 mM Tris, 2% w/v 3-[(3-cholamidopropyl)dimethylammonio]-1-propanesulfonate (CHAPS), 2% w/v 3-[N,N-Dimethyl(3-myristoylamino)propyl]ammonio]propanesulfonate (ASB14). After adjusting the pH of the sample solutions [pH 8.5 - 9], the protein concentrations were determined using the 2D Quant kit (GE Healthcare, UK) with bovine serum albumin (2 mg/mL) as standard.

*2D-DIGE, imaging of gels and protein identification.* Cytosolic proteins were labeled with the CyDyes minimal labeling method (GE Healthcare, UK). 2D-DIGE separation, imaging of the gels, picking and identification of the spot of interest were carried out as described before with minor modifications (Lasserre et al. 2012; Pasquali et al. 2013). The

labeling was performed according to the manufacturer's instructions. Forty  $\mu\text{g}$  of cytosolic proteins were used for each sample and labeled using the CyDyes minimal labeling method (GE Healthcare, UK). The internal standard was constituted by an equal fraction of each sample included in the experiment in order to correct the quantification of the proteins for potential uneven loading and electrophoretic conditions. Briefly, each sample plus internal standard were individually labeled for 30 minutes on ice in the dark with 320 pmol of either Cy3, Cy5 (for the analytical samples) or Cy2 (for the internal standard). Labeling reaction was stopped by the addition of 1  $\mu\text{L}$  10 mM lysine solution and incubation for 15 minutes on ice in the dark. Labeled samples were pooled such that each pool contained an equal ratio of proteins marked with Cy2, Cy3, and Cy5: two samples of 40  $\mu\text{g}$  each (one labeled with Cy3 and one labeled with Cy5) and 40  $\mu\text{g}$  of internal standard were then mixed and their final volume was adjusted to 120  $\mu\text{L}$  using lysis buffer (7 M urea, 2 M thiourea, 2% w/v CHAPS, 2% w/v ASB14). Prior to electrophoresis, ampholytes (Biolytes 3-10, 3% v/v, BioRad, Belgium) and Destreak reagent (0.6% v/v, GE Healthcare, Belgium) were added to each tube.

Each pool was then loaded onto a strip for the isoelectric separation (1<sup>st</sup> dimension). After re-hydration of the strips with 450  $\mu\text{L}$  of Destreak re-hydration solution (GE) for at least 12 h, the samples were directly applied on re-hydrated strips via sample loading cups. Separation was achieved using an Ettan IPGphor III (GE Healthcare, Belgium) at 20 °C allowing the strip to reach a total electric current of 80 k Vh in 25 hours. Following the 1<sup>st</sup> dimension, proteins were reduced and alkylated by incubating the strip in two consecutive steps of 15 minutes at room temperature in an equilibration buffer (2DGel DALT, SERVA electrophoresis gmbh, Germany) containing 1% DTT (Sigma, Belgium) and 2.5% iodoacetamide (Sigma, Belgium), respectively. Equilibrated strips were orthogonally loaded on large format precast gels (24 cm 2D DALT NF large gel 12.5%, SERVA electrophoresis gmbh, Germany) using the Flap cassette system (sealed with agarose) and subjected to electrophoretic separation with an Ettan DALT XII system (GE Healthcare, Belgium) by applying 0.5 W/gel for 2 h and then then 2.5 W/gel for 14 h at 25 °C (2<sup>nd</sup> dimension). Acquisition of gel images was carried out using a Typhoon 9400 (GE Healthcare, Belgium) at a special resolution of 100  $\mu\text{m}$ . CyDyes were visualized using excitation at 488 nm, 532 nm, and 633 nm (Cy2, Cy3 and Cy5, respectively) and emission at 520 nm, 610 nm and 670 nm (Cy2, Cy3 and Cy5, respectively). Gels were analyzed for the differentially abundant proteins by the DeCyder 2D Differential Analysis v.7.0 software package (GE Healthcare, Belgium).

Criteria for the selection were: spot present in at least 75% of the spot maps, fold change of at least  $\pm 1.3$ , statistical significance ( $P \leq 0.05$ ).

*Protein identification by MALDI-TOF/TOF.* Spots of interest were used to generate a “pick list” which was submitted to the Ettan Spot Handling Workstation (GE Healthcare, Belgium) for automatic picking, trypsin digestion and spotting of the peptides on the MALDI target plates with an equal volume of  $\alpha$ -cyano-4-hydroxy cinnamic acid (HCCA). On spots of interest a combined approach of protein mass fingerprint (PMF) and MS/MS using the Applied Biosystems MALDI-TOF/TOF 4800 Proteomics Analyser was applied. Calibration was carried out with the peptide mass calibration kit 4700 (Applied Biosystems, Belgium). For each spot PMF spectra were acquired and up to 8 MS/MS fragmentations were allowed on the most abundant precursors. Protein identification was achieved by searching the acquired spectra against the NCBI nr database (version 20100924 with 11888344 sequences; 4060865000 residues) with “*Homo sapiens*” as taxonomy (541459 sequences, downloaded on May 2011), using GPS Explorer Software v3.6 (Applied Biosystems) including MASCOT (Matrix Science, www.matrixscience.com, London, UK). Settings chosen for the dataset search were: 150 ppm tolerance on PMF, 0.75 Da tolerance for parent ion, up to two missed cleavages allowed, carboamidomethyl cysteine as fixed modification, oxidation of methionine and oxidation of tryptophan (single oxidation, double oxidation and kynurenin) as variable modification. Proteins with probability-based MOWSE scores ( $P < 0.05$ ) were considered to be positively identified. Univariate statistical analysis and multivariate analysis, including principal component analysis (PCA) of differentially abundant proteins, were carried out using the EDA module which is present inside the Decyder 7.0 software package.

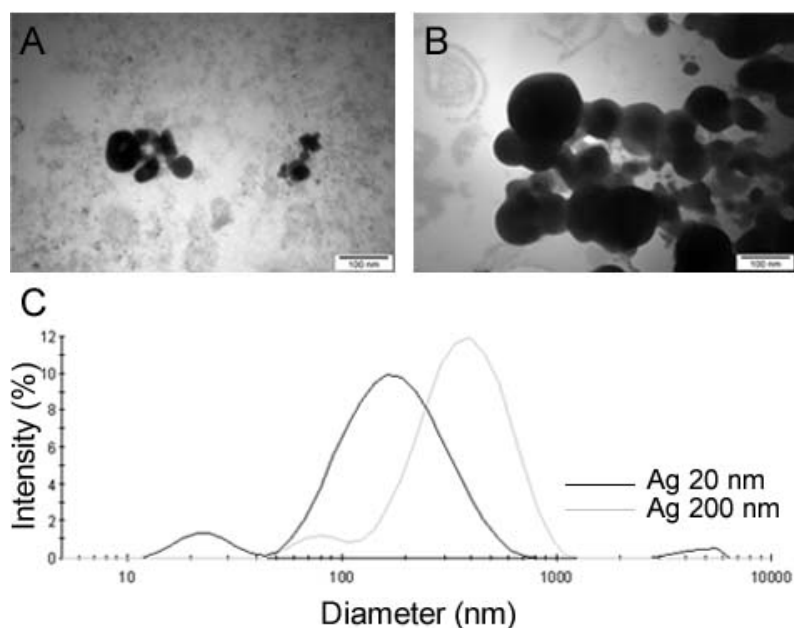
### *Statistical analysis*

The data are expressed as mean values with standard deviations of three independent experiments each containing 3 replicates. Data were analyzed with SigmaPlot 12 (Systat Software, Inc. SigmaPlot for Windows) and SPSS (IBM SPSS Statistics for Windows, Version 21.0. Armonk, NY: IBM Corp) using a general linear model (univariate analysis) with a Tukey’s post Hoc test for comparison of means. When necessary the data was transformed to achieve normal distribution and equal variances. Differences among means were considered to be significant at  $P < 0.05$ .

## Results

### *Ag particle characterization in cell culture medium*

After suspension of the particles in full cell culture medium, containing 10% FBS, both Ag 20 and 200 nm agglomerated and resulted in a broad size distribution with higher hydrodynamic sizes (Figure 1, Table 1). The  $\zeta$  potential for both particles in the FBS-containing cell culture medium was around -13 mV suggesting an unstable dispersion.

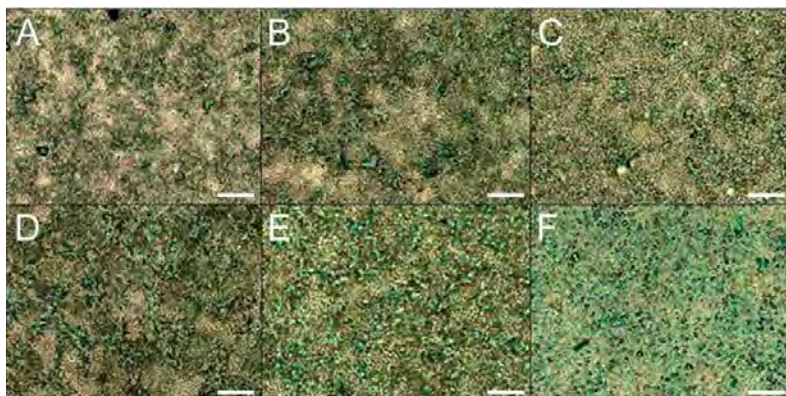


**Figure 1.** Transmission electron microscopy (TEM) images of (A) Ag 20 nm and (B) Ag 200 nm. (C) Size distribution of the particles Ag 20 nm and Ag 200 nm in the cell culture medium with 10% FBS at the highest exposure concentration used (100 mg/L).

The soluble silver present in medium with FBS after 6 and 24 hours of exposure to Ag NPs 20 and 200 nm was found to be less than 10  $\mu\text{g/L}$ , which corresponds to less than 0.01% release (Table 1).

**Table 1.** Main characteristics of the Ag particles studied and the ions released in cell culture medium containing 10% FBS after 6 and 24 hrs at the highest concentration at which the cells were exposed to (100 mg/L).

Particles	Primary size (nm)	Hydrodynamic diameter (nm)	Z potential (mV)	Soluble Ag released ( $\mu\text{g/L}$ )
Ag 20 nm	20	129	-12.8	< 10 (0.01%)
Ag 200 nm	200	308	-13.9	< 10 (0.01%)

*Co-culture system characterization*

**Figure 2.** Mucus layer stained with alcian blue in Caco-2/TC7:HT29-MTX mixed cultures 14 days after seeding with increasing densities of HT29-MTX cells (A) 0%, (B) 10%, (C) 25%, (D) 50%, (E) 75% and (F) 100%. Scale bar is 50  $\mu\text{m}$ .

The number of HT29-MTX cells present in the co-cultures after 14 days were increased with increasing the HT29-MTX initial cell seeding ratio (Figure 2). At a 90:10 ratio (Figure 2B) clusters of HT29-MTX cells were observed to be surrounded by Caco-2/TC7 that would increase with increasing HT29-MTX ratio.

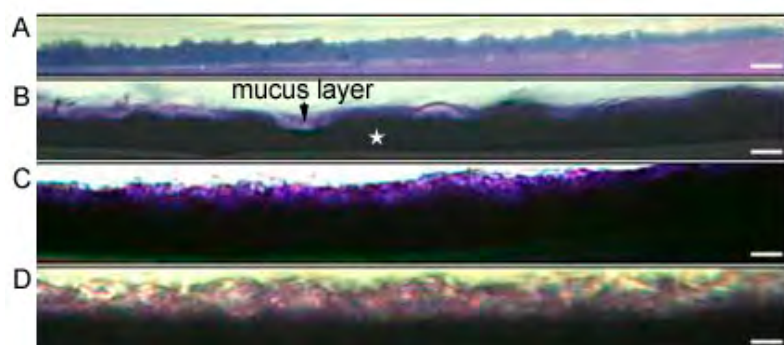


**Figure 3.** Profile of the Caco-2/TC7:HT29-MTX cells after 14 days in culture. The HT29-MTX cells were seeded at increasing densities (A) 0%, (B) 10%, (C) 50%, (D) 100%. The mucus layer is stained light purple while the cell monolayer is stained dark blue (Toluidine blue staining). The arrow head shows the mucus layer while the star shows the cell monolayer. No mucus layer is present in (A). Scale bars are 200  $\mu\text{m}$  in (A) and 100  $\mu\text{m}$  in (B-D).

No mucus layer is present in (A). Scale bars are 200  $\mu\text{m}$  in (A) and 100  $\mu\text{m}$  in (B-D).

After 14 days of culture in trans-well inserts, the mucus layer was present at all seeding densities of 10% or more of HT29-MTX cells (Figure 3 B, C, D). Already at the ratio of 90:10 Caco-2/TC7:HT29-MTX the monolayer was completely covered by mucus (B). The thickness of the mucus layer increased with the increasing initial seeding density of HT29-MTX. As expected no mucus was detected in Caco-2/TC7 cells cultured alone (A). For further experiments the 90:10 ratio was used.

## Alamar Blue assay

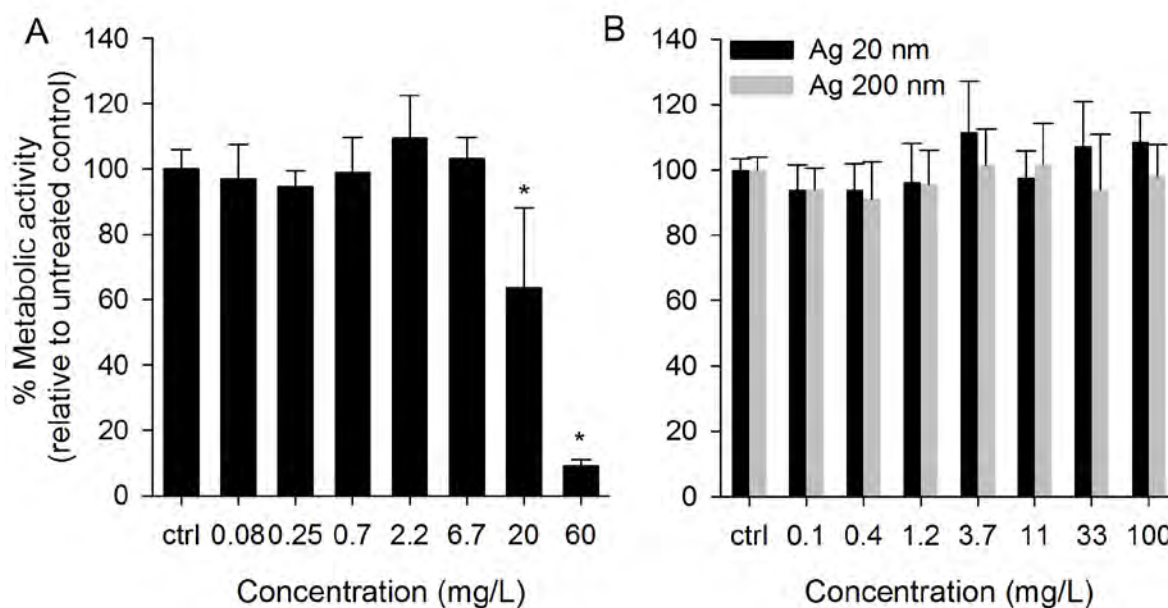


**Figure 4.** Effects of (A) AgNO<sub>3</sub> and (B) Ag 20 and 200 nm on the viability (determined as metabolic activity) of Caco-2/TC7 and HT29-MTX cells in co-culture at a 90:10 ratio. After 14 days in culture the cells were exposed for 24 hours. Error bars represent the mean ± SD of 3 independent experiments performed in triplicate. \* indicates significant differences of the treatments from the respective untreated controls ( $P < 0.05$ ).

The viability of the cells (determined as metabolic activity) significantly decreased in a dose dependent manner in 90:10 co-culture exposed to AgNO<sub>3</sub> for 24 hours (Figure 4A). Neither Ag 20 nm nor Ag 200 nm induced cytotoxicity at any of the tested concentrations (0-100 mg/L) (Figure 4B). Also no cytotoxicity was induced by the Ag particles in Caco-2/TC7 HT29-MTX cell lines cultured alone (data not shown).

## Intracellular reactive oxygen species formation

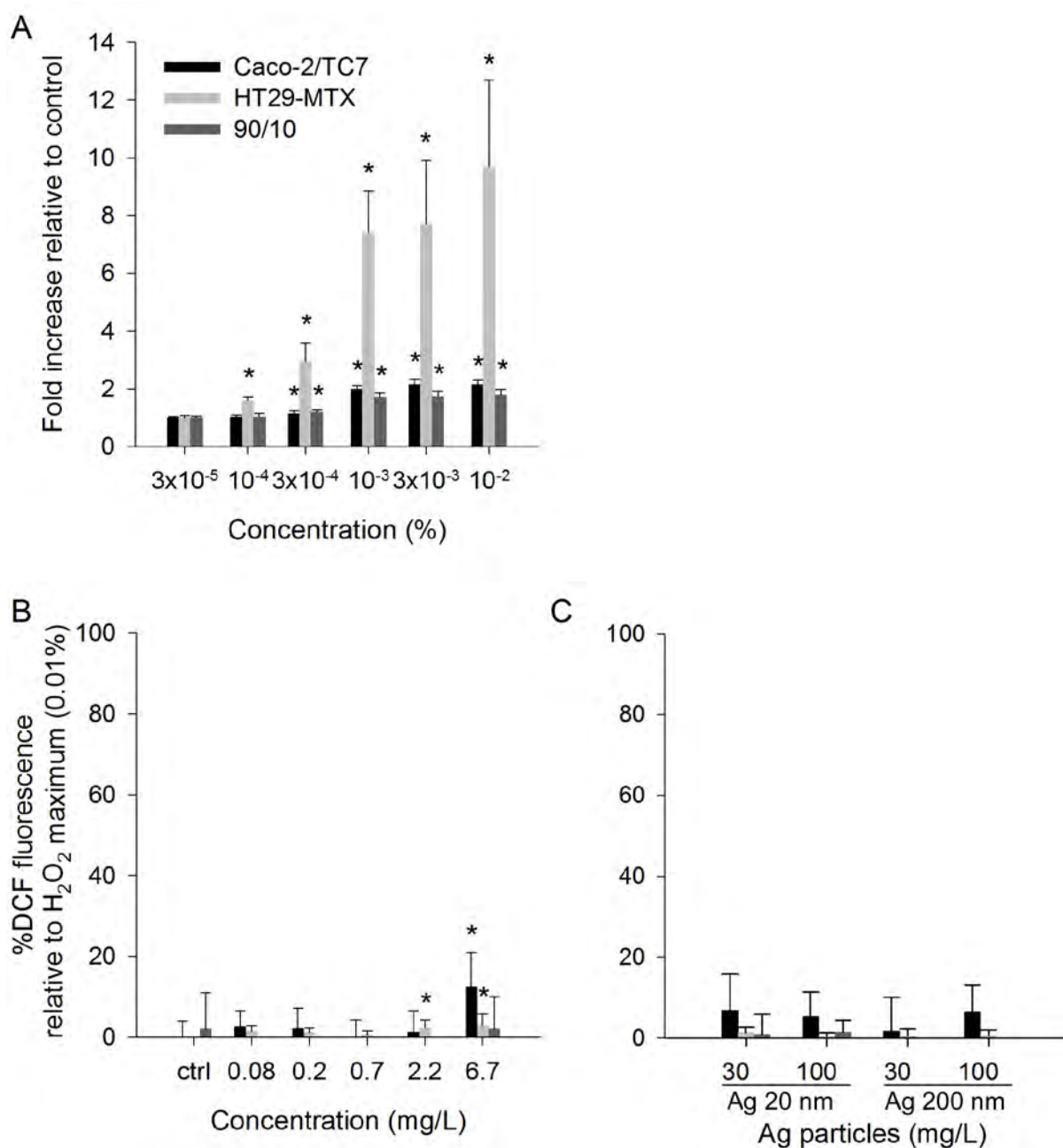
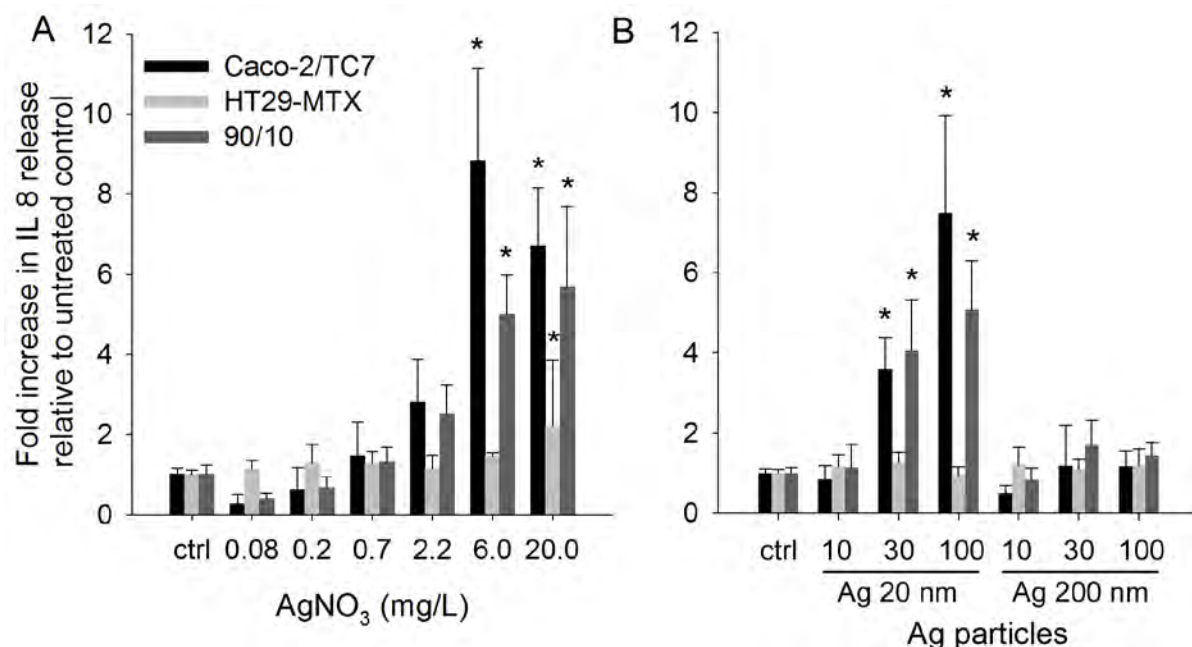


**Figure 5.** Effect of (A) H<sub>2</sub>O<sub>2</sub> (positive control) and (B) AgNO<sub>3</sub> and (C) Ag 20 and 200 nm particles on the reactive oxygen species formation. After 14 days in culture Caco-2/TC7, HT29-MTX and the 90:10 co-culture were exposed for 2 hours. Error bars represent the mean  $\pm$  SD of 3 independent experiments performed in triplicate. Significant differences from respective untreated controls are marked with asterisks (\* for  $P < 0.05$ ).

Figure 5A shows a dose-dependent enhanced production of ROS in both cell lines as well as in the co-culture, upon exposure to the positive control H<sub>2</sub>O<sub>2</sub>. The highest levels of ROS were observed with the HT29-MTX cells upon exposure to the positive control. The response in co-culture was lower than in Caco-2/TC7 and HT29-MTX alone. The Ag NPs

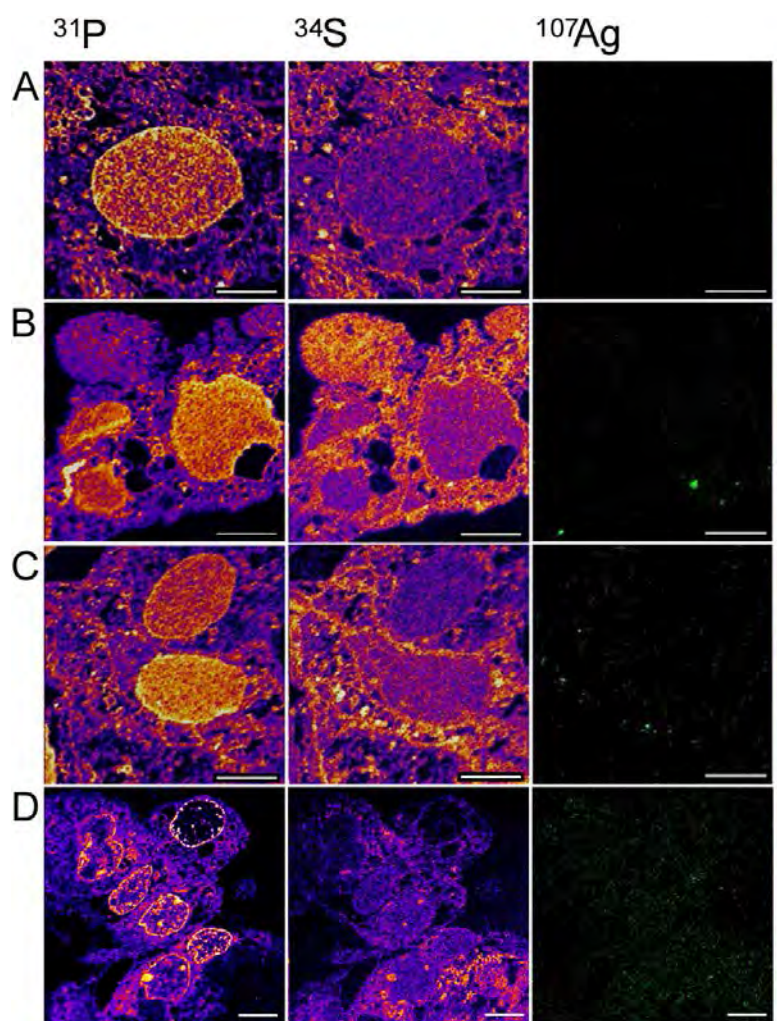
and AgNO<sub>3</sub> led to ROS production only in the Caco-2/TC7 and HT29-MTX mono-cultures with ROS levels of less than 15% of the maximal levels induced by the positive control H<sub>2</sub>O<sub>2</sub>.

### IL-8 release



**Figure 6.** IL-8 release in exposed Caco-2/TC7, HT29-MTX cells and their co-culture to (A) AgNO<sub>3</sub> and (B) Ag 20 and 200 nm particles. Differentiated cells (after 14 days of culture) were exposed for 24 hours. Error bars represent the mean  $\pm$  SD of 3 independent experiments performed in duplicate. Significant differences from respective untreated controls are marked with asterisks (\* for  $P < 0.05$ ).

The pro-inflammatory effects of Ag NPs and AgNO<sub>3</sub>, measured as secretion of interleukine-8 (IL-8), clearly revealed a dose-dependent effect for AgNO<sub>3</sub> in both Caco-2/TC7 (7-fold) as well as in the co-culture (6-fold) after 24 hours of exposure at the highest concentration used (Figure 6A). The amount of IL-8 measured in the supernatant of exposed cells in co-culture was 2 times lower compared to the Caco-2/TC7 cells cultured alone at a concentration of 6 mg/L. The HT29-MTX cells alone did not respond to stimulation by AgNO<sub>3</sub>. Ag 20 NPs induced a dose-dependent increase in IL-8 release in the Caco-2/TC7 cells and the co-culture while no statistically significant differences were observed for Ag 200 nm, showing a clear size-dependent effect (6- and 3.5-fold increase in IL 8 release compared to Ag 200 nm-exposed Caco-2/TC7 and cells in co-culture, respectively) (Figure 6B).

*Nanoparticle uptake in the co-culture-NanoSIMS*

**Figure 7.** Elemental distribution of  $^{31}\text{P}$ ,  $^{34}\text{S}$  and  $^{107}\text{Ag}$  (green), in 300 nm cuts. Caco-2/TC7:HT29-MTX cells in 90:10 co-culture were exposed to (B) Ag 20 nm (C) Ag 200 nm and (D)  $\text{AgNO}_3$  for 24 hours while (A) represents the untreated control cells. Scale bar is 5  $\mu\text{m}$ .

In figure 7, the elemental distribution of  $^{31}\text{P}$ ,  $^{34}\text{S}$  and  $^{107}\text{Ag}$  (representing NPs) in cells in co-culture is shown. Intracellular presence of Ag was observed for both Ag 20 and 200 nm as well as  $\text{AgNO}_3$ . After 24 hours of exposure to 100 mg/L of particles, Ag 20 nm (Figure 7B) was found to be present in specific areas having a high content of sulfur or phosphorus whereas Ag was more homogeneously distributed in Ag 200 nm exposed cells (Figure 7C). A high signal of Ag was detected in  $\text{AgNO}_3$ -exposed cells where a homogeneous distribution was observed.

*Proteomic analysis 2D-DIGE*

At a non-cytotoxic concentration (1 mg/L) changes in relative abundance were found for 61 proteins upon exposure to Ag 20, 200 nm or AgNO<sub>3</sub> compared to the untreated control in the co-culture model. In the AgNO<sub>3</sub>, Ag 20 nm and Ag 200 nm- treated cells in co-culture, 16, 50 and 6 proteins were altered, respectively (Table 2). The 61 differentially expressed proteins were used to cluster the samples by principal component analysis (PCA) compared to the negative control (Figure 8). Co-cultures treated with Ag 200 nm clustered very close to the negative control, while the Ag 20 nm and AgNO<sub>3</sub> treatments showed bigger differences in the proteome compared to the untreated cells or the Ag 200 nm-treated cells. The Ag 20 nm and AgNO<sub>3</sub>-induced proteome changes clustered far away from each other. The hierarchical clustering, based on these proteins provided the same overall picture (Figure S2).

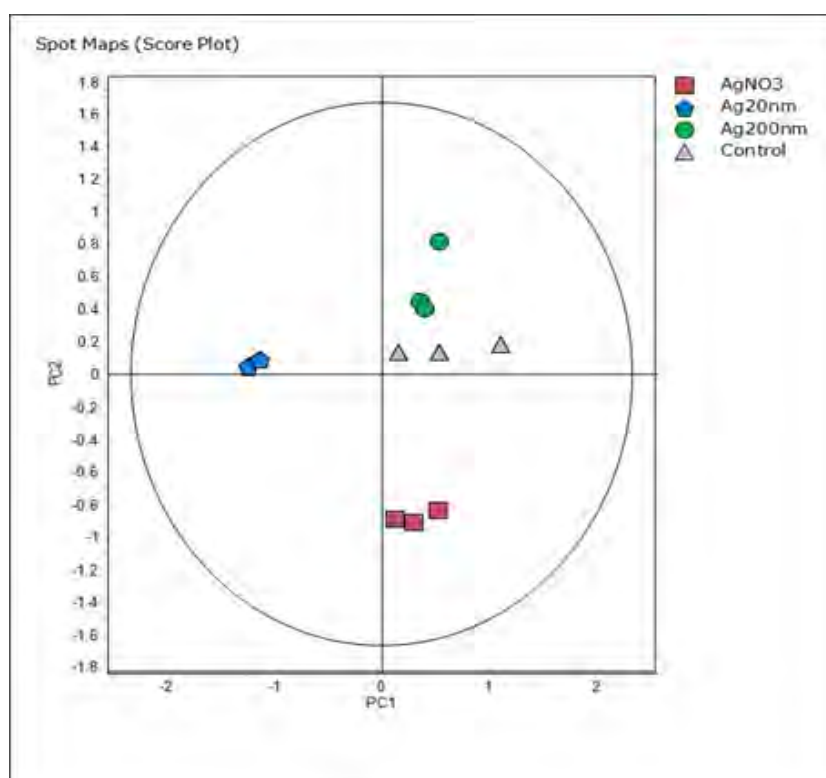


**Figure 8.** Principal component analysis of differentially expressed proteins in Caco-2/TC7:HT29-MTX cells in 90:10 co-culture exposed to 1 mg/L of Ag 20 nm, Ag 200 nm or AgNO<sub>3</sub> for 24 hours.



**Table 2.** Proteins with altered abundance upon exposure of the cells in co-culture to the non-toxic concentration of 1 mg/L of Ag 20nm NPs, Ag 200 nm NPs or AgNO<sub>3</sub><sup>a)</sup>

Spot N°	Protein name	UniProt Ac. N°	UniProt ID	NCBI GI	Cov. %	MOWSE Score	p-value	Queries matched	Mr (Da)	pI (pH)	AgNO <sub>3</sub> vs Control		Ag 20 nm vs Control		Ag 200 nm vs Control	
											Fold Change	t-test	Fold Change	t-test	Fold Change	t-test
<b>Cytoskeleton-associated proteins</b>																
260	villin-1	<a href="#">P09327</a>	VILI	194394237	40%	153	2.7e-010	40	93093	5.99	-1.13	0.351	-1.03	0.792	1.55	0.047
701	keratin, type II cytoskeletal 8	<a href="#">P05787</a>	K2C8	4504919	64%	274	2.2e-022	38	53671	5.52	-1.29	0.451	2.05	0.026	-1.97	0.12
800	keratin, type II cytoskeletal 8	<a href="#">P05787</a>	K2C8	4504919	67%	345	1.7e-029	43	53671	5.52	1.13	0.468	1.7	0.002	1.16	0.18
1083	keratin, type II cytoskeletal 8	<a href="#">P05787</a>	K2C8	4504919	59%	412	3.4e-036	44	53671	5.52	3.1	0.001	1.59	0.022	1.1	0.598
841	cytokeratin 18 (424 AA)	<a href="#">P05783</a>	K1C18	30311	77%	387	1.1e-033	46	47305	5.27	1.1	0.502	1.49	0.029	1.02	0.802
263	gelsolin isoform a precursor	<a href="#">B7Z9A0</a>	B7Z9A0	221045118	35%	130	5.4e-008	34	83451	5.58	-1.1	0.751	1.77	0.033	1.33	0.218
984	actin, cytoplasmic 1	<a href="#">P60709</a>	ACTB	14250401	72%	527	1.1e-047	38	41321	5.56	-1.1	0.114	-1.74	0.004	-1.05	0.282
993	actin, cytoplasmic 1	<a href="#">Q53G99</a>	Q53G99	62897625	85%	642	3.4e-059	42	42080	5.37	-1.22	0.083	-1.94	0.001	-1.1	0.319
683	tubulin alpha-1B chain	<a href="#">P68363</a>	TBA1B	119578453	60%	317	1.1e-026	30	46797	4.96	-2.16	0.009	-1.55	0.077	1.07	0.815
713	tubulin, beta 2C, isoform CRA_b	<a href="#">Q8N6N5</a>	Q8N6N5	119608775	55%	272	3.4e-022	38	49250	4.88	-3.8	0.003	-1.22	0.331	1.32	0.267
538	dihydropyrimidinase-related protein 2	<a href="#">Q16555</a>	DPYL2	4503377	62%	347	1.1e-029	40	62711	5.95	-1.62	0.052	1.44	0.08	1.44	0.117
<b>Oxidative stress-associated proteins</b>																
1492	peroxiredoxin-6	<a href="#">P30041</a>	PRDX6	4758638	89%	718	8.6e-067	46	25133	6.00	-1.45	0.005	-1.25	0.036	-1.33	0.032
627	protein disulfide-isomerase A3	<a href="#">P30101</a>	PDIA3	220702506	58%	271	4.3e-022	38	55328	5.61	1.1	0.383	2.01	0.004	1.38	0.038
629	protein disulfide-isomerase A3	<a href="#">P30101</a>	PDIA3	220702506	64%	795	1.7e-074	43	54541	5.61	1.34	0.18	2.63	0.007	1.42	0.106
635	protein disulfide-isomerase A3	<a href="#">P30101</a>	PDIA3	220702506	63%	645	1.7e-059	44	54541	5.61	1.32	0.146	2.53	0.003	1.22	0.2
655	protein disulfide isomerase family A, member 3, isoform CRA_a	<a href="#">B3KQT9</a>	B3KQT9	119597640	40%	81	0.0039	21	54454	6.78	1.69	0.043	1.1	0.247	-1.06	0.514
765	protein disulfide-isomerase A6	<a href="#">Q15084</a>	PDIA6	1710248	63%	419	6.8e-037	38	46512	4.95	1.32	0.118	1.52	0.04	-1.11	0.618
769	protein disulfide-isomerase A6	<a href="#">Q15084</a>	PDIA6	1710248	63%	467	1.1e-041	43	46512	4.95	1.25	0.104	1.53	0.02	1.05	0.757
767	glutathione synthetase	<a href="#">P48637</a>	GSHB	4504169	70%	580	5.4e-053	50	52523	5.67	-1.08	0.367	1.48	9E-04	1.01	0.79

<b>Apoptosis-associated proteins</b>																
1203	annexin A4	<a href="#">P09525</a>	ANXA4	1703319	73%	453	2.7e-040	39	36088	5.84	-1.27	0.021	-1.54	0.01	-1.04	0.703
1208	annexin A4	<a href="#">P09525</a>	ANXA4	1703319	69%	346	1.4e-029	37	36088	5.84	-1.16	0.434	-1.1	0.611	1.88	0.009
1226	annexin A4	<a href="#">P09525</a>	ANXA4	1703319	73%	731	4.3e-068	42	36088	5.84	-1.24	0.119	-1.63	0.006	-1.06	0.676
1769	histidine triad nucleotide-binding protein 1	<a href="#">P49773</a>	HINT1	227968190	94%	105	1.7e-005	18	13887	6.24	1.16	0.224	1.36	0.013	1.24	0.037
1773	programmed cell death protein 5	<a href="#">O14737</a>	PDCD5	159163907	84%	217	1.1e-016	22	12911	9.85	1.72	0.011	1.03	0.896	-1.45	0.115
<b>Stress-associated proteins</b>																
408	heat shock cognate 71 kDa protein isoform 2	<a href="#">Q53HF2</a>	Q53HF2	24234686	57%	419	6.8e-037	39	53598	5.62	-1.03	0.896	1.55	0.023	-1.04	0.845
414	heat shock 70 kDa protein 1A/1B	<a href="#">P08107</a>	HSP71	147744565	62%	248	8.6e-020	33	70294	5.48	1.46	0.016	1.57	0.017	1.1	0.493
429	heat shock 70 kDa protein 1A/1B	<a href="#">P08107</a>	HSP71	147744565	56%	515	1.7e-046	45	70294	5.48	1.33	0.01	1.61	3E-04	1.28	0.269
438	heat shock 70 kDa protein 1A/1B	<a href="#">P08107</a>	HSP71	147744565	51%	203	2.7e-015	31	70294	5.48	1.54	0.034	2.04	0.021	1.04	0.913
573	60 kDa heat shock protein, mitochondrial	<a href="#">P10809</a>	CH60	31542947	53%	357	1.1e-030	43	61187	5.70	-1.03	0.884	1.74	0.029	-1.22	0.44
576	60 kDa heat shock protein, mitochondrial	<a href="#">P10809</a>	CH60	31542947	45%	138	8.6e-009	30	61187	5.70	-1	0.86	1.75	0.004	-1.15	0.356
577	60 kDa heat shock protein, mitochondrial	<a href="#">P10809</a>	CH60	31542947	57%	641	4.3e-059	47	61187	5.70	-1.04	0.889	1.85	0.048	-1.21	0.577
578	60 kDa heat shock protein, mitochondrial	<a href="#">P10809</a>	CH60	31542947	72%	684	2.2e-063	49	61187	5.70	-1.04	0.869	1.66	0.067	-1.26	0.469
473	stress-induced-phosphoprotein 1	<a href="#">P31948</a>	STIP1	5803181	54%	131	4.3e-008	29	68721	7.81	1.05	0.57	2.02	0.002	1.37	0.012
479	stress-induced-phosphoprotein 1	<a href="#">P31948</a>	STIP1	5803181	58%	122	3.4e-007	28	68721	7.81	1.08	0.404	2.03	0.003	1.29	0.032
<b>Metabolism-associated proteins</b>																
625	liver carboxylesterase 1	<a href="#">P23141</a>	EST1	30749518	45%	133	2.7e-008	38	60692	6.06	-1.06	0.869	-1.91	0.028	-1.18	0.488
631	liver carboxylesterase 1	<a href="#">P23141</a>	EST1	30749518	51%	109	6.8e-006	31	60692	6.06	-1.13	0.732	-2.59	0.017	-1.48	0.191
1543	glutathione S-transferase P	<a href="#">P09211</a>	GSTP1	4504183	75%	716	1.4e-066	29	23569	5.43	-1.14	0.435	-1.95	0.008	-1.29	0.19
1569	glutathione S-transferase P	<a href="#">P09211</a>	GSTP1	4504183	75%	681	4.3e-063	26	23569	5.43	-1.03	0.791	-1.68	0.008	-1.17	0.266
1866	fatty acid binding protein	<a href="#">P07148</a>	FABPL	182356	91%	408	8.6e-036	21	14226	6.60	1.26	0.195	1.88	0.008	-1.07	0.706
1177	inorganic pyrophosphatase	<a href="#">Q15181</a>	IPYR	11056044	77%	234	2.2e-018	29	33095	5.54	-1.16	0.332	1.41	0.05	1.2	0.366
1199	inorganic pyrophosphatase	<a href="#">Q15181</a>	IPYR	11056044	68%	169	6.8e-012	25	33095	5.54	-1.03	0.975	1.91	0.031	1.26	0.309
1045	sialic acid synthase	<a href="#">Q9NR45</a>	SIAS	12056473	76%	397	1.1e-034	39	40738	6.29	-1.15	0.548	1.58	0.046	1.37	0.109
1133	pyridoxal kinase	<a href="#">O00764</a>	PDXK	119629883	45%	123	2.7e-007	24	42931	7.59	-1.06	0.702	-1.7	0.008	1.01	0.988
1320	purine nucleoside phosphorylase	<a href="#">P00491</a>	PNPH	157168362	73%	244	2.2e-019	29	32758	6.71	-1.25	0.249	-2.03	0.028	-1.18	0.405

Chapter 2

941	aspartate aminotransferase, cytoplasmic	<a href="#">P17174</a>	AATC	4504067	72%	298	8.6e-025	39	46447	6.52	1.85	0.039	1.03	0.966	1.11	0.632
1938	polyubiquitin-C	<a href="#">F5H7Y5</a>	F5H7Y5	228311825	80%	556	1.4e-050	24	17081	6.22	1.36	0.016	1.09	0.514	-1.19	0.268
185	elongation factor 2	<a href="#">P13639</a>	EF2	4503483	37%	197	1.1e-014	38	96246	6.41	1.24	0.164	-1.82	0.021	1.15	0.595
200	elongation factor 2	<a href="#">P13639</a>	EF2	4503483	46%	258	8.6e-021	45	96246	6.41	-1.15	0.164	-1.67	0.009	1.21	0.646
1734	peptidyl-prolyl cis-trans isomerase A	<a href="#">P62937</a>	PPIA	1633054	93%	443	2.7e-039	23	18098	7.82	1.78	0.05	-1.48	0.037	-1.27	0.125
994	leukocyte elastase inhibitor	<a href="#">P30740</a>	ILEU	13489087	56%	563	2.7e-051	39	42829	5.90	-1.65	0.003	-2	0.001	-1.25	0.147
1007	leukocyte elastase inhibitor	<a href="#">P30740</a>	ILEU	13489087	52%	266	1.4e-021	27	42829	5.90	-1.65	0.02	-1.75	0.009	-1.39	0.151
1020	leukocyte elastase inhibitor	<a href="#">P30740</a>	ILEU	13489087	56%	662	3.4e-061	39	42829	5.90	-1.22	0.024	-1.32	0.005	1.11	0.021
703	retinal dehydrogenase 1	<a href="#">P00352</a>	AL1A1	21361176	52%	318	8.6e-027	45	55454	6.30	-1.28	0.064	-1.62	0.01	1.19	0.18
815	alpha-enolase	<a href="#">P06733</a>	ENOA	203282367	78%	531	4.3e-048	48	47350	6.99	1.07	0.614	1.92	0.008	1.12	0.479
816	alpha-enolase	<a href="#">P06733</a>	ENOA	203282367	80%	383	2.7e-033	45	47350	6.99	-1.03	0.803	1.54	0.008	1.05	0.737
1426	triosephosphate isomerase isoform 1	<a href="#">P60174</a>	TPIS	4507645	97%	631	4.3e-058	51	26938	6.45	1.13	0.515	1.95	0.025	1.09	0.582
1443	triosephosphate isomerase isoform 1	<a href="#">P60174</a>	TPIS	4507645	94%	830	5.4e-078	53	26938	6.45	-1.02	0.946	1.92	0.049	1.18	0.501
1461	triosephosphate isomerase isoform 1	<a href="#">P60174</a>	TPIS	66360365	55%	171	4.3e-012	26	26938	6.45	-1.56	0.033	-1.08	0.667	-1.13	0.494
1008	fructose-bisphosphate aldolase C	<a href="#">P09972</a>	ALDOC	61680382	61%	138	8.6e-009	23	37940	6.67	-1.23	0.047	-1.07	0.334	1.35	0.003
<b>Others</b>																
1357	chloride intracellular channel protein 1	<a href="#">O00299</a>	CLIC1	14251209	81%	322	3.4e-027	31	27248	5.09	1.2	0.107	-1.55	0.009	-1.2	0.064
1370	chloride intracellular channel protein 1	<a href="#">O00299</a>	CLIC1	14251209	75%	506	1.4e-045	38	27248	5.09	-1.04	0.808	-1.65	0.013	-1.22	0.213

<sup>a)</sup> The spot number; protein name; UniProt accession number; UniProt ID; NCBI accession number; sequence coverage; MOWSE score; p-value relative to the MASCOT identification; number of queries matched; theoretical molecular weight (expressed in Da) and isoelectric point (expressed in pH units); the fold change and relative t-test value for co-cultures treated with AgNO<sub>3</sub>, Ag 20 nm NPs and Ag 200 nm NPs, respectively, are reported for each protein. Dark grey = protein is more abundant; light grey = protein is less abundant

## Discussion

Ag NPs with their increased use in consumer products are likely to reach the environment and humans through either direct or indirect exposure. Although an important uptake route for humans is via ingestion, the effects of NPs and their fate in the gastrointestinal tract are largely unknown. This study describes the evaluation of the uptake, intracellular localization and effects of Ag NPs and AgNO<sub>3</sub> on a gastrointestinal co-culture model simulating the epithelium incorporating a mucus layer

In the gastrointestinal epithelium the mucus layer provides a protective barrier against pathogens, digestive enzymes and damage (Mahler et al. 2009). The staining performed showed that the mucus layer was formed after 14 days in culture and the thickness of the mucus layer increased with increasing HT29-MTX ratio. The mucus layer covered the whole surface of the cell monolayer and was continuous for Caco-2/TC7 and HT29-MTX even at the lowest ratio of HT29-MTX cells present (90:10). The concentration of goblet cells in the small intestine and under healthy conditions is approximately 10% (Walter et al. 1996) and for that reason this ratio was chosen for the study.

Ag NPs did not exert adverse effects in the metabolic activity of Caco-2/TC7, HT29-MTX as well as the co-culture as measured with the Alamar blue assay. This is in accordance with previous studies where the metabolic activity of Caco-2 upon exposure to different-sized Ag NPs up to 50 mg/L was always above 80% (Bouwmeester et al. 2011).

The soluble silver present in medium was found to be less than 10 µg/L under all conditions, which corresponds to less than 0.01% release. However, it has to be noted that the actual concentration of Ag may be underestimated due to binding of Ag in the filter membrane. In addition, due to complexation of Ag with proteins and aminoacids present in the cell culture medium, low levels of Ag can be measured in the filtrates in full cell culture medium with FBS (concentration of AgNO<sub>3</sub> was 139 µg/L which corresponds to 0.7% of total Ag).

The NanoSIMS analysis revealed that both 20 and 200 nm Ag NPs were taken up by the cells in co-culture. Although the exact compartment in which they were accumulated could not be identified, they were found to be localized in regions with high phosphorus and sulfur content, possibly in late endosomes or lysosomes, and they were not found in the nucleus but close to the nuclear membrane. Ag 200 nm NPs were more homogeneously distributed in the cells whereas Ag 20 nm NPs were found to be localized in specific areas

which may point to different uptake or intracellular distribution mechanisms depending on the size or surface area of the particle. SiO<sub>2</sub> NPs were reported to be localized in lysosomes and cytosol in HT29 cells but not found in the nucleus (Gehrke et al. 2013). In previous studies, starch-capped Ag NPs were found in endosomes, lysosomes, mitochondria and nucleus (AshaRani et al. 2009). No particle localization was observed in the nucleus in our study, probably due to the bigger size of our particles as well as the lack of a capping agent that could affect the distribution of the NPs in the medium and the cell, confirming once more that several factors such as size and surface coating can influence uptake and intracellular localization.

However, none of the Polyvinyl pyrrolidone (PVP), citrate or uncoated Ag NPs were found to be localized in the nucleus of BEAS-2B cells which is in agreement with our results (Gluga et al. 2014). When NPs are localized in lysosomes, whose major function is to break down material that is taken up by the cell, the low pH could affect the dissolution of Ag NPs with subsequent consequences for the Ag availability and possibly the toxic effects within the cells. Studies with polymeric NPs have shown that the surface charge of the particle affects cell-particle interactions and their interference with membrane-bound proteins (Bhattacharjee et al. 2013). Also interactions with serum proteins are to be expected and it has been shown that the fetal bovine serum (FBS) content of the medium influenced the extent of NPs' toxic effects. In medium with 1% FBS a concentration and size-dependent cytotoxicity of SiO<sub>2</sub> NPs was observed while no cytotoxicity was reported in the 10% FBS-containing medium (Brownlee et al. 2007). In our study 10% FBS was used which is the minimum content required for optimal growth and function of the Caco-2/TC7 and HT29-MTX cells. The extent of Ag NPs' surface interaction with the proteins is still unknown but complexation processes are to be expected. The zeta potential of both particles in culture medium with 10% FBS was very similar and slightly negatively charged (-13 mV). Therefore, the differences in uptake observed in our study cannot be explained by the charge differences of the particles.

Although oxidative stress is one of the proposed mechanisms for NP toxicity, the studied Ag NPs did not lead to a significant increase in intracellular ROS formation which is in agreement with previous studies using Caco-2 (Abbott Chalew and Schwab 2013) and BEAS-2B cells (Gluga et al. 2014). The cells in co-culture were less responsive to oxidative stress induced by H<sub>2</sub>O<sub>2</sub> compared to Caco-2/TC7 cells alone. It has been previously shown that the mucus layer has ROS scavenging abilities and resists to ROS attack while low levels of

ROS increase the barrier protection by increasing the mucus layer thickness (Brownlee et al. 2007). Therefore, it seems that the presence of the mucus layer protects against ROS damage.

A significant size-dependent increased IL-8 release was observed with the smaller Ag 20 nm eliciting an 8 and 4 times higher inflammatory response compared to the larger Ag 200 nm in Caco-2/TC7 cells alone and the co-culture, respectively. This is in accordance with previous findings using the same set of NPs and only 20 nm Ag NPs up-regulated the IL-8 expression (Stepkowski et al. 2014). An increase in IL-8 gene and protein expression in a macrophage cell line exposed to 5 nm Ag NPs has been previously found while 100 nm Ag NPs did not induce IL-8 release (Lim et al. 2012). A possible explanation for this effect could be that bigger particles are better retained in the mucus layer than smaller ones that may thus cross the mucus layer and reach the cells faster and induce higher effects. The levels of IL-8 produced by the cells in co-culture exposed to non-toxic concentrations of AgNO<sub>3</sub> (up to 20 mg/L) were lower compared to the IL-8 production in Caco-2/TC7 cells alone. The mucus layer could serve as a barrier against ions and impede the access to the microvilli (Pontier et al. 2001).

In order to have a comprehensive understanding of changes that occur upon Ag 20, Ag 200 nm and AgNO<sub>3</sub> exposure in the co-culture model, a proteomic study was included. The biggest changes in protein expression were induced by Ag 20 nm (50 differentially regulated proteins) followed by AgNO<sub>3</sub> (16 modified proteins), while treatment with Ag 200 nm NPs only induced changes to 6 cytosolic proteins. These results are in agreement with the IL-8 release findings and with a recent study with LoVo human colon cancer cells showing that more proteins were differentially regulated after exposure to Ag 20 nm than Ag 100 nm NPs regulating different sets of proteins (Verano-Braga et al. 2014). Also in HepG2 cells exposed to the same 200 nm NPs, only minor changes in gene expression were previously found (Stepkowski et al. 2014). The altered protein expression profile found in the current study was involved in cytoskeleton organization and cell cycle, apoptosis, metabolism/detoxification, stress and oxidative stress.

*Cytoskeleton- and cell cycle-associated proteins:* Ag 20 nm triggered an up-regulation of the cytoskeleton proteins cytokeratin 8 (CK8) and cytokeratin 18 (424 AA) (CK18) that are essential for the integrity of the epithelial cells and beyond their mechanical function they have been found to be involved in the protection against stress, apoptosis and in cell cycle regulation (Moll et al. 2008). They are co-expressed in a variety of tissues including the gastrointestinal tract (Weng et al. 2012) playing an important role in maintaining barrier

function under stress. CK8/CK18 have been reported to be involved in IL-6 mediated barrier protection (Wang et al. 2007) whereas a re-arrangement of CK18 has been reported upon rotavirus infection in differentiated Caco-2 cells (Brunet et al. 2000). Gelsolin and villin are actin-binding proteins that regulate cell morphology and motility and their upregulation has been linked with resistance to apoptosis (Wang et al. 2012a), while villin-1 (a brush-border actin-binding protein) has been reported to be a cell-specific anti-apoptotic protein (Wang et al. 2008). The up-regulation of gelsolin and villin observed in our study in Ag 20 nm and 200 nm-treated cells, respectively, suggests a protection of the cells against injury, stress and apoptosis. In addition, actin, cytoplasmic 1 (ACTB) that is essential for maintaining the epithelial integrity and regulating the structure of tight junctions (Baranwal et al. 2012; Ku et al. 1999) was down-regulated in Ag 20 nm-exposed cells that can lead to the disruption of tight junctions and subsequent increased epithelial permeability. The paracellular permeability, however, was not changed upon exposure to Ag NPs as measured with a paracellular permeability marker (lucifer yellow) and transepithelial electrical resistance (TEER) (Figure S1). All these results suggest that treatment with Ag 20 nm NPs and AgNO<sub>3</sub>, even though in the latter case to a lesser extent, interferes with the structure and organization of the cytoskeleton of Caco-2 and HT29 cells in co-culture. A clear particle-size effect on the proteins that were differentially expressed was seen, that was also different from the pattern observed for AgNO<sub>3</sub>, which is in accordance with a recent study showing that particles of different sizes regulate different sets of proteins (Verano-Braga et al. 2014). Similar findings have been observed in a proteomic study of the plant *Eruca sativa* after exposure to either ionic or particulate silver indicating that the effects of Ag NPs are not due to ion release (Vannini et al. 2013). In addition, a proteomic study with Cu NPs and Cu ion-exposed macrophages showed that the responses could only be partly attributed to the free ions (Triboulet et al. 2013).

AgNO<sub>3</sub> led to down-regulation of the microtubule-involved proteins tubulin alpha 1B chain (TUBA1B) and tubulin beta 2C, isoform CRA\_b that play a major role in cell motion and in cell division (Downing and Nogales 1998) and collapsin response mediator protein 2 (CRMP-2) involved in axonal growth and differentiation and microtubule assembly (Charrier et al. 2003; Fukata et al. 2002). An interference of Au NPs (40 nm) with microtubule polymerization and a subsequent cell cycle arrest and induction of apoptosis have been observed in A549 cells (Choudhury et al. 2013). Although the A549 cells were viable after 48 hours of exposure to Au NPs, the initiation of damage of microtubules started at 24 hours

that was followed by apoptosis (Choudhury et al. 2013). These results suggest that AgNO<sub>3</sub> could lead to altered mitosis and subsequent cell cycle arrest.

*Apoptosis-associated proteins:* A key apoptosis regulator, Annexin A4 (ANXA4), was altered under Ag 20 nm (less abundant) and Ag 200 nm treatment (more abundant). ANXA4, a water soluble Ca<sup>2+</sup> binding protein that can reversibly associate with membranes and cytoskeletal proteins and that is involved in endocytotic and exocytotic processes (Weinman et al. 1994), was suggested to be an early marker of apoptosis (Herzog et al. 2004). In the intestine, ANXA4 is present in both mature villus enterocytes (along the basolateral membrane) and goblet cells (Massey et al. 1991). Higher levels of histidine triad nucleotide-binding protein 1 (HINT1) in Ag 20 nm treated cells were also observed. HINT1 is involved in apoptotic processes and may also have tumor suppressor functions (Weiske and Huber 2006). These results suggest that Ag NPs treatment affects apoptotic signaling in cells. The balance in cell proliferation and apoptosis is essential in the gastrointestinal epithelium for the maintenance of the normal function as a barrier (Wang et al. 2008).

*Metabolism-associated proteins:* Ag 20 nm altered the expression of proteins that play an important role in xenobiotic metabolism probably compromising the detoxification process. The protein liver carboxylesterase 1 (CES1), responsible for the hydrolysis and metabolism of endogenous and exogenous compounds (Imai et al. 2005), and glutathione S-transferase P (GSTP1) were found to be less abundant in the Ag 20 nm-treated cells in co-culture. GSTP1 belongs to the family of phase II detoxification enzymes, responsible for the metabolism of xenobiotics and secondary metabolites/by-products of oxidative stress (Hayes et al. 2005). The activity of GST has been previously found to be reduced in the digestive gland of freshwater snails exposed to Ag NPs (Ali et al. 2014). Ag 20 nm induced higher levels of the liver type fatty acid-binding protein-1 (FABPL), that regulates absorption and transport of fatty acids (Levy et al. 2009) and has been reported to be a marker of intestinal tissue injury (Pelsers et al. 2003). Inorganic pyrophosphatase (IPYR), an important enzyme in cell energy metabolism was also more abundant in Ag 20 nm-treated cells. It was previously shown that it is essential for *C. elegans* development and intestinal function (Ko et al. 2007). Furthermore, higher levels of sialic acid synthase (SAS, also known as N-acetylneuraminase synthase) were observed in Ag 20 nm-treated cells. It regulates the synthesis of sialic acids that play an important role in biological properties of the cell (Lawrence et al. 2000). Sialic acids may have a structural role due their presence in the outer surface of the cell and their negative charge and they are part of binding and recognition sites for pathogens and toxins

(Varki 2008) as well as they may mask recognition sites such as antigenic sites (Schauer 1985). In addition, sialic acids are also localized in mucus glycoprotein and they contribute to the high viscosity of the mucus barrier and are of high importance for the maintenance of mucosal integrity (Yusuf et al. 2005). Ag 20 nm reduced the levels of pyridoxal kinase (PDXK) that is involved in Vitamin B6 activation (Albersen et al. 2013). Purine nucleoside phosphorylase (PNP) is a purine metabolism enzyme (Bzowska et al. 2001) and was found to be less present in Ag 20 nm-treated cells. PNP deficiency has been associated with immune dysfunction (Gudas et al. 1978; Papinazath et al. 2011).

The protein elongation factor 2 (EF2) that is involved in protein biosynthesis and has been implicated in cell cycle progression (Nakamura et al. 2009), was present in a lower amount in Ag 20 nm-exposed cells. Peptidyl-prolyl cis-trans isomerase A (PPIA), also known as cyclophilin A (CYPA), is known to be involved in protein folding and trafficking and is the target for the immunosuppressive drug cyclosporine A (CsA) (Chen et al. 2008). CYPA can be released in the presence of inflammatory stimuli and it has been involved in several diseases (e.g. cardiovascular and inflammatory diseases, cancer) and plays a role in the regulation of infection and replication of several viruses (Nigro et al. 2013). CYPA overexpression has been related with increased IL-8 levels and proliferation (Sun et al. 2011) as well as increased drug resistance (Chen et al. 2008). AgNO<sub>3</sub>-induced higher CYPA abundance could therefore be involved in the increased IL-8 levels found in our study.

*Oxidative stress-associated proteins:* Normally cells have a defense system against oxidative stress with a variety of enzymes being involved. Both Ag NPs treatments and AgNO<sub>3</sub> triggered a down-regulation of peroxiredoxin-6 (PRDX6, the only overlap observed for all treatments) that is a member of peroxiredoxins and is involved in redox regulation of the cell and protection against oxidative injury (Manevich and Fisher 2005). A previous suppression of PRDX6 led to increased ROS levels and apoptosis of cancer cells (Wang et al. 2012b). This implies that both Ag NPs and ions lead to a compromised oxidative defense system. Ag 20 nm activated proteins related to redox homeostasis. Increased levels of protein disulfide isomerases A3 and A6 (PDIA3 and PDIA6) were observed in Ag 20 nm-treated cells. They are members of the protein disulfide isomerase family (PDI) that catalyzes disulfide bond formation. They are part of the cell protective mechanism against oxidative stress and glycoprotein folding control (Turano et al. 2011). Thus, the increased levels observed could counteract the effects induced by oxidative stress such as protein misfolding or damage. In addition, Ag 20 nm treatment led to increased levels of glutathione synthetase (GSS) that is

critical for the synthesis of glutathione (GSH), a major anti-oxidant and detoxification agent (Zhang and Forman 2012) that provides defense against metabolite toxicity (Spielberg and Gordon 1981). Therefore, these results indicate that both Ag NPs and AgNO<sub>3</sub> but mainly Ag 20 nm, lead to the activation of mechanisms in order to deal with oxidative stress and maintain cellular homeostasis.

*Stress-associated proteins:* Both Ag 20 nm and AgNO<sub>3</sub>, though the latter to a lower extent, were found to induce stress response proteins such as heat shock 70 kDa protein 1A/1B (HSP70s). These proteins participate in many processes related to normal protein folding and assembly (Mayer and Bukau 2005). An increased expression of HSP70 has only been reported for the smaller sized Ag NPs (5 nm)-treated macrophage cells (Lim et al. 2012), which is in accordance with our study. An overexpression of the HSP70 gene has been previously reported in the earthworm *E. fetida* treated with both Ag NPs and AgNO<sub>3</sub> (Tsyusko et al. 2012) which was rather related to the total Ag concentration than the Ag form. Therefore, the higher levels of HSP70 could be more of an indication of generic stress in the presence of Ag NPs and AgNO<sub>3</sub>. Interestingly, only Ag 20 nm NPs significantly increased the levels of the heat shock 60 kDa mitochondrial protein (HSP60). HSP60 plays an important role in protein folding quality control, in regulating apoptotic processes and in organelle biogenesis (Ghosh et al. 2008; Takada et al. 2010). An over-representation of HSP60 had a protective role against H<sub>2</sub>O<sub>2</sub>-induced damage of small intestinal mucosal cells and exhibited a protective role against apoptosis and necrosis (Takada et al. 2010). These results indicate that over-expression of HSPs may protect the epithelium against protein misfolding and Ag NPs-induced cellular damage. Stress-induced-phosphoprotein 1(STIP1) was found to have higher levels in Ag 20 nm exposed cells. STIP1 is a co-chaperone that binds with HSP70 and HSP90 and regulates their action and specificity (Odunuga et al. 2004).

*Other functions:* Only the exposure to Ag 20 nm led to lower levels of chloride intracellular channel protein 1(CLIC1) that is expressed in the apical part of columnar epithelia including the small intestine (Ulmasov et al. 2007) and has been suggested to be associated with actin cytoskeleton (Singh et al. 2007). It has been previously shown that CLIC1 is involved in cell cycle regulation and cell division and the over-expression of CLIC1 led to the inhibition of the proliferation of gastric cells and apoptosis induction (Ma et al. 2012). In addition, the role of CLIC1 as a sensor of cell oxidation has been previously reported (Averaimo et al. 2010), which could suggest protection against apoptosis or response to oxidative conditions.

In the current study, the proteomic results revealed an altered expression of proteins related to the maintenance of the redox balance of the cell, protection against oxidative damage and apoptosis as well as tissue damage and adaptation. The mechanisms of intestinal adaptation upon several internal and external stimuli involve altered expression levels of carrier proteins, changes in barrier permeability etc. (Drozdowski and Thomson 2006) and proteins involved in the maintenance of the balance between cell proliferation and apoptosis which is a physiological event in the gastrointestinal epithelium. Our results revealed that Ag 20 nm NPs could result in a compromised intestinal barrier integrity and function as was shown with the increased levels of IL-8 as well as the altered levels of proteins that have been reported to be involved in intestinal injury and adaptation (e.g. ANXA4 and villin, CK8/CK18, gelsolin, ACTB, IPYR, FABPL, SAS) that could have implications on the physiological processes occurring in the gastrointestinal epithelium such as normal nutrient absorption and transport as well as protection against pathogens and xenobiotics. In addition, Ag NPs 20 nm led to an up-regulation of several proteins (GSTP1, CES1, GSS) that together with the multidrug efflux transporters are involved in the defense of the cells against xenobiotics and metabolites in several tissues. Certain NPs can inhibit multidrug efflux transporters (Anselmo et al. 2012; Bhattacharjee et al. 2013) and this could possibly result in up-regulation of compensation mechanisms.

This study describes the effects of Ag NPs on a co-culture model that represents a more physiological and relevant *in vivo*-like model compared to the Caco-2 cells alone, with the presence of mucus which has an impact on modulating the induced toxicity of NPs. NP-specific effects were observed for uptake, pro-inflammatory response and changes at the proteome level. The nanoSIMS analysis showed that especially the Ag 20 nm NPs were taken up by the cells and were localized in areas with high sulfur content, most likely in late endosomes or lysosomes, but not in the nucleus. Further research should elucidate the uptake mechanisms in the co-culture and the mechanism leading to increased inflammatory response. The proteomic results revealed that Ag NPs 20 nm regulated different sets of proteins with a distinct pattern of cellular responses compared to Ag 200 nm and AgNO<sub>3</sub>, indicating a different mode of action with effects being particle and size-dependent.

## Supporting Information

Cell monolayer integrity evaluation (TEER) (Figure S1), hierarchical clustering (Figure S2) and detailed information on protein identification (Table S1).

## Acknowledgements

These experiments were supported by the Fonds National de la Recherche of Luxembourg within the projects NanEAU (FNR/08/SR/07) and NanEAU II (C10/SR/799842). Parts of the work have been performed in the framework of the “Small Particles-environmental behaviour and toxicity of nanomaterials and particulate matter” project. The authors would like to thank C. Carlson (Norwegian School of Veterinary Science, Oslo, Norway) and T.G. Iversen (The Norwegian Radium Hospital, Oslo, Norway) for their valuable help and advice on the size and zeta potential measurements. The work of A. El Moul (Department of Material Sciences, Centre de Recherche Public-Gabriel Lippmann, Luxembourg) for sample cutting for NanoSIMS analyses is gratefully acknowledged. We also thank V. Peardon for editing the English of the manuscript.

## References

- Abbott Chalew TE, Schwab KJ. 2013. Toxicity of commercially available engineered nanoparticles to Caco-2 and SW480 human intestinal epithelial cells. *Cell Biol. Toxicol.* 29:101–16.
- Albersen M, Bosma M, Knoers NVVAM, de Ruiter BHB, Diekman E, de Ruijter J, et al. 2013. The intestine plays a substantial role in human vitamin B6 metabolism: a Caco-2 cell model. *Plos* 8:e54113.
- Ali D, Yadav PG, Kumar S, Ali H, Alarifi S, Harrath AH. 2014. Sensitivity of freshwater pulmonate snail *Lymnaea luteola* L., to silver nanoparticles. *Chemosphere* 104:134–140.
- Anselmo HMR, van den Berg JHJ, Rietjens IMCM, Murk AJ. 2012. Inhibition of cellular efflux pumps involved in multi xenobiotic resistance (MXR) in echinoid larvae as a possible mode of action for increased ecotoxicological risk of mixtures. *Ecotoxicology* 21:2276–87.
- AshaRani P V, Low Kah Mun G, Prakash Hande M, Valiyaveetil S. 2009. Cytotoxicity and genotoxicity of silver nanoparticles in human cells. *ACS Nano* 3: 279–290.
- Audinot J-N, Senou M, Migeon H-N, Many M-C. 2008. Visualisation of thyroid hormone synthesis by ion imaging. *Appl. Surf. Sci.* 255:1185–1189.
- Averaimo S, Milton RH, Duchon MR, Mazzanti M. 2010. Chloride intracellular channel 1 (CLIC1): sensor and effector during oxidative stress. *FEBS Lett.* 584:2076–2084.
- Bailey CA, Bryla P, Malick AW. 1996. The use of the intestinal epithelial cell culture model, Caco-2, in pharmaceutical development. *Adv. Drug Deliv. Rev.* 22:85–103.
- Baranwal S, Naydenov NG, Harris G, Dugina V, Morgan KG, Chaponnier C, et al. 2012. Nonredundant roles of cytoplasmic  $\beta$ - and  $\gamma$ -actin isoforms in regulation of epithelial apical junctions. *Mol. Biol. Cell* 23:3542–3553.

- Bhattacharjee S, Opstal EJ, Alink GM, Marcelis ATM, Zuilhof H, Rietjens IMCM. 2013. Surface charge-specific interactions between polymer nanoparticles and ABC transporters in Caco-2 cells. *J. Nanoparticle Res.* 15:1695.
- Böhmert L, Niemann B, Thünemann AF, Lampen A. 2012. Cytotoxicity of peptide-coated silver nanoparticles on the human intestinal cell line Caco-2. *Arch. Toxicol.* 86:1107–15.
- Boscher A, Gobert S, Guignard C, Ziebel J, L'Hoste L, Gutleb AC, et al. 2010. Chemical contaminants in fish species from rivers in the North of Luxembourg: potential impact on the Eurasian otter (*Lutra lutra*). *Chemosphere* 78:785–792.
- Bouwmeester H, Poortman J, Peters RJ, Wijma E, Kramer E, Makama S, et al. 2011. Characterization of translocation of silver nanoparticles and effects on whole-genome gene expression using an *in vitro* intestinal epithelium coculture model. *ACS Nano* 5: 4091–4103.
- Brownlee IA, Knight J, Dettmar PW, Pearson JP. 2007. Action of reactive oxygen species on colonic mucus secretions. *Free Radic. Biol. Med.* 43:800–8.
- Brunet J, Jourdan N, Cotte-Laffitte J, Linxe C, Géniteau-Legendre M, Servin A, et al. 2000. Rotavirus infection induces cytoskeleton disorganization in human intestinal epithelial cells: implication of an increase in intracellular calcium concentration. *J. Virol.* 74:10801–10806.
- Bzowska A, Kulikowska E, Shugar D. 2001. Purine nucleoside phosphorylases: properties, functions, and clinical aspects. *Pharmacol. Ther.* 88: 349–425.
- Charrier E, Reibel S, Rogemond V, Aguera M, Thomasset N, Honnorat J. 2003. Collapsin response mediator proteins (CRMPs). *Mol. Neurobiol.* 28: 51–63.
- Chen S, Zhang M, Ma H, Saiyin H, Shen S, Xi J, et al. 2008. Oligo-microarray analysis reveals the role of cyclophilin A in drug resistance. *Cancer Chemother. Pharmacol.* 61:459–469.
- Choudhury D, Xavier PL, Chaudhari K, John R, Dasgupta AK, Pradeep T, et al. 2013. Unprecedented inhibition of tubulin polymerization directed by gold nanoparticles inducing cell cycle arrest and apoptosis. *Nanoscale* 5:4476–4489.
- Colorado State University. Pathophysiology of the digestive system. Hypertexts Biomed. Sci. Available: <http://www.vivo.colostate.edu/hbooks/pathophys/digestion/index.html> [accessed 4 February 2014].
- Cone RA. 2009. Barrier properties of mucus. *Adv. Drug Deliv. Rev.* 61:75–85.
- Downing KH, Nogales E. 1998. Tubulin structure: insights into microtubule properties and functions. *Curr. Opin. Struct. Biol.* 8: 785–791.
- Drozdowski L, Thomson ABR. 2006. Intestinal mucosal adaptation. *World J. Gastroenterol.* 12: 4614–4627.
- Fukata Y, Itoh TJ, Kimura T, Ménager C, Nishimura T, Shiromizu T, et al. 2002. CRMP-2 binds to tubulin heterodimers to promote microtubule assembly. *Nat. Cell Biol.* 4:583–591.
- Gaiser BK, Fernandes TF, Jepson MA, Lead JR, Tyler CR, Baalousha M, et al. 2012. Interspecies comparisons on the uptake and toxicity of silver and cerium dioxide nanoparticles. *Environ. Toxicol. Chem.* 31:144–54.
- Gehrke H, Frühmesser A, Pelka J, Esselen M, Hecht LL, Blank H, et al. 2013. In vitro toxicity of amorphous silica nanoparticles in human colon carcinoma cells. *Nanotoxicology* 7:274–93.
- Georgantzopoulou A, Balachandran YL, Rosenkranz P, Dusinska M, Lankoff A, Wojewodzka M, et al. 2013. Ag nanoparticles: size- and surface-dependent effects on model aquatic organisms and uptake evaluation with NanoSIMS. *Nanotoxicology* 7:1168–78.
- Gerloff K, Albrecht C, Boots AW, Förster I, Schins RPF. 2009. Cytotoxicity and oxidative DNA damage by nanoparticles in human intestinal Caco-2 cells. *Nanotoxicology* 3:355–364.

- Gerloff K, Pereira DIA, Faria N, Boots AW, Kolling J, Förster I, et al. 2013. Influence of simulated gastrointestinal conditions on particle-induced cytotoxicity and interleukin-8 regulation in differentiated and undifferentiated Caco-2 cells. *Nanotoxicology* 7:353–66.
- Ghosh JC, Dohi T, Heon Kang B, Altieri DC. 2008. Hsp60 regulation of tumor cell apoptosis. *J. Biol. Chem.* 283:5188–5194.
- Gluga AR, Skoglund S, Wallinder IO, Fadeel B, Karlsson HL. 2014. Size-dependent cytotoxicity of silver nanoparticles in human lung cells: the role of cellular uptake, agglomeration and Ag release. *Part. Fibre Toxicol.* 11:11.
- Grès M-C, Julian B, Bourrié M, Meunier V, Roques C, Berger M, et al. 1998. Correlation between oral drug absorption in humans, and apparent drug permeability in TC-7 cells, a human epithelial intestinal cell line: comparison with the parental Caco-2 cell line. *Pharm. Res.* 15: 726–733.
- Gudas L, Ullman B, Cohen A, Martin Jr D. 1978. Deoxyguanosine toxicity in a mouse T lymphoma: relationship to purine nucleoside phosphorylase-associated immune dysfunction. *Cell* 14: 531–538.
- Gutleb AC, Freitas J, Murk AJ, Verhaegen S, Ropstad E, Udelhoven T, et al. 2012. NanoSIMS50- a powerful tool to elucidate cellular localization of halogenated organic compounds. *Anal. Bioanal. Chem.* 404:2693–2698.
- Hayes JD, Flanagan JU, Jowsey IR. 2005. Glutathione transferases. *Annu. Rev. Pharmacol. Toxicol.* 45:51–88.
- Herzog A, Kuntz S, Daniel H, Wenzel U. 2004. Identification of biomarkers for the initiation of apoptosis in human preneoplastic colonocytes by proteome analysis. *Int. J. cancer* 109:220–229.
- Hilgendorf C, Spahn-Langguth H, Regårdh CG, Lipka E, Amidon GL, Langguth P. 2000. Caco-2 versus Caco-2/HT29-MTX co-cultured cell lines: permeabilities via diffusion, inside- and outside-directed carrier-mediated transport. *J. Pharm. Sci.* 89:63–75.
- Imai T, Imoto M, Sakamoto H, Hashimoto M. 2005. Identification of esterases expressed in Caco-2 cells and effects of their hydrolyzing activity in predicting human intestinal absorption. *Drug Metab. Dispos.* 33:1185–1190.
- Jin F, Welch R, Glahn R. 2006. Moving toward a more physiological model: application of mucin to refine the *in vitro* digestion/Caco-2 cell culture system. *J. Agric. Food Chem.* 54:8962–7.
- Ko KM, Lee W, Yu J-R, Ahnn J. 2007. PYP-1, inorganic pyrophosphatase, is required for larval development and intestinal function in *C. elegans*. *FEBS Lett.* 581:5445–5453.
- Kruszewski M, Brzoska K, Brunborg G, Asare N, Dobrzynska M, Dusinska M, et al. 2011. Toxicity of silver nanomaterials in higher eukaryotes. In *Advances in Molecular Toxicology*, Vol. 5 of, pp. 179–218, Elsevier B.V.
- Kruszewski M, Grądzka I, Bartłomiejczyk T, Chwastowska J, Sommer S, Grzelak A, et al. 2013. Oxidative DNA damage corresponds to the long term survival of human cells treated with silver nanoparticles. *Toxicol. Lett.* 219:151–9.
- Ku N-O, Zhou X, Toivola D, Omary BM. 1999. The cytoskeleton of digestive epithelia in health and disease. *Am. J. Physiol. Gastrointest. Liver Physiol.* 277: G1108–1137.
- Lankoff A, Sandberg WJ, Wegierek-ciuk A, Lisowska H, Refsnes M, Schwarze PE, et al. 2012. The effect of agglomeration state of silver and titanium dioxide nanoparticles on cellular response of HepG2, A549 and THP-1 cells. *Toxicol. Lett.* 208:197–213.
- Larhed A, Artursson P, Björk E. 1998. The influence of intestinal mucus components on the diffusion of drugs. *Pharm. Res.* 15: 66–71.
- Lasserre J-P, Fack F, Serchi T, Revets D, Planchon S, Renaut J, et al. 2012. Atrazine and PCB 153 and their effects on the proteome of subcellular fractions of human MCF-7 cells. *Biochim. Biophys. Acta* 1824:833–41.

- Lawrence SM, Huddleston KA, Pitts LR, Nguyen N, Lee YC, Vann WF, et al. 2000. Cloning and expression of the human N-acetylneuraminic acid phosphate synthase gene with 2-keto-3-deoxy-D- glycero-D-galactononic acid biosynthetic ability. *J. Biol. Chem.* 275:17869–17877.
- Lesuffleur T, Barbat A, Dussaulx E, Zweibaum A. 1990. Growth adaptation to methotrexate of HT-29 human colon carcinoma cells is associated with their ability to differentiate into columnar absorptive and mucus-secreting cells. *Cancer Res.* 50: 6334–43.
- Levy E, Ménard D, Delvin E, Montoudis A, Beaulieu J-F, Mailhot G, et al. 2009. Localization, function and regulation of the two intestinal fatty acid-binding protein types. *Histochem. Cell Biol.* 132:351–367.
- Lim D, Jang J, Kim S, Kang T, Lee K, Choi I. 2012. The effects of sub-lethal concentrations of silver nanoparticles on inflammatory and stress genes in human macrophages using cDNA microarray analysis. *Biomaterials* 33:4690–4699.
- Ma P-F, Chen J-Q, Wang Z, Liu J-L, Li B-P. 2012. Function of chloride intracellular channel 1 in gastric cancer cells. *World J. Gastroenterol.* 18:3070–3080.
- Mahler GJ, Shuler ML, Glahn RP. 2009. Characterization of Caco-2 and HT29-MTX cocultures in an *in vitro* digestion/cell culture model used to predict iron bioavailability. *J. Nutr. Biochem.* 20:494–502.
- Manevich Y, Fisher AB. 2005. Peroxiredoxin 6, a 1-Cys peroxiredoxin, functions in antioxidant defense and lung phospholipid metabolism. *Free Radic. Biol. Med.* 38:1422–1432.
- Massey D, Traverso V, Rigal A, Maroux S. 1991. Cellular and subcellular localization of annexin IV in rabbit intestinal epithelium, pancreas and liver. *Biol. Cell* 73: 151–156.
- Mayer MP, Bukau B. 2005. Hsp70 chaperones : cellular functions and molecular mechanism. *Cell. Mol. Life Sci.* 62:670–684.
- Moll R, Divo M, Langbein L. 2008. The human keratins: biology and pathology. *Histochem. Cell Biol.* 129:705–33.
- Nakamura J, Aoyagi S, Nanchi I, Nakatsuka S, Hirata E, Shibata S, et al. 2009. Overexpression of eukaryotic elongation factor eEF2 in gastrointestinal cancers and its involvement in G2/M progression in the cell cycle. *Int. J. Oncol.* 34:1181–1189.
- Nigro P, Pompilio G, Capogrossi MC. 2013. Cyclophilin A: a key player for human disease. *cell death Dis.* 4:e888.
- Odunuga OO, Longshaw VM, Blatch GL. 2004. Hop: more than an Hsp70/Hsp90 adaptor protein. *BioEssays* 26:1058–1068.
- Papinazath T, Min W, Sujiththa S, Cohen A, Ackerley C, Roifman C, et al. 2011. Effects of purine nucleoside phosphorylase deficiency on thymocyte development. *J. Allergy Clin. Immunol.* 128:854–863.e1.
- Pasquali M, Serchi T, Renaut J, Hoffmann L, Bohn T. 2013. 2D difference gel electrophoresis reference map of a *Fusarium graminearum* nivalenol producing strain. *Electrophoresis* 34:505–9.
- Pelsers MMAL, Namiot Z, Kisielewski W, Namiot A, Januszkiewicz M, Hermens WT, et al. 2003. Intestinal-type and liver-type fatty acid-binding protein in the intestine. Tissue distribution and clinical utility. *Clin. Biochem.* 36:529–535.
- Piret J-P, Vankoningsloo S, Mejia J, Noël F, Boilan E, Lambinon F, et al. 2012. Differential toxicity of copper (II) oxide nanoparticles of similar hydrodynamic diameter on human differentiated intestinal Caco-2 cell monolayers is correlated in part to copper release and shape. *Nanotoxicology* 6:789–803.
- Pontier C, Pachot J, Botham R, Lenfant B, Arnaud P. 2001. HT29-MTX and Caco-2/TC7 monolayers as predictive models for human intestinal absorption: role of the mucus layer. *J. Pharm. Sci.* 90: 1608–19.
- Schauer R. 1985. Sialic acids and their role as biological masks. *Trends Biochem. Sci.* 10: 357–360.

- Singh H, Cousin MA, Ashley RH. 2007. Functional reconstitution of mammalian “chloride intracellular channels” CLIC1, CLIC4 and CLIC5 reveals differential regulation by cytoskeletal actin. *FEBS J.* 274:6306–6316.
- Spielberg S, Gordon G. 1981. Glutathione synthetase-deficient lymphocytes and acetaminophen toxicity. *Clin. Pharmacol. Ther.* 29: 51–55.
- Stepkowski TM, Brzóska K, Kruszewski M. 2014. Silver nanoparticles induced changes in the expression of NF- $\kappa$ B related genes are cell type specific and related to the basal activity of NF- $\kappa$ B. *Toxicol. Vitro.* 28:473–478.
- Sun S, Wang Q, Giang A, Cheng C, Soo C, Wang C-Y, et al. 2011. Knockdown of CypA inhibits interleukin-8 (IL-8) and IL-8-mediated proliferation and tumor growth of glioblastoma cells through down-regulated NF- $\kappa$ B. *J. Neurooncol.* 101:1–14.
- Takada M, Otaka M, Takahashi T, Izumi Y, Tamaki K, Shibuya T. 2010. Overexpression of a 60-kDa heat shock protein enhances cytoprotective function of small intestinal epithelial cells. *Life Sci.* 86:499–504.
- Triboulet S, Aude-garcia C, Carriere M, Diemer H, Proamer F, Habert A, et al. 2013. Molecular responses of mouse macrophages to copper and copper oxide nanoparticles inferred from proteomic analyses. *Mol. Cell. proteomics* 12:3108–3122.
- Tsyusko OV, Hardas SS, Shoultz-Wilson WA, Starnes CP, Joice G, Butterfield DA, et al. 2012. Short-term molecular-level effects of silver nanoparticle exposure on the earthworm, *Eisenia fetida*. *Environ. Pollut.* 171:249–255.
- Turano C, Gaucci E, Grillo C, Chichiarelli S. 2011. ERp57/GRP58: a protein with multiple functions. *Cell. Mol. Biol. Lett.* 16:539–563.
- Ulmasov B, Bruno J, Woost PG, Edwards JC. 2007. Tissue and subcellular distribution of CLIC1. *BMC Cell Biol.* 8.
- Vannini C, Domingo G, Onelli E, Prinsi B, Marsoni M, Espen L, et al. 2013. Morphological and proteomic responses of *Eruca sativa* exposed to silver nanoparticles or silver nitrate. *PLoS One* 8:e68752.
- Varki A. 2008. Sialic acids in human health and disease. *Trends Mol. Med.* 14:351–60.
- Verano-Braga T, Miethling-Graff R, Wojdyla K, Rogowska-Wrzesinska A, Brewer JR, Erdmann H, et al. 2014. Insights into the cellular response triggered by silver nanoparticles using quantitative proteomics. *ACS Nano* 8: 2161–2175.
- Walter E, Janich S, Roessler BJ, Hilfinger JM, Amidon GL. 1996. HT29-MTX/Caco-2 cocultures as an *in vitro* model for the intestinal epithelium: *in vitro-in vivo* correlation with permeability data from rats and humans. *J. Pharm. Sci.* 85:1070–6.
- Wang L, Srinivasan S, Theiss AL, Merlin D, Sitaraman S V. 2007. Interleukin-6 induces keratin expression in intestinal epithelial cells. Potential role of keratin-8 in interleukin-6-induced barrier function alterations. *J. Biol. Chem.* 282.
- Wang Y, George SP, Srinivasan K, Patnaik S, Khurana S. 2012a. Actin reorganization as the molecular basis for the regulation of apoptosis in gastrointestinal epithelial cells. *Cell Death Differ.* 19:1514–1524.
- Wang Y, Srinivasan K, Siddiqui MR, George SP, Tomar A, Khurana S. 2008. A novel role for villin in intestinal epithelial cell survival and homeostasis. *J. Biol. Chem.* 283:9454–9464.
- Wang Z, Cheng Y, Wang N, Wang D, Li Y, Han F, et al. 2012b. Dioscin induces cancer cell apoptosis through elevated oxidative stress mediated by downregulation of peroxiredoxins. *Cancer Biol. Ther.* 13: 138–147.
- Weinman JS, Feinberg JM, Rainteau DP, Gaspera B Della, Weinman SJ. 1994. Annexins in rat enterocyte and hepatocyte: an immunogold electron-microscope study. *Cell Tissue Res.* 278: 389–397.
- Weiske J, Huber O. 2006. The histidine triad protein Hint1 triggers apoptosis independent of its enzymatic activity. *J. Biol. Chem.* 281:27356–27366.

- Weng Y, Cui Y, Fang J. 2012. Biological functions of cytokeratin 18 in cancer. *Mol. cancer Res.* 10:485–493.
- Wikman A, Karlsson J, Carlstedt I, Artursson P. 1993. A drug absorption model based on the mucus layer producing human intestinal goblet cell line HT29-H. *Pharm. Res.* 10: 843–52.
- Yuan H, Chen C, Chai G, Du Y, Hu F. 2013. Improved transport and absorption through gastrointestinal tract by PEGylated solid lipid nanoparticles. *Mol. Pharm.* 10: 1865–1873.
- Yusuf S, Nok AJ, Ameh DA, Adelaiye AB, Balogun EO. 2005. Correlation of gastric mucosal damage with sialic acid profile in rats: effect of hydrochloric acid , pepsin and hypertonic saline. *cell Biochem. Funct.* 23: 339–345.
- Zhang H, Forman HJ. 2012. Glutathione synthesis and its role in redox signaling. *Semin. Cell Dev. Biol.* 23:722–728.

## Supporting Information for Chapter 2

### Cell monolayer integrity evaluation: transepithelial electrical resistance (TEER)

Caco-2/TC7, HT29-MTX cells and cells in co-culture at a ratio of 90:10 (Caco-2/TC7:HT29:MTX) were seeded onto polycarbonate 0.4  $\mu\text{M}$  pore size 12-well hanging trans-well inserts at an initial concentration of  $1.2 \times 10^5$  cells/mL (0.5 mL/insert) and cultured for 14 days. The medium was changed every other day in the apical (0.5 mL) and the basolateral (1.5 mL) compartment. The integrity of the monolayer was monitored using an epithelial volt-ohmmeter fitted with planar electrodes (Millipore, MILLICELL<sup>®</sup>-ERS) during the medium change. At the end of the growth period, fresh growth medium containing the Ag NPs 20 nm, 200 nm or AgNO<sub>3</sub> was added to the apical compartment of each insert. After a 24-hour exposure to the TEER of the monolayers were measured.

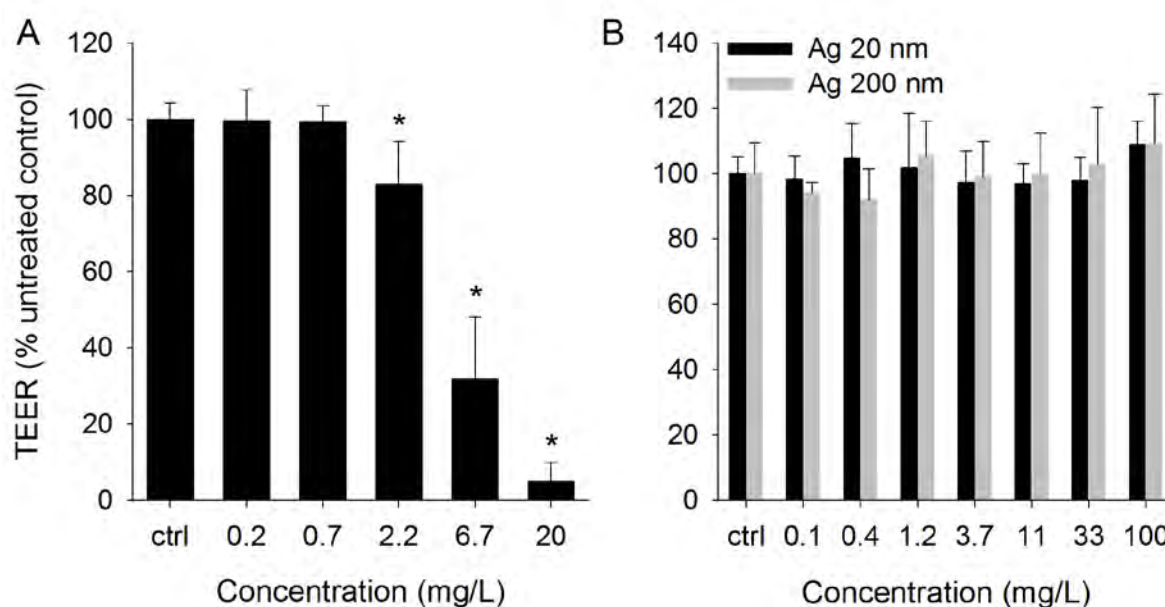


**Figure S1.** Effects of (A) AgNO<sub>3</sub> and (B) Ag NPs 20 and 200 nm on the trans-epithelial resistance (TEER) expressed as percentage of untreated control. Differentiated cells (after 14 days of culture) were exposed for 24 hours. Error bars represent the mean  $\pm$  SD of 2 independent experiments performed in triplicate. Significant differences from respective untreated controls are marked with asterisks (\* for  $P < 0.05$ ).

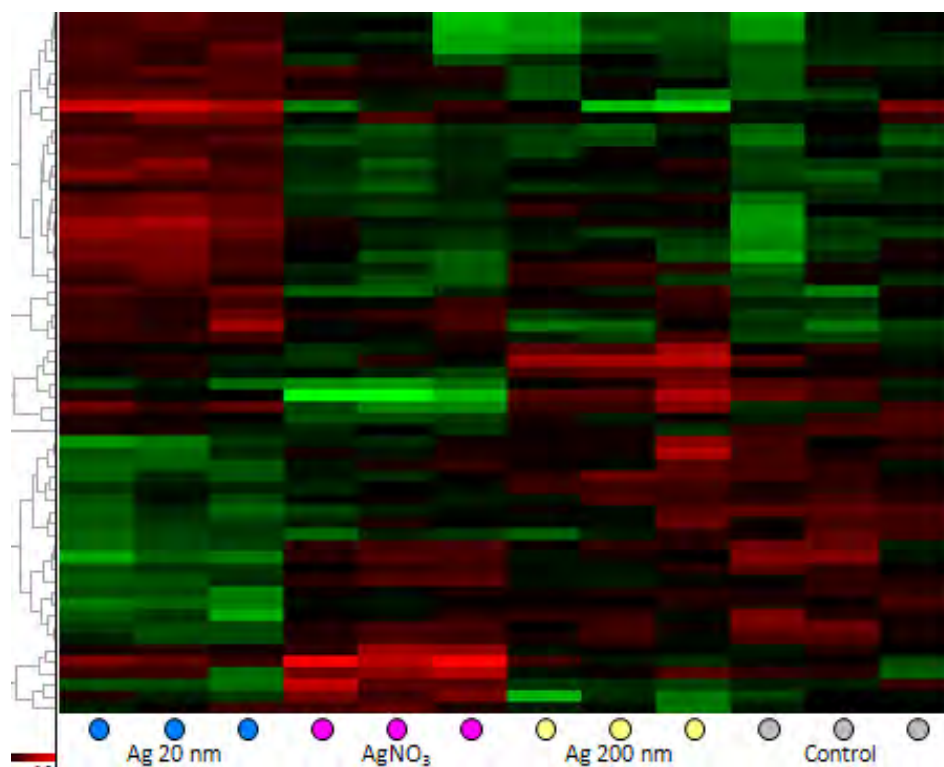


**Figure S2.** Hierarchical clustering of differentially expressed proteins in Caco-2/TC7:HT29-MTX cells in 90:10 co-culture exposed to 1mg/L of Ag NPs 20 nm, 200 nm or AgNO<sub>3</sub> for 24 hours.

**Table S1.** For each identified protein UniProt Accession number, UniProt ID, NCBI accession number, percentage of sequence coverage, cumulative MOWSE score with corresponding p-value, number of queries matched, theoretical molecular mass and isoelectric points are reported (Table S1.xls).

# Chapter 3

## Ag nanoparticles: size- and surface-dependent effects on model aquatic organisms and uptake evaluation with NanoSIMS

Anastasia Georgantzopoulou, Yekkuni L. Balachandran, Philipp Rosenkranz, Maria Dusinska, Anna Lankoff, Maria Wojewodzka, Marcin Kruszewski, Cédric Guignard, Jean-Nicolas Audinot, Shanmugam Girija, Lucien Hoffmann, & Arno C. Gutleb

*Nanotoxicology* 2013; 7(7): 1168-1178

DOI: 10.3109/17435390.2012.715312

### **Abstract**

This study aims to assess the effects of Ag particles synthesized by a chemical (Ag 20, 200 nm) and biological method (Ag 23, 27 nm) in aquatic organisms: the bacterium *Vibrio fischeri*, the alga *Desmodesmus subspicatus* and the crustacean *Daphnia magna*. Ag particles exerted toxic effects in all organisms studied with Ag particles 23 nm being the most potent. Although soluble Ag was released in all media, the differences between the tested Ag particles still cannot be explained solely based on soluble Ag. NanoSIMS analysis performed with *D. magna* showed that apart from their localization in the gut lumen, Ag 200 nm and Ag NPs 23 nm seemed to pass through the epithelial barrier as well. Ag NPs 23 nm localized in specific areas seemed to be within the ovaries. This study strengthens the argument that size, method of synthesis as well as surface chemistry may affect the uptake and toxic effects of Ag NPs.

## Introduction

There is no doubt that nanotechnology is very promising having hundreds of applications, from electronics, medicine and environmental remediation to personal care products, food industry and agriculture (Ju-Nam and Lead 2008; Nair et al. 2010; Perez-de-Luque and Rubiales 2009). Although nanoparticles (NPs, particles with all dimensions less than 100 nm) have been naturally occurring in the environment through forest fires, volcano eruptions, soil erosion, etc. (Handy et al. 2008; Wiesner et al. 2009), man-made NPs are unique in that their surface and size can be manipulated providing them with novel properties and enhanced reactivity that do not exist in the larger scale.

Among the NPs currently used, nano-silver is by far the most frequently employed in consumer products. Nano silver (Ag NPs) has found many applications in food packaging, sports clothing and equipment, home cleaning disinfectants, wound dressings, cosmetics, etc. due to its broad spectrum antimicrobial properties (Ju-Nam and Lead 2008; Woodrow Wilson International Center for Scholars 2014).

The large scale of manufacture and potential release in the environment during the life cycle of a product, e.g. release of Ag particles during washing of Ag NP incorporated textiles (Benn and Westerhoff 2008; Benn et al. 2010; Geranio et al. 2009), raise concerns on safety and potential effects on humans, animals and environment (Som et al. 2010). The number of studies on the effects of Ag nanoparticles on living systems, although still limited, has increased rapidly within the past few years (Kruszewski et al. 2011) and there is already evidence for size-dependent effects (Hartmann et al. 2010; Hund-Rinke and Simon 2006; Roh et al. 2010). Ag NPs were found to induce oxidative stress, DNA damage and apoptosis in *Drosophila melanogaster* (Ahamed et al. 2010) as well as developmental, reproductive and genotoxic effects in *Chironomus riparius* (Nair et al. 2011). The green alga *Chlamydomonas reinhardtii* exposed to Ag NPs showed a decrease in photosynthesis activity that could not be fully attributed to free Ag ions (Navarro et al. 2008). In addition, a study using the plant *Lolium multiflorum* has shown that the reduced growth and altered root morphology was due to the particulate form of Ag (Yin et al. 2011). However, there is still a big knowledge gap with the mechanism of action, behavior and fate of NPs in the environment being far from understood (Ju-Nam and Lead 2008; Kruszewski et al. 2011).

One step towards understanding the NPs' adverse effects is by investigating their potential of being accumulated and distributed in tissues which is normally done by

transmission electron microscopy (TEM) (Heinlaan et al. 2011; Lovern et al. 2008). However, as direct elemental information cannot be obtained, identification of NPs is ambiguous (Brandenberger et al. 2010). In the present study, we have used the latest generation of Secondary Ion Mass Spectrometry instruments, the NanoSIMS 50 (CAMECA, France), which scans the object surface with a 50–100 nm primary Cs<sup>+</sup> beam. NanoSIMS could provide an additional powerful tool for NPs visualization and intracellular localization due to its high sensitivity and high lateral resolution (Eybe et al. 2008), thus giving the potential of further understanding the differences in toxicity.

The aim of the present study was to assess the ecotoxicological effects of Ag NPs for which the potential exposure is expected to be very high (Wijnhoven et al. 2009). Chemically synthesized Ag particles of different sizes (20 and 200 nm) were used to get insight into the relation between size and toxicity, as well as AgNO<sub>3</sub> in order to account for the ionic form of Ag that may leach out from the NPs. In addition, Ag NPs synthesized by *Azadirachta indica* (Ag 27 nm) (Balachandran et al. 2012) and *Ocimum sanctum* (Ag 23 nm) plant leaf extracts were used to evaluate whether effects are dependent on the surface coating. The bacterium *Vibrio fischeri* was used in the standard inhibition of bioluminescence assay as a fast and high-throughput prescreening tool for the toxicity assessment of the selected Ag nanoparticles. Representatives of different trophic levels (the alga *Desmodesmus subspicatus* and the crustacean *Daphnia magna*) were selected, as they are model organisms in toxicity tests. Furthermore, NanoSIMS was used as a novel approach to assess the potential of *Daphnia magna* to ingest NPs and to visualize the uptake and localization of particles in the gut or show possible translocation across the gastrointestinal tract (GIT).

## **Organisms, materials and methods**

### *Particles and Chemicals*

Characterized Ag particles (20 and 200 nm) were obtained from PlasmaChem GmbH (Berlin, Germany) (Supporting Information, Figures S1, S2, S3). *Azadirachta indica* (Ag NPs 27 nm) and *Ocimum sanctum* (Ag NPs 23 nm) plant leaf extract synthesized Ag NPs were characterized and provided by the Department of Biotechnology, Barathiar University, India (Supporting Information, Figures S1, S2, S3, S4, Table S1). Potassium dichromate (K<sub>2</sub>Cr<sub>2</sub>O<sub>7</sub>, CAS no. 7778-50-9) and silver nitrate (AgNO<sub>3</sub>, CAS no. 8012-12-2) were purchased from VWR (Leuven, Belgium), and 3,5-dichlorophenol (CAS no. 591-35-5), osmium tetroxide (OsO<sub>4</sub>, CAS

no. 20816-12-0), glutaraldehyde (CAS no. 111-30-8) and the epoxy resin embedding kit from Sigma Aldrich (Bornem, Belgium). Phosphate buffer saline (PBS) and heat-inactivated fetal bovine serum (FBS) were both obtained from Invitrogen (Merelbeke, Belgium).

#### *Particles dispersion protocols*

*Ag 20 and Ag 200 nm.* Two milligrams of the particles were weighed and 1mL of 5% DMSO in Milli-Q water (Millipak Express, Millipore) was added. Then the solution was sonicated (cycle 1) on ice for 3 min using a UP200S probe ultra sonicator (Hielscher, Germany). Stocks were always prepared fresh before each experiment. This dispersion protocol was adapted from the one used in the PNRF122 project (<http://www.pnrf122.org>) (Lankoff et al. 2012), to enable the comparison of results.

*Ag NPs 23 nm and 27 nm.* The NPs were provided as stocks in MilliQ water and stored at 4°C in glass vials. Before use the vials were gently vortexed and no further sonication step was included.

#### *Particle physical characterization in exposure media*

Dynamic light scattering and zeta ( $\zeta$ ) potential measurements of NPs in solution were performed with a nanoZetasizer (Malvern Instruments Ltd, UK). The stocks were added to 2% NaCl, NBBM medium and Volvic water in order to achieve the highest concentration at which the organisms were exposed.

#### *Vibrio fischeri inhibition of luminescence assay*

The assay is an adaptation of the ISO standard (International Organisation for Standardization (ISO 11348-1) 1999) in a 96-well plate format (Hamers et al. 2001; Macova et al. 2010). *V. fischeri* (DSMZ, Germany) culture conditions were the same as in the guideline. Briefly, bacterial stock in 10% glycerol was stored in -80°C. After thawing, activation solution was added to the bacterial suspension which was further diluted in 2% NaCl. Fifty microliters of the diluted bacterial suspension was added in the wells of a 96-well plate. Test compounds were serially diluted in 2% NaCl (isotonic solution) and 100  $\mu$ L of appropriate concentration was added in order to reach final concentrations of 0.1–300 mg/L Ag 20 nm and 200 nm, 0.05–100 mg/L Ag NPs 23 nm and Ag NPs 27 nm and 0.05–7 mg/L AgNO<sub>3</sub>. Diluent (2% NaCl) as well as diluent with the maximum concentration of the carrier solvent (0.75 % MilliQ water or

DMSO) were used as controls. After a 30-min incubation, the ability of the bacteria to produce light was measured with the use of a luminometer (Synergy 2, BioTek Instruments, Inc.). For every treatment and control, three replicates were measured.

#### *Desmodesmus subspicatus* 72-h growth inhibition assay

The growth inhibition test was performed with the green algal species *Desmodesmus subspicatus* (SAG 86.81, CCALA, Czech Republic). The test is a modification of the ISO standard (International Organisation for Standardization (ISO 8692) 2004) in a 12-well plate format. A pre-culture of algae was started 3 days before the beginning of the experiment and algae in exponential growth phase were used. The NBBM algal medium (Andersen et al. 2005) was used in order to prepare the test concentrations, which were inoculated with exponentially growing algae in a concentration of  $10^4$  cells/mL. 1.5 mL of algae with or without the different particles and AgNO<sub>3</sub> at increasing concentrations (Ag NPs 20 nm and Ag 200 nm: 0.003–10 mg/L, Ag NPs 23 nm: 0.0003–1 mg/L, Ag NPs 27 nm: 0.003–10 mg/L and AgNO<sub>3</sub>: 0.0046–0.4 mg/L) were placed in the wells of 12-well plates and were continuously shaken at 50 rpm (Gerhardt Analytical Systems, Germany) under a cool white fluorescent light ( $46.2 \mu\text{mol m}^{-2} \text{s}^{-1}$ ) and temperature  $20 \pm 1^\circ\text{C}$ . *D. subspicatus* suspension with the highest concentration of the carrier solvent (0.025% DMSO of MilliQ water) was used as control. Three replicates per concentration and for the control were used. After 72 h the cell concentration was determined manually in a Bürker-Türk haemocytometer. Growth rates were calculated as indicated in the guideline and the results were expressed as % inhibition of growth rate relative to untreated control. The tests were in accordance to validity criteria with a mean control growth rate of  $1.68 \text{ d}^{-1}$  and an EC50 for the positive control potassium dichromate of 0.7 mg/L.

#### *Daphnia magna* immobilization assay

The assay is a modification of the OECD 202 guideline (Organisation for Economic Co-operation and Development (OECD) 2004). Dormant eggs (ephippia) of *Daphnia magna* were obtained from MicroBioTests Inc. (Belgium). Eggs were incubated in Petri dishes containing the natural mineral water Volvic (Source Clairvic, Société des Eaux de Volvic, France) for 4 days at  $21^\circ\text{C}$  under continuous light. Once hatched the daphnids were fed for 2 h with the green alga *Desmodesmus subspicatus*. Daphnids less than 24 h old were transferred in the wells of a six-well plate. The final volume of each well was 10 mL (Volvic water  $\pm$  increasing

concentrations of particles). All tests were conducted at  $20 \pm 1^\circ\text{C}$  under a 16 h:8 h light: dark photoperiod. For every concentration or control (water with highest concentration of carrier solvent: 0.025% DMSO or MilliQ water) four replicates were used (five animals per replicate). The daphnids were exposed to particles and  $\text{AgNO}_3$  (serially diluted in Volvic water, Ag NPs 20 nm: 0.0001–10 mg/L, Ag 200 nm: 0.01–3 mg/L, Ag NPs 23 nm: 0.0015–10  $\mu\text{g/L}$ , Ag NPs 27 nm: 0.0015–0.35 mg/L,  $\text{AgNO}_3$ : 0.041–10  $\mu\text{g/L}$ ) for 48 h and their ability to swim was evaluated at the end of the exposure period. Animals that would not respond after gentle agitation were considered as immobilized. In all tests immobilization in control was lower than 10%, which was in accordance with the validity criteria.

#### *Total dissolved Ag release over time in different media (Ultrafiltration and ICP-MS)*

It is important to assess the amount of soluble Ag ionic species released from the Ag particles in the different media during exposure. Therefore, 2 mL of exposure medium (medium + Ag particles at the highest working concentration or only medium in the absence of organisms) from the different assays was taken at different time points ( $t = 0.5, 6, 24, 48$  and  $72$  h depending on the duration of the exposure of the test organism) and were centrifuged for 40 min at 4000 g using centrifugal filter devices (Amicon ultra-4, Millipore, Ireland) with 3 kDa cut-off. The ultrafiltrates were evaluated for the total dissolved Ag content with Inductively Coupled Plasma Mass Spectrometry (ICP-MS) (Elan DRC-e, Perkin Elmer, Waltham, MA, USA) as previously described (Boscher et al. 2010). In addition, the stock solutions of all Ag particles were analyzed with ICP-MS for the presence of the metals chromium (Cr), manganese (Mn), iron (Fe), cobalt (Co), nickel (Ni), copper (Cu), zinc (Zn), arsenic (As), cadmium (Cd) and lead (Pb).

#### *Particle uptake in daphnids - NanoSIMS analysis*

*Sample preparation.* The daphnids exposed to 0.1 mg/L Ag NPs 20 nm or Ag 200 nm, 0.001 mg/L Ag 23 nm and 0.004 mg/L Ag 27 nm (concentrations corresponding close to EC50 or lower) for 48 h were embedded in 1% agar. After agar solidification (5 min) they were cut into small cubes as described earlier (Eybe et al. 2008). The first fixation was done with 5% glutaraldehyde in PBS overnight. Glutaraldehyde was removed and the cubes were washed in pure PBS. They were then postfixated with 1% osmium tetroxide in water for 2 h. After an additional washing step with PBS and dehydration with five increasing acetone concentrations

(30%, 50%, 70%, 90% and 100% acetone), the blocks with the daphnids were embedded in epoxy resin (Epon 812 substitute). The samples were cut to 300 nm semi-thin sections (Leica ultracut UCT, Le Pecq Cedex, France) and placed on silicon wafers (Siltronix, Archamps, France) for NanoSIMS 50 analysis.

*NanoSIMS analysis.* Samples were analysed with a NanoSIMS 50 (Cameca, Courbevoie, France) using a Cs<sup>+</sup> primary source (8 keV), rasterizing the surface of the sample (-8 keV) with a raster between 40 x 40 μm and 20 x 20 μm to generate secondary negative ions. The energy of the impact of the primary beam was 16 keV with an intensity range of 1.0-0.8 pA. In these conditions the probe-working diameter was in the range 80-100 nm. The masses studied simultaneously in multicollection mode were: <sup>12</sup>C<sup>14</sup>N<sup>-</sup> (m = 26.00307), <sup>31</sup>P<sup>-</sup> (30.97376), <sup>34</sup>S<sup>-</sup> (m = 33.96786), <sup>107</sup>Ag<sup>-</sup> (106.90486) and <sup>107</sup>Ag<sup>16</sup>O<sup>-</sup> (m = 124.8996). Here, only <sup>12</sup>C<sup>14</sup>N<sup>-</sup> and NPs images are represented. The <sup>12</sup>C<sup>14</sup>N<sup>-</sup> image allows us to recognize the essential anatomical features and gives a very similar image to that obtained with light microscopy (Audinot et al. 2008). Images were recorded in a pixel format of 256 x 256 image points with a counting time of 20 ms per pixel.

#### *Statistical analysis*

The data are expressed as mean values with standard deviations of at least two independent experiments each containing three or four replicates. Dose-response curves and EC50 were obtained with SigmaPLOT 7.101 (SPSS Inc. SigmaPlot for Windows) using a logistic four- parameter model.

## Results

### *Particle characterization in media*

The estimated hydrodynamic size of the particles at the time of exposure is much larger than their nominal size (Table 1, Figure 1).

**Table 1.** Hydrodynamic size and z potential determination of the different Ag particles in the exposure media used in the different assays as obtained with the nanoZetasizer (Malvern Instruments Ltd, UK).

	Ag 20	Ag 200	Ag 23	Ag 27
Primary Size (nm)	20	200	23	27
Surface area (m <sup>2</sup> /g)	2.2419	2.9345	8.1757	2.2232
Hydrodynamic diameter in 2% NaCl (nm)	504.9	424	1372	224
Concentration (mg/L)	300	300	100	100
Hydrodynamic diameter in NBBM (nm)	199.9	265	220.9	79.2
Concentration (mg/L)	10	10	1	10
Hydrodynamic diameter in Volvic (nm)	198.9	259.1	577.6	75.9
Concentration (mg/L)	10	10	0.01	0.35
ζ potential in 2% NaCl (mV)	-11	-12.65	-10.845	-13.5
ζ potential in NBBM (mV)	-20	-22	-16.45	-21.1
ζ potential in Volvic (mV)	-14.2	-19.8	-12.3	-20.05

2% NaCl, isotonic solution for the bacterium *V. fischeri*; NBBM, algal medium; Volvic, water used for the *D. magna* immobilisation assay; Stocks were prepared as described in material and methods and added to the different media in order to reach the highest concentration at which the organisms were exposed.

Aggregation was seen for all types of Ag particles in all the media that were used in the assays with the highest levels of aggregation being observed when 2% NaCl was used as a diluent and exposure medium (Figure 1). Ag NPs 27 nm (*A. indica* synthesized) were shown to have the smallest size of all particles in the NBBM medium and water (average size of 76–79 nm). In addition, the z potential of the particles dispersed in 2% NaCl showed low negative values suggesting a decreased electrostatic repulsion (Table 1).

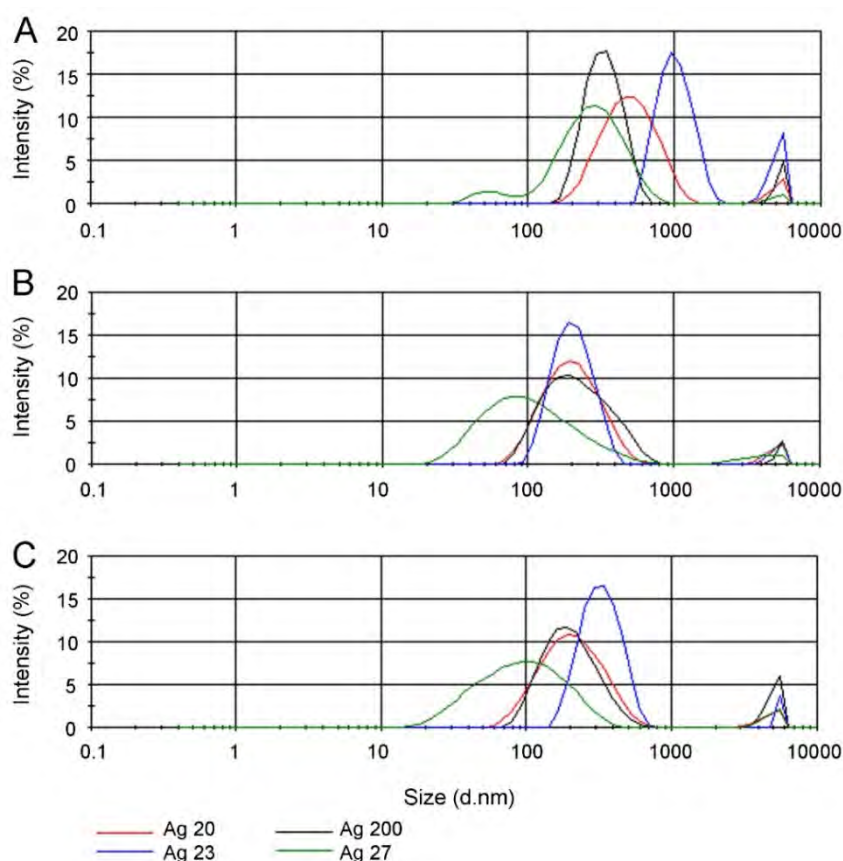


**Figure 1.** Particle size distribution of Ag particles in (A) 2%NaCl solution, (B) NBBM medium and (C) Volvic water used for the toxicological assays. Stocks were prepared as described in Organisms, materials and methods and added to the different media in order to reach the highest concentration at which the organisms were exposed. The measurements were performed with a nanoZetasizer (Malvern Instruments Ltd, UK). Data are presented as % intensity of light scattered.

### *Vibrio fischeri* luminescence assay

Luminescence-inhibiting effects were observed when *Vibrio fischeri* was exposed to Ag particles (Figure 2). Although Ag 20 nm and 200 nm were tested at high concentrations (0.05-300 mg/L) no full dose–response curves could be obtained. However, EC50 could be calculated that were 182 and 458.9 mg/L for Ag 20 and 200 nm, respectively (Table 2). Ag 23 nm was the most toxic of all Ag NPs with an EC50 of 0.42 mg/L.

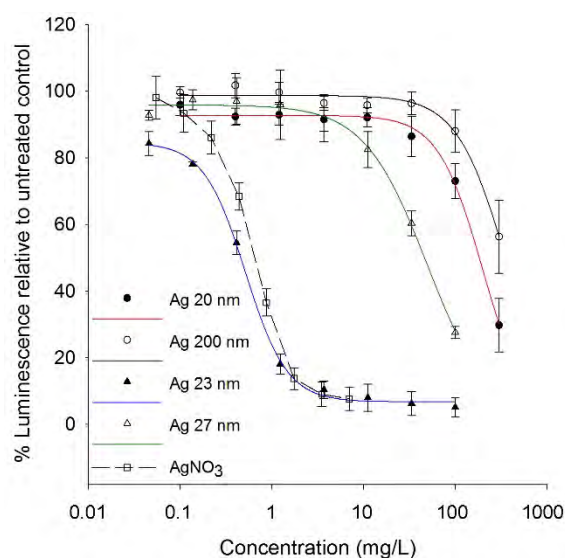


**Figure 2.** Dose–response curves obtained in the *Vibrio fischeri* luminescence assay after exposure of the bacteria to increasing doses of AgNO<sub>3</sub> and Ag particles 20, 200 nm, Ag 23 nm (*Ocimum sanctum* leaf extract), Ag 27 nm (*Azadirachta indica* leaf extract). The assay was performed in 96-well plates and decrease in luminescence upon exposure to the compounds was assessed after 30 min. Error bars represent the mean with standard deviation of two independent experiments.

#### *Desmodium subspicatus* 72-h growth inhibition assay

Dose-dependent effects of all Ag particles on algal growth were observed (Figure 3). Amongst the particles tested Ag 23 nm was the most potent (EC<sub>50</sub> = 0.034 mg/L) followed by Ag 27 nm, Ag 20 nm and Ag 200 nm (Table 2). A full dose response could not be obtained for Ag 200 nm despite the high concentrations used (0.01–100 mg/L).

**Table 2.** EC<sub>10</sub> and EC<sub>50</sub> (mg/L, with the 95% confidence intervals between parentheses) obtained from the toxicity tests using the organisms *V. fischeri*, *D. subspicatus* and *D. magna* upon exposure to Ag 20, Ag 200, Ag 23 (*Ocimum sanctum* leaf extract) and Ag 27 nm (*Azadirachta indica* leaf extract) particles.

Particle	<i>V. fischeri</i>		<i>D. subspicatus</i>		<i>D. magna</i>	
	EC <sub>10</sub>	EC <sub>50</sub>	EC <sub>10</sub>	EC <sub>50</sub>	EC <sub>10</sub>	EC <sub>50</sub>
Ag 20 nm	N.D.	182 (163.1-202.9)	0.28 (0.21-0.38)	2.2 (1.6-3.7)	0.035 (0.014-0.09)	0.12 (0.09-0.16)
Ag 200 nm	N.D.	458.9 (401.9-523.9)	0.9 (0.62-1.28)	3.7 (2.3-6)	0.57 (0.25-1.4)	0.65 (0.17-2.5)
Ag 23 nm	0.16 (0.13-0.19)	0.42 (0.37-0.47)	0.01 (0.009-0.014)	0.034 (0.031-0.037)	0.0004 (0.00028-0.00058)	0.0012 (0.00098-0.0014)
Ag 27 nm	8.9 (6-13)	46 (39.7-52.6)	0.012 (0.004-0.038)	0.33 (0.2-0.53)	0.009 (0.0074-0.01)	0.02 (0.019-0.027)
AgNO <sub>3</sub>	0.2 (0.19-0.24)	0.6 (0.59-0.65)	0.02 (0.01-0.05)	0.042 (0.035-0.051)	0.0009 (N.D.)	0.0014 (N.D.)

N.D., Not determined because the 95% confidence intervals were too wide.

*Daphnia magna* immobilization assay

A size-dependent effect was observed in daphnids exposed to Ag particles (Figure 4). Ag 23 nm was the most toxic one followed by Ag 27 nm, 20 nm and 200 nm as already observed in the previous two assays. The same EC<sub>50</sub> was obtained for AgNO<sub>3</sub> and Ag 23 nm (0.001 mg/L). The internal concentrations of Ag as measured with ICP-MS were found to be below the detection limits for Ag NPs 23 nm (Table S2).

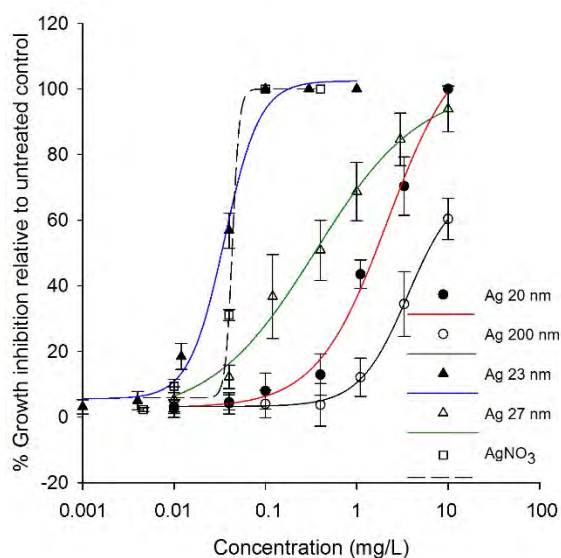


**Figure 3.** Dose–response curves of Ag particles 20 nm, 200 nm, 23 nm (*Ocimum sanctum* leaf extract), 27 nm (*Azadirachta indica* leaf extract) and AgNO<sub>3</sub> obtained in the *Desmodosmus subspicatus* growth inhibition assay after exposure to the compounds for 72 h. The assay was performed in 12-well plates under continuous shaking and illumination. Error bars represent the mean with standard deviation of two independent experiments.

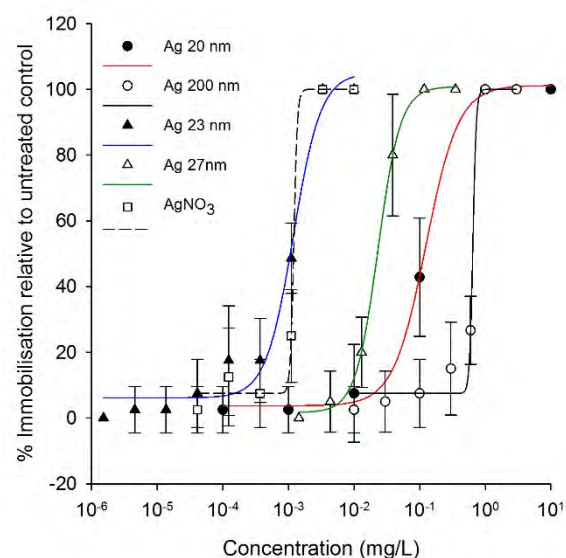


**Figure 4.** Effect of Ag particles 20 nm, 200 nm, 23 nm (*Ocimum sanctum* leaf extract), 27 nm (*Azadirachta indica* leaf extract) as well as AgNO<sub>3</sub> on the mobility of *Daphnia magna*. The experiments were performed in six-well plates and the inhibition of mobility was evaluated after 48 h exposure. Each treatment consisted of four replicates and the experiment was repeated twice. Error bars represent the mean with standard deviation of two independent experiments.

*Total dissolved Ag release over time in different media (Ultrafiltration and ICP-MS)*

The technique of ultrafiltration in combination with ICP-MS does not make a distinction between different Ag ionic species. Ag 200 nm showed the lowest release of soluble Ag in 2% NaCl after 30 min (Figure 5A). The other Ag NPs released approximately 1.7 times higher more soluble Ag species than Ag 200 nm. In both NBBM (Figure 5B) and Volvic water (Figure 5C), the soluble Ag content released from Ag NPs 23 nm remained stable over time. In contrast, the other Ag NPs showed a time-dependent increase in Ag released. When comparing identical concentrations for Ag NPs 20 nm, different amounts of soluble Ag were measured

after 48 h (27.5% less in NBBM than in Volvic water). Ag NPs 27 nm exhibited the lowest release of soluble Ag (16.7 µg/L, 0.2% of the mass) among all Ag particles in NBBM medium.

The tested particles contained only 0.004–0.007% of Ni and 0.007–0.01% of Cu while Cr, Mn, Fe, Co, Zn, As, Cd and Pb were not detected at all.

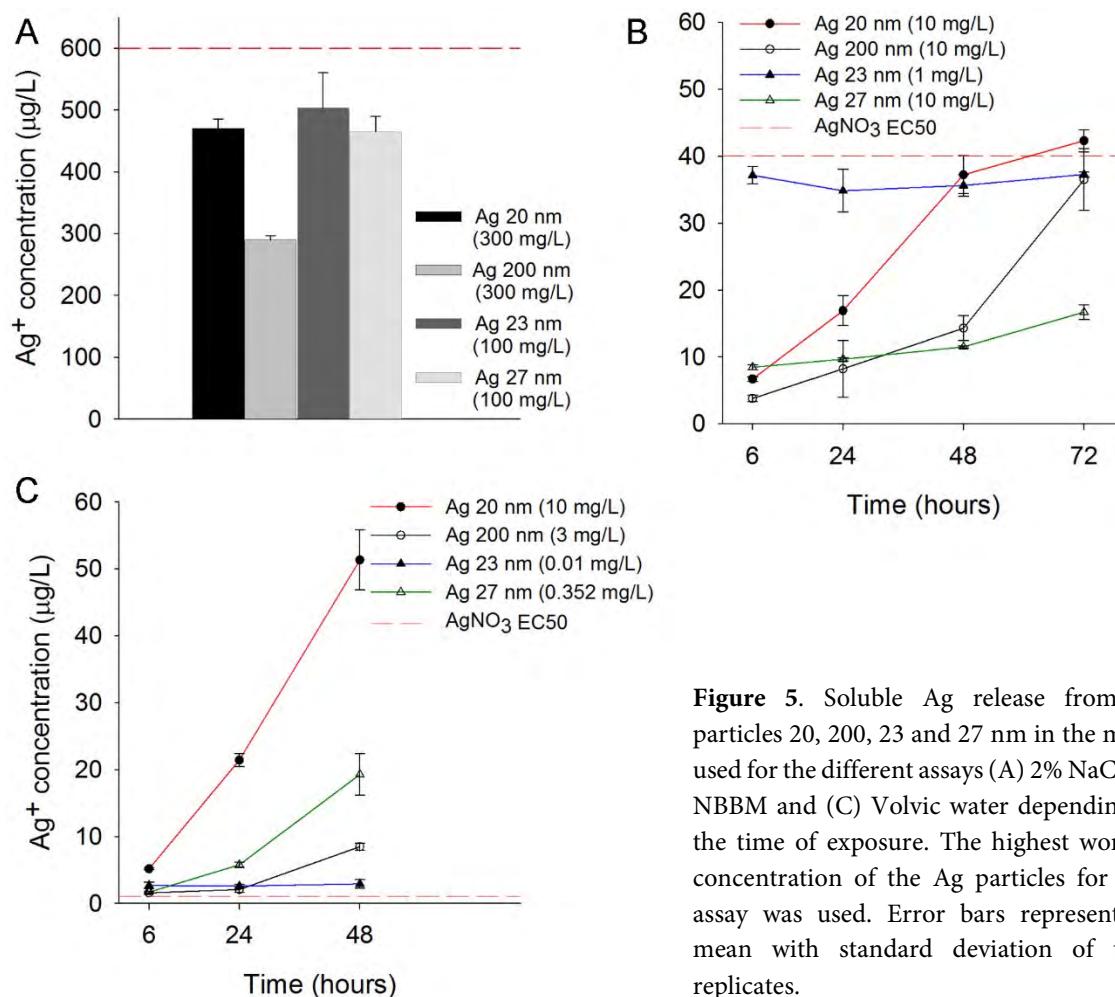


**Figure 5.** Soluble Ag release from Ag particles 20, 200, 23 and 27 nm in the media used for the different assays (A) 2% NaCl, (B) NBBM and (C) Volvic water depending on the time of exposure. The highest working concentration of the Ag particles for each assay was used. Error bars represent the mean with standard deviation of three replicates.

#### NPs uptake in *Daphnids* – NanoSIMS analysis

The Ag 20 nm, Ag 200 nm and Ag 23 nm particles (Figure 6A, B, C) are seen as bigger aggregates in the gut lumen and possibly attached to food particles or debris, while the Ag 27 nm particles (Figure 6D) did not seem to be present in the gut. There was no evidence that the Ag 20 nm particles were able to cross the GIT however, the Ag 200 nm particles were observed to have passed the peritrophic membrane and possibly entered intercellular spaces within the epithelial layer (B). Although the Ag 23 nm particles were not observed to have passed the GIT barrier and seemed to be present in the gut lumen at only very low concentrations, they were

found to accumulate around what is thought to be developing oocytes or oogonia in the ovaries (C) as reported in a previous study (Hiruta et al. 2010).

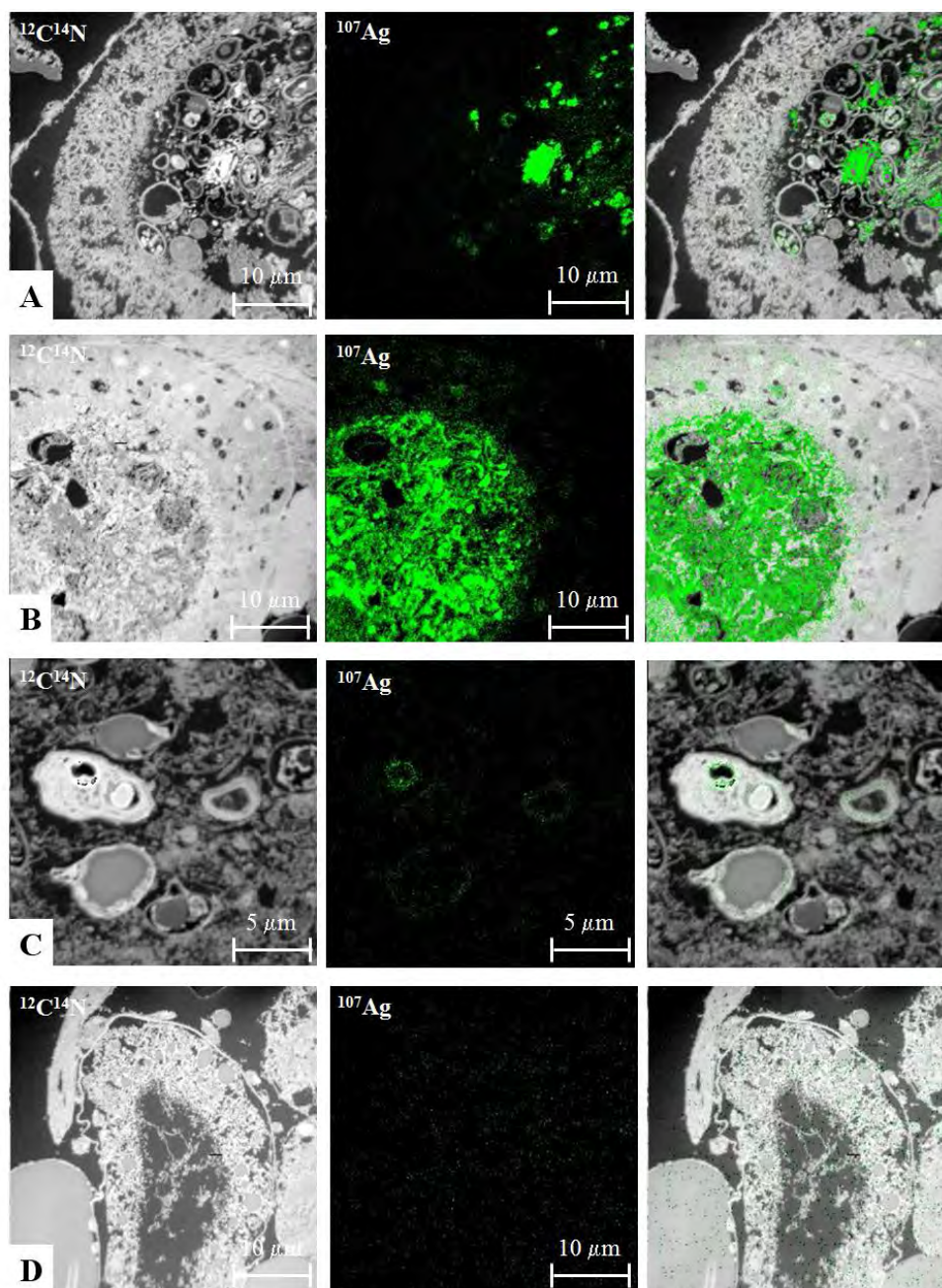


**Figure 6.** Elemental distribution of  $^{12}\text{C}^{14}\text{N}$  (black and white) and  $^{107}\text{Ag}$  (green) in 300 nm cuts. The last pictures show the overlap of  $^{12}\text{C}^{14}\text{N}$  and  $^{107}\text{Ag}$ . Daphnids were exposed to (A) Ag 20 nm, (B) Ag 200 nm, (C) Ag 23 nm and (D) Ag 27 nm. Scale bar is 10  $\mu\text{m}$  in A, B, D and 5  $\mu\text{m}$  in C.

## Discussion

In the present study, the effects of Ag NPs which are widely used were evaluated with the use of the alga *Desmodesmus subspicatus* and the crustaceans *Daphnia magna*, which are key

organisms in the ecosystem due to their importance in the food chain. In addition, the *Vibrio fischeri* inhibition of bioluminescence assay, which is commonly used for sediment toxicity testing, was modified and employed as a fast pre-screening assay.

The order of toxicity was identical for the different Ag particles across all organisms tested, with Ag 20 nm being always more toxic than Ag 200 nm. According to DLS results from the exposure solutions, the size between the two particles is not dramatically different. The two Ag NPs that were produced by a biological method were always more potent compared to commercially available ones. It has been shown that bare Ag NPs were less toxic to mammalian cell lines than biogenic Ag NPs with surface charge and coating affecting the interaction with cellular components (Suresh et al. 2012). Of the two biologically synthesized NPs, Ag 23 nm was the most toxic in all organisms. The DLS results, however, show that especially in the case of the *V. fischeri* assay, Ag 23 nm was the one with the biggest agglomerates (average diameter of 1372 nm). However, the limitations of the DLS method should be kept in mind. The particle size is correlated with the light scattered and the presence of few large particles could mask the presence of a high number of small particles (Handy et al. 2008).

The NP surface area could be more relevant in nanotoxicology studies than the mass unit (Oberdörster et al. 2005). While the differences in effects between Ag 23 nm and the rest of the Ag particles were decreased by a factor of about 3 when the dose was expressed as particle surface area, the differences were still clear with Ag NPs 23 nm being always the most potent (Figure S5).

NanoSIMS analysis showed that Ag NPs 23 nm were taken up and localized in the gut as well as in specific areas of *D. magna*, which are hypothesized to be developing oocytes (Bodar et al. 1990) within the ovaries. An uptake of 20 nm polystyrene beads and a translocation into lipid storage droplets or fat cells was reported for *D. magna* earlier (Rosenkranz et al. 2009). Although these storage droplets or fat cells were not directly observed here, it is known that the lipid-containing storage droplets are normally partially transferred to the oocytes (Goulden and Hornig 1980; Tessier and Goulden 1982) and a side-by-side transport of Ag NPs could be possible. The nearly similar-sized Ag 27 nm particles were not found to have translocated across the GIT, which might be due to different surface properties. The Ag 200 nm particles were detected to have slightly entered the intercellular spaces within the epithelial layer. Similar observations were already reported for diamond nanoparticles (Mendonça et al. 2011). Here, also a degeneration of epithelial cells as well as loss of adhesion to each other was observed, resulting in intercellular spaces. Another report observed Cu NPs passing the peritrophic

membrane allowing the particles to come in contact with the microvilli (Heinlaan et al. 2011). According to ICP-MS results of *D. magna* exposed to either Ag NPs 23 nm or 27 nm, Ag was below the detectable limits in the case of Ag NPs 23 nm (Table S2). Thus, NanoSIMS could be a useful tool for studying the uptake of NPs and their potential localization since ICP-MS alone could not detect the presence of Ag NPs in this case. TEM was performed in order to make ultrastructural observations, however Ag NPs cannot be distinguished from dark stained particles due to sample preparation (e.g., OsO<sub>4</sub>, uranyl acetate, etc.). The TEM used was equipped with an EDS detector in order to identify the particles. However, this method requires high concentrations and therefore the presence of the particles could be overlooked. While the elimination route was not assessed in this study, a slow elimination from the body has been reported for Ag NPs (Zhao and Wang 2010) and TiO<sub>2</sub> NPs (Zhu et al. 2010) that might affect food intake with subsequent effects on growth and development.

The observed differences in effects between the two biologically synthesized Ag NPs (using *A. indica* and *O. sanctum*) may be due to the nature and distribution of biomolecules on the surface of NPs indicated by the observed differences in the FTIR peaks and intensities (Figure S4, Table S1) (Balachandran et al. 2012). Although most of the band assignments were common for both NPs, an additional IR peak was observed at position 1385 cm<sup>-1</sup> for Ag 27 nm NPs (*A. indica* synthesized) that could be assigned to germinal methyl or symmetric stretching of carbonyl group. The difference in the FTIR peak assignments may be attributed to the number of molecules present as well as the distribution of biomolecules on the nanoparticle surface. The biomolecules present on the surface of 23 nm sized (*O. sanctum* synthesized) Ag NPs may be unevenly packed thereby possibly decreasing the capability of electrostatic repulsion and consequently the stability in the medium. The surface or chemical barrier of the particle plays a major role in the physicochemical properties such as aggregation and dissolution that could influence the toxicity (Kittler et al. 2010; Verma and Stellacci 2010). Previously, it has already been suggested that the extent of effects is dependent on the nature of the proteins on the surface of the particles (Lynch and Dawson 2008). In a study using mammalian cells as a model, it was found that polysaccharide-coated Ag NPs induce more severe DNA damage than uncoated ones also suggesting that different surface chemistry can lead to different effects (Ahamed et al. 2008). Thus, it is possible that the nature of molecules present on the Ag NPs 23 nm and 27 nm due to the plant extracts could have affected their uptake and distribution in the daphnias. In addition, ICP-MS analysis was performed with the stock Ag NP solutions in order to assess the potential contribution of impurities to toxicity.

These low concentrations of contaminants in the NP stock solutions are unlikely to explain the observed differences in toxicity.

For metallic NPs it is hard to differentiate effects due to the NPs themselves or the ions that are released (Zook et al. 2011). Ag ions are reactive binding to various inorganic ligands forming complexes such as silver chloride, silver sulphide, silver thiosulphate (LeBlanc et al. 1984), as well as to organic ligands commonly present in the environment (Choi et al. 2009) that could lead to decreased bioavailability and toxicity to organisms. It has been shown that Ag dissolution is medium-, concentration- and time-dependent (Zhao and Wang 2012). In 2% NaCl and NBBM, the fraction of dissolved Ag (total amount of dissolved non-particulate Ag after filtration through a 3kD cut-off membrane) was found to be lower than the EC50 obtained for AgNO<sub>3</sub> in *V. fischeri* and *D. subspicatus*. All particles except for Ag 27 nm showed similar soluble Ag concentrations after 72 h incubation in NBBM medium while EC50 values differed by a factor of 100. Although dissolved Ag may have contributed to the observed effects, the measured concentrations cannot explain alone differences in toxicity of the different Ag particles.

At this stage the concentrations at which Ag NPs are present in the environment are not known, as there are no analytical methods to detect NPs in water, soil or sediment (Benn and Westerhoff 2008; UK Environmental Nanoscience Initiative (ENI)). Therefore, the concentrations used in the study may not be environmentally relevant. However, the predicted environmental concentration of Ag NPs in water in a realistic scenario was suggested to be 0.03 µg/L (Mueller and Nowack 2008). In addition, at the moment it is not easy to correlate the situation between the laboratory and the field since it is difficult to estimate the interaction of NPs with environmental matrices and to what extent the organism will be actually exposed in the environment. Addition of 1.5 mg/L of total organic carbon (TOC) in the exposure medium decreased the TiO<sub>2</sub> NPs toxicity to *Ceriodaphnia dubia* (Hall et al. 2009). This suggests a potential for overestimation of toxicity since natural waters contain TOC. However, this study presents findings concerning the potential hazards of NPs on aquatic organisms of different trophic levels, which is of high importance since these organisms form the base of the food chain.

In addition, our findings further support the suggestion that apart from the size, the surface coating and the nature of biomolecules present in the surface could influence toxicity and affect uptake and localization as visualized with NanoSIMS. It is obvious that the

relationship between toxicity and NPs properties is not simple and cannot be predicted by just relating it with size.

### Acknowledgements

The authors would like to thank Camilla Carlson (Norwegian School of Veterinary Science, Oslo, Norway) and Tore-Geir Iversen (The Norwegian Radium Hospital, Oslo, Norway) for their valuable help and advice on the size and zeta potential measurements. The work of Esther Lentzen and Patrick Grysan (Department of Material Sciences, Centre de Recherche Public-Gabriel Lippmann, Luxembourg) on NanoSIMS analysis as well as the expertise of Sylvie Migot (Ecole des Mines, Nancy, France) in TEM are gratefully acknowledged. The authors also thank Johanna Ziebel for the ICP-MS analysis and Servane Contal, Henry- Michel Cauchie and Delphine Collard (Department of Environment and Agrobiotechnologies, Centre de Recherche Public-Gabriel Lippmann, Luxembourg) for their support with the set-up of the assays. In addition, many thanks to Hans van den Berg (Wageningen University, the Netherlands) for his advice on *Daphnia magna* anatomy. This study was supported by the Fonds National de la Recherche of Luxembourg within the project NanEAU (FNR/08/SR/07).

### References

- Ahamed M, Karns M, Goodson M, Rowe J, Hussain SM, Schlager JJ, et al. 2008. DNA damage response to different surface chemistry of silver nanoparticles in mammalian cells. *Toxicol. Appl. Pharmacol.* 233:404–410.
- Ahamed M, Posgai R, Gorey TJ, Nielsen M, Hussain SM, Rowe JJ. 2010. Silver nanoparticles induced heat shock protein 70, oxidative stress and apoptosis in *Drosophila melanogaster*. *Toxicol. Appl. Pharmacol.* 242:263–9.
- Andersen R, Berges J, Harrison P, Watanabe M. 2005. Appendix A-recipes for freshwater and seawater media. In *Algal culturing techniques*, pp. 429–538, Elsevier Inc.
- Audiot J-N, Senou M, Migeon H-N, Many M-C. 2008. Visualisation of thyroid hormone synthesis by ion imaging. *Appl. Surf. Sci.* 255:1185–1189.
- Balachandran YL, Peranantham P, Selvakumar R, Gutleb AC, Girija S. 2012. Size-controlled green synthesis of silver nanoparticles using dual functional plant leaf extract at room temperature. *Int. J. Green Nanotechnol.* 4:310–325.
- Benn T, Cavanagh B, Hristovski K, Posner JD, Westerhoff P. 2010. The release of nanosilver from consumer products used in the home. *J. Environ. Qual.* 39:1875.
- Benn TM, Westerhoff P. 2008. Nanoparticle silver released into water from commercially available sock fabrics. *Environ. Sci. Technol.* 42: 4133–4139.
- Bodar CWM, van Donselaar EG, Herwig HJ. 1990. *Morphological aspects of Daphnia magna*. Health Council of the Netherlands, University of Utrecht, The Hague, the Netherlands.

- Boscher A, Gobert S, Guignard C, Ziebel J, L'Hoste L, Gutleb AC, et al. 2010. Chemical contaminants in fish species from rivers in the North of Luxembourg: potential impact on the Eurasian otter (*Lutra lutra*). *Chemosphere* 78:785–792.
- Brandenberger C, Clift MJD, Vanhecke D, Mühlfeld C, Stone V, Gehr P, et al. 2010. Intracellular imaging of nanoparticles: is it an elemental mistake to believe what you see? Part. *Fibre Toxicol.* 7:15.
- Choi O, Clevenger TE, Deng B, Surampalli RY, Ross LJ, Hu Z. 2009. Role of sulfide and ligand strength in controlling nanosilver toxicity. *Water Res.* 43:1879–1886.
- Eybe T, Audinot J-N, Bohn T, Guignard C, Migeon HN, Hoffmann L. 2008. NanoSIMS 50 elucidation of the natural element composition in structures of cyanobacteria and their exposure to halogen compounds. *J. Appl. Microbiol.* 105:1502–10.
- Geranio L, Heuberger M, Nowack B. 2009. The behavior of silver nanotextiles during washing. *Environ. Sci. Technol.* 43:8113–8.
- Goulden CE, Hornig LL. 1980. Population oscillations and energy reserves in planktonic cladocera and their consequences to competition. *Proc. Natl. Acad. Sci. USA* 77: 1716–20.
- Hall S, Bradley T, Moore JT, Kuykindall T, Minella L. 2009. Acute and chronic toxicity of nano-scale TiO<sub>2</sub> particles to freshwater fish, cladocerans, and green algae, and effects of organic and inorganic substrate on TiO<sub>2</sub> toxicity. *Nanotoxicology* 3:91–97.
- Hamers T, Smit MGD, Murk AJ, Koeman JH. 2001. Biological and chemical analysis of the toxic potency of pesticides in rainwater. *Chemosphere* 45: 609–624.
- Handy RD, von der Kammer F, Lead JR, Hassellöv M, Owen R, Crane M. 2008. The ecotoxicology and chemistry of manufactured nanoparticles. *Ecotoxicology* 17:287–314.
- Hartmann NB, von der Kammer F, Hofmann T, Baalousha M, Ottofuelling S, Baun A. 2010. Algal testing of titanium dioxide nanoparticles-testing considerations, inhibitory effects and modification of cadmium bioavailability. *Toxicology* 269:190–7.
- Heinlaan M, Kahru A, Kasemets K, Arbeille B, Prensier G, Dubourguier H-C. 2011. Changes in the *Daphnia magna* midgut upon ingestion of copper oxide nanoparticles: a transmission electron microscopy study. *Water Res.* 45:179–90.
- Hiruta C, Nishida C, Tochinali S. 2010. Abortive meiosis in the oogenesis of parthenogenetic *Daphnia pulex*. *Chromosome Res.* 18:833–40.
- Hund-Rinke K, Simon M. 2006. Ecotoxic effect of photocatalytic active nanoparticles (TiO<sub>2</sub>) on algae and daphnids. *Environ. Sci. Pollut. Res. Int.* 13: 225–32.
- International Organisation for Standardization (ISO 11348-1). 1999. Water quality-Determination of the inhibitory effect of water samples on the light emission of *Vibrio fischeri* (Luminescent bacteria test).
- International Organisation for Standardization (ISO 8692). 2004. Water quality- freshwater algal growth inhibition test with unicellular green algae.
- Ju-Nam Y, Lead JR. 2008. Manufactured nanoparticles: an overview of their chemistry, interactions and potential environmental implications. *Sci. Total Environ.* 400:396–414.
- Kittler S, Greulich C, Diendorf J, Köller M, Epple M. 2010. Toxicity of silver nanoparticles increases during storage because of slow dissolution under release of silver ions. *Chem. Mater.* 22:4548–4554.
- Kruszewski M, Brzoska K, Brunborg G, Asare N, Dobrzynska M, Dusinska M, et al. 2011. Toxicity of silver nanomaterials in higher eukaryotes. In *Advances in Molecular Toxicology*, Vol. 5 of, pp. 179–218, Elsevier B.V.

- Lankoff A, Sandberg WJ, Wegierek-ciuk A, Lisowska H, Refsnes M, Schwarze PE, et al. 2012. The effect of agglomeration state of silver and titanium dioxide nanoparticles on cellular response of HepG2, A549 and THP-1 cells. *Toxicol. Lett.* 208:197–213.
- LeBlanc GA, Mastone JD, Paradice AP, Wilson BF. 1984. The influence of speciation on the toxicity of silver to fathead minnow (*Pimephales promelas*). *Environ. Toxicol. Chem.* 3: 37–46.
- Lovern SB, Owen HA., Klaper R. 2008. Electron microscopy of gold nanoparticle intake in the gut of *Daphnia magna*. *Nanotoxicology* 2:43–48.
- Lynch I, Dawson KA. 2008. Protein-nanoparticle interactions. *Nano Today* 3: 40–47.
- Macova M, Escher BI, Reungoat J, Carswell S, Lee Chue K, Keller J, et al. 2010. Monitoring the biological activity of micropollutants during advanced wastewater treatment with ozonation and activated carbon filtration. *Water Res.* 44:477–92.
- Mendonça E, Diniz M, Silva L, Peres I, Castro L, Correia JB, et al. 2011. Effects of diamond nanoparticle exposure on the internal structure and reproduction of *Daphnia magna*. *J. Hazard. Mater.* 186:265–71.
- Mueller NC, Nowack B. 2008. Exposure modeling of engineered nanoparticles in the environment. *Environ. Sci. Technol.* 42: 4447–53.
- Nair PMG, Park SY, Lee S-W, Choi J. 2011. Differential expression of ribosomal protein gene, gonadotrophin releasing hormone gene and Balbiani ring protein gene in silver nanoparticles exposed *Chironomus riparius*. *Aquat. Toxicol.* 101:31–7.
- Nair R, Varghese SH, Nair BG, Maekawa T, Yoshida Y, Kumar DS. 2010. Nanoparticulate material delivery to plants. *Plant Sci.* 179:154–163.
- Navarro E, Piccapietra F, Wagner B, Marconi F, Kaegi R, Odzak N, et al. 2008. Toxicity of silver nanoparticles to *Chlamydomonas reinhardtii*. *Environ. Sci. Technol.* 42: 8959–64.
- Oberdörster G, Oberdörster E, Oberdörster J. 2005. Nanotoxicology : an emerging discipline evolving from studies of ultrafine particles. *Environ. Health Perspect.* 113:823–839.
- Organisation for Economic Co-operation and Development (OECD). 2004. OECD Guidelines for the testing of chemicals/ section 2: effects on biotic systems, Test No. 202: *Daphnia* sp. acute immobilisation test.
- Perez-de-Luque A, Rubiales D. 2009. Nanotechnology for parasitic plant control. *Pest Manag. Sci.* 65:540–545.
- Roh J, Park Y, Park K, Choi J. 2010. Ecotoxicological investigation of CeO<sub>2</sub> and TiO<sub>2</sub> nanoparticles on the soil nematode *Caenorhabditis elegans* using gene expression, growth, fertility, and survival as endpoints. *Environ. Toxicol. Pharmacol.* 29:167–172.
- Rosenkranz P, Chaudhry Q, Stone V, Fernandes TF. 2009. A comparison of nanoparticle and fine particle uptake by *Daphnia magna*. *Environ. Toxicol. Chem.* 28:2142–9.
- Som C, Berges M, Chaudhry Q, Dusinska M, Fernandes TF, Olsen SI, et al. 2010. The importance of life cycle concepts for the development of safe nanoproducts. *Toxicology* 269:160–169.
- Suresh AK, Pelletier DA, Wang W, Morrell-Falvey JL, Gu B, Doktycz MJ. 2012. Cytotoxicity induced by engineered silver nanocrystallites is dependent on surface coatings and cell types. *Langmuir* 28:2727–2735.
- Tessier AJ, Goulden CE. 1982. Estimating food limitation in cladoceran populations. *Limnol. Oceanogr.* 27: 707–717.
- UK Environmental Nanoscience Initiative (ENI). Small world. Available: <http://www.nerc.ac.uk/>.
- Verma A, Stellacci F. 2010. Effect of surface properties on nanoparticle-cell interactions. *Small* 6:12–21.
- Wiesner MR, Lowry GV, Jones KL, Tech V, Giulio RTDI. 2009. Decreasing uncertainties in assessing environmental exposure, risk, and ecological implications of nanomaterials. *Environ. Sci. Technol.* 43:6458–6462.

- Wijnhoven SWP, Dekkers S, Hagens WI, De Jong WH. 2009. Exposure to nanomaterials in consumer products. Available: <http://www.rivm.nl/bibliotheek/>.
- Woodrow Wilson International Center for Scholars. 2014. Project on emerging nanotechnologies. Available: <http://www.nanotechproject.org/> [accessed 15 August 2014].
- Yin L, Cheng Y, Espinasse B, Colman BP, Auffan M, Wiesner M, et al. 2011. More than the ions: the effects of silver nanoparticles on *Lolium multiflorum*. *Environ. Sci. Technol.* 45:2360–7.
- Zhao C-M, Wang W. 2010. Biokinetic uptake and efflux of silver nanoparticles in *Daphnia magna*. *Environ. Sci. Technol.* 44: 7699–7704.
- Zhao C-M, Wang W-X. 2012. Importance of surface coatings and soluble silver in silver nanoparticles toxicity to *Daphnia magna*. *Nanotoxicology* 6:361–370.
- Zhu X, Chang Y, Chen Y. 2010. Toxicity and bioaccumulation of TiO<sub>2</sub> nanoparticle aggregates in *Daphnia magna*. *Chemosphere* 78:209–215.
- Zook JM, Long SE, Cleveland D, Geronimo CLA, MacCuspie RI. 2011. Measuring silver nanoparticle dissolution in complex biological and environmental matrices using UV-visible absorbance. *Anal. Bioanal. Chem.* 401:1993–2002.

### Supporting Information for Chapter 3

#### *NP characterisation by Scanning (SEM) and Transmission (TEM) Electron Microscopy*

*Ag 20 nm and Ag 200 nm.* Observations were performed using a scanning electron microscope (SEM) type DSM942 (Zeiss, Germany) in the secondary electron (SE) mode. SEM worked with parameters: high voltage EHT 2kV, working distance from 4 to 4.8 mm. Ag NPs of nominal size 20 and 200 nm were dispersed in distilled water containing 5% DMSO at a concentration 2 mg/mL and were sonicated (cycle 1) on ice for 3 minutes using a UP200S probe ultra sonicator (Hielscher, Germany). Stock solutions of the NPs were diluted 1:10 in distilled water and were deposited on the microscopic holders. After evaporation of the solvent (24 hours), the samples were coated with a thin layer of Au (about 10 nm) using a vacuum evaporator (JEE-4X, JEOL, Japan) to protect the sample from heat destruction and to keep real parameters of the observed details. It operated with ultimate pressure  $6 \times 10^{-4}$  Pa with rotating and tilting specimen stage. The images were collected at 10 kV and either 10 000 $\times$  or 20 000 $\times$  magnification. The morphology of NPs was also observed by transmission electron microscopy (TEM) (JEOL 1200 EXII, JEOL, Japan) operating at an acceleration voltage of 120 kV. The samples were prepared on the copper mesh covered with a carbon film as the carrier. Digital images were recorded by CD camera SIS Morada 11 megapixels and processed using AnalySIS.

*Ag 23 nm and Ag 27 nm.* High Resolution Scanning Electron Microscope (HRSEM) images were obtained on Sirion HRSEM (FEI company) operated at 3.0 kV. Samples for HRSEM were prepared on a silicon wafer by drop coating of colloidal Ag nanoparticles (0.1 OD absorbance). TEM images were obtained on a CM20 Philips microscope and FEI Technai 20U TWIN STEM equipped with energy dispersive X-ray (EDX, EDAX) spectra that operated at 200 kV. Samples were prepared by evaporating a drop of Ag colloidal solution on carbon coated copper grid.

#### *NPs size distribution*

*Ag 20 and Ag 200 nm.* DLS was performed at 25°C with a scattering angle of 90° on the Zetasizer NanoZS (Malvern, Malvern Hills, UK). Stock solutions were diluted 1:4 in distilled water and measured in triplicate with 20 sub-runs.

*Ag 23 nm and Ag 27 nm.* Size distribution was determined with TEM as explained in the previous section. Over 200 particles were counted and values were converted to percentile to plot histogram and size distribution pattern. Particle size measurements were carried out using ImageJ 1.44 software.

*FTIR spectra for Ag 23 nm and Ag 27 nm*

The surface chemistry of the Ag NPs 23 nm and 27 nm was characterized using Shimadzu FTIR-8400S FTIR (Fourier Transform Infrared) spectrometer, over a spectral range of 4000-450  $\text{cm}^{-1}$  at a spectral resolution of 4  $\text{cm}^{-1}$ . Samples were prepared by drying the colloidal Ag NPs on a clean glass slide, and then the particles were scraped from the glass slide and mixed with KBr (2 mg of Ag NPs per 100 mg of dry KBr Sigma-Aldrich spectroscopic grade) and pressed into a pellet for measurements. A background spectrum was obtained before each measurement session using pure KBr at the same instrumental conditions used for sample acquisition.

*Total Ag content in daphnids*

Daphnids were exposed to 0.1 mg/L Ag NPs 20 nm, 0.4 mg/L Ag NPs 200 nm, 0.001 mg/L Ag NPs 23 nm and 0.04 mg/L Ag NPs 27 nm (concentrations corresponding close to the EC50s) for 48 hours as already described in the previous section. At the end of exposure 10 daphnids were collected, transferred in clean Volvic water and digested with 700  $\mu\text{l}$   $\text{HNO}_3$  (Plasma Pure quality, 67-70%, SCP Science, Courtaboeuf, France) and 300  $\mu\text{l}$   $\text{H}_2\text{O}_2$  (30% w/w for metals traces analysis, Fisher Scientific, Belgium) and left to react overnight. Then the volume was completed to 10 ml with demineralized water and the obtained solution was diluted 5 times with 1%  $\text{HNO}_3$  before analysis. Silver was analyzed by Inductively Coupled Plasma Mass Spectrometry (ICP-MS) (Elan DRC-e, Perkin Elmer, Waltham, MA, USA).

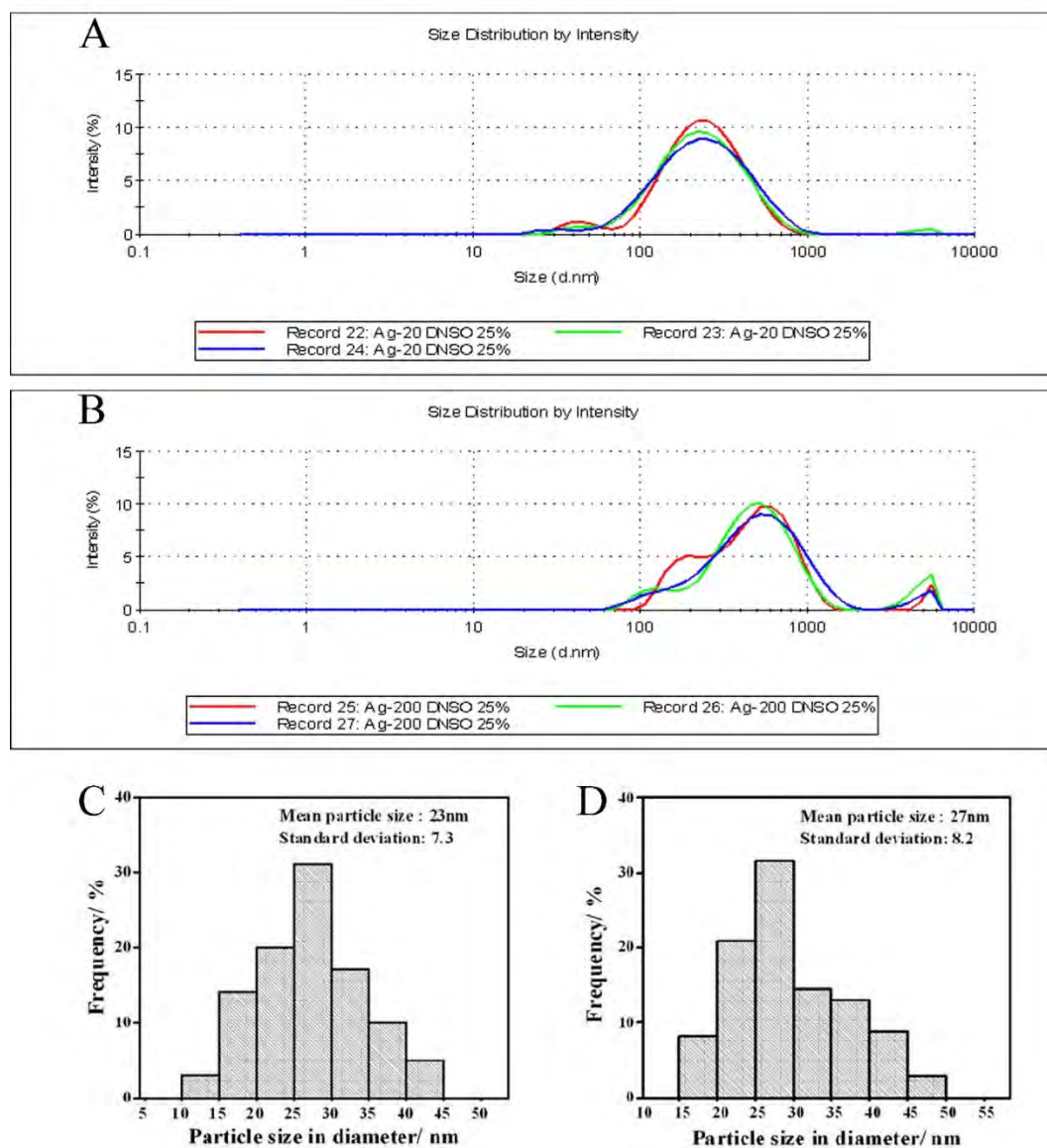


**Figure S1.** Particle size distribution of Ag NPs (A) 20 nm, (B) 200 nm, (C) 23 nm (synthesized using *O. sanctum* plant extract), (D) 27 nm (synthesized using *A. indica*). Data are presented as % intensity of light scattered (A-B) and as % frequency (C-D).

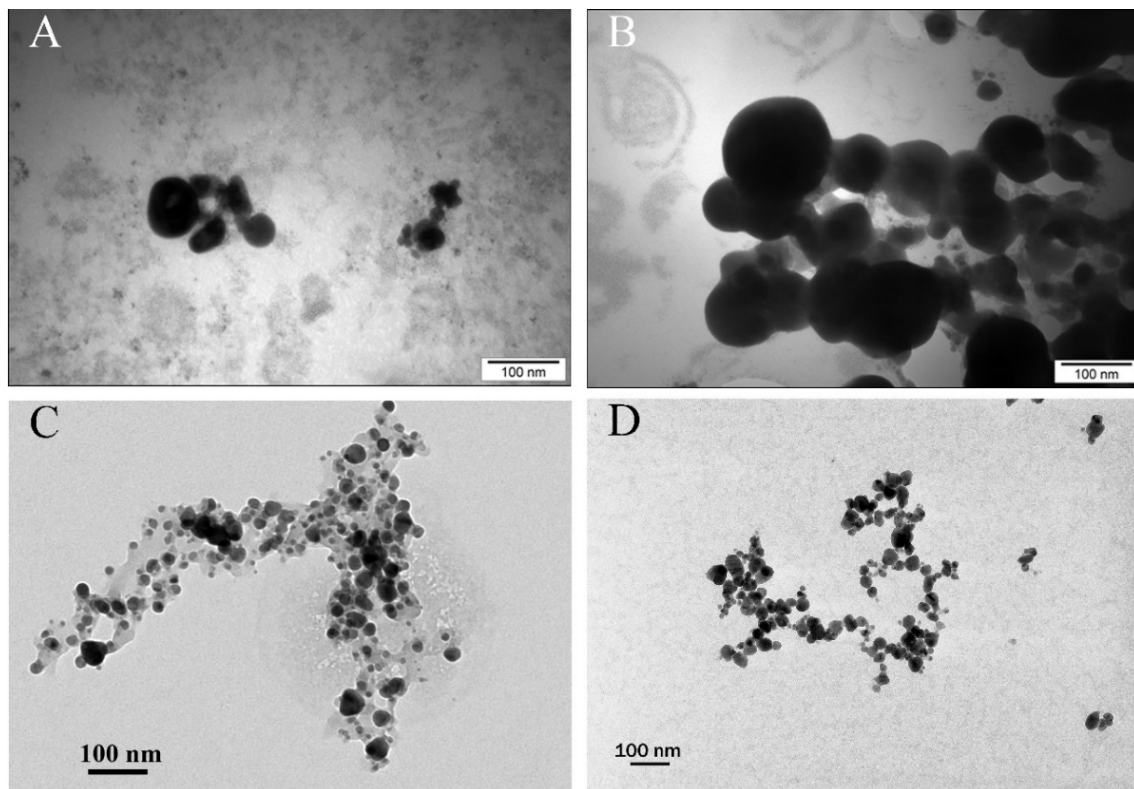


**Figure S2.** TEM micrographs of Ag NPs (A) 20 nm, (B) 200 nm, (C) 23 nm (synthesized using *O. sanctum* plant extract), (D) 27 nm (synthesized using *A. indica*).

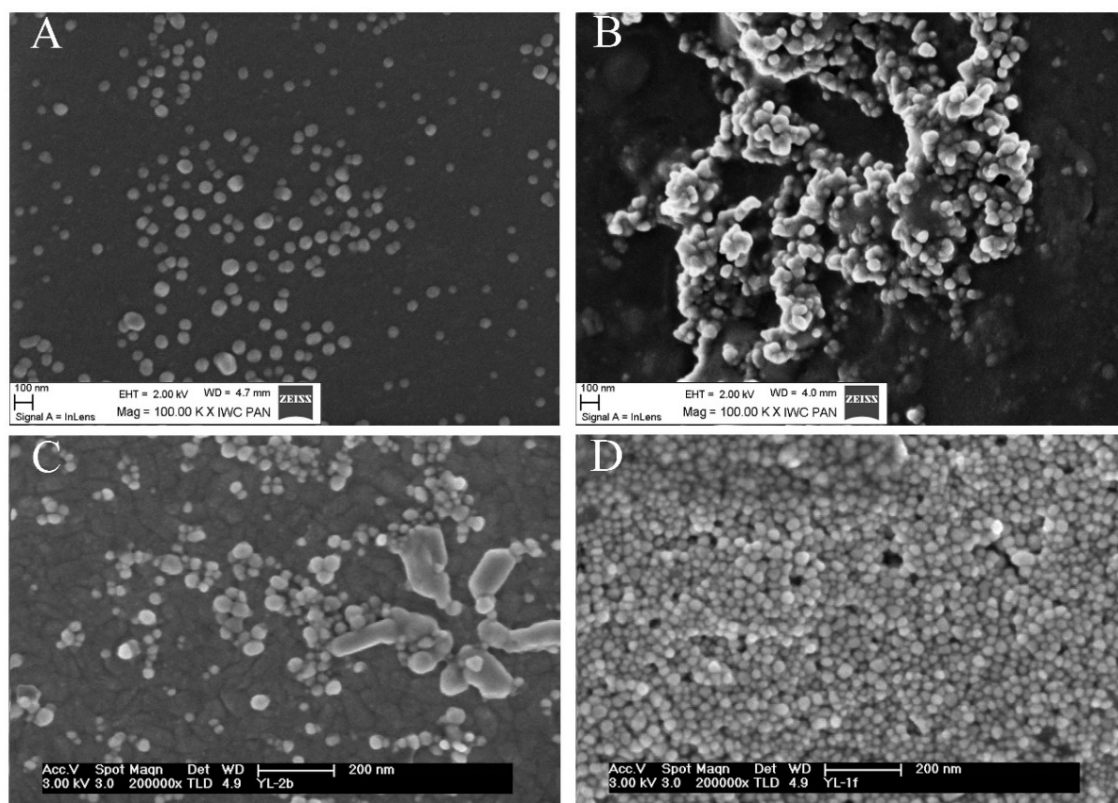


**Figure S3.** SEM images of Ag NPs (A) 20 nm, (B) 200 nm, (C) 23 nm (synthesized using *O. sanctum* plant extract), (D) 27 nm (synthesized using *A. indica*).

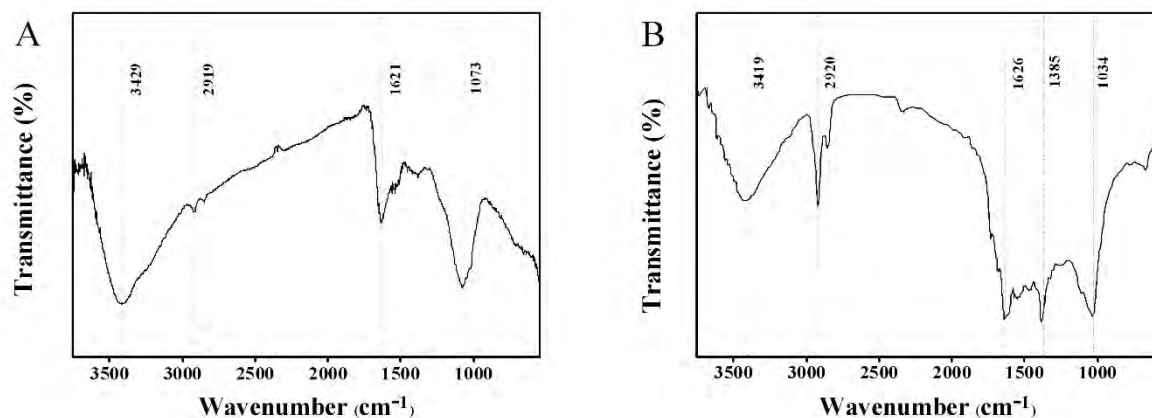


**Figure S4.** FTIR spectrum of Ag NPs synthesized in aqueous leaf extract of (A) *O. sanctum* and (B) *A. indica*.

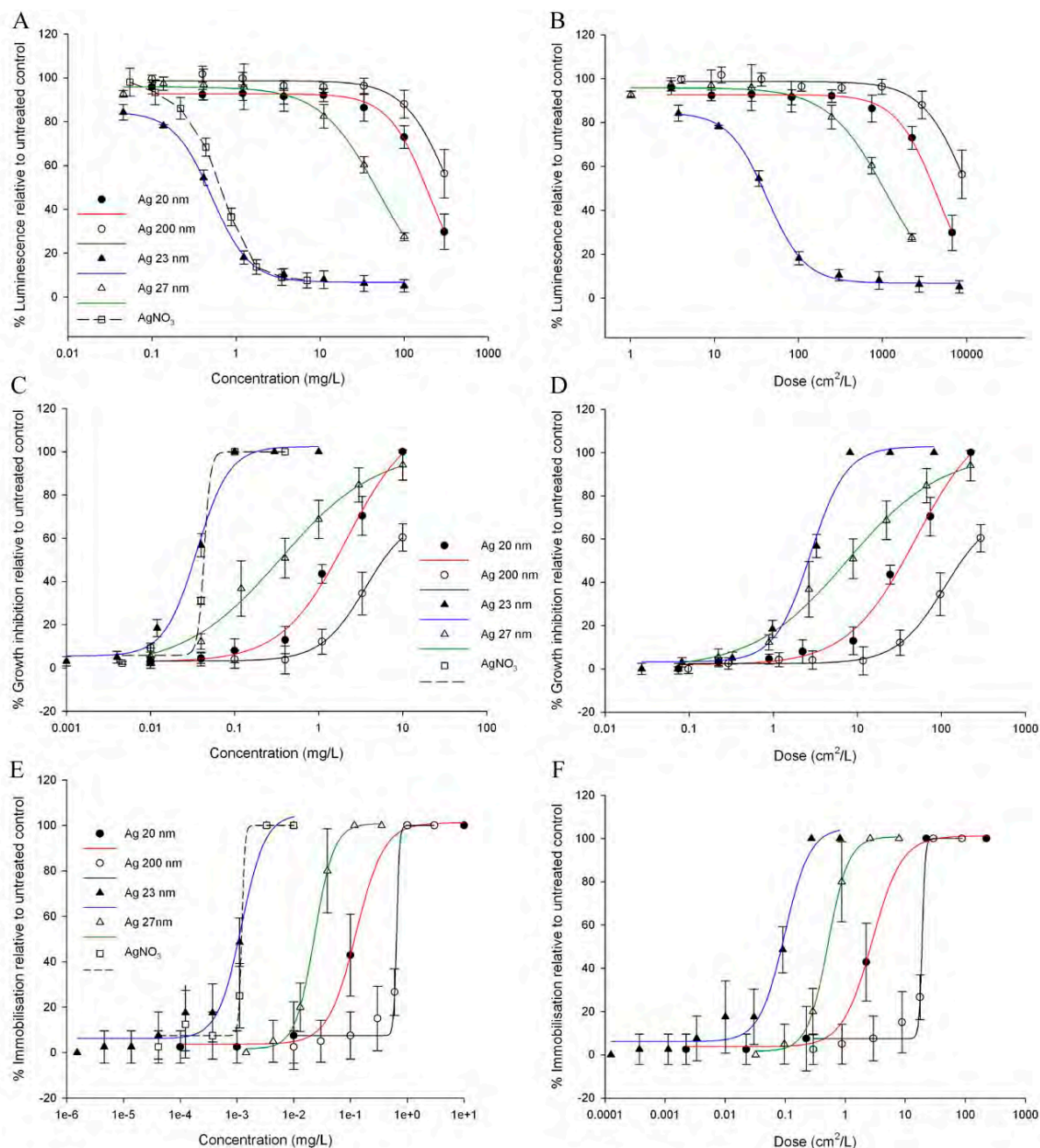


**Figure S5.** Effects of Ag NPs 20 nm, 200 nm, Ag 23 nm (*Ocimum sanctum* leaf extract) and Ag 27 nm (*Azadirachta indica* leaf extract) on (A, B) *Vibrio fischeri*, (C, D) *Desmodemus subspicatus* and (E, F) *Daphnia magna*. Data show mean with standard deviation of 2 independent experiments. (B, D, F) are the (A, C, E) dose-response relationships when dose is expressed as particle surface area.

**Table S1.** Summary of the dominant peak positions and their corresponding functional groups obtained with FTIR for Ag NPs synthesized in aqueous leaf extract of *O. sanctum* and *A. indica*.

<i>A. indica</i> Ag NPs (27nm)	<i>O. sanctum</i> Ag NPs (23nm)	Functional groups
Wave numbers (cm <sup>-1</sup> )		
1034( <i>s</i> )	1073( <i>s</i> )	C-O stretch
1385( <i>s</i> )	-	Geminal methyls
1626( <i>s</i> )	1621( <i>s</i> )	Amide
2920( <i>s</i> )	2919( <i>w</i> )	C-H stretch
3419( <i>s</i> )	3429( <i>s</i> )	O-H stretch, H-bond

(*s*) =strong; (*w*) = weak

**Table S2.** Total Ag content in daphnids at the end of the exposure period (after 48 hours).

Treatment	Exposure conc (mg/L)	Ag content (ng)/sample
Control	0	<5
Ag 20 nm	0.1	133
Ag 200 nm	0.4	398.8
Ag 23 nm	0.001	<5
Ag 27 nm	0.04	7.35

# Chapter 4

## P-gp efflux pump inhibition potential of common environmental contaminants determined *in vitro*

Anastasia Georgantzopoulou, Ewa Skoczynska, Johannes H.J. van den Berg, Walter Brand, Sylvain Legay, Sebastian G. Klein, Ivonne M.C.M. Rietjens and Albertinka J. Murk

*Env. Toxicol. Chem.* 2014; 33(4): 804–813

DOI: 10.1002/etc.2493

## **Abstract**

Across different species, cellular efflux pumps such as P-glycoprotein (P-gp; also termed multidrug resistance protein 1 [MDR1]) serve as a first line of defense by transporting toxic xenobiotics out of the cell. This mechanism is also active in aquatic organisms such as mussels, fish, and their larvae. Modulation of this resistance mechanism by chemical agents occurring in the environment could result in either higher or lower internal concentrations of toxic or endogenous compounds in cells. The aim of the present study was to explore and quantify the inhibition of the P-gp efflux pumps by several ubiquitous aquatic contaminants. The calcein-acetoxymethyl ester (calcein-AM) assay commonly used in pharmacological research was established with P-gp-overexpressing Madin-Darby canine kidney cells (MDCKII-MDR1) in a 96-well plate, avoiding extra washing, centrifugation, and lysis steps. This calcein-AM-based P-gp cellular efflux pump inhibition assay (CEPIA) was used to study the inhibition by commonly occurring environmental contaminants. Among others, the compounds pentachlorophenol, perfluorooctane sulfonate, and perfluorooctanoate strongly inhibited the P-gp-mediated efflux of calcein-AM while the chlorinated alkanes did not seem to interact with the transporter. The fact that common pollutants can be potent modulators of the efflux transporters is a motive to further study whether this increases the toxicity of other contaminants present in the same matrices.

## Introduction

Chemical agents occur in the environment as mixtures, often resulting in unexpected and unpredictable combination effects, for example, because the internal concentration of toxic compounds is increased as a result of inhibition of the normal function of cellular efflux pumps. Cellular efflux pumps are membrane-bound, energy-dependent efflux pumps that bind and actively excrete the compounds into the extracellular environment (Bolhuis et al. 1997; Endicott and Ling 1989; Higgins 2007; Loo et al. 2004). An important adenosine triphosphate (ATP) binding cassette (ABC) transport protein is the well-preserved P-glycoprotein (P-gp, or ABCB1), also referred to as multidrug resistance protein 1 (MDR1). Other ABC transport proteins are also known, including the multidrug resistance associated proteins 1 (MRP1, or ABCC1) and 2 (MRP2, or ABCC2), as well as the breast cancer resistance protein (BCRP, or ABCG2) (Schinkel and Jonker 2003). P-glycoprotein has been localized in mammalian tissues with barrier functions, such as the intestines, brain, placenta, ovaries, and testis, as well as those with excretory functions, such as the liver and kidney (Brand et al. 2006; Chan et al. 2004; Gottesman and Pastan 1993; Schinkel and Jonker 2003). Also, in aquatic organisms the efflux pumps are located at the interface between the outside and inside world as well as between the body and special tissues involved in the excretion of xenobiotics or endogenous metabolites, such as the gills, liver, hepatopancreas, kidney, and intestines, suggesting the importance of these proteins in the defense against toxic agents (Smital et al. 2004).

Cellular efflux pumps form a first line of defense against toxic compounds as they lower the internal concentrations in the cells. In pharmacological sciences, cellular efflux pumps have already been studied for decades because they have been shown to be involved in the phenomenon of multidrug resistance (MDR), in which cancer patients do not benefit from chemotherapy because of an overexpression of transport proteins that act as efflux pumps for medicines in tumor cells (Ambudkar et al. 1999; van Tellingen 2001). A phenomenon analogous to MDR in aquatic ecotoxicology is called multixenobiotic resistance (MXR) (Kurelec 1992), which has been observed in the gills and larvae of all marine organisms tested to date (Bard 2000). The phenomenon of MDR is undesired in cancer research as it limits the success of chemotherapy (Ferguson and De Flora 2005); MXR, however, because of overexpression of the efflux proteins, results in enhanced protection of organisms against environmental contaminants.

Given the relevance of this defense mechanism, fast *in vitro* assays for high-throughput screening and mixture testing are extremely valuable. The present study describes the

application of the calcein-acetoxymethyl ester (calcein-AM) assay for exploration and quantification of the inhibition of cellular efflux pumps by environmental contaminants. The assay is based on the well-known calcein-AM assay that has been described before using several cell models (Caminada et al. 2008; Ebert et al. 2012; Holló et al. 1994; Homolya et al. 1993; Laska et al. 2002; Liminga et al. 1994; Pivčević and Zaja 2006; Tiberghien and Loor 1996), modified to avoid extra washing, centrifugation, and lysis steps. Calcein-AM is a non-fluorescent, highly lipid-soluble molecule that diffuses across the cell membrane and can be pumped out by both P-gp and MRP1 (Essodaigui et al. 1998). Inside the cell, calcein-AM is metabolized by cytosolic esterases into the hydrophilic and fluorescent calcein. Calcein is not a P-gp substrate, and therefore it will accumulate in the cell (Holló et al. 1994). The calcein retention is measured as increased intracellular fluorescence, indicating the degree of inhibition of the efflux pumps P-gp and MRP1 (Eneroth et al. 2001; Laska et al. 2002).

The P-gp-overexpressing Madin–Darby canine kidney cells stably transfected with the human MDR1 gene (MDCKII-MDR1) were used as well as the parental MDCKII cells for comparison, with the use of calcein-AM as a model substrate, and verapamil and PSC-833 as specific inhibitors that are well established and commonly used agents known for their ability to inhibit P-gp in drug-resistant cell lines (Ford 1996; Tan et al. 2000; Teodori et al. 2002). A known specific inhibitor of the MRP1 transporter (Gekeler et al. 1995), MK571, was also evaluated in the assay to assess the potential contribution of MRP1 in the calcein efflux. After validation of the method with these model inhibitors, we studied several groups of environmentally relevant compounds for which there were indications of mixture or supramaximal effects (pentachlorophenol [PCP], hexabromocyclododecane [HBCD], bisphenol A [BPA], nonylphenol (NP), genistein, and quercetin (Montaño et al. 2010; Schriks et al. 2006); A. Georgantzopoulou et al., unpublished results), as well as interference with intercellular communication (perfluorinated compounds such as perfluorooctanoic acid [PFOA] and perfluorooctane sulfonate [PFOS] (Hu et al. 2003; Stevenson et al. 2006; Upham et al. 2009) and with membrane sodium ion channels (the organochlorine pesticides o,p'-DDT, methoxychlor, and dieldrin). In addition, compounds suggested to interact with MDR (the organophosphate pesticides malathion, fenitrothion, and diazinon (Lecoeur et al. 2006) and interfere with MDR as well as the thyroxine transporters (amiodarone) (Cermanova et al. 2010; Schriks et al. 2006) and widespread soil and groundwater contaminants with high bioaccumulation potential and persistence in the environment (chlorinated alkanes)

(Zvinavashe et al. 2008) were studied for their effect relative to that of verapamil in the calcein-AM-based P-gp cellular efflux pump inhibition assay (CEPIA).

## Materials and Methods

### *Chemicals*

Amiodarone (CAS number 1951-25-3), genistein ( $\geq 98\%$ , CAS number 446-72-0), PCP (98%, CAS number 87-86-5), diethylstilbesterol (DES; CAS number 56-53-1), and verapamil ( $\geq 99\%$ , CAS number 152-11-4) were obtained from Sigma-Aldrich. Bisphenol A (CAS number 80-05-7) and PFOA (CAS number 335-67-1) were obtained from Aldrich Chemical. The PSC-833 (valsopodar; CAS number 121584-18-7) was kindly provided by Novartis. The MK571 was purchased from Enzo Life Sciences. The technical mixture of HBCD (CAS number 25637-99-4) was a kind gift from the Dutch National Institute for Public Health and the Environment (RIVM). Triphenyltin chloride (TPT-Cl; CAS number 639-58-7), 17- $\beta$ -estradiol (E2; CAS number 50-28-2), dieldrin (CAS number 60-57-1), diazinon (CAS number 333-41-5), fenitrothion (CAS number 122-14-5), malathion (CAS number 121-75-5), methoxychlor (CAS number 72-43-5), and *o,p'*-DDT (CAS number 789-02-6) were all obtained from Riedel de Haën, and butyl benzyl phthalate (BBP; CAS number 85-68-7) was obtained from TCI. The compounds perfluorobutansulfonate (potassium salt; PFBS; CAS number 29420-43-3), perfluorodecanoic acid (PFDCa; CAS number 335-76-2), 1,3-dichloropropane (CAS number 142-28-9), 1-chloro-2-methylbutane (CAS number 616-13-7), 1,1-dichloro-3,3-dimethylbutane (CAS number 6130-96-7), 1,9-dichlorononane (CAS number 821-99-8), 1-chlorodecane (CAS number 1002-69-3), and 1-chlorotetradecane (CAS number 2425-54-9) were all obtained from IMARES. A technical mixture of 4-nonylphenol (NP; CAS number 104-40-5) and PFOS were obtained from Fluka. Quercetin (CAS number 117-39-5) was acquired from Acros Organics. Calcein-AM was purchased from Molecular Probes.

All compounds were dissolved in dimethyl sulfoxide (DMSO; Sigma) except for PFBS and PFDCa, which were prepared in methanol. For exposure, the compounds were further diluted in phosphate-buffered saline (PBS) to the desired concentrations with a final DMSO or methanol concentration of 0.5% (v/v).

### *Cell culture*

Dulbecco's minimum essential medium with Glutamax (DMEM-Glutamax), PBS, penicillin, streptomycin, and fetal bovine serum (FBS) were all obtained from Gibco, Invitrogen. The MDCKII-MDR1 cells were kindly provided by A.H. Schinkel (The Netherlands Cancer Institute, Amsterdam, the Netherlands) (Evers et al. 2000). The MDCKII-wild type (MDCKII-wt) cells were obtained from the European Collection of Cell Cultures. Both cell lines were cultured in DMEM-Glutamax supplemented with 10% (v/v) FBS, 1% (v/v) penicillin and streptomycin, and grown in conditions of 37 °C and 5% CO<sub>2</sub> in a humidified atmosphere. The culture medium was changed 3 times per week. When 70% to 90% confluency was reached, the cells were split with trypsin-ethylenediamine tetraacetic acid.

### *Reverse transcription quantitative polymerase chain reaction*

The MDCKII-wt (passage numbers 35, 36, 38, and 39) and MDCKII-MDR1 cells (passage numbers 40, 41, 43, and 44) were seeded in 6-well plates in triplicate at a concentration of  $1 \times 10^5$  cells/mL (3 mL/well) and grown for 2 d. Cells were collected using 0.2 mL trypsin, and after 2 washing steps with PBS, 0.35 mL RLT buffer (RNeasy Plant Mini Kit, Qiagen) supplemented with 1% mercaptoethanol was added to the cell pellet. The total RNA was extracted by using the RNeasy Plant Mini Kit (Qiagen) including deoxyribonuclease (DNase) treatment (following the manufacturer's instructions). Quality control was performed with the RNA Nano 6000 assay (Agilent Technologies) using a 2100 Bioanalyzer (Agilent Technologies). All RNA samples displayed RNA integrity numbers above 8. The purity and concentration of RNA were assessed by measuring the absorbance at 230 nm, 260 nm, and 280 nm using a Nanodrop ND1000 spectrophotometer (Thermoscientific).

Quantitative polymerase chain reaction (qPCR) primers for canine glyceraldehyde-3-phosphate dehydrogenase (dGAPDH; GenBank accession number AB038240.1; forward: 5'-ATTCCACGGCACAGTCAAG-3'; reverse: 5'-TACTCAGCACCAGCATCACC-3') and canine MDR1 (dMDR1; GenBank accession number DQ068953.1; forward: 5'-TTGCTGGTTTTGATGATGGA-3'; reverse: 5'-CTGGACCCTGAATCTTTTGG-3') were obtained from K. Kuteykin-Teplyakov (Kuteykin-Teplyakov et al. 2010). Primers for human MDR1 (hMDR1; GenBank accession number NM\_000927.3; forward: 5'-ACGGAAGGCCTAATGCCG-3'; reverse: 5'-GGGATAGTTGAATACAACCTTCACC-3'; amplicon size: 69 bp) were designed using the Primer3 software (<http://frodo.wi.mit.edu/>) with

the following criteria: primer size between 18 base pairs (bp) and 25 bp, guanosine-cytosine (GC) content between 30% and 70%, amplicon size from 50 bp to 150 bp, and  $T_m$  of primers in the 57 °C to 61.8 °C range. Matching primer sets were checked using NetPrimer (<http://www.premierbiosoft.com/netprimer/index.html>) for unexpected secondary structures (DG should be below -5 kcal/mol with default settings). To test the specificity of primers, a BLASTn (<http://blast.ncbi.nlm.nih.gov/Blast.cgi>) search was used.

Reverse transcription (RT) was performed using M-MuLV Reverse Transcriptase (RNase H-), Murine RNase Inhibitor (New England Biolabs), and Random primers (Invitrogen) following the manufacturers' guidelines. Five micrograms of RNA in a 20  $\mu$ L final volume were used. The PCR was performed on a Vii7 Real-time PCR system (Life Technologies) using Mesa Green Low Rox Real-time PCR Kits (Eurogentec) with the following final concentrations in a 25  $\mu$ L final volume: 1xMasterMix, 100 nM forward and reverse primers, 0.4 ng/ $\mu$ L complementary (c)DNA. No template control and RT-control samples were included in each plate, and each sample was run in triplicate. Thermal cycling conditions were as follows: initial 5-min denaturation at 95 °C, followed by 45 cycles of 15 s at 95 °C and 1 min at 60 °C, and a final dissociation step. Primer specificity was controlled by the presence of a single peak in the melting curve, and PCR efficiency (hMDR1: 1.8756; dMDR1: 1.9325; dGAPDH: 1.8816) was assessed using decreasing 5-fold dilutions (from 25 ng to 0.04 ng and no cDNA). Relative expression was calculated taking into account gene-specific PCR efficiency [39], and the dGAPDH gene was used as the reference gene for normalization. Expression of dMDR1 in MDCKII-wt was used as the calibrator.

#### *Confocal laser scanning microscopy for visualization of P-gp*

The MDCKII-wt and MDCKII-MDR1 cells were seeded in Lab-Tek II chambers (Thermoscientific) at a concentration of  $1.7 \times 10^5$  cells/mL (0.4 mL/well). After 24 h, the medium was removed, the cells were washed twice in PBS, and cellular membranes were stained for 10 min using 200-fold diluted *Ricinus communis* agglutinin 1 coupled to fluorescein isothiocyanate (RCA-1-FITC; Vector Labs). After washing with PBS, the cells were fixed and permeabilized with ice-cold methanol (100%) at -20 °C for 10 min. Fixed cells were incubated for 30 min with 10% bovine serum albumin fraction V (BSA) in PBS (w/v) to block nonspecific binding. Cells were then incubated for 1 h at room temperature with the 100-fold diluted primary antibody against P-gp C219 (MA1-26528, Thermoscientific). After being washed 3

times with PBS containing 2% BSA, the cells were incubated with the 200-fold diluted secondary antibody goat anti-mouse Cy3 (405309; Biolegend). Nuclei were counterstained with 1:10 000 diluted Hoechst 33342 (AnaSpec). Antibodies were diluted in PBS containing 2% BSA. A Zeiss LSM 510 Meta with an inverted Zeiss microscope (Axiovert 200M, lasers: HeNe 633 nm, HeNe 543 nm, Ar 488 nm, and Diode 405 nm) was used. Image processing and visualization were done with the Zeiss Software ZEN Lite 2011 and ImageJ (<http://rsbweb.nih.gov/ij/>).

#### *Optimization of the calcein-AM assay*

The cells were seeded in 96-well plates with a clear flat bottom (100  $\mu$ L/well) at a density of  $5 \times 10^5$  cells/mL. Subsequently, they were cultured for 24 h at 5% CO<sub>2</sub> and 37 °C in a humidified atmosphere, after which they formed the confluent monolayer needed to produce the highest fluorescence signal after 30 min of incubation with calcein-AM. When the confluent monolayer was formed, the medium was removed and the cells were washed with pre-warmed (37 °C) PBS. Next, the cells were exposed to the test compounds diluted in 100  $\mu$ L PBS (final DMSO concentration 0.5% [v/v]). After 30 min of exposure, 100  $\mu$ L of 5  $\mu$ M calcein-AM in PBS was added, without an additional washing step, reaching a final concentration of 2.5  $\mu$ M; then 30 min later, the fluorescence was directly measured using a microplate reader (Synergy 2; BioTek Instruments) at 485-nm excitation and 530-nm emission. The lowest concentration of calcein-AM in the linear range of the standard curve that produced a sufficient and significant signal (maximizing the fluorescent signal to background noise ratio, 7-fold increase) was chosen for both cell lines, which was 2.5  $\mu$ M calcein-AM (Homolya et al. 1993; Laska et al. 2002). In addition, the shortest incubation period that produced that signal was selected to avoid interference by spontaneous hydrolysis of calcein-AM. The exposure medium chosen was PBS because background fluorescence of this buffer was lower than that of DMEM without phenol red and FBS. However, PBS is not suitable for longer exposures, because the condition of the cells will then deteriorate.

For evaluation of potential calcein fluorescence quenching by the tested compounds, we measured the fluorescence of the cells incubated with only calcein-AM for 60 min and the cells incubated with calcein-AM followed by the addition of a test compound at the highest and lowest test concentrations for another 20 min. The added test compounds never influenced the fluorescence signal, indicating no fluorescence quenching.

The potential of the contaminants to inhibit the cytosolic esterases was evaluated by pre-exposing the cells to the compounds for 20 min, followed by incubation with 300  $\mu\text{M}$  verapamil for another 15 min, and finally by a calcein-AM addition according to the CEPIA protocol. When the calcein fluorescence after the addition of verapamil did not reach the maximal levels (verapamil alone), the esterases were considered to be (partly) inhibited (Pivčević and Zaja 2006).

### *Cytotoxicity evaluation*

Immediately after the end of exposure, the exposure medium was removed, cells were washed with PBS, and 120  $\mu\text{L}$  of MTS solution [3-(4,5-dimethylthiazol-2-yl)-5-(3-carboxymethoxyphenyl)-2-(4-sulfophenyl)-2H-tetrazolium salt] (Promega) was added to each well. After 1 h of incubation (37 °C, 5%  $\text{CO}_2$ ), the absorbance was measured at 490 nm with a microplate reader (Synergy 2, BioTek Instruments). The concentrations that were proved to be non-toxic to the cells in the MTS assay are shown in the P-gp inhibition assay.

### *Data analysis*

The results are expressed as mean  $\pm$  standard deviation (SD) of at least 2 independent experiments in triplicate. The curve fitting, regression analyses, and determination of the 50% effect concentration (EC50) to characterize the potencies of the compounds were performed with GraphPad Prism 5 (GraphPad Software) and SigmaPlot (Systat Software). Statistical comparisons among mean values of the different treatments as well as the solvent controls were performed by one-way analysis of variance followed by a Tukey's Multiple Comparison Test (GraphPad Prism 5). Results with a  $p$  value below 0.05 were considered significant.

Spontaneous hydrolysis of calcein-AM was corrected by subtracting the mean value obtained from 2.5  $\mu\text{M}$  calcein-AM in PBS incubated at 37 °C for 30 min without cells (relative fluorescence units RFUs). On each plate, verapamil calibration points were included to correct plate-to-plate variation. The 10% effect concentrations (EC10s) were used to express inhibitory as well as inductive effects as relative potencies (REPs) by dividing the EC10 of verapamil by the EC10 of the test compounds ( $\text{REP} = \text{EC}_{10\text{verapamil}} / \text{EC}_{10\text{test compound}}$ ). The maximal inhibition of the P-gp activity (maximal fluorescence values) by the test compounds was expressed relative to maximal inhibition by verapamil set at 100% (% P-gp Inhibition =  $[(\text{RFU}_{\text{test compound}} - \text{RFU}_{\text{control}}) / (\text{RFU}_{\text{verapamil}} - \text{RFU}_{\text{control}})] \times 100$ ). The

calcein retention induced by the compounds in the MDCKII-MDR1 cells was expressed relative to the calcein retention in their own DMSO-treated response set at 1. For the MDCKII-wt cells, the calcein retention was calculated in the same way.

## Results

Expression of the endogenous (canine) MDR1 gene was significantly but only slightly (1.6-fold) higher in the parental MDCKII cell line in comparison with the MDCKII-MDR1 cells (Figure 1A). As expected, no human MDR1 expression was detected in the MDCKII-wt cells (Figure 1B). Relative expression of human hMDR1 in the MDCKII-MDR1 cells was approximately 17 times higher than the canine dMDR1 in the MDCKII-wt cells.

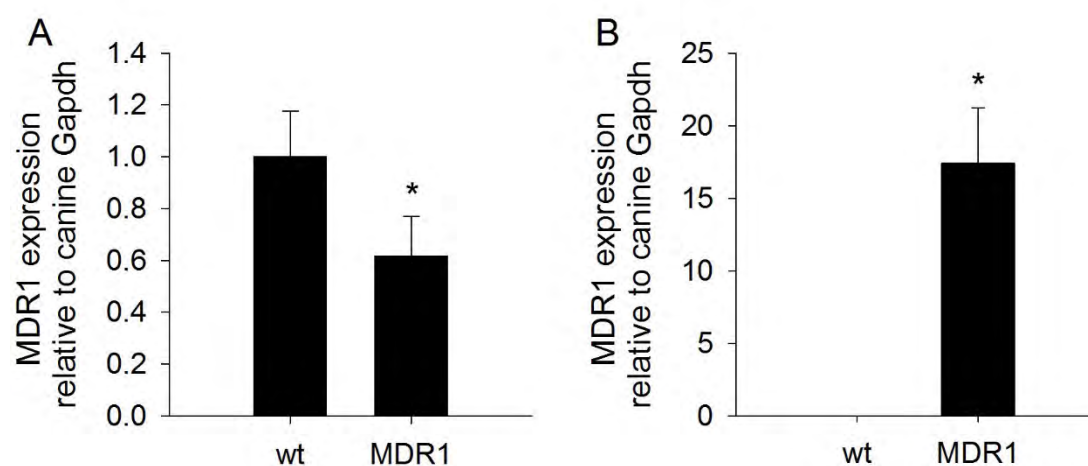


**Figure 1.** Expression of (A) endogenous MDR1 (canine, dMDR1) and (B) human MDR1 (hMDR1) in the parental (wild-type) and MDR1 overexpressing MDCKII cells. Results are expressed as relative expression normalized by the reference gene GAPDH. Data are shown as mean  $\pm$  standard deviation of 4 biological replicates in duplicate (4 different passages). \*  $p < 0.05$ , significant differences between groups.

The cellular localization of total P-gp (endogenous plus human) was confirmed with confocal laser scanning microscopy (Figure 2). P-glycoprotein was widely detectable in the P-gp-overexpressing MDCKII cells, with the signal obtained by the C219 antibody being much stronger than in the parental MDCKII cells (Figure 2).

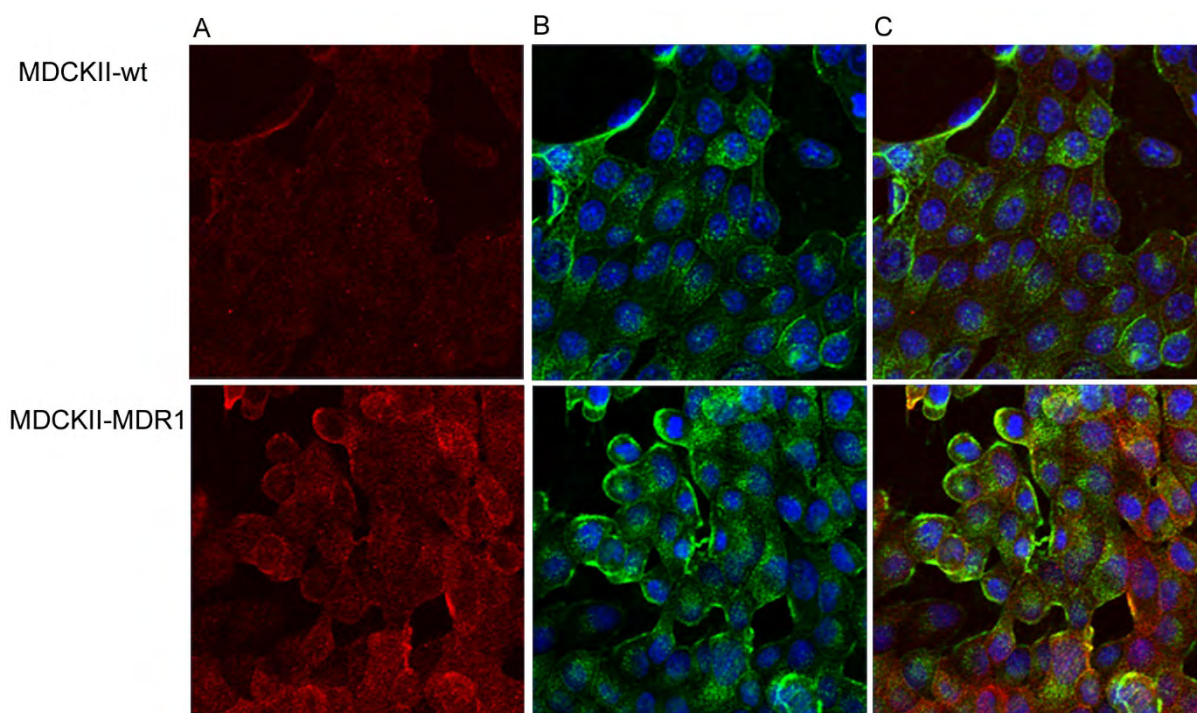


**Figure 2.** Immunolocalization of total P-glycoprotein (P-gp) in wild-type and MDR1 overexpressing MDCKII cells by confocal microscopy. P-gp was detected by goat anti-mouse Cy3 secondary antibody (red, A). Cellular membranes were stained using *Ricinus communis* agglutinin 1 coupled to fluorescein isothiocyanate (RCA-1-FITC; green, B). Nuclei were counterstained with Hoechst 33342 (blue, B). (C) Represents an overlay of all 3 channels combined (A and B).

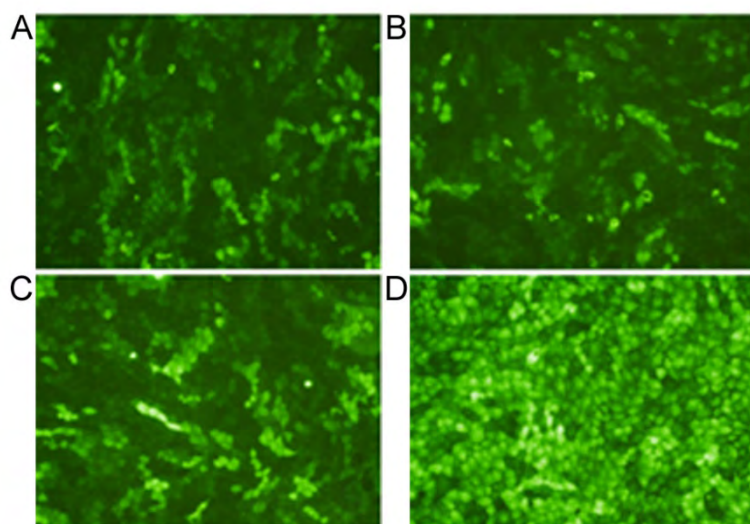


**Figure 3.** Fluorescence images of calcein accumulation in MDCKII-MDR1 cells incubated for 30 min in the absence (A) or presence of verapamil in concentrations of (B) 1  $\mu$ M, (C) 10  $\mu$ M, and (D) 100  $\mu$ M. An increased calcein accumulation was observed at 10  $\mu$ M and 100  $\mu$ M.

Figures 3 and 4 show the dose–response curves for increased accumulation of calcein in MDCKII-MDR1 and MDCKII-wt cells on exposure to the model P-gp inhibitor verapamil, PSC-833, and amiodarone in the CEPIA optimized for exposure medium, cell concentration, incubation time, and calcein-AM substrate concentration. In the absence of an inhibitor, the MDCKII-MDR1 cells showed much lower fluorescence values compared with the wild type (10

times lower). The MDCKII-wt cells were little affected by the increasing concentrations of the test compounds. At the highest concentration of amiodarone, a 28-fold increase in calcein fluorescence in the MDCKII-MDR1 cells was observed compared with a 2-fold increase in the MDCKII-wt cells (Figure 4). Concentrations of approximately 50  $\mu\text{M}$  verapamil increased the calcein fluorescence in MDCKII-MDR1 cells to a level comparable to the control MDCKII-wt cells. As expected, the selective inhibitor PSC-833 was found to be the most potent compound, followed by verapamil and amiodarone (Table 1).

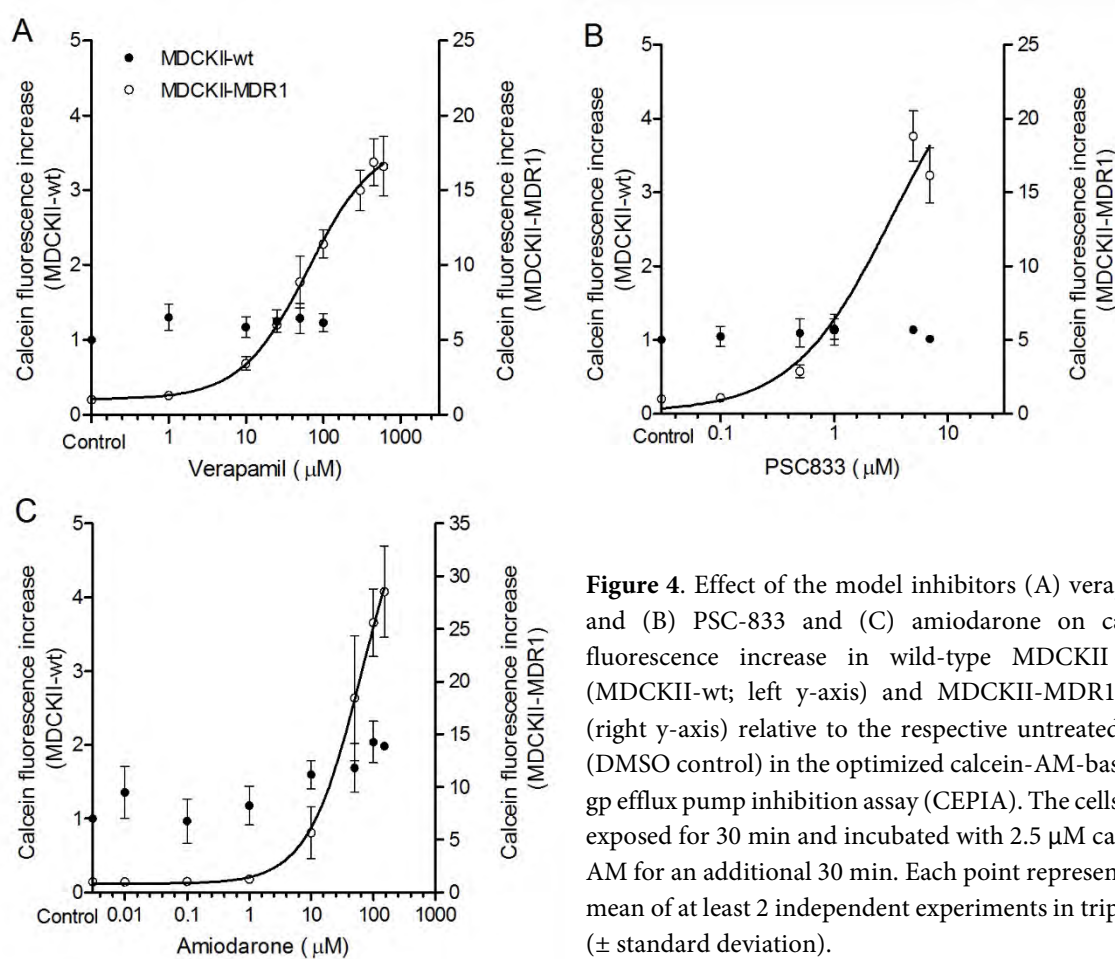


**Figure 4.** Effect of the model inhibitors (A) verapamil and (B) PSC-833 and (C) amiodarone on calcein fluorescence increase in wild-type MDCKII cells (MDCKII-wt; left y-axis) and MDCKII-MDR1 cells (right y-axis) relative to the respective untreated cells (DMSO control) in the optimized calcein-AM-based P-gp efflux pump inhibition assay (CEPIA). The cells were exposed for 30 min and incubated with 2.5  $\mu\text{M}$  calcein-AM for an additional 30 min. Each point represents the mean of at least 2 independent experiments in triplicate ( $\pm$  standard deviation).

Among the compounds tested in the CEPIA in the MDCKII-MDR1 cells, several inhibited the efflux of calcein-AM (Table 1). In particular, PCP, BPA, PFOS, and PFOA increased the fluorescence in the assay in a dose-dependent manner (Table 1 and Figure 5), some with potencies even higher than the model inhibitor verapamil. For instance, PCP had an REP of 64, although it only reached 12% of maximal verapamil response. For some compounds, (e.g. BPA, PFOS, and PFOA), the dose-response curve did not reach maximum effect at the exposure concentrations chosen. As a result of the efflux pump inhibition by PFOS, the calcein

fluorescence increased to 64% relative to verapamil in the MDCKII-MDR1 cells while treatment with PFOA resulted in calcein accumulation up to 34% of the verapamil maximum (Figure 5 and Table 1).

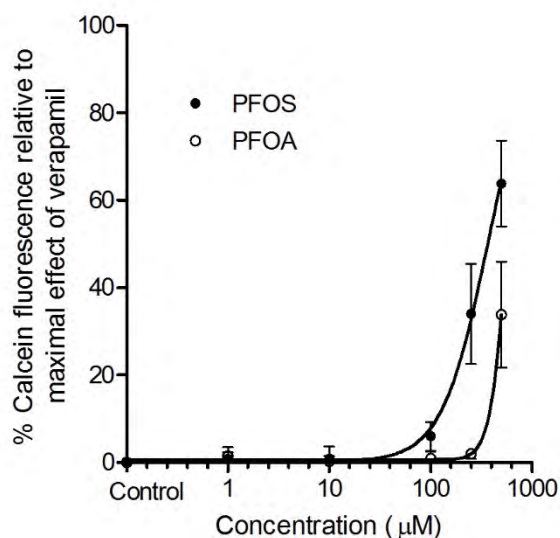


**Figure 5.** Effects of the perfluorinated organic compounds perfluorooctane sulfonate (PFOS) and perfluorooctanoic acid (PFOA) in MDCKII-MDR1 expressed as percentage calcein fluorescence relative to the maximal effect of verapamil (set at 100%). Each point represents the mean of 3 independent experiments in triplicate ( $\pm$  standard deviation).

At the highest concentrations tested, PFOS and PFOA led to 10-fold and 5.4-fold increases in fluorescence levels compared with unexposed MDCKII-MDR1 cells, respectively, while 1.2-fold and 1.4-fold increases were observed in the case of MDCKII-wt. The compounds tested without cells or calcein-AM did not give rise to fluorescence, nor did they quench the verapamil-induced fluorescence, even at the highest concentration tested (data not shown). The standard MRP1 inhibitor MK571 had only a minor effect on the calcein efflux from MDCKII-MDR1 cells, with fluorescence levels being only 7% of verapamil maximum at the highest concentration tested (50  $\mu$ M; Table 1).

In the CEPIA some compounds decreased the control fluorescence. For instance, fenitrothion showed the strongest decrease at 250  $\mu\text{M}$  (76% reduction relative to the DMSO-exposed controls set at 100%; Table 1) whereas *o,p'*-DDT reduced the signal by 38% compared with fenitrothion at the same concentration (Figure 6 and Table 1). On addition of 300  $\mu\text{M}$  verapamil at the end of the exposure period, the fluorescence levels increased but did not reach the fluorescence levels induced by 300  $\mu\text{M}$  of verapamil (set at 100%; Figure 6). At the highest concentrations of methoxychlor and *o,p'*-DDT, decreases in fluorescence were still observed, of 29% and 53%, respectively.

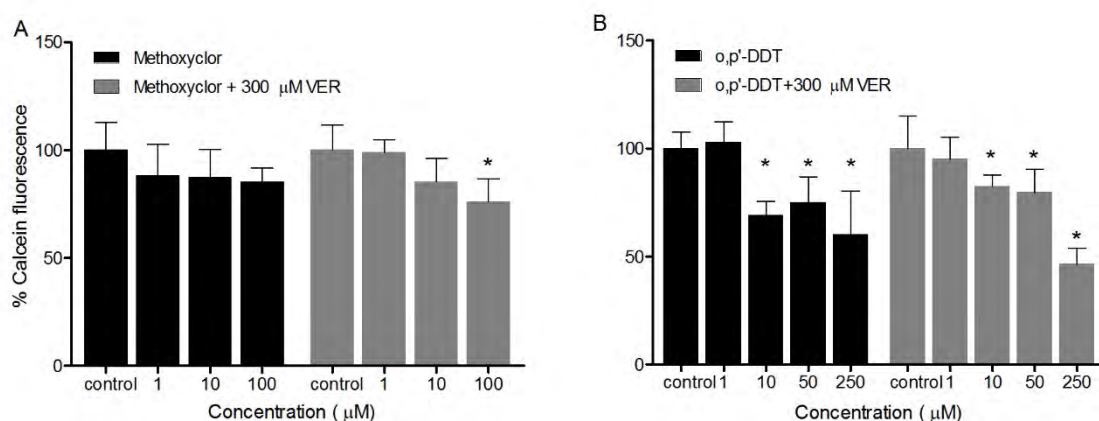


**Figure 6.** Response MDCKII-MDR1 cells of compounds that reduced the signal, as percentage fluorescence relative to solvent control (black bars) or to maximal levels reached with 300  $\mu\text{M}$  verapamil (VER) (gray bars) on exposure to (A) methoxychlor and (B) *o,p'*-DDT in the absence or presence of 300  $\mu\text{M}$  verapamil. Verapamil was added at the end of the exposure for 15 min. Each point represents the mean of at least 2 independent experiments in triplicate ( $\pm$  standard deviation). \*  $p < 0.05$ , significant differences between different treatment groups and control.

**Table 1.** Overview of results obtained in the calcein-AM-based P-gp cellular efflux pump inhibition assay (CEPIA) with MDCKII-MDR1 cells

Compound	Max Conc Tested ( $\mu\text{M}$ ) <sup>b</sup>	Response <sup>c</sup>	EC10/EC50 ( $\mu\text{M}$ ) <sup>d</sup>	NOEC ( $\mu\text{M}$ ) <sup>d</sup>	REP <sup>d</sup>	Max effect at highest dose tested (% relative to VER max) <sup>d</sup>
<i>Model Inhibitors<sup>a</sup></i>						
Verapamil	600	++	6.4 (4.1-9.9)/ 63.9 (52.5-77.7)	1	1	100 (450 $\mu\text{M}$ )
PSC-833	7	++	0.66 (0.08-5.4)/ 3.2 (0.2-46.6)	0.1	9.7	112 (5 $\mu\text{M}$ )
Amiodarone	150	++	7.8 (7.1-8.5)/ 65.4 (52.7-81.3)	1	0.8	173 (150 $\mu\text{M}$ )
MK571	50	0	N.D.	N.D.	N.D.	7 (50 $\mu\text{M}$ )
<i>Supermaximal effects reported<sup>a</sup></i>						
Bisphenol A	250	±	11.8 (1.7-80.4)/ N.D.	10	0.5	14 (250 $\mu\text{M}$ )
Nonylphenol	10	0	N.D.	N.D.	N.D.	N.D. (10 $\mu\text{M}$ )
Genistein	50	0	N.D.	N.D.	N.D.	N.D. (50 $\mu\text{M}$ )
Quercetin	250	±	24.6 (N.D.)/ N.D.	10	0.3	11 (250 $\mu\text{M}$ )
<i>Potentiators in some assays<sup>a</sup></i>						
PCP	10	±	0.1 (0.04-0.4)/ 1.6 (0.7-1.9)	0.01	64	12 (10 $\mu\text{M}$ )
TBT-O	0.5	0	N.D.	N.D.	N.D.	N.D. (0.5 $\mu\text{M}$ )
TPT-Cl	0.1	0	N.D.	N.D.	N.D.	N.D.
<i>Indications for interference with cell membranes<sup>a</sup></i>						
BBP	50	±	3 (1.2-8)/ N.D.	1	1.3	24 (50 $\mu\text{M}$ )
PFOS	500	++	116.4 (92.1-147) / N.D.	100	0.05	64 (500 $\mu\text{M}$ )
PFOA	500	+	374.2 (325.7-430)/ N.D.	250	0.01	34 (500 $\mu\text{M}$ )
PFBS	10	0	N.D.	N.D.	N.D.	N.D. (10 $\mu\text{M}$ )
PFDCa	10	0	N.D.	N.D.	N.D.	N.D. (10 $\mu\text{M}$ )
Dieldrin	25	0	N.D.	N.D.	N.D.	N.D. (25 $\mu\text{M}$ )
Malathion	150	0	N.D.	N.D.	N.D.	N.D. (150 $\mu\text{M}$ )
Diazinon	0.4	0	N.D.	N.D.	N.D.	N.D. (0.4 $\mu\text{M}$ )

<i>Widespread persistent, bioaccumulative contaminants<sup>a</sup></i>						
1,3-dichloropropane	500	0	N.D.	N.D.	N.D.	N.D. (500 µM)
1-chloro-2-methylbutane	500	0	N.D.	N.D.	N.D.	N.D. (500 µM)
1,1-dichloro-3,3-dimethylbutane	250	0	N.D.	N.D.	N.D.	N.D. (250 µM)
1,9-dichlorononane	500	±	N.D.	N.D.	N.D.	N.D. (500 µM)
1-chlorodecane	500	0	N.D.	N.D.	N.D.	N.D. (500 µM)
1-chlorotetradecane	100	0	N.D.	N.D.	N.D.	N.D. (100 µM)
<i>Potentiators in some assays<sup>a</sup></i>						
HBCD	5	-	0.4 (0.2-0.9)/ 4 (2.2-7.1)	<1	1.8	-55° (10 µM)
<i>Indications for interference with cell membranes<sup>a</sup></i>						
Fenitrothion	250	--	0.7 (N.D.)/ 10.9 (2.7-44.6)	<10	1	-100° (250 µM)
o,p'-DDT	250	-	0.9 (N.D.)/ 2.2 (0.02-282.1)	<1	0.8	-38.5° (250 µM)
Methoxychlor	100	-	N.D.	N.D.	N.D.	-17.3° (100 µM)

<sup>a</sup>Rationale for choosing the compound.

<sup>b</sup>The maximum concentration tested differed between the compounds.

<sup>c</sup>The response is qualified on the following scale: ++ = strong increase in calcein fluorescence (>60% relative to verapamil); + = increase in calcein fluorescence; ± = increase in calcein fluorescence but not very strong (<30% inhibition relative to verapamil); 0 = no effect in the concentration range tested; -- = strong decrease in calcein fluorescence.

<sup>d</sup>The responses are quantified as 10% and 50% effective concentrations (EC10 and EC50, respectively, with the 95% confidence intervals in parentheses); the highest concentration without observed effect (NOEC); the relative potency (REP) compared with verapamil at the EC10; and the maximal response as a percentage relative to the maximal effect of verapamil at 450 µM, reached at the concentration given in parentheses.

<sup>e</sup>Fenitrothion is used as reference for compounds reducing the fluorescence.

N.D. = not determined because these compounds did not induce a significant effect in the CEPIA or the 95% confidence intervals were too wide to calculate a reliable effective concentration; PCP = pentachlorophenol; TBT-O = tributyltin oxide; TPT-Cl = triphenyltin chloride; BBP = butyl benzyl phthalate; PFOS = perfluorooctane sulfonate; PFOA = perfluorooctanoic acid; PFBS = perfluorobutansulfonate; PFDcA = perfluorodecanoic acid; HBCD = hexabromocyclododecane.

## Discussion

The aim of the present study was to explore and quantify the inhibition of the P-gp cellular efflux pump by several ubiquitous aquatic contaminants. Based on methods commonly used in pharmacological research, the calcein-AM method was optimized with P-gp-overexpressing MDCKII-MDR1 as well as MDCKII-wt cells in a 96-well plate format.

### *Method optimization*

The basis of the calcein-AM assay has been described in the field of pharmacological and toxicokinetic research (Homolya et al. 1993; Tiberghien and Loor 1996; van Zanden et al. 2005). It has also been used in ecotoxicological studies with several modifications, with various cell lines (Pivčević and Zaja 2006) including some from fish as models (Caminada et al. 2008). Omission of the washing, centrifugation, and lysis steps between exposure; substrate addition; and final reading allowed a fast and reproducible quantification of the inhibition of the cellular efflux of calcein-AM in the P-gp-overexpressing MDCKII-MDR1 cells. The MDCKII-MDR1 cells had much lower baseline values (10 times lower) of calcein fluorescence (in control with 2.5  $\mu$ M calcein-AM) compared with MDCKII-wt. This was to be expected because of the higher membrane density of P-gp pumps in the transfected cells and the subsequent increased numbers of P-gp transporter-substrate complexes formed, allowing a larger increase in fluorescence on blocking of the efflux pumps compared with the MDCKII-wt cells. The maximum increase in fluorescence was more than 17 times higher in the MDCKII-MDR1 cells exposed to verapamil or amiodarone compared with the control MDCKII-MDR1 cells exposed to the solvent DMSO only. Verapamil-sensitive P-gp activity in MDCKII-wt cells was observed showing the presence of a functional canine P-gp. In the MDCKII-wt cells, exposure to verapamil and amiodarone increased the fluorescence only up to 2 times.

Functional differences between the human and canine P-gp in terms of substrate binding affinities are not yet fully understood and cannot be excluded, because interspecies differences could affect substrate recognition and transport. It has been previously observed that the transport relationship between MDCKII-wt and MDCKII-MDR1 for different substrates was not always consistent (Taub et al. 2005). The assay was specific for P-gp because the well-known specific MRP1 inhibitor MK571 had only a minor effect (7% accumulation of calcein relative to the maximum of verapamil), suggesting that the increase in fluorescence observed by the compounds in the assay is indeed mainly resulting from the presence of P-gp.

*Effects of the compounds*

After optimization of the assay, several classes of compounds were evaluated for their potential to interfere with the P-gp efflux pump. Of all compounds tested, PCP, BPA, and quercetin were the most potent, as indicated by their low EC<sub>10</sub>s (Table 1). The strong inhibition by PCP is in accordance with the reported inhibition of the efflux of rhodamine B (a fluorescence dye known to be a P-gp substrate) in gill tissue of the marine mussel *Mytilus californiacus* reaching saturation at a concentration of 7.5  $\mu$ M (Cornwall et al. 1995). The maximal P-gp inhibition could not be reached for all compounds (e.g. Figure 5), as the maximum concentration that could be tested for practical reasons (as well as the cytotoxicity) differed between compounds. The P-gp inhibition by PFOS and PFOA was strong and dose dependent between 100  $\mu$ M and 500  $\mu$ M (Figure 5). The maximal response had not yet been reached and the compounds were not yet toxic for the cells at 500  $\mu$ M. It has been suggested that the fatty acid-mimicking effect of perfluorinated organic compounds (PFOCs) increases the fluidity of biological membranes thereby altering the membrane structure and function (Hu et al. 2003). This could be an alternative explanation for the strong increase in calcein accumulation. However, the same extent of response was not observed in the case of MDCKII-wt cells, which showed only a 1.4-fold increase in fluorescence at the highest concentration compared with the 11-fold increase in MDCKII-MDR1 cells, excluding this alternative mode of action. The maximum exposure concentrations for PFBS and PFDcA (<100  $\mu$ M) were probably too low to have an effect in the CEPIA. In a study comparing the effects of 2 PFOCs with different chain lengths for their effect on cell membrane permeability, PFBS, with the shortest carbon chain length (C4), had no effect on cell membrane permeability whereas PFOS, with a longer carbon chain length (C8), had a higher potential for interacting with membranes (Jones et al. 2003). Longer chain perfluoroalkyl acids inhibited P-gp activity in the mussel *Mytilus californiacus*, with perfluorononanoate leading to an increase of P-gp levels in the gill (Stevenson et al. 2006).

Of the 2 flavonoids studied (genistein and quercetin), only quercetin exhibited a dose-related increase in inhibition. In previous studies, quercetin as well as other flavonoids have been shown to interfere with P-gp by acting on both the ATP-binding site and the substrate-binding site of P-gp (Castro and Altenberg 1997; Teodori et al. 2002). Possibly the exposure concentration of genistein was not high enough to elicit a significant effect in the CEPIA. Genistein previously has been shown to inhibit the MRP1- and P-gp-mediated transport in P-gp-overexpressing cell lines at concentrations greater than 200  $\mu$ M (Castro and Altenberg

1997). Nonylphenol did not interfere at all with the P-gp efflux pump, which is in agreement with previous research showing that NP ethoxylates (and not NP) are substrates of P-gp, whereas a lack of ATPase activity stimulation on exposure to NP was observed (Loo and Clarke 1998). Nonylphenol diethoxylate inhibited the efflux of rhodamine 123 (a P-gp substrate) from rainbow trout hepatocytes (Sturm et al. 2001), whereas NP had no effect on P-gp-overexpressing fish hepatoma cells (Caminada et al. 2008).

Surprisingly, HBCD and the pesticides *o,p'*-DDT, methoxychlor, and fenitrothion decreased the calcein fluorescence, which was not caused by the quenching of the fluorescence (data not shown). These results may suggest stimulation of P-gp by these compounds or inhibition of the esterase activity that leads to the conversion of calcein-AM into calcein. This would be expected for acetylcholinesterase inhibitors such as organophosphate pesticides (Hamers et al. 2000). At the end of the exposure period, the addition of 300  $\mu$ M verapamil led to an increase of calcein fluorescence levels across all concentrations although not as high as the maximal levels reached with exposure to 300  $\mu$ M verapamil alone (Figure 6). This observation suggests that the esterases could have been partially inhibited. The organophosphate pesticide malathion, however, did not induce a response in the CEPIA, whereas parathion and chlorpyrifos have been previously reported to inhibit P-gp-mediated efflux of doxorubicin (Bain and LeBlanc 1996). Another potential mechanism behind the decrease in fluorescence in the cells could be allosteric activation of P-gp. It has been suggested that P-gp may contain allosteric sites in addition to the drug binding sites (Litman et al. 2000; Martin et al. 1999). Binding of HBCD or fenitrothion, for example, to the allosteric binding sites of P-gp could increase the transporter's activity, resulting in enhanced calcein-AM efflux. The phenomenon of putative stimulation of P-gp activity clearly requires further mechanistic study before its meaning can be interpreted.

Despite their structural differences, the compounds that interact with P-gp seem to share some common characteristics including a molecular mass of over 300 Da (optimal 391–490 Da) and the fact that they are moderately hydrophobic with an octanol–water partition coefficient ( $\log K_{ow}$ ) of 3.6–4.5 (Bain and LeBlanc 1996). However, none of the chlorinated alkanes used in the present study interacted with the transporter despite the moderate hydrophobicity of 1-chloro-2-methylbutane and 1,1-dichloro-3,3-dimethylbutane. These results suggest that the potential for interaction with P-gp, at least in the case of the chlorinated alkanes tested, does not depend on hydrophobicity. This is in accordance with a previously reported absence of a relation between lipophilicity and potential for P-gp interaction; the log

$K_{ow}$  values of strong P-gp inhibitors were lower than the reported optimal (Pivčević and Zaja 2006). In a previous study establishing structure- activity relationships of xenobiotics with P-gp, compounds with a molecular weight of approximately 290 Da were classified as non-interactors, while P-gp-interacting compounds had a high potential to form H-bonds with the efflux pump (Bain et al. 1997). Some of the chlorinated alkanes tested had molecular masses of less than 250 Da, and all of them lacked hydrogen bond donor and acceptor groups, which could explain the lack of interaction observed with the transporter. It is clearly a combination of multiple factors that determines whether and to what extent a compound is able to interact with the efflux transporter. These factors include size, lipophilicity, and electrostatic parameters (Bain et al. 1997).

#### *Implications for ecotoxicology*

The compounds that were shown to decrease P-gp activity, such as PCP, BPA, and PFOCs, are widespread environmental contaminants that are common in aquatic environments and are sometimes present at high levels. In addition, some of them are widely distributed in organisms including aquatic invertebrates, fish, fish-eating birds, and mammals; and because of their persistence, they reach much higher concentrations in higher trophic level organisms (Giesy et al. 2006; Kannan et al. 2005; Taniyasu et al. 2003)]. For example, PFOS was found at a concentration of up to 17 ng/L in river water (~0.034 nM), and the mean levels in liver of salmon, bald eagle, and mink were as high as 100 ng/g wet weight, 1740 ng/g wet weight, and 18 000 ng/g wet weight (~0.2  $\mu$ M, ~3.5  $\mu$ M, and ~36  $\mu$ M), respectively (Kannan et al. 2005). In a study evaluating the distribution of PFOCs in water, sediment, and eel in different locations in the Netherlands, levels of PFOS up to 32 ng/L in water (~0.06 nM), 8.7 ng/g dry weight in sediment (~0.02 nM), and 58 ng/g wet weight in eel (~0.1 nM) were found (Kwadijk et al. 2010). Also, PFOS was detected at levels as high as 5900 ng/L (~12 nM) in selected tributaries of the German river Moehne (Skutlarek et al. 2006). The PFOCs concentrations used in the present study (maximum-tolerated concentrations) are much higher than the concentrations measured in water, but for these bioaccumulating compounds the internal concentrations are much more relevant. The high levels found in top predators, such as in the liver of a male mink (59 500 ng/g wet w, ~120  $\mu$ M), exceeded the lowest observed effect concentration found in the present study.

Tissues that act as barriers between organisms and the outside world need functional transport proteins such as P-gp to reduce the body burdens of pollutants that the organisms are exposed to. However, a broad range of contaminants could block this natural defense system, resulting in higher cellular xenobiotic concentrations (Epel et al. 2008). Organisms are in general exposed to mixtures of different compounds, so additive effects are to be expected. Synergistic effects of compounds such as pesticides on the inhibition of P-gp have been observed (Pivčević and Zaja 2006). Unexpected effects may occur when (possibly even nontoxic) compounds in a mixture may modulate the toxicity of other compounds. Therefore, it is of major interest to study further the compounds that may modulate the cellular transporter systems including the P-gp efflux pumps. This should include the widespread class of personal care products (e.g., detergents and cosmetics) such as galaxolide, musk xylene, triclosan, and pharmaceuticals that may be not toxic themselves, but that bioaccumulate and (are suspected to) interfere with the efflux pumps (Anselmo et al. 2012; Luckenbach and Epel 2004).

In the present study, the evaluation of the interference of common environmental contaminants with the MDR/MXR defense system displayed a modulation of the P-gp efflux pump by some widely distributed environmental contaminants such as PFOS and PFOA. Compounds with low molecular mass and lacking H-bond donor and acceptor groups (such as chlorinated alkanes) were not found to interact with the transporter. Pesticides such as o,p'-DDT and methoxychlor decreased fluorescent calcein accumulation. The exact mechanism behind this phenomenon still needs to be elucidated. Further research is needed to investigate mixture effects in the case of realistic field mixtures including bioaccumulating compounds [60] and new emerging contaminants, both in cells and in small aquatic organisms such as sea urchin (Anselmo et al. 2012; Bosnjak et al. 2009) and mussel larvae (Faria et al. 2011). This allows for *in vivo* validation of the *in vitro* results, facilitating future non-vertebrate animal testing and monitoring of the P-gp-inhibiting potency of environmental mixtures.

### **Acknowledgments**

The authors thank A.H. Schinkel for providing the MDCKII-MDR1 cell line, M. Montano for the fluorescence microscopy images, A.C. Gutleb for helpful discussions. Part of the work was funded by NanEAUII within the FNR-funded 'Core2010' program (C10/SR/799842).

### **References**

- Ambudkar SV, Dey S, Hrycyna CA, Ramachandra M, Pastan I, Gottesman MM. 1999. Biochemical, cellular, and pharmacological aspects of the multidrug transporter. *Annu. Rev. Pharmacol. Toxicol.* 39:361–98.
- Anselmo HMR, van den Berg JHJ, Rietjens IMCM, Murk AJ. 2012. Inhibition of cellular efflux pumps involved in multi xenobiotic resistance (MXR) in echinoid larvae as a possible mode of action for increased ecotoxicological risk of mixtures. *Ecotoxicology* 21:2276–87.
- Bain LJ, LeBlanc GA. 1996. Interaction of structurally diverse pesticides with the human MDR1 gene product P-glycoprotein. *Toxicol. Appl. Pharmacol.* 141:288–98.
- Bain LJ, McLachlan JB, LeBlanc GA. 1997. Structure-activity relationships for xenobiotic transport substrates and inhibitory ligands of P-glycoprotein. *Environ. Health Perspect.* 105: 812–8.
- Bard S. 2000. Multixenobiotic resistance as a cellular defense mechanism in aquatic organisms. *Aquat. Toxicol.* 48: 357–389.
- Bolhuis H, van Veen HW, Poolman B, Driessen AJ, Konings WN. 1997. Mechanisms of multidrug transporters. *FEMS Microbiol. Rev.* 21: 55–84.
- Bosnjak I, Uhlinger KR, Heim W, Smital T, Franekić-Colić J, Coale K, et al. 2009. Multidrug efflux transporters limit accumulation of inorganic, but not organic, mercury in sea urchin embryos. *Environ. Sci. Technol.* 43:8374–80.
- Brand W, Schutte ME, Williamson G, van Zanden JJ, Cnubben NHP, Groten JP, et al. 2006. Flavonoid-mediated inhibition of intestinal ABC transporters may affect the oral bioavailability of drugs, food-borne toxic compounds and bioactive ingredients. *Biomed. Pharmacother.* 60:508–19.
- Caminada D, Zaja R, Smital T, Fent K. 2008. Human pharmaceuticals modulate P-gp1 (ABCB1) transport activity in the fish cell line PLHC-1. *Aquat. Toxicol.* 90:214–22.
- Castro AF, Altenberg GA. 1997. Inhibition of drug transport by genistein in cells expressing P-glycoprotein. *Biochem. Pharmacol.* 53: 89–93.
- Cermanova J, Fuksa L, Brckova E, Hroch M, Kucera O, Kolouchova G, et al. 2010. Up-regulation of renal Mdr1 and Mrp2 transporters during amiodarone pretreatment in rats. *Pharmacol. Res.* 61: 129–135.
- Chan LM., Lowes S, Hirst BH. 2004. The ABCs of drug transport in intestine and liver: efflux proteins limiting drug absorption and bioavailability. *Eur. J. Pharm. Sci.* 21:25–51.
- Cornwall R, Toomey BH, Bard S, Bacon C, Jarman WM, Epep D. 1995. Characterization of multixenobiotic/multidrug transport in the gills of the mussel *Mytilus californianus* and identification of environmental substrates. *Aquat. Toxicol.* 31: 277–296.
- Ebert SP, Wetzel B, Myette RL, Conseil G, Cole SPC, Sawada GA, et al. 2012. Chalcogenopyrylium compounds as modulators of the ATP-binding cassette transporters P-glycoprotein (P-gp/ABCB1) and multidrug resistance protein 1 (MRP1/ABCC1). *J. Med. Chem.* 55:4683–99.
- Endicott JA, Ling V. 1989. The biochemistry of P-glycoprotein-mediated multidrug resistance. *Annu. Rev. Biochem.* 58:137–171.
- Eneroth A, Aström E, Hoogstraate J, Schrenk D, Conrad S, Kauffmann HM, et al. 2001. Evaluation of a vincristine resistant Caco-2 cell line for use in a calcein AM extrusion screening assay for P-glycoprotein interaction. *Eur. J. Pharm. Sci.* 12: 205–214.
- Epel D, Luckenbach T, Stevenson CN, Macmanus-Spencer LA, Hamdoun A, Smital T. 2008. Efflux transporters: newly appreciated roles in protection against pollutants. *Environ. Sci. Technol.* 42: 3914–20.
- Essodaigui M, Broxterman HJ, Garnier-Suillerot a. 1998. Kinetic analysis of calcein and calcein-acetoxymethylester efflux mediated by the multidrug resistance protein and P-glycoprotein. *Biochemistry* 37:2243–50.

- Evers R, Kool M, Smith AJ, Van Deemter L, de Haas M, Borst P. 2000. Inhibitory effect of the reversal agents V-104, GF120918 and Pluronic L61 on MDR1 Pgp-, MRP1- and MRP2-mediated transport. *Br J Cancer* 83: 366–374.
- Faria M, Navarro A, Luckenbach T, Piña B, Barata C. 2011. Characterization of the multixenobiotic resistance (MXR) mechanism in embryos and larvae of the zebra mussel (*Dreissena polymorpha*) and studies on its role in tolerance to single and mixture combinations of toxicants. *Aquat. Toxicol.* 101:78–87.
- Ferguson LR, De Flora S. 2005. Multiple drug resistance, antimutagenesis and anticarcinogenesis. *Mutat. Res.* 591:24–33.
- Ford JM. 1996. Experimental reversal of P-glycoprotein-mediated multidrug resistance by pharmacological chemosensitisers. *Eur. J. Cancer* 32A: 991–1001.
- Gekeler V, Ise W, Sanders KH, Ulrich WR, Beck J. 1995. The leukotriene LTD4 receptor antagonist MK571 specifically modulates MRP associated multidrug resistance. *Biochem. Biophys. Res. Commun.* 208:345–52.
- Giesy JP, Mabury SA, Martin JW, Kannan K, Jones PD, Newsted JL, et al. 2006. Perfluorinated compounds in the Great Lakes. In *The Handbook of Environmental Chemistry*, pp. 391–438, Springer.
- Gottesman MM, Pastan I. 1993. Biochemistry of multidrug resistance mediated by the multidrug transporter. *Annu. Rev. Biochem.* 62:385–427.
- Hamers T, Molin KR, Koeman JH, Murk AJ. 2000. A small-volume bioassay for quantification of the esterase inhibiting potency of mixtures of organophosphate and carbamate insecticides in rainwater: development and optimization. *Toxicol. Sci.* 58: 60–67.
- Higgins CF. 2007. Multiple molecular mechanisms for multidrug resistance transporters. *Nature* 446: 749–757.
- Holló Z, Homolya L, Davis CW, Sarkadi B. 1994. Calcein accumulation as a fluorometric functional assay of the multidrug transporter. *Biochim. Biophys. Acta - Biomembr.* 1191: 384–388.
- Homolya L, Holló Z, Germann UA, Pastan I, Gottesman MM, Sarkadi B. 1993. Fluorescent cellular indicators are extruded by the multidrug resistance protein. *J. Biol. Chem.* 268: 21493–21496.
- Hu W, Jones PD, DeCoen W, King L, Fraker P, Newsted J, et al. 2003. Alterations in cell membrane properties caused by perfluorinated compounds. *Comp. Biochem. Physiol. C Toxicol. Pharmacol.* 135: 77–88.
- Jones PD, Hu W, De Coen W, Newsted JL, Giesy JP. 2003. Binding of perfluorinated fatty acids to serum proteins. *Environ. Toxicol. Chem.* 22: 2639–2649.
- Kannan K, Tao L, Sinclair E, Pastva SD, Jude DJ, Giesy JP. 2005. Perfluorinated compounds in aquatic organisms at various trophic levels in a Great Lakes food chain. *Arch. Environ. Contam. Toxicol.* 48: 559–566.
- Kurelec B. 1992. The multixenobiotic resistance mechanism in aquatic organisms. *Crit. Rev. Toxicol.* 22:23–43.
- Kuteykin-Teplyakov K, Luna-Tortós C, Ambroziak K, Löscher W. 2010. Differences in the expression of endogenous efflux transporters in MDR1-transfected versus wildtype cell lines affect P-glycoprotein mediated drug transport. *Br. J. Pharmacol.* 160:1453–63.
- Kwadijk CJAF, Korytár P, Koelmans AA. 2010. Distribution of perfluorinated compounds in aquatic systems in The Netherlands. *Environ. Sci. Technol.* 44:3746–51.
- Laska DA, Houchins JO, Pratt SE, Horn J, Xia X, Hanssen BR, et al. 2002. Characterization and application of a vinblastine-selected Caco-2 cell line for evaluation of P-glycoprotein. *In Vitro Cell. Dev. Biol. Anim.* 38:401–10.
- Lecoeur S, Videmann B, Mazallon M. 2006. Effect of organophosphate pesticide diazinon on expression and activity of intestinal P-glycoprotein. *Toxicol. Lett.* 161:200–9.
- Liminga G, Nygren P, Larsson R. 1994. Microfluorometric evaluation of calcein acetoxymethyl ester as a probe for P-glycoprotein-mediated resistance: effects of cyclosporin A and its nonimmunosuppressive analogue SDZ PSC 833. *Exp. Cell Res.* 212: 291–296.

- Litman T, Brangi M, Hudson E, Fetsch P, Abati A, Ross DD, et al. 2000. The multidrug-resistant phenotype associated with overexpression of the new ABC half-transporter, MXR (ABCG2). *J. Cell Sci.* 113: 2011–2021.
- Loo TW, Bartlett MC, Clarke DM. 2004. The drug-binding pocket of the human multidrug resistance P-glycoprotein is accessible to the aqueous medium. *Biochemistry* 43:12081–9.
- Loo TW, Clarke DM. 1998. Nonylphenol ethoxylates, but not nonylphenol, are substrates of the human multidrug resistance P-glycoprotein. *Biochem. Biophys. Res. Commun.* 247:478–80.
- Luckenbach T, Epel D. 2004. Nitromusk and polycyclic musk compounds as long-term inhibitors of cellular xenobiotic defense systems mediated by multidrug transporters. *Environ. Health Perspect.* 113:17–24.
- Martin C, Berridge G, Mistry P, Higgins C, Charlton P, Callaghan R. 1999. The molecular interaction of the high affinity reversal agent XR9576 with P-glycoprotein. *Br. J. Pharmacol.* 128:403–11.
- Montaño M, Bakker E, Murk AJ. 2010. Meta-analysis of supramaximal effects in *in vitro* estrogenicity assays. *Toxicol. Sci.* 115:462–474.
- Pivčević B, Zaja R. 2006. Pesticides and their binary combinations as P-glycoprotein inhibitors in NIH 3T3/MDR1 cells. *Environ. Toxicol. Pharmacol.* 22:268–76.
- Schinkel AH, Jonker JW. 2003. Mammalian drug efflux transporters of the ATP binding cassette (ABC) family: an overview. *Adv. Drug Deliv. Rev.* 55: 3–29.
- Schriks M, Vrabie C, Gutleb A, Faassen E, Rietjens IMCM, Murk AJ. 2006. T-screen to quantify functional potentiating, antagonistic and thyroid hormone-like activities of poly halogenated aromatic hydrocarbons (PHAHs). *Toxicol. In Vitro* 20: 490–498.
- Skutlarek D, Exner M, Färber H. 2006. Perfluorinated surfactants in surface and drinking waters. *Environ. Sci. Pollut. Res. Int.* 13: 299–307.
- Smital T, Luckenbach T, Sauerborn R, Hamdoun AM, Vega RL, Epel D. 2004. Emerging contaminants-pesticides, PPCPs, microbial degradation products and natural substances as inhibitors of multixenobiotic defense in aquatic organisms. *Mutat. Res.* 552:101–17.
- Stevenson CN, MacManus-Spencer LA, Luckenbach T, Luthy RG, Epel D. 2006. New perspectives on perfluorochemical ecotoxicology: inhibition and induction of an efflux transporter in the marine mussel, *Mytilus californianus*. *Environ. Sci. Technol.* 40: 5580–5.
- Sturm A, Cravedi JP, Segner H. 2001. Prochloraz and nonylphenol diethoxylate inhibit an mdr1-like activity *in vitro*, but do not alter hepatic levels of P-glycoprotein in trout exposed *in vivo*. *Aquat. Toxicol.* 53: 215–28.
- Tan B, Piwnica-Worms D, Ratner L. 2000. Multidrug resistance transporters and modulation. *Curr. Opin. Oncol.* 12: 450–8.
- Taniyasu S, Kannan K, Horii Y, Hanari N, Yamashita N. 2003. A survey of perfluorooctane sulfonate and related perfluorinated organic compounds in water, fish, birds, and humans from Japan. *Environ. Sci. Technol.* 37: 2634–2639.
- Taub ME, Podila L, Ely D, Almeida I. 2005. Functional assessment of multiple P-glycoprotein (P-gp) probe substrates: influence of cell line and modulator concentration on P-gp activity. *Drug Metab. Dispos.* 33: 1679–1687.
- Teodori E, Dei S, Scapecchi S, Gualtieri F. 2002. The medicinal chemistry of multidrug resistance (MDR) reversing drugs. *Farmacol.* 57: 385–415.
- Tiberghien F, Loo F. 1996. Ranking of P-glycoprotein substrates and inhibitors by a calcein-AM fluorometry screening assay. *Anticancer. Drugs* 7: 568–78.
- Upham BL, Park JS, Babica P, Sovadinova I, Rummel AM, Trosko JE, et al. 2009. Structure-activity-dependent regulation of cell communication by perfluorinated fatty acids using *in vivo* and *in vitro* model systems. *Environ. Health Perspect.* 117: 545–551.

- Van Tellingen O. 2001. The importance of drug-transporting P-glycoproteins in toxicology. *Toxicol. Lett.* 120: 31–41.
- Van Zanden JJ, Wortelboer HM, Bijlsma S, Punt A, Usta M, Bladeren PJ, et al. 2005. Quantitative structure activity relationship studies on the flavonoid mediated inhibition of multidrug resistance proteins 1 and 2. *Biochem. Pharmacol.* 69: 699–708.
- Zvinavashe E, van den Berg H, Soffers AEMF, Vervoort J, Freidig A, Murk AJ, et al. 2008. QSAR models for predicting *in vivo* aquatic toxicity of chlorinated alkanes to fish. *Chem. Res. Toxicol.* 21: 739–745.



# Chapter 5

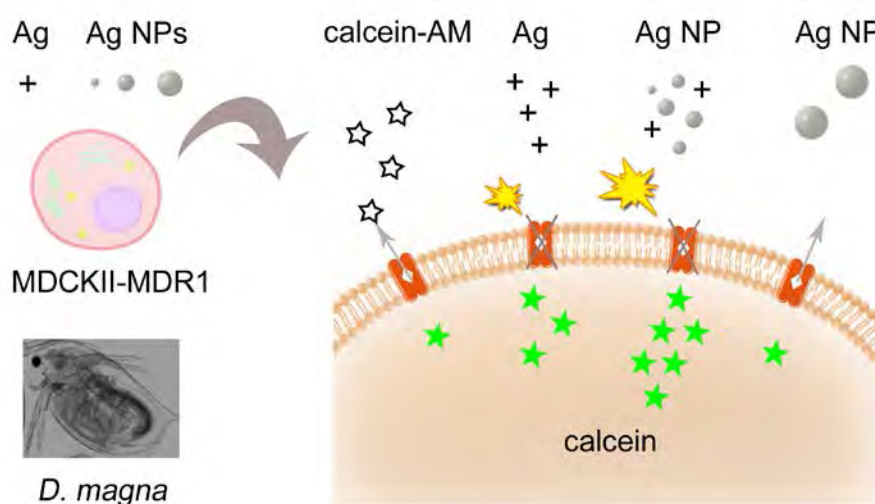
## Inhibition of multixenobiotic resistance transporters (MXR) by silver nanoparticles and ions *in vitro* and *in vivo*

Anastasia Georgantzopoulou, Sébastien Cambier, Tommaso Serchi, Anna Lankoff, Marcin Kruszewski, Yekkuni L. Balachandran, Patrick Grysan, Jean-Nicolas Audinot, Johanna Ziebel, Cédric Guignard, Arno C. Gutleb and AlberTinka J. Murk

*Environ. Sci. Technol.* (Submitted)

### Abstract

The P-glycoprotein (P-gp, ABCB1) and multidrug resistance associated protein 1 (MRP1), important members of the ABC (ATP-binding cassette) transporters, protect cells and organisms *via* efflux of xenobiotics and are responsible for the phenomenon of multidrug or multixenobiotic resistance (MXR). In this study we first evaluated, *in vitro*, the interaction of silver nanoparticles (Ag NPs, 20-200 nm) and Ag ions (AgNO<sub>3</sub>) with MXR efflux transporters using MDCKII and the P-gp over-expressing MDCKII-MDR1 cells and calcein-AM as a substrate of the transporters. Next the *in vivo* modulation of MXR activity was studied in *D. magna* juveniles with the model P-gp and MRP1 inhibitors verapamil-HCl and MK571, respectively. The common environmental contaminants perfluorooctane sulfonate and bisphenol A also inhibited the efflux of calcein from daphnids. Small-sized Ag NPs and AgNO<sub>3</sub> inhibited the MXR activity in daphnids and MDCKII-MDR1 cells, but *abcb1* gene expression remained unchanged. Both Ag NPs and dissolved ions contributed to the effects. This study provides for the first time evidence of the interference of Ag NPs and AgNO<sub>3</sub> with the MXR activity both *in vitro* and *in vivo*, and should be taken into account when Ag NP toxicity is assessed.



## Introduction

The multixenobiotic resistance (MXR) mechanism represents a first line of defense protecting the cells and organisms against xenobiotics (Kurelec 1992). It is a phenomenon analogous to the multidrug resistance (MDR) which is the resistance observed in cancer cells/tissues against anticancer drugs limiting the efficiency of chemotherapy (Ambudkar et al. 1999; van Tellingen 2001). It is mediated by energy dependent efflux transporters located in the cell membrane belonging to the ATP-binding cassette (ABC) transporter superfamily that recognize and actively pump drugs/contaminants or their metabolites out of the cell decreasing the intracellular concentrations (Ambudkar et al. 1999; Endicott and Ling 1989; Loo et al. 2004). Important members of the ABC family related to MXR/MDR are the P-glycoprotein (P-gp, ABCB1, MDR1) and multidrug resistance associated protein 1 (MRP1, ABCC1) and they are localized in tissues with excretory (e.g. liver and kidney) or barrier functions such as intestines, brain, placenta (Schinkel and Jonker 2003). In aquatic organisms they represent an environment-tissue barrier and they are localized in eggs, embryos, larvae and gills (Campos et al. 2014; Faria et al. 2011; Shipp and Hamdoun 2012; Smital et al. 2004). They recognize and transport a wide range of structurally diverse compounds against a concentration gradient. Due to this lack of specificity they are vulnerable to modulation by several different classes of chemicals leading to the transporters' compromised activity and as a consequence, xenobiotics that would normally be excluded from the cell can now accumulate, thus lowering the EC<sub>50</sub> or LC<sub>50</sub> concentrations (Epel et al. 2008; Anselmo et al. 2012).

Besides organic compounds, several metals such as mercury have also been found to be transported or interfere with efflux pumps in sea urchin embryos (Bosnjak et al. 2009), whereas cadmium was reported to increase the P-gp protein levels in exposed oysters *Crassostrea virginica* (Ivanina and Sokolova 2008). Human and bacterial MDR transporters conferred resistance against mercury, zinc and cadmium that was abolished in the presence of verapamil (Achard-Joris and Bourdineaud 2006; Achard-Joris et al. 2005). The expression of the transporters is inducible upon chemical stress (Campos et al. 2014; de Cerio et al. 2012; Navarro et al. 2012), however other factors, such as oxidative stress, can also alter their expression profile (Callaghan et al. 2008). Also some nanoparticles (NPs, particles with all dimensions less than 100 nm) have been shown to interfere with multidrug transporters in sea urchin larvae (Anselmo et al. 2012). Furthermore polystyrene NPs have been shown to

interact with the P-gp and MRP1 in the Caco-2 cell line in a surface charge-dependent manner (Bhattacharjee et al. 2013).

Among the different NP groups, Ag NPs have drawn great attention because of their increased use and incorporation in consumer products, textiles, medical devices, food packaging etc. due to their broad spectrum antimicrobial activity (Wijnhoven et al. 2009; Woodrow Wilson International Center for Scholars 2014). This increased use and potential release in the environment has raised concerns for human and environmental health. Several *in vitro* and *in vivo* studies using fish and other organisms have shown size-dependent toxicity, with smaller sized Ag NPs being more toxic than larger ones (Gaiser et al. 2012; Gliga et al. 2014; Park et al. 2011). Moreover, surface coating influences the NP toxicity (Kwok et al. 2012). In addition to the NP-specific also Ag ions released from the NPs could contribute to the toxic effects (Gaiser et al. 2012; Griffitt et al. 2008; Kwok et al. 2012).

The aim of this study was to assess to what extent Ag NPs and Ag ions ( $\text{AgNO}_3$ ) interfere with the MXR transporters. The previously optimized calcein-AM based cellular efflux pump inhibition assay (CEPIA) (Georgantzopoulou et al. 2014) was used with the P-gp over-expressing MDCKII-MDR1 cells, a widely used tool for the identification of P-gp substrates/inhibitors and drug permeability, as well as with the wild type MDCKII-WT cells for comparison. *D. magna* neonates were used as an environmentally relevant organism for *in vivo* studies in an adaptation of the *in vitro* assay. *D. magna* is a model organism widely used in freshwater eco-toxicological studies. As a filter-feeder *D. magna* can be easily exposed to NPs and its transparency makes it a very suitable model for the visualization of the accumulation of fluorophores. Studies on the uptake and translocation of NPs have been previously performed with *D. magna* (Feswick et al. 2013; Georgantzopoulou et al. 2013; Rosenkranz et al. 2009) and it has been recently found that MXR-involved transporters are expressed in different developmental stages of *D. magna* with high levels especially in the neonate and adult life stage (Campos et al. 2014). Calcein-AM was used as a model substrate and verapamil-HCl and MK571 were used as model inhibitors of the efflux transporters both *in vitro* and *in vivo*. The environmental contaminants perfluorooctane sulfonate (PFOS) and bisphenol A (BPA) that have previously been shown to interfere with MXR both *in vitro* (Georgantzopoulou et al. 2014) and *in vivo* (marine mussels *M. californiacus*) (Stevenson et al. 2006) and induce mixture effects (Montaño et al. 2010), were also evaluated for their modulatory potential in *D. magna*. *In vitro* membrane localization of Ag was visualized by using a high resolution nanoprobe (nanoSIMS50). Finally, the effects of Ag NPs of different

sizes and AgNO<sub>3</sub> on the MXR mechanism were assessed *in vitro* and *in vivo*. In *D. magna* the effect of the Ag NPs on the *abcb1* gene expression levels was also studied to assess whether the transporter can be chemically induced.

## Organisms, Materials and Methods

### *NPs and chemicals*

Ag NPs (20 and 200 nm) (Lankoff et al. 2012) were obtained from PlasmaChem GmbH (Berlin, Germany) and Ag NPs synthesized by *Ocimum sanctum* (Ag 23 nm) and *Azadirachta indica* (Ag 27 nm) plant leaf extracts (Balachandran et al. 2013, 2012) from Bharathiar University (Coimbatore, India). Silver nitrate (AgNO<sub>3</sub>) was purchased from VWR (Leuven, Belgium) and BPA, calcein-AM and verapamil-HCl from Sigma Aldrich (Bornem, Belgium). MK571 was purchased from Enzo Life Sciences and PFOS from Fluka (Steinheim, Germany).

### *NPs dispersion protocols and characterization in media*

Stock solutions of particles Ag 20 and Ag 200 nm (2 mg/mL) were prepared in 5% DMSO in sterile Milli-Q water (Millipak Express, Millipore). Then the solution was sonicated on ice for 3 minutes using a UP200S probe ultra sonicator (Hielscher, Germany). Stocks were always prepared fresh before each experiment. Ag 23 and Ag 27 nm NPs were provided as stocks in MilliQ water. Particle size distribution of the Ag NPs in mineral water (Volvic, France) as well as in DMEM without phenol red and fetal bovine serum (FBS) was evaluated with Nanoparticle Tracking Analysis (Hole et al. 2013) (NTA, NanoSIGHT, UK).

### *Cell culture*

Dulbecco's minimum essential medium with Glutamax (DMEM-Glutamax), Dulbecco's minimum essential medium without phenol red (DMEM), phosphate buffer saline (PBS), penicillin/ streptomycin and heat-inactivated FBS were all obtained from Gibco, Invitrogen (Merelbeke, Belgium).

The MDCKII-MDR1 cells were kindly provided by A.H. Schinkel (The Netherlands Cancer Institute, Amsterdam, The Netherlands). The MDCKII-wild type (MDCKII-WT) cells were obtained from the European Collection of Cell Cultures (Salisbury, UK). Both cell lines were maintained in Dulbecco's Modified Eagle Medium-Glutamax (DMEM-Glutamax,

Invitrogen, Merelbeke, Belgium) supplemented with 10% foetal bovine serum and 1% penicillin/streptomycin solution at 37 °C in a 5% CO<sub>2</sub> humidified incubator. The medium was replaced every other day and the cells were split with Trypsin-EDTA when 70-90% confluency was reached.

#### *Cellular efflux pump inhibition assay (CEPIA)-in vitro*

The assay was performed as previously described (Georgantzopoulou et al. 2014). Briefly, MDCKII-WT or MDCKII-MDR1 were seeded in 96-well plates at a concentration of  $5 \times 10^5$  cells/mL and were grown overnight in a humidified atmosphere at 37 °C and 5% CO<sub>2</sub>. The cells were exposed to increasing concentrations (0.6-5 mg/L) of Ag NPs 20, 23, 27 and 200 nm or AgNO<sub>3</sub> (100 µL/well) for 30 minutes. Then, calcein-AM was added (100 µL/well) reaching a final concentration of 2.5 µM for another 30 minutes. DMEM without phenol red nor FBS was used for the dilutions of the compounds/Ag NPs. The calcein fluorescence was finally measured using a microplate reader (Synergy 2, BioTek Instruments, Inc.) at 485 nm excitation and 530 nm emission. No interference of calcein with Ag ions and Ag NPs was observed.

In order to assess the membrane localization of Ag in Ag NP and AgNO<sub>3</sub>-exposed MDCKII-WT and MDCKII-MDR1 cells a secondary ion mass spectrometry analysis was performed as described in the Supporting Information.

#### *Cytotoxicity assay*

Cytotoxicity was determined based on the metabolic activity assay using MTS [3-(4,5-dimethylthiazol-2-yl)-5-(3-carboxymethoxyphenyl)-2-(4-sulfophenyl)-2H tetrazolium salt] as a probe. At the end of the exposure period the exposure medium was removed and 120 µL of MTS solution (Promega) was added to each well. After 1 hour of incubation the absorbance at 490 nm was measured (Synergy 2, BioTek Instruments, Inc.). The non-cytotoxic concentrations of the compounds/NPs as determined by the MTS assay are used in the CEPIA.

#### *D. magna culture and maintenance*

*Daphnia magna* cultures were stabilized for a period of 5 months and were in accordance with the OECD guideline. Cultures of 40 animals/L were maintained in LC

medium (Ca(NO<sub>3</sub>)<sub>2</sub>(H<sub>2</sub>O)<sub>4</sub>: 40g/L; KNO<sub>3</sub>: 100g/L; MgSO<sub>4</sub>(H<sub>2</sub>O)<sub>7</sub>: 30g/L; K<sub>2</sub>HPO<sub>4</sub>: 40g/L; CuSO<sub>4</sub>(H<sub>2</sub>O)<sub>5</sub>: 30mg/L; (NH<sub>4</sub>)<sub>6</sub>Mo<sub>7</sub>(H<sub>2</sub>O)<sub>4</sub>: 60mg/L; ZnSO<sub>4</sub>(H<sub>2</sub>O)<sub>7</sub>: 60mg/L; CoCl<sub>2</sub>(H<sub>2</sub>O)<sub>6</sub>: 60mg/L, Mn(NO<sub>3</sub>)<sub>2</sub>(H<sub>2</sub>O)<sub>4</sub>: 60mg/L; C<sub>6</sub>H<sub>8</sub>O<sub>7</sub>(H<sub>2</sub>O) : 60mg/L; H<sub>3</sub>BO<sub>3</sub>: 60mg/L; citrate iron: 1625mg/L; FeSO<sub>4</sub>(H<sub>2</sub>O)<sub>7</sub>: 625mg/L; FeCl<sub>3</sub>(H<sub>2</sub>O)<sub>6</sub>: 625mg/L): mineral water (1:4) supplemented with Thiamine HCl (75µg/L), Vitamine B12 (1 µg/L) and Biotine (0.75 µg/L) in glass tanks (1 L/ tank). Cultures were fed three times daily with a mixture of the algae *Scenedesmus subspicatus* and *Chlorella vulgaris* (200 × 10<sup>6</sup>cells/mL each). The culture medium was changed twice a week and neonates were removed every 24 hours. The photoperiod was adjusted to 16 hours light: 8 hours dark at 20±2 °C.

#### *In vivo cellular efflux pump inhibition assay (CEPIA)*

*D. magna* juveniles of 48 hours old were exposed in 6-well plates with 5 organisms/well in 10 mL mineral water (Source Clairvic, Société des Eaux de Volvic, France) to increasing concentrations of the standard inhibitors MK571 (5-10 µM), Verapamil-HCl (25-100 µM), or the environmental contaminants PFOS (45-120 µM) and BPA 12.5-50 µM for 60 minutes in duplicates. The concentration range was chosen based on previous *in vivo* studies using sea urchins (Anselmo et al. 2012). Then, calcein-AM at a final concentration of 1 µM was added to each well for another 60 minutes. At the end of the exposure period the animals were transferred in clean mineral water for 5 minutes to remove excess dye. Subsequently, the animals were transferred in Eppendorf tubes with the use of a Pasteur pipette, the remaining water was removed and replaced with 100 µL of mineral water. The tubes containing the daphnids were placed at -20 °C for 10 minutes and upon thawing they were sonicated for 2 minutes in order to extract the accumulated calcein as previously described.(Campos et al. 2014) The samples were centrifuged for 5 minutes at 1500 rpm and 80 µL of the supernatant was transferred in white 96-well plates and calcein fluorescence was measured using a microplate reader (Synergy 2, BioTek Instruments, Inc.) at 485 nm excitation and 530 nm emission. The protein content was determined according to the Bradford method (Biorad, Munich, Germany) using bovine serum albumin (BSA) as a standard and the calcein fluorescence signal was normalized to the protein content of each sample (calcein fluorescence/µg protein).

To visualize the calcein accumulation within the animals, after the exposure period the daphnids were transferred in coverslips and immobilized using a drop of Mowiol 4-88

(Sigma-Aldrich). Calcein accumulation in the organisms was observed under an epifluorescent microscope equipped with FITC filter (Zeiss LSM 510 Meta with an inverted Zeiss microscope). Image processing and visualization were done with the Zeiss Software ZEN 2012.

#### *Abcb1* induction in Ag NP-exposed daphnias (RT-qPCR)

*Daphnia magna* juveniles (48 hours old) were exposed to Ag NPs or AgNO<sub>3</sub> at the EC<sub>10</sub> level (Georgantzopoulou et al. 2013) (Ag 23 nm: 0.4 µg/L; Ag 27 nm: 9 µg/L; Ag 20 nm: 35 µg/L; Ag 200 nm: 570 µg/L; AgNO<sub>3</sub>: 0.9 µg/L) and 0.001% DMSO (solvent control) for 24 hours in a 6-well plate (12 daphnids/well in 10 mL). Each exposure was performed in 5 replicates. At the end of the exposure 10 daphnids were washed with clean water before the total RNA extraction. The total RNA extraction was done using the RNeasy Plant Mini Kit (Qiagen, Leusden, The Netherlands) including a DNaseI treatment following the manufacturer's instructions. The quality of RNA was controlled with the RNA Nano 6000 assay (Agilent Technologies, Diegem, Belgium) using a 2100 Bioanalyzer (Agilent Technologies). All RNA samples had RNA integrity numbers above 8. The purity and concentration of RNA were assessed by measuring the absorbance at 230 nm, 260 nm, and 280 nm using a Nanodrop ND1000 spectrophotometer (Thermo scientific). Primers for *abcb1* (Fw: 5'-GTATCCAGTGC GGAAGTGGC-3'; Rev: 5'-ACAGCGTATCGCTATTGCCC-3') were obtained from Campos et al. (Campos et al. 2014) and those for *18S* (Fw: 5'-CGCTCTGAATCAAGGGTGTT-3'; Rev: 5'-TGTCCGACCGTGAAGAGAGT-3') and *actin* (Fw: 5'-CCACACTGTCCCCATTTATGAA-3'; Rev: 5'-CGCGACCAGCCAAATCC-3') were obtained from Heckmann et al. (Heckmann et al. 2006). The PCR were performed on a ViiA7 Real-time PCR system (Life technologies) using Mesa Green Low Rox Real-time PCR Kits (Eurogentec, Liège, Belgium) with the following final concentrations in a 12.5 µL final volume: 1X MasterMix, 100 nM forward and reverse primers, 0.4 ng/µL cDNA. No template control and RT- control samples were included in each plate and each sample was run in triplicate. Thermal cycling conditions were: initial 5 min denaturation at 95 °C, followed by 45 cycles of 15 s at 95 °C and 1 min at 60 °C, and a final dissociation step. Primer specificity was controlled by the presence of a single peak in the melting curve. *18S* and *actin* were used as reference genes for the normalization prior to relative quantification of gene expression data. The suitability of these 2 genes as references was determined with GeNorm (qbase+ 2.5, Biogazelle) and used for the normalization. Relative expression quantity between each

exposed condition to the control was then calculated following qBase model (Hellemans et al. 2007).

#### *Ag measurements (total soluble silver, total organism concentrations)*

Ag ions may leach from Ag NPs and therefore the total amount of soluble Ag ionic species released from the Ag NPs into the DMEM exposure medium was evaluated as previously described (Georgantzopoulou et al. 2013). At the end of the exposure of the MDCKII cells, 2 mL of exposure medium (at a concentration of 1 mg/L) was taken and centrifuged for 40 min at 4000 g using centrifugal filter devices (Amicon ultra-4, Millipore, Ireland) with 3 kDa cut-off. The ultrafiltrates were evaluated for the total soluble Ag content with Inductively Coupled Plasma Mass Spectrometry (ICP-MS) (Elan DRC-e, Perkin Elmer, Waltham, MA, USA) as previously described (Georgantzopoulou et al. 2013). Concentrations of Ag released in daphnid's media have been reported previously (Georgantzopoulou et al. 2013).

At the end of the 24-hr exposure period, 10 daphnids per treatment were collected, transferred into clean volvic water, pooled and analysed for the amount of total silver by Inductively Coupled Plasma Mass Spectrometry (ICP-MS) (Georgantzopoulou et al. 2013) (Elan DRC-e, Perkin Elmer, Waltham, MA, USA) as described in the Supporting Information.

#### *Data analysis*

The data are expressed as mean values with standard deviations of three independent experiments each containing 3 replicates. Data were analyzed with SigmaPlot 12 (Systat Software, Inc. SigmaPlot for Windows) and SPSS (IBM SPSS Statistics for Windows, Version 21.0. Armonk, NY: IBM Corp) using a general linear model (univariate analysis) with a Tukey's post Hoc test for comparison of means. When necessary the data were transformed to achieve normal distribution and equal variances. Differences among means were considered to be significant at  $P < 0.05$ . Dose-response curves and  $EC_{50}$ s were obtained with SigmaPLOT 7.101 (SPSS Inc. SigmaPlot for Windows) using a logistic four-parameter model. The maximal response (maximal calcein fluorescence values) reached by the compounds and Ag NPs or  $AgNO_3$  was expressed as a percentage relative to the effect of verapamil at 100  $\mu M$  set at 100% ( $\% P\text{-gp Inhibition} = [(RFU_{\text{test compound}} - RFU_{\text{control}})/(RFU_{\text{Verapamil}} - RFU_{\text{control}})] \times 100$ ).

The calcein accumulation induced was expressed relative to the calcein accumulation observed in the solvent control set at 1.

## Results

### *Ag particles characterization in different media and Ag measurements*

The NPs in both water and DMEM agglomerated as can be seen from the sizes (Table 1). Except for the Ag 200 nm particles this effect was greatest in DMEM medium. The  $\zeta$  potential was in the range of -4.5 to +7 mV, also suggesting agglomeration and unstable dispersions in both media (Table 1, Figure S2). In both media, the number of peaks in the size distribution increased with the NP size (Supplementary Figure S2).

**Table 1.** Size distribution (mode  $\pm$  standard deviation of triplicate measurements) and  $\zeta$  potential in Volvic water and DMEM without phenol red and FBS of the Ag NPs used in the study.

Particle	Volvic water		DMEM	
	Size (nm)	$\zeta$ potential (mV)	Size (nm)	$\zeta$ potential (mV)
Ag 23 nm	56 $\pm$ 3.2	- 3.49	82 $\pm$ 12.3	+ 7.14
Ag 27 nm	63 $\pm$ 3.2	- 3.55	91 $\pm$ 13.3	- 1.53
Ag 20 nm	69 $\pm$ 8.4	- 3.49	90 $\pm$ 3.8	+ 3.5
Ag 200 nm	135 $\pm$ 18.7	- 4.55	114 $\pm$ 16.5	+ 0.45

The dissolved Ag concentrations measured in the DMEM medium at the end of the exposure period with Ag NPs 23 nm were at the same levels as for AgNO<sub>3</sub>-treated cells and corresponds to 0.8-0.9% of total Ag administered (Table S1), while for Ag NPs 27 nm this percentage was much lower (0.03%) and for the rest of the NPs the Ag concentrations were even below the limit of detection. Similarly, the levels of dissolved Ag in volvic water were lower in the case of Ag NPs 23 nm (29% of total Ag added) compared to AgNO<sub>3</sub> (40% of total Ag), whereas lower levels were found for the other particles (less than 5.5% of total Ag administered) (Table S1).

At the end of the 24 hour exposure period at the EC<sub>10</sub> level of Ag NPs or AgNO<sub>3</sub>, 41% of the total Ag administered as Ag NPs 23 nm was measured in the daphnids while the lowest levels were found for AgNO<sub>3</sub> (0.17% of total Ag) (Table S1).

*Cellular Efflux Pump Inhibition Assay (CEPIA)- in vitro*

Only AgNO<sub>3</sub> and Ag NPs 23 nm inhibited the efflux of calcein fluorescence in the MDCKII-MDR1 cell line (Figure 1B), reaching 22.5% and 55%, respectively of the maximum response of the positive control (100 µM of Verapamil) (Table 2).

**Table 2.** *In vitro* and *in vivo* effects obtained in the calcein-AM based cellular efflux pump inhibition assay (CEPIA) with MDCKII-MDR1, MDCKII-WT cells and 48 hours old *D. magna* juveniles.

Ag NP/ compound	LOEC <sup>a</sup>	EC <sub>50</sub> <sup>a</sup>	Fold increase (over control)	Max effect <sup>a</sup> (% 100 µM VER)
<b>MDCKII-WT</b>				
AgNO <sub>3</sub>	N.D.	N.D.	1.1	14 (5 mg/L)
Ag 23 nm	5 (mg/L)	N.D.	1.2	19 (5 mg/L)
Ag 27 nm	N.D.	N.D.	0.87	-4 (5 mg/L)
Ag 20 nm	N.D.	N.D.	0.94	-3 (5 mg/L)
Ag 200 nm	N.D.	N.D.	1	0.2 (5 mg/L)
<b>MDCKII-MDR1</b>				
AgNO <sub>3</sub>	2.5 (mg/L)	3.2 (mg/L)	2.8	23 (5 mg/L)
Ag 23 nm	1.3 (mg/L)	2.9 (mg/L)	4.1	55 (5 mg/L)
Ag 27 nm	N.D.	N.D.	0.93	-1.5 (5 mg/L)
Ag 20 nm	N.D.	N.D.	1	0.8 (5 mg/L)
Ag 200 nm	N.D.	N.D.	1	0.9 (5 mg/L)
<b><i>D. magna</i></b>				
VER	50 (µM)	23.4 (µM)	1.6	100 (100 µM)
MK571	5 (µM)	2.5 (µM)	1.9	158 (10 µM)
PFOS	45 (µM)	45 (µM)	2.5	246 (120 µM)
BPA	25 (µM)	11.2 (µM)	2	176 (25 µM)
AgNO <sub>3</sub>	<0.44 (µg/L)	0.44 (µg/L)	1.5	89 (1.8 µg/L)
Ag 23 nm	<0.18 (µg/L)	0.18 (µg/L)	2.5	194 (0.4 µg/L)
Ag 27 nm	4.5 (µg/L)	4.8 (µg/L)	1.9	166 (9 µg/L)
Ag 20 nm	N.D.	N.D.	1.3	66 (17.5 µg/L)
Ag 200 nm	N.D.	N.D.	1.2	51.8 (1140 µg/L)

<sup>a</sup> The responses are quantified as lowest observed effect concentration (LOEC) and 50% effective concentration (EC<sub>50</sub>); and the maximal response as a percentage relative to the maximal effect of verapamil at 100 µM, reached at the concentration given in parentheses.

N.D.= not determined because these compounds did not induce a significant effect; VER= verapamil-HCl; PFOS= perfluorooctane sulfonate; BPA= Bisphenol A.

Only Ag 23 nm increased the calcein accumulation in MDCKII-WT cells, at the highest exposure concentration of 5 mg/L reaching a 1.2-fold increase compared to control (Figure 1A). In addition, the baseline levels of calcein fluorescence in the presence of only 2.5 µM calcein-AM were 10 times lower in MDCKII-MDR1 cells compared to MDCKII-WT.

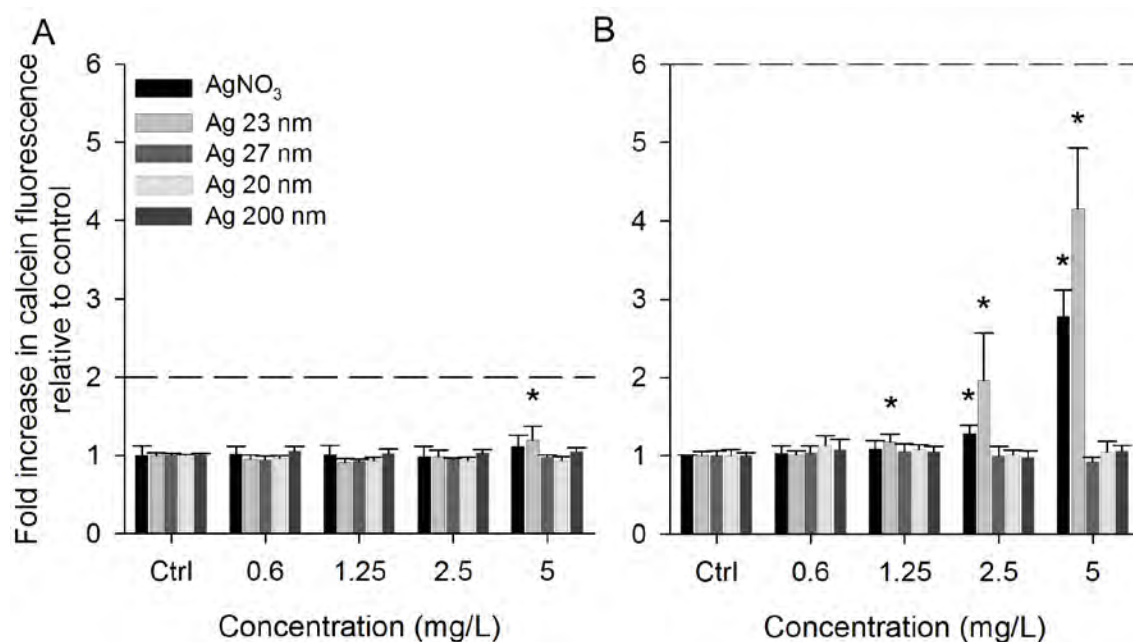


**Figure 1.** Effects of AgNO<sub>3</sub> and Ag NPs 23, 27, 20 and 200 nm on (A) MDCKII-WT and (B) MDCKII-MDR1 cells. The cells were exposed to Ag NPs and AgNO<sub>3</sub> for 30 min and incubated with 2.5 μM calcein-AM for an additional 30 min. Error bars represent the mean ± standard deviation of 3 independent experiments performed in triplicate. The dashed line denotes the calcein fluorescence induction by 100 μM verapamil. \* indicates significant differences of the treatments from the respective untreated controls (P<0.05).

#### *Cellular efflux pump inhibition assay (CEPIA)-in vivo (D. magna)*

The *in vivo* CEPIA assay, using *D. magna* juveniles, was established with the model inhibitors verapamil-HCl and MK571 (Figure 2A-B, Table 2), with MK571 inducing 12% higher calcein fluorescence levels than verapamil. Also the environmental contaminants PFOS and BPA enhanced the calcein fluorescence in a concentration-dependent manner, even reaching higher maximal levels than the reference inhibitors (Figure 2C-D, Table 2).

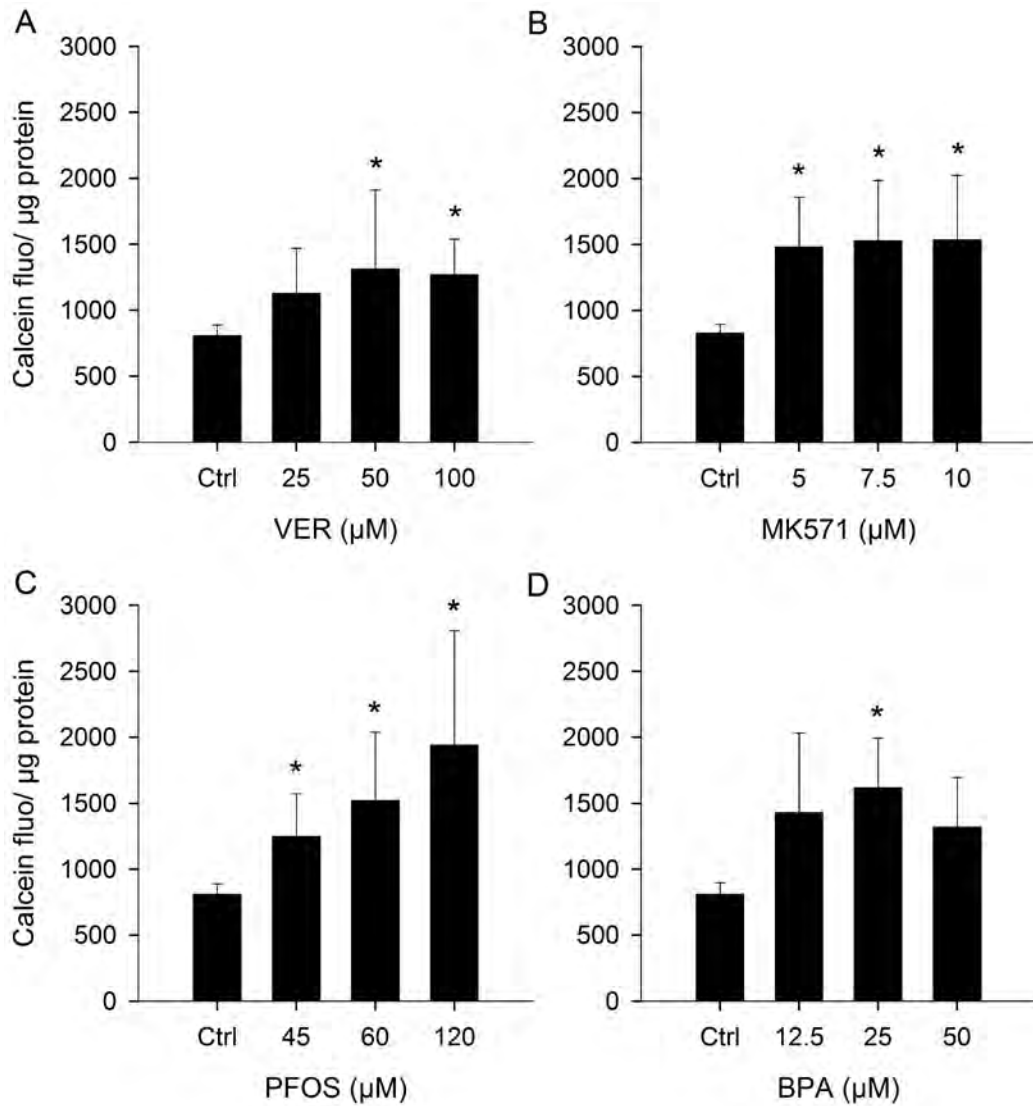


**Figure 2.** Effect of the model inhibitors (A) Verapamil-HCl and (B) MK571 and the environmental contaminants (C) PFOS and (D) BPA on the calcein accumulation in 48 hours old *D. magna* exposed for 60 min followed by 60 min exposure to 1 µM calcein-AM. Error bars represent the mean  $\pm$  standard deviation of 3 independent experiments performed in duplicate. Significant differences from respective untreated controls are marked with asterisks ( $P < 0.05$ ).

One hour of exposure to Ag NPs 23 and 27 nm as well as AgNO<sub>3</sub> resulted in higher calcein fluorescence in the daphnids compared to the untreated animals (Figure 3). Especially Ag NPs 23 nm were very potent in the *in vivo* CEPIA, with a response that was almost twice that of the positive control verapamil, with an EC<sub>50</sub> of 0.18 µg/L while Ag 20 and 200 nm did not induce an effect (Table 2).

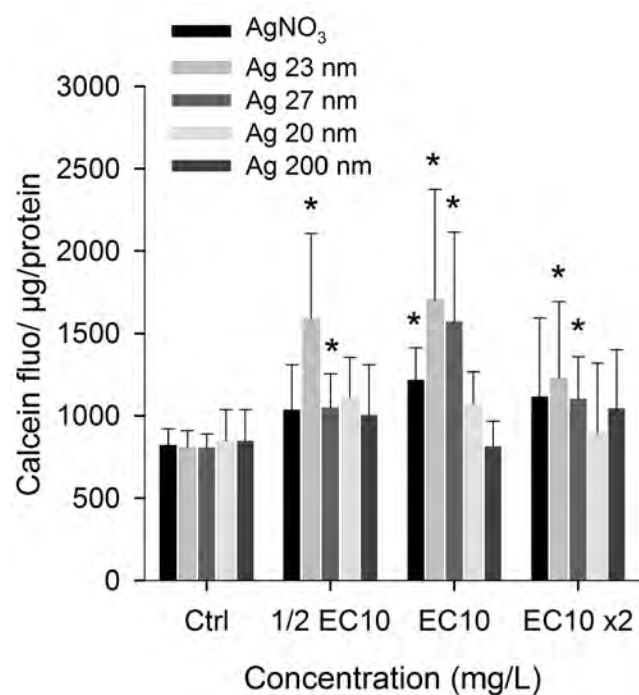


**Figure 3.** Calcein accumulation increase in 48 hours old daphnids upon exposure for 60 min to  $\frac{1}{2}$ EC<sub>10</sub>, EC<sub>10</sub> and EC<sub>10</sub>x2 of AgNO<sub>3</sub> (0.45, 0.9, 1.8 µg/L) and Ag NPs 23 nm (0.2, 0.4, 0.8 µg/L), 27 nm (4.5, 9, 18 µg/L), 20 nm (17.5, 35, 70 µg/L) and 200 nm (285, 570, 1140 µg/L). The substrate calcein-AM (1 µM) was added for another 60 min. Error bars represent the mean  $\pm$  SD of 3 independent experiments performed in duplicate. Significant differences from untreated controls are marked with asterisks ( $P < 0.05$ ).

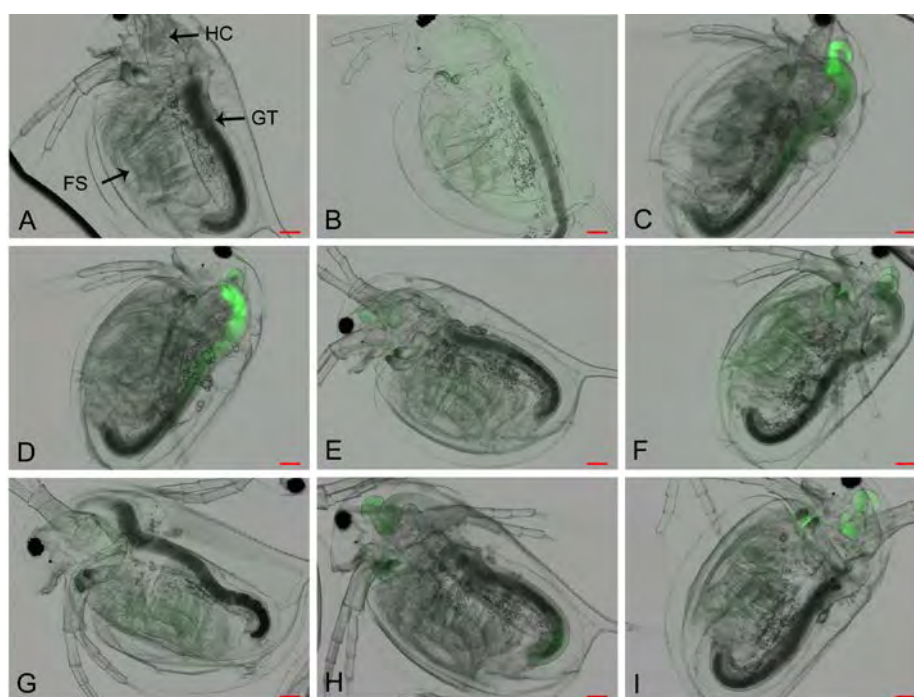


**Figure 4.** Representative fluorescence microscopy images of *D. magna* either unexposed (A), exposed to 1 µM of the substrate Calcein-AM (B), plus the inhibitors 50 µM Verapamil-HCl (C), 7.5 µM MK571 (D), 45 µM PFOS (E), 12.5 µM BPA (F), 0.9 µg/L AgNO<sub>3</sub> (G), 0.4 µg/L Ag 23 nm (H), or 9 µg/L Ag 27 nm (I). Scale bar is 100 µM. HC: hepatic ceca; GT: gut; FS: filtering setae.

As can be seen in Figures 4C-D, calcein accumulated in the gut and hepatic ceca especially of verapamil and MK571-exposed daphnids (Figure 4C-D), and to a lesser extent in

the PFOS and BPA exposed animals (Figure 4E-F). Calcein was also detectable in the thoracic appendages where the filtering setae are localized. In the AgNO<sub>3</sub>-exposed daphnids calcein fluorescence was mainly detected in the filtering setae (Figure 4G) (for details see the calcein channel in Figure S5). Both Ag 23 nm and 27 nm-exposed animals showed high calcein fluorescence signals in the intestinal ceca while calcein was also localized in the shell gland of Ag 23 nm-exposed animals (Figure 4H and I). All the images with the different filters can be found in the Supporting Information (Figure S5). Due to the absence of effects of Ag NPs 20 and 200 nm both in *in vitro* and *in vivo* CEPIA, fluorescence microscopy was not performed with these particles.

### *Abcb1* induction in Ag NP-exposed daphnids

**Table 3.** Relative quantity and quantification cycles of *abcb1* and the housekeeping genes *18S* and *actin* in 48 hour old daphnids exposed for 24 hours to Ag NPs 20, 23, 27, 200 nm and AgNO<sub>3</sub> (mean ± standard deviation, n=5).

Treatment	<i>18S</i>		<i>actin</i>		<i>abcb1</i>	
	CNRQ	Cq	CNRQ	Cq	CNRQ	Cq
Ctrl	1.00 ± 0.07	4.92 ± 0.42	1.01 ± 0.14	15.37 ± 0.49	1.01 ± 0.18	23.13 ± 1.16
Ag 23	1.01 ± 0.13	4.99 ± 0.34	1.09 ± 0.07	15.26 ± 0.12	0.89 ± 0.15	23.02 ± 0.31
Ag 27	1.02 ± 0.05	5.10 ± 0.23	1.13 ± 0.07	15.42 ± 0.22	0.96 ± 0.06	23.10 ± 0.21
Ag 20	1.05 ± 0.06	5 ± 0.23	1.06 ± 0.09	15.34 ± 0.26	1.09 ± 0.15	22.73 ± 1.11
Ag 200	1.13 ± 0.10	5.11 ± 0.24	1.21 ± 0.08	15.42 ± 0.27	1.13 ± 0.19	24.33 ± 1.36
AgNO <sub>3</sub>	1.11 ± 0.13	5.02 ± 0.14	1.13 ± 0.11	15.40 ± 0.23	0.95 ± 0.14	24.21 ± 1.66

CNRQ= calibrated normalized relative quantity; Cq= quantification cycle

The *abcb1*, one of the genes responsible for MXR in organisms and cells, was expressed in 72 hr old *D. magna* juveniles, although at lower levels compared to the housekeeping genes *18S* and *actin*. Exposure to Ag NPs or AgNO<sub>3</sub> for 24 hours at the EC<sub>10</sub> level (based on the previously performed acute toxicity test (Georgantzopoulou et al. 2013)) did not result in altered *abcb1* expression levels (Table 3).

## Discussion

In the present study we examined the *in vitro* and *in vivo* modulation of MXR activity by Ag NPs (Ag 20, 200, 23 and 27 nm) and AgNO<sub>3</sub> along with common environmental contaminants such as PFOS and BPA. In the *in vitro* model MDCKII-MDR1, Ag NPs 23 nm and AgNO<sub>3</sub> inhibited the calcein efflux demonstrating that they can lead to a compromised MXR function. In the juvenile *D. magna*, the biologically synthesized Ag NPs (Ag 23 and 27 nm) and AgNO<sub>3</sub> as well as the common environmental contaminants PFOS and BPA led to increased levels of calcein accumulation.

The wild type MDCKII cells showed 3.5 times lower calcein accumulation than the P-gp overexpressing MDCKII-MDR1 cells upon exposure to Ag NPs 23 nm, supporting the conclusion that the effects of the Ag NPs are through interference with the P-gp protein and not due to a specific effect via e.g. interference with the cell membrane permeability.

The Ag NPs clearly release Ag ions in the DMEM medium (Table S1), especially the Ag 23 NPs synthesized by *Ocimum sanctum*. Although these results suggest that Ag ions contribute to the toxicity, the differences in responses between the Ag NPs and AgNO<sub>3</sub> cannot be explained solely based on the Ag ions released as a higher fold induction was observed in the case of Ag NPs 23 nm compared to AgNO<sub>3</sub> with comparable dissolved Ag concentrations in the medium. In addition to size effects, factors such as surface charge and the specific molecules present on the NP surface can play important roles on the interaction with the cell and uptake. (Zhao et al. 2011) (Lundqvist et al. 2008) Positively charged NPs are more readily taken up by cells than neutral or negatively charged NPs, probably due to the more efficient binding to the negatively charged groups of the cell membrane. (Zhao et al. 2011) Ag NPs 23 and 27 nm are plant leaf extracts-synthesized which results in the presence of biomolecules on the surface of the NPs as shown with Fourier transform infrared spectroscopy (FTIR) in previous studies. (Balachandran 2012; Balachandran et al. 2012; Georgantzopoulou et al. 2013) Most of the bands assigned for the different functional molecules present were common for both NPs (as revealed with FTIR), an additional band was observed in Ag NPs 27 nm that may confer higher stability in the media. (Balachandran 2012; Balachandran et al. 2012; Georgantzopoulou et al. 2013)

The *in vivo* CEPIA method with *D. magna* was optimized for life stage, sample size and method that would allow less steps to be taken. Based on a recent study showing an increase in levels of the efflux transporters *abcb1* and *abcc1/3* with the developmental stage of

*D. magna* (Campos et al. 2014) combined with the transparency of the animal, 48 hours old juveniles were chosen as test animals. The *abcb1* expression at the juvenile stage (Campos et al. 2014) was confirmed in the current study. The *in vivo* CEPIA method was technically optimized with daphnids using the model inhibitors verapamil-HCl and MK571. The results with these specific inhibitors confirm that the inhibition of the MXR activity in 48-hour old daphnids was indeed P-gp and MRP-mediated. The results with 5  $\mu$ M MK571 are in accordance with a previous study using sea urchin embryos as a model organism (Bosnjak et al. 2009). The environmental contaminants PFOS and BPA also modulated the transporter activity in daphnids, resulting in even higher calcein accumulation than the model inhibitors verapamil and MK571 (Table 2). This is also in accordance with the study using sea urchin larvae (Anselmo et al. 2012). PFOS has been shown before to inhibit the P-gp activity in MDCKII-MDR1 cells (Georgantzopoulou et al. 2014) and this and other long chain perfluoroalkyl acids interfered with MXR activity in the gills of the mussels *Mytilus californianus* (Stevenson et al. 2006) and in the zebra mussels *Dreissena polymorpha* (Fernández-Sanjuan et al. 2013).

An increase in calcein accumulation was observed in AgNO<sub>3</sub>, Ag 23 nm and Ag 27 nm-exposed daphnids while Ag 20 and 200 nm treatment did not exert any significant effect. The fluorescence microscopy images reveal that calcein was mainly accumulated in the gut and intestinal ceca of the daphnids exposed to the model inhibitors verapamil-HCl and MK571. Exposure to PFOS and BPA led to calcein accumulation in the filter setae of the thoracic appendages where the gills are located. In crustaceans the gills are the main sites of interaction and accumulation of metals and toxic compounds that can be adsorbed on the cuticular side of the gills (Henry et al. 2012). AgNO<sub>3</sub> exposure led to a calcein fluorescence signal present in the filter setae while Ag NPs 23 and 27 nm resulted in increased fluorescence in the intestinal ceca as well as the shell gland that is the organ responsible for excretion (Ebert 2005; Smirnov 2014). Therefore it seems that different xenobiotics interfere with different parts of the daphnid's body and MXR-related transporters seem to be localized in different organs such as the gut, intestinal ceca, filter setae and shell glands that are all associated with barrier or excretory function. It has been suggested that the gills of fish are the initial uptake sites for Ag NPs although Ag was also present in the gut, liver and brain depending on the surface coating (Kwok et al. 2012). The intestinal ceca participate in the production of digestive fluids (Ebert 2005) and were reported of being the sites of Cd and Ca<sup>2+</sup> uptake (Smirnov 2014).

As previously shown the Ag release is medium-dependent (Georgantzopoulou et al. 2013) and in the daphnids' exposure medium the highest levels of dissolved Ag were measured. Ag 23 nm NPs released more ions compared to the rest of the particles (5 times more compared to Ag 27 nm NPs) (Table S1) indicating that the differences observed between the similar sized Ag NPs can be attributed to the Ag released. The dissolved Ag concentration was higher though in the case of AgNO<sub>3</sub> (1.4 times higher compared to Ag NPs 23 nm), that cannot explain the differences in calcein accumulation increase suggesting a particle effect as well. However, the Ag ion concentration may be underestimated due to the potential binding of Ag species on the centrifugal filter. In the daphnids exposed for 24 hrs, 41% of the Ag administered as Ag NPs 23 nm was recovered from daphnids. For AgNO<sub>3</sub> and the other particles this was in the range of 0.17-0.43% of the total Ag dosed. Likewise, Ag signal was detected with secondary ion mass spectrometry (NanoSIMS) in the MDCKII-MDR1 and MDCKII-WT cells in the case of Ag 23 nm but not in the case of AgNO<sub>3</sub> (Figures S3-4). It cannot be excluded that Ag 23 nm has a different route and rate of transport rate than the other NPs and AgNO<sub>3</sub> tested. There is a different route for intracellular uptake of Ag NPs and dissolved Ag *in vivo* for the estuarine polychaete *N. diversicolor* (García-Alonso et al. 2011). It seems that the Ag NPs 23 nm are more readily taken up by cells and in organisms and may more readily release the ions intracellularly after uptake.

Although the chemicals that interfere with efflux transporters are chemically and structurally unrelated it has been suggested that the optimal characteristics required for a compound to interact with P-gp, include the presence of a cyclic structure, molecular weight of 391-490 Da, a log Kow between 3.6-4.5 (Bain and LeBlanc 1996) and a hydrogen bonding potential (Bain et al. 1997) although several metal have been found to interfere with the MXR activity (Achard-Joris and Bourdineaud 2006; Bosnjak et al. 2009; Della Torre et al. 2012). AgNO<sub>3</sub> and Ag NPs, however, do not meet these requirements to interact with the transporters. As in the case of NPs these structure-activity relationships are not applicable, the presence of functional groups, capping agents as well as charge seems to be very important. It has been previously shown that the transport of positively and negatively charged polystyrene NPs is mediated by P-gp and MRP1, respectively in the colon cancer cell line Caco-2 (Bhattacharjee et al. 2013). It is not known whether Ag acts directly on the transporter by binding to the substrate site or indirectly by blocking the ATPase activity or by acting on the membrane environment and thus causing conformational changes and affecting the transporter functionality. Ag NPs inhibit the Na<sup>+</sup>/K<sup>+</sup>-ATPase activity in the gills of

zebrafish (Katuli et al. 2014) and rainbow trout (Schultz et al. 2012). However, addition of verapamil at the end of the Ag NP exposure in MDCKII-MDR1 and MDCKII-WT cells in our experiments led to an increase in the calcein accumulation reaching the verapamil levels suggesting that the transporters are still functional (Figure S6). Ag has a high affinity for cysteine and sulfhydryl groups so Ag ions and Ag NPs may react with the sulfhydryl and amino groups of the transporters and alter their functionality. It has been previously suggested that MRP2 may be involved in the transport of Hg while Cd affects the P-gp activity (Achard-joris et al. 2005; Della Torre et al. 2012). The MRPs were suggested to be responsible for inorganic Hg elimination after association with glutathione whereas that was not the case for organic Hg (Bosnjak et al. 2009). Further research should elucidate the exact mechanism of Ag NP/ions-MXR transporters interaction.

*Abcb1* transcripts were present in 48 hours old *D. magna* but no changes in transcript expression were observed upon treatment with any of the Ag NPs and AgNO<sub>3</sub> at the EC<sub>10</sub> level for 24 hours. An increase in *abcb1* and *abcc* transcript levels was previously observed in zebra mussel larvae exposed to dacthal and HgCl<sub>2</sub> while the changes in gills of adults were less evident although higher efflux activity was observed for treated animals. Changes at the transcription level do not necessarily correspond to changes in the protein level of transporters (Navarro et al. 2012). Some perfluorinated compounds have been shown to increase P-gp protein levels in the mussels *M. californianus* after 48 hours of exposure, and it was suggested that this was the result of a general stress response involving the expression of several stress proteins (Stevenson et al. 2006). The daphnids in our study were exposed to the EC<sub>10</sub> level for only 24 hours, and the basal level of the existing MXR and other protecting mechanisms seem to be sufficient for daphnids to be able to cope with the chemical stress induced by the Ag NPs and AgNO<sub>3</sub>, as no impact was detected on the expression level of *abcb1*.

Currently environmental concentrations of Ag NPs cannot yet be determined. Based on probabilistic material flow analysis the maximum predicted environmental concentrations (PEC) for Ag NPs in Europe are 0.764 ng/L and 42.5 ng/L for surface water and sewage treatment plant effluent, respectively (Gottschalk et al. 2009). In an intermediate scenario the maximum PEC for Ag in river water was 140 ng/L (Blaser et al. 2008) which is only slightly lower than the EC<sub>50s</sub> obtained in our study for AgNO<sub>3</sub> and Ag 23 nm of 440 and 180 ng/L, while 320 ng/L are expected in maximum scenario (Blaser et al. 2008) so e.g. potentiation of

effects of compounds that are MXR substrates (Anselmo et al. 2012) cannot be excluded in those aquatic environments.

The results we obtained with the *in vitro* study correspond well with the data obtained with *D. magna* juveniles, indicating a similar specificity and role of these transporters in *D. magna* tissues. This means that the *in vitro* tests can indicate whether effects are to be expected in *D. magna*, which is in accordance with the results obtained with sea urchin larvae. The Ag 27 nm NPs, however, only gave an effect in *D. magna*, possibly via other transporters than the P-gp that is over-expressed in the MDCKII MDR1 cells. This would be in accordance with the reports that sea urchin embryos also express *abcc* and *abcg2* transporter genes (Shipp and Hamdoun 2012) and that in *D. magna* the ABC transporters *abcc1/3*, *abcc4* and *abcc5* also contribute to MXR (Campos et al. 2014). Therefore, the increase in calcein fluorescence observed in Ag 27 nm-exposed daphnids could be due to the inhibition of other MXR-related transporters.

In the current study, Ag 23 and 27 NPs and AgNO<sub>3</sub> were found to modulate the efflux activity of MXR-involved transporters both *in vitro* and *in vivo*, and this effect was mediated by the contribution of both released Ag ions and the Ag NP themselves. *D. magna* proved to be a good *in vivo* model for studying the MXR mechanism and its modulation by NPs. The *in vivo* CEPIA method with *D. magna* was optimized, and combined with the fact that it is a model species in standard ecotoxicity tests (OECD guideline 202)(Organisation for Economic Co-operation and Development (OECD) 2004) makes it a relatively easy assay to incorporate in testing of compounds and NPs for potential mixture toxicity. The modulation by NPs of the MXR as a first line of defense, which is present in all organisms tested, may have broader implications, even for human health. Therefore, the new insights in the toxicology of Ag NPs this study brings should be further elaborated for real world exposures in which exposure to Ag NPs always occurs in combination with mixtures of chemicals.

### **Supporting Information**

Supporting Information includes TEM images and Ag NP size distributions in different media, Ag localization *in vitro* (NanoSIMS), fluorescence microscopy images of CEPIA with daphnids with all channels, calcein accumulation *in vitro* after co-exposure of Ag NPs/AgNO<sub>3</sub> with verapamil, Ag release in different media and Ag concentration in exposed daphnids.

## Acknowledgements

This study was funded by NanEAUII within the FNR-funded 'Core2010' program (C10/SR/799842). The authors would like to thank A.H. Schinkel for providing the MDCKII-MDR1 cell line and D. Collard and S. Bonot (Department of Environment and Agro-biotechnologies, Centre de Recherche Public-Gabriel Lippmann, Luxembourg) for maintenance of the *D. magna* cultures and their helpful advice. The authors also thank S. Contal (Department of Environment and Agro-biotechnologies, Centre de Recherche Public-Gabriel Lippmann, Luxembourg) for the excellent assistance with the cell culture assays experiments, L. Hoffmann (Department of Environment and Agro-biotechnologies, Centre de Recherche Public-Gabriel Lippmann, Luxembourg) for the useful comments on the manuscript and V. Peardon for the English editing of the manuscript. The contribution of S. Girija (Department of Biotechnology, Bharathiar University, India) in the development of the plant-synthesized Ag NPs is gratefully acknowledged.

## References

- Achard-Joris M, Bourdineaud J-P. 2006. Heterologous expression of bacterial and human multidrug resistance proteins protect *Escherichia coli* against mercury and zinc contamination. *Biometals* 19:695–704.
- Achard-joris M, van den Berg van Saparoea HB, Driessen AJM, Bourdineaud J. 2005. Heterologously expressed bacterial and human multidrug resistance proteins confer cadmium resistance to *Escherichia coli*. *Biochemistry* 44: 5916–5922.
- Ambudkar SV, Dey S, Hrycyna CA, Ramachandra M, Pastan I, Gottesman MM. 1999. Biochemical, cellular, and pharmacological aspects of the multidrug transporter. *Annu. Rev. Pharmacol. Toxicol.* 39:361–98.
- Anselmo HMR, van den Berg JHJ, Rietjens IMCM, Murk AJ. 2012. Inhibition of cellular efflux pumps involved in multi xenobiotic resistance (MXR) in echinoid larvae as a possible mode of action for increased ecotoxicological risk of mixtures. *Ecotoxicology* 21:2276–87.
- Bain LJ, LeBlanc GA. 1996. Interaction of structurally diverse pesticides with the human MDR1 gene product P-glycoprotein. *Toxicol. Appl. Pharmacol.* 141:288–98.
- Bain LJ, McLachlan JB, LeBlanc GA. 1997. Structure-activity relationships for xenobiotic transport substrates and inhibitory ligands of P-glycoprotein. *Environ. Health Perspect.* 105: 812–8.
- Balachandran YL. 2012. Bio-molecules templated silver nanoparticles: synthesis, characterization and their applications. Bharathiar University.
- Balachandran YL, Girija S, Selvakumar R, Tongpim S, Gutleb AC, Suriyanarayanan S. 2013. Differently environment stable bio-silver nanoparticles: study on their optical enhancing and antibacterial properties. *PLoS One* 8:e77043.
- Balachandran YL, Peranantham P, Selvakumar R, Gutleb AC, Girija S. 2012. Size-controlled green synthesis of silver nanoparticles using dual functional plant leaf extract at room temperature. *Int. J. Green Nanotechnol.* 4:310–325.

- Bhattacharjee S, Opstal EJ, Alink GM, Marcelis ATM, Zuilhof H, Rietjens IMCM. 2013. Surface charge-specific interactions between polymer nanoparticles and ABC transporters in Caco-2 cells. *J. Nanoparticle Res.* 15:1695.
- Blaser SA, Scheringer M, Macleod M, Hungerbühler K. 2008. Estimation of cumulative aquatic exposure and risk due to silver: contribution of nano-functionalized plastics and textiles. *Sci. Total Environ.* 390:396–409.
- Bosnjak I, Uhlinger KR, Heim W, Smital T, Franekić-Colić J, Coale K, et al. 2009. Multidrug efflux transporters limit accumulation of inorganic, but not organic, mercury in sea urchin embryos. *Environ. Sci. Technol.* 43:8374–80.
- Callaghan R, Crowley E, Potter S, Kerr ID. 2008. P-glycoprotein: so many ways to turn it on. *J. Clin. Pharmacol.* 48:365–78.
- Campos B, Altenburger R, Gómez C, Lacorte S, Piña B, Barata C, et al. 2014. First evidence for toxic defense based on the multixenobiotic resistance (MXR) mechanism in *Daphnia magna*. *Aquat. Toxicol.* 148:139–51.
- De Cerio OD, Bilbao E, Cajaraville MP, Cancio I. 2012. Regulation of xenobiotic transporter genes in liver and brain of juvenile thicklip grey mullets (*Chelon labrosus*) after exposure to Prestige-like fuel oil and to perfluorooctane sulfonate. *Gene* 498:50–8.
- Della Torre C, Zaja R, Loncar J, Smital T, Focardi S, Corsi I. 2012. Interaction of ABC transport proteins with toxic metals at the level of gene and transport activity in the PLHC-1 fish cell line. *Chem. Biol. Interact.* 198:9–17.
- Ebert D. 2005. Introduction to *Daphnia* biology. In *Ecology, Epidemiology, and Evolution of Parasitism in Daphnia [Internet]*, National Center for Biotechnology Information.
- Endicott JA, Ling V. 1989. The biochemistry of P-glycoprotein-mediated multidrug resistance. *Annu. Rev. Biochem.* 58:137–171.
- Epel D, Luckenbach T, Stevenson CN, Macmanus-Spencer LA, Hamdoun A, Smital T. 2008. Efflux transporters: newly appreciated roles in protection against pollutants. *Environ. Sci. Technol.* 42: 3914–20.
- Faria M, Navarro A, Luckenbach T, Piña B, Barata C. 2011. Characterization of the multixenobiotic resistance (MXR) mechanism in embryos and larvae of the zebra mussel (*Dreissena polymorpha*) and studies on its role in tolerance to single and mixture combinations of toxicants. *Aquat. Toxicol.* 101:78–87.
- Fernández-Sanjuan M, Faria M, Lacorte S, Barata C. 2013. Bioaccumulation and effects of perfluorinated compounds (PFCs) in zebra mussels (*Dreissena polymorpha*). *Environ. Sci. Pollut. Res. Int.* 20:2661–9.
- Feswick A, Griffitt RJ, Siebein K, Barber DS. 2013. Uptake, retention and internalization of quantum dots in *Daphnia* is influenced by particle surface functionalization. *Aquat. Toxicol.* 130-131:210–218.
- Gaiser BK, Fernandes TF, Jepson MA, Lead JR, Tyler CR, Baalousha M, et al. 2012. Interspecies comparisons on the uptake and toxicity of silver and cerium dioxide nanoparticles. *Environ. Toxicol. Chem.* 31:144–54.
- García-Alonso J, Khan FR, Misra SK, Turmaine M, Smith BD, Rainbow PS, et al. 2011. Cellular internalization of silver nanoparticles in gut epithelia of the estuarine polychaete *Nereis diversicolor*. *Environ. Sci. Technol.* 45:4630–6.
- Georgantzopoulou A, Balachandran YL, Rosenkranz P, Dusinska M, Lankoff A, Wojewodzka M, et al. 2013. Ag nanoparticles: size- and surface-dependent effects on model aquatic organisms and uptake evaluation with NanoSIMS. *Nanotoxicology* 7:1168–78.
- Georgantzopoulou A, Skoczyńska E, van den Berg JHJ, Brand W, Legay S, Klein SG, et al. 2014. P-gp efflux pump inhibition potential of common environmental contaminants determined *in vitro*. *Environ. Toxicol. Chem.* 33:804–13.

- Gliga AR, Skoglund S, Wallinder IO, Fadeel B, Karlsson HL. 2014. Size-dependent cytotoxicity of silver nanoparticles in human lung cells: the role of cellular uptake, agglomeration and Ag release. Part. Fibre Toxicol. 11:11.
- Gottschalk F, Sonderer T, Scholz RW, Nowack B. 2009. Modeled environmental concentrations of engineered nanomaterials (TiO<sub>2</sub>, ZnO, Ag, CNT, fullerenes ) for different regions. Environ. Sci. Technol. 43: 9216–9222.
- Griffitt RJ, Luo J, Gao J, Bonzongo J-C, Barber DS. 2008. Effects of particle composition and species on toxicity of metallic nanomaterials in aquatic organisms. Environ. Toxicol. Chem. 27:1972–8.
- Heckmann L-H, Connon R, Hutchinson TH, Maund SJ, Sibly RM, Callaghan A. 2006. Expression of target and reference genes in *Daphnia magna* exposed to ibuprofen. BMC Genomics 7:175.
- Hellemans J, Mortier G, De Paepe A, Speleman F, Vandesomepele J. 2007. qBase relative quantification framework and software for management and automated analysis of real-time quantitative PCR data. Genome Biol. 8:R19.
- Henry RP, Lucu C, Onken H, Weihrauch D. 2012. Multiple functions of the crustacean gill: osmotic/ionic regulation, acid-base balance, ammonia excretion, and bioaccumulation of toxic metals. Front. Physiol. 3:431.
- Hole P, Sillence K, Hannell C, Maguire CM, Roesslein M, Suarez G, et al. 2013. Interlaboratory comparison of size measurements on nanoparticles using nanoparticle tracking analysis (NTA). J. Nanopart. Res. 15:2101.
- Ivanina A V, Sokolova IM. 2008. Effects of cadmium exposure on expression and activity of P-glycoprotein in eastern oysters, *Crassostrea virginica* Gmelin. Aquat. Toxicol. 88:19–28.
- Katuli KK, Massarsky A, Hadadi A, Pourmehran Z. 2014. Silver nanoparticles inhibit the gill Na<sup>+</sup>/K<sup>+</sup>-ATPase and erythrocyte AChE activities and induce the stress response in adult zebrafish (*Danio rerio*). Ecotoxicol. Environ. Saf. 106:173–80.
- Kurelec B. 1992. The multixenobiotic resistance mechanism in aquatic organisms. Crit. Rev. Toxicol. 22:23–43.
- Kwok KWH, Auffan M, Badireddy AR, Nelson CM, Wiesner MR, Chilkoti A, et al. 2012. Uptake of silver nanoparticles and toxicity to early life stages of Japanese medaka (*Oryzias latipes*): effect of coating materials. Aquat. Toxicol. 120-121:59–66.
- Lankoff A, Sandberg WJ, Wegierek-ciuk A, Lisowska H, Refsnes M, Schwarze PE, et al. 2012. The effect of agglomeration state of silver and titanium dioxide nanoparticles on cellular response of HepG2 ,A549 and THP-1 cells. Toxicol. Lett. 208:197–213.
- Loo TW, Bartlett MC, Clarke DM. 2004. The drug-binding pocket of the human multidrug resistance P-glycoprotein is accessible to the aqueous medium. Biochemistry 43:12081–9.
- Lundqvist M, Stigler J, Elia G, Lynch I, Cedervall T, Dawson KA. 2008. Nanoparticle size and surface properties determine the protein corona with possible implications for biological impacts. Proc. Natl. Acad. Sci. USA 105: 14265–14270.
- Montaño M, Bakker E, Murk AJ. 2010. Meta-analysis of supramaximal effects in *in vitro* estrogenicity assays. Toxicol. Sci. 115:462–474.
- Navarro A, Weißbach S, Faria M, Barata C, Piña B, Luckenbach T. 2012. Abcb and Abcc transporter homologs are expressed and active in larvae and adults of zebra mussel and induced by chemical stress. Aquat. Toxicol. 122-123:144–52.
- Organisation for Economic Co-operation and Development (OECD). 2004. OECD Guidelines for the testing of chemicals/ section 2: effects on biotic systems, Test No. 202: *Daphnia* sp. acute immobilisation test.

- Park MVDZ, Neigh AM, Vermeulen JP, de la Fonteyne LJJ, Verharen HW, Briedé JJ, et al. 2011. The effect of particle size on the cytotoxicity, inflammation, developmental toxicity and genotoxicity of silver nanoparticles. *Biomaterials* 32:9810–9817.
- Rosenkranz P, Chaudhry Q, Stone V, Fernandes TF. 2009. A comparison of nanoparticle and fine particle uptake by *Daphnia magna*. *Environ. Toxicol. Chem.* 28:2142–9.
- Schinkel AH, Jonker JW. 2003. Mammalian drug efflux transporters of the ATP binding cassette (ABC) family: an overview. *Adv. Drug Deliv. Rev.* 55: 3–29.
- Schultz AG, Ong KJ, MacCormack T, Ma G, Veinot JGC, Goss GG. 2012. Silver nanoparticles inhibit sodium uptake in juvenile rainbow trout (*Oncorhynchus mykiss*). *Environ. Sci. Technol.* 46:10295–301.
- Shipp LE, Hamdoun A. 2012. ATP-binding cassette (ABC) transporter expression and localization in sea urchin development. *Dev. Dyn.* 241:1111–24.
- Smirnov NN. 2014. Excretion. In *Physiology of the cladocera*, pp. 99–106, Elsevier Inc.
- Smital T, Luckenbach T, Sauerborn R, Hamdoun AM, Vega RL, Epel D. 2004. Emerging contaminants-pesticides, PPCPs, microbial degradation products and natural substances as inhibitors of multixenobiotic defense in aquatic organisms. *Mutat. Res.* 552:101–17.
- Stevenson CN, MacManus-Spencer LA, Luckenbach T, Luthy RG, Epel D. 2006. New perspectives on perfluorochemical ecotoxicology: inhibition and induction of an efflux transporter in the marine mussel, *Mytilus californianus*. *Environ. Sci. Technol.* 40: 5580–5.
- Van Tellingen O. 2001. The importance of drug-transporting P-glycoproteins in toxicology. *Toxicol. Lett.* 120: 31–41.
- Wijnhoven SWP, Peijnenburg WJGM, Herberts CA, Hagens WI, Oomen AG, Heugens EHW, et al. 2009. Nano-silver a review of available data and knowledge gaps in human and environmental risk assessment. *Nanotoxicology* 3:109–138.
- Woodrow Wilson International Center for Scholars. 2014. Project on emerging nanotechnologies. Available: <http://www.nanotechproject.org/> [accessed 15 August 2014].
- Zhao F, Zhao Y, Liu Y, Chang X, Chen C, Zhao Y. 2011. Cellular uptake , intracellular trafficking , and cytotoxicity of nanomaterials. *Small* 7:1322–1337.

## Supporting Information for Chapter 5

### *Ag localization in vitro (NanoSIMS)*

Cells were seeded on sterile silicon wafers (Siltronix, Archamps, France) in 12-well plates at a concentration of  $4 \times 10^5$  cells/mL and were incubated overnight at 5% CO<sub>2</sub> and 37°C. The cells were then exposed to 1 mg/L, Ag 20, Ag 200, Ag 23, Ag 27 or AgNO<sub>3</sub> diluted in DMEM without phenol red or FBS for 30 minutes or they were pre-exposed to 120 µM PFOS for 30 minutes. At the end of the exposure period, the monolayers were washed with MilliQ water and fixed with 5% glutaraldehyde in PBS overnight. Glutaraldehyde was removed and the cells were washed with MilliQ water. Samples were analyzed with a NanoSIMS 50 (Cameca, Courbevoie, France) using a Cs<sup>+</sup> primary source (+8 keV), scanning the polarized surface of the sample (-8 keV) with a raster from 20 x 20 µm<sup>2</sup> to 40 x 40 µm<sup>2</sup>. In these conditions with a primary intensity range of 1.0–0.8 pA, the probe-working diameter was in the range 80–100 nm. With a mass resolution  $M/\Delta M$  higher than 4000 to separate isobaric masses (e.g. <sup>12</sup>C<sup>14</sup>N and <sup>13</sup>C<sub>2</sub>), the secondary negative ions recorded simultaneously in the multicollection mode were: <sup>19</sup>F<sup>-</sup> (m= 18,9984), <sup>12</sup>C<sup>14</sup>N<sup>-</sup> (m = 26.00307), <sup>34</sup>S<sup>-</sup> (m = 33.96786) and <sup>107</sup>Ag<sup>-</sup> (m=106.90486). Images were recorded in a pixel format of 256 x 256 image points with a counting time of 20 ms per pixel.

### *Total Ag content in daphnids*

At the end of the exposure as already described for the *abcb1* expression experiment, a pool of 10 daphnids per treatment were collected, transferred in clean Volvic water and digested with 700 µl HNO<sub>3</sub> (Plasma Pure quality, 67-70%, SCP Science, Courtaboeuf, France) and 300 µl H<sub>2</sub>O<sub>2</sub> (30% w/w for metals traces analysis, Fisher Scientific, Belgium) and left to react overnight. Then the volume was completed to 10 ml with demineralized water and the obtained solution was diluted 5 times with 1% HNO<sub>3</sub> before analysis. Silver was analyzed by Inductively Coupled Plasma Mass Spectrometry (ICP-MS)(Georgantzopoulou et al. 2013) (Elan DRC-e, Perkin Elmer, Waltham, MA, USA).

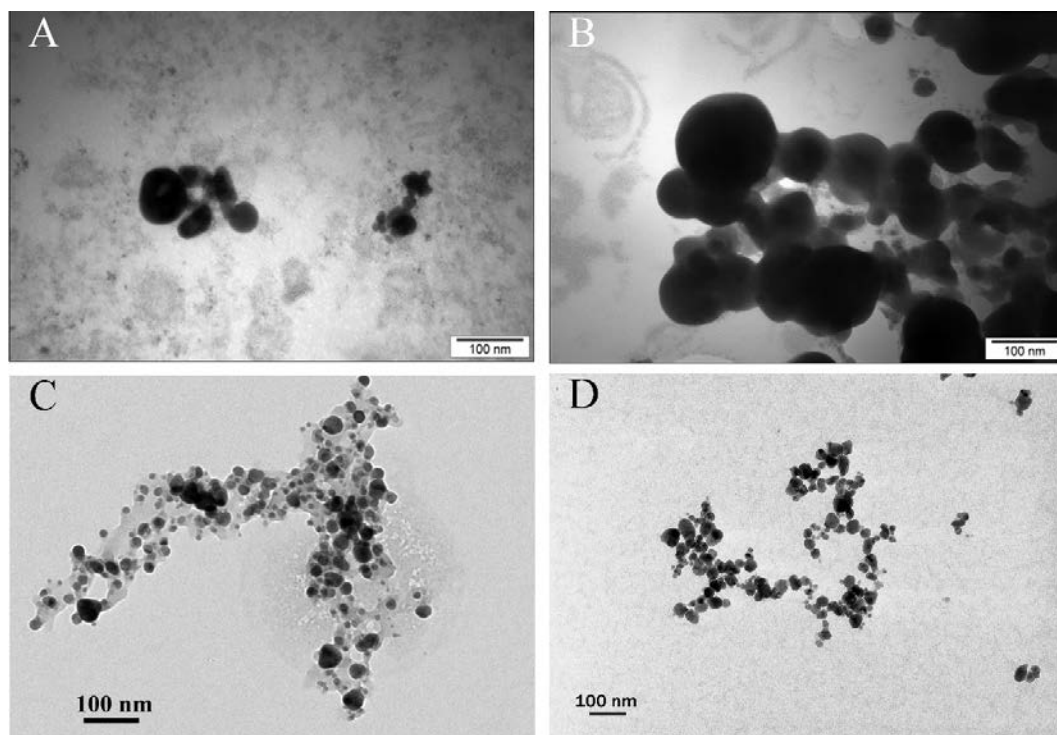


**Figure S1.** TEM micrographs of Ag NPs (A) 20 nm, (B) 200 nm, (C) 23 nm (synthesized using *O. sanctum* plant extract), (D) 27 nm (synthesized using *A. indica*). (Balachandran 2012; Balachandran et al. 2012; Georgantzopoulou et al. 2013; Lankoff et al. 2012).

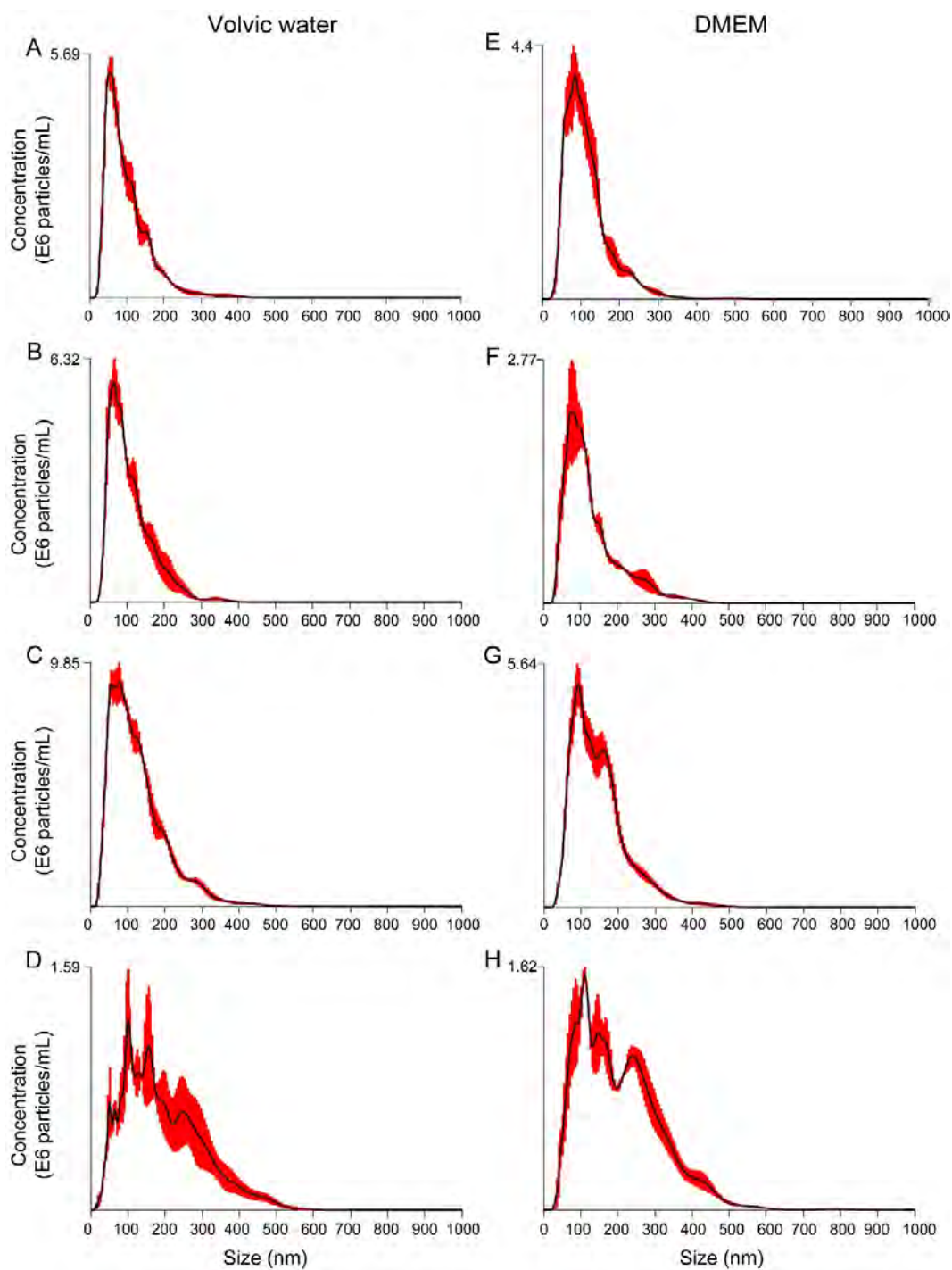


**Figure S2.** Size distribution of Ag NPs 23 nm (A, E), 27 nm (B, F), 20 nm (C, G) and 200 nm (D, H) in Volvic water and DMEM without phenol red and FBS expressed as particle concentration E6/mL. The red error bars indicate the  $\pm$  SD of the mean of triplicate measurements.

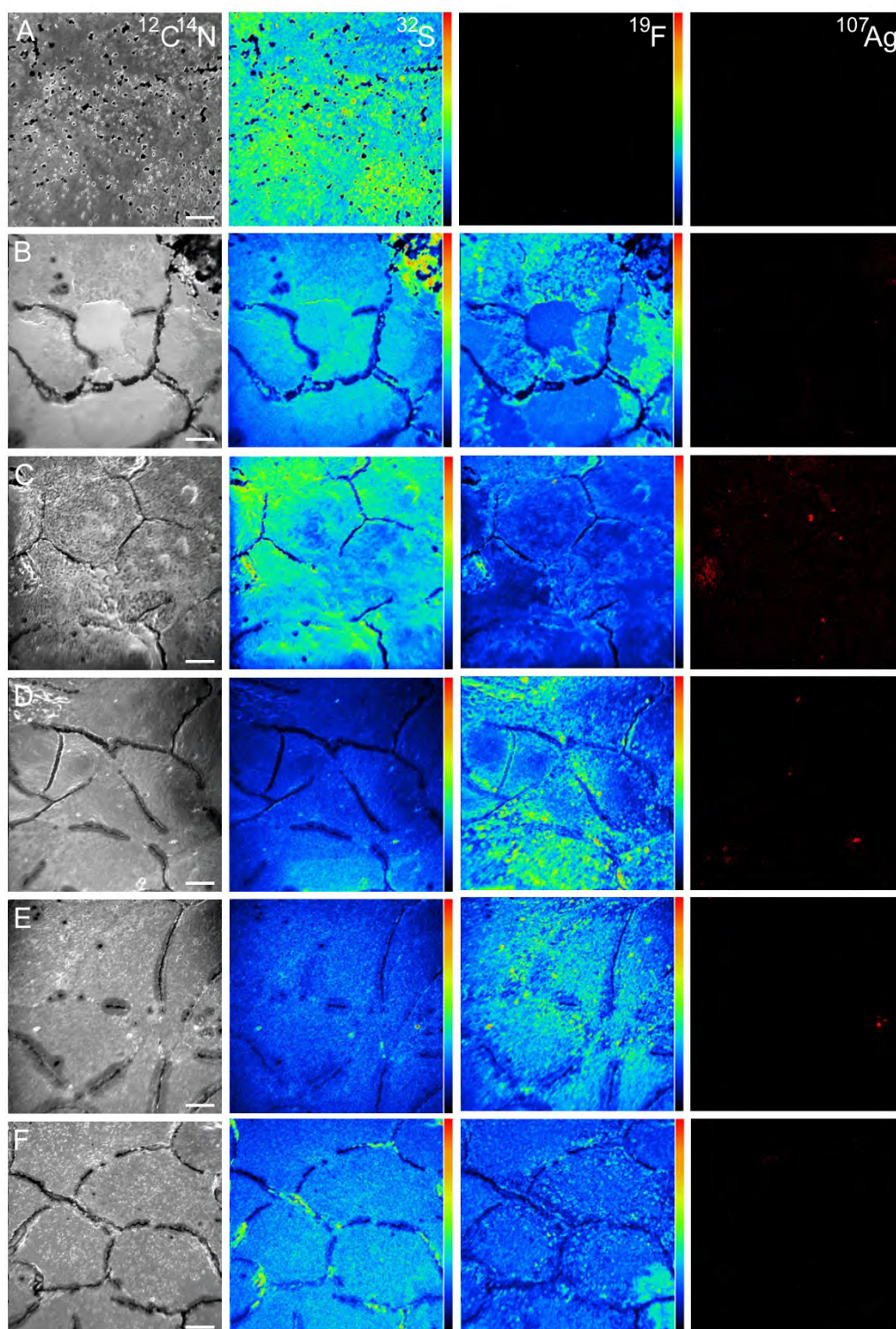


**Figure S3.** Elemental distribution of  $^{12}\text{C}^{14}\text{N}$ ,  $^{34}\text{S}$ ,  $^{19}\text{F}$  and  $^{107}\text{Ag}$  in MDCKII-WT cells exposed to 120  $\mu\text{M}$  PFOS and 1 mg/L of (B)  $\text{AgNO}_3$ , (C) Ag 23 nm, (D) Ag 27 nm, (E) Ag 20 nm and (F) Ag 200 nm. (A) Represents the untreated control. Scale bar is 5  $\mu\text{M}$ .

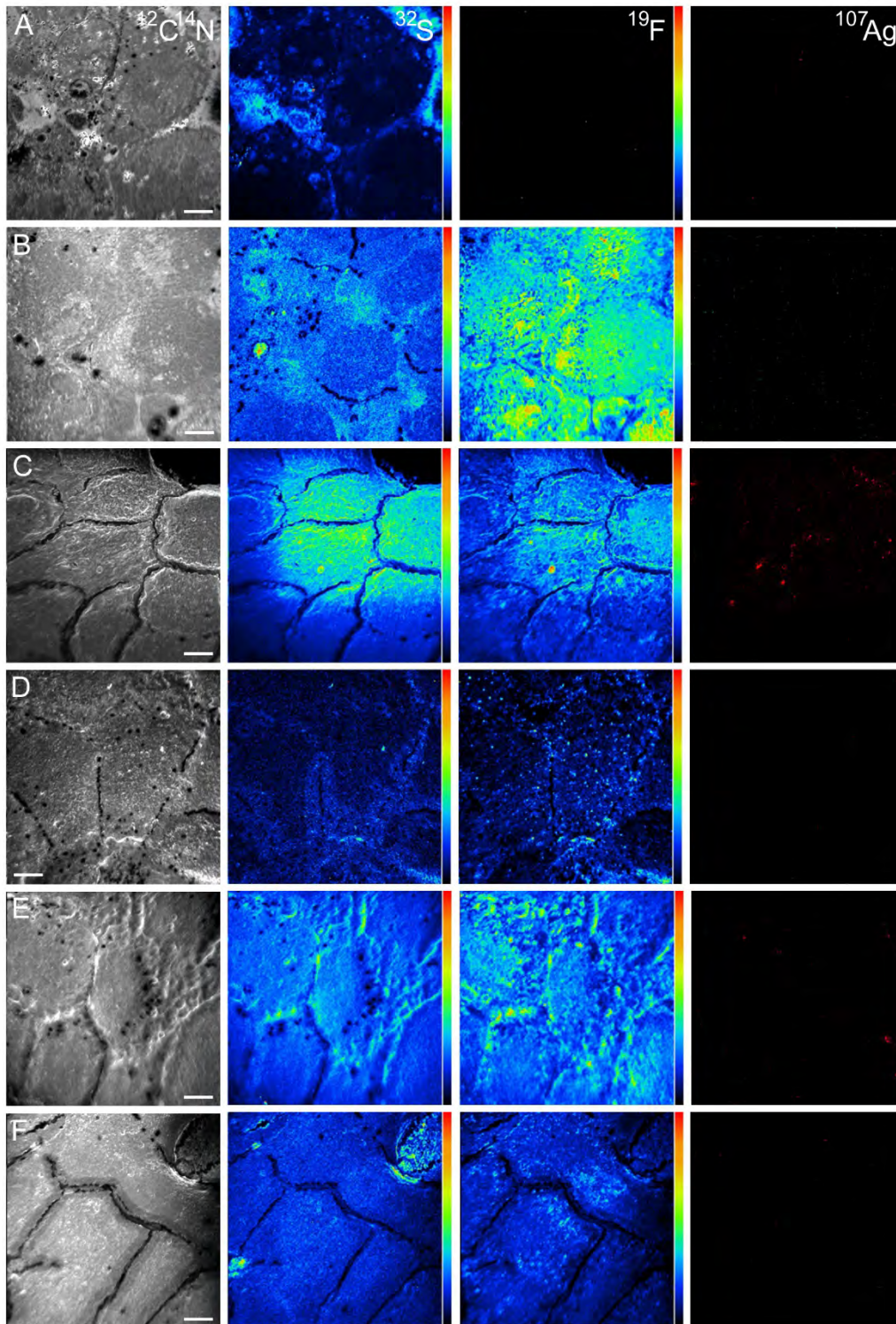


**Figure S4.** Elemental distribution of  $^{12}\text{C}^{14}\text{N}$ ,  $^{34}\text{S}$ ,  $^{19}\text{F}$  and  $^{107}\text{Ag}$  in MDCKII-MDR1 cells exposed to 120  $\mu\text{M}$  PFOS and 1 mg/L of (B)  $\text{AgNO}_3$ , (C) Ag 23 nm, (D) Ag 27 nm, (E) Ag 20 nm and (F) Ag 200 nm. (A) Represents the untreated control. Scale bar is 5  $\mu\text{M}$ .

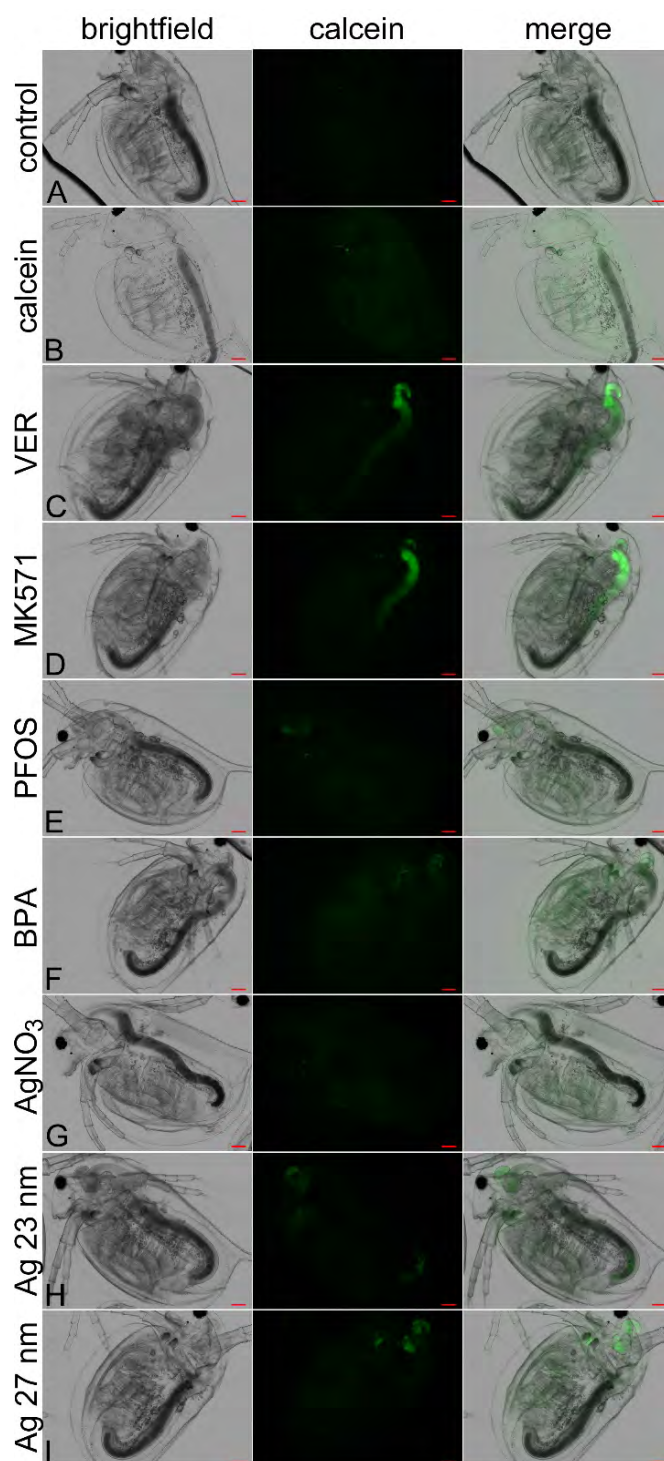


**Figure S5.** Fluorescence microscopy images of *D. magna* exposed to (B) only 1  $\mu\text{M}$  calcein-AM or (C) 50  $\mu\text{M}$  verapamil-HCl, (D) 7.5  $\mu\text{M}$  MK571, (E) 45  $\mu\text{M}$  PFOS, (F) 12.5  $\mu\text{M}$  BPA, (G) 0.9  $\mu\text{g/L}$   $\text{AgNO}_3$ , (H) 0.4  $\mu\text{g/L}$  Ag 23 nm, (I) 9  $\mu\text{g/L}$  Ag 27 nm and 1  $\mu\text{M}$  calcein-AM while (A) is the negative control. The first column shows the bright field image while the second shows the calcein channel. The last column represents the overlay of all channels. Pictures of ten individuals were taken. Scale bar is 100  $\mu\text{M}$ .

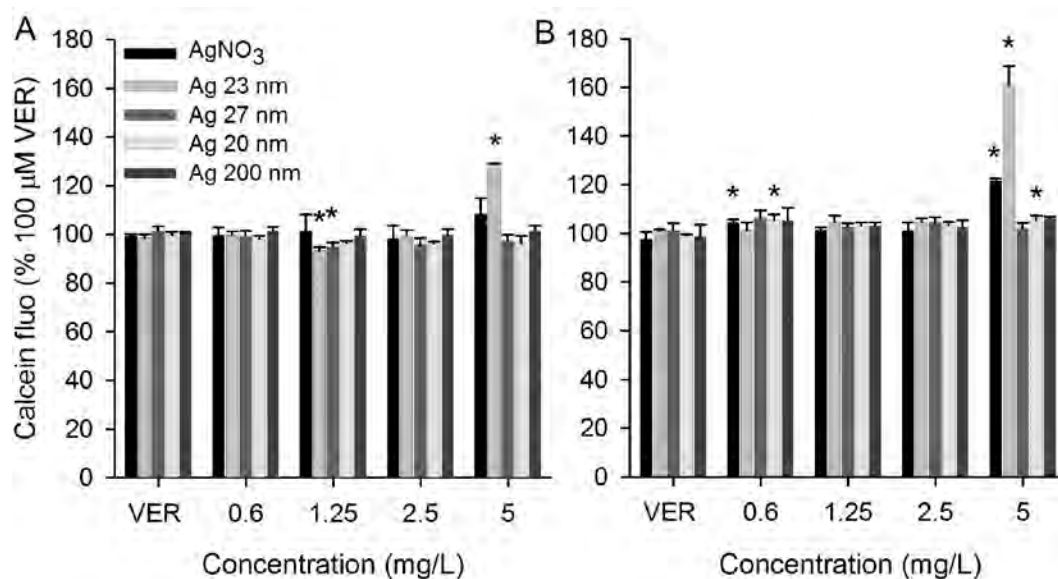


**Figure S6.** Calcein accumulation in (A) MDCKII-WT and (B) MDCKII-MDR1 after exposure to Ag NPs 23 nm, 27 nm, 20 nm, 200 nm and AgNO<sub>3</sub> for 30 min. Calcein-AM was then added for another 30 min and in the end the cells were incubated with 100 μM verapamil-HCl for 15 min. Error bars represent the mean ± SD of triplicates. Significant differences from respective untreated controls are marked with asterisks (P < 0.05).

**Table S1.** Quantification of Ag released in media and present in daphnids. The amount of Ag present in the exposure medium DMEM without phenol red and FBS is expressed as % from the total Ag added. Results are presented as mean ± standard deviation of triplicates.

	Ag released in medium (% total Ag added)		Ag in daphnids (% total Ag added)
	DMEM <sup>a</sup>	volvic water <sup>b,d</sup>	Daphnids <sup>c</sup>
AgNO <sub>3</sub>	0.8 ± 0.11	40.5 ± 2.96	0.17
Ag 23 nm	0.9 ± 0.15	29.2 ± 6.49	40.9
Ag 27 nm	0.03 ± 0.007	5.47 ± 0.87	0.43
Ag 20 nm	< 0.025	0.51 ± 4.47	0.25
Ag 200 nm	< 0.025	0.28 ± 0.018	0.32

<sup>a</sup> the quantification was performed with UF/ICP-MS after exposure of the cells with Ag NPs or AgNO<sub>3</sub> for 1 hr (1 mg/L).

<sup>b</sup> the quantification was performed with UF/ICP-MS after incubation of the Ag NPs or AgNO<sub>3</sub> with volvic water for 48 hours (duration of the standard acute test) and at the highest concentration to which the organisms were exposed.

<sup>c</sup> the quantification was performed with ICP-MS after exposure of *D. magna* juveniles (48 hours old, pool of 10 animals) to Ag NPs or AgNO<sub>3</sub> for 24 hrs at the EC10 level.

<sup>d</sup> (Georgantzopoulou et al. 2013)



# Chapter 6

General discussion



Silver nanoparticles (Ag NPs) are among the most promising groups of NPs for application in numerous consumer products due to their broad spectrum antimicrobial activities. Examples are incorporation in textiles and plastics, personal care products, water filters, food supplements etc. The extensive application and use together with the not yet fully understood properties of Ag NPs as well as the toxicity of Ag itself has raised concerns on potential impact of Ag NPs on human and environmental health.

The research conducted within this thesis aimed at the evaluation of potential hazards of Ag NPs and identification of some key factors that determine the toxicity of Ag NPs. One of the main uptake routes for Ag NPs is through ingestion making the gastrointestinal epithelium one of the first ports of potential NP uptake and cell-particle interactions. An *in vitro* co-culture model incorporating a mucus layer mimicking the gastrointestinal epithelium was established for a more realistic evaluation of Ag NP potential toxicity than using intestinal epithelial cells alone. Indeed, the absence of mucus resulted in an overestimation of Ag NP toxicity (Chapter 2). To be able to elucidate subtle changes in cellular functions and identification of particle specific effects and NP modes of action, a proteomic approach was employed. Differences and commonalities were observed between the cellular responses induced Ag NPs of different sizes and AgNO<sub>3</sub> as a source of free Ag ions (Chapter 2).

As the Ag NPs are expected to reach the aquatic environment, a combination of adapted standard ecotoxicity assays with organisms of different trophic levels were used to evaluate the toxic effects Ag NPs (Chapter 3). Synthetically produced Ag NPs of different sizes (Ag 20 and 200 nm) as well as Ag NPs synthesized by a biological method (using plant leaf extracts of *Ocinum sanctum* and *Azadirachta indica*, Ag 23 and 27 nm, respectively) were used as model particles in order to elucidate the relation between size, synthesis method, NP surface properties, ion dissolution and toxicity. Based on earlier indications of interference of another type of NPs with the multi xenobiotic resistance mechanism (MXR), a first line of defense against xenobiotics, the effects of Ag NPs on the MXR mechanism were studied as well. The MXR mechanism is present in all animals studied, including humans and aquatic organisms. MXR can be compromised by chemical agents that are structurally and chemically unrelated, and could be the basis for enhanced toxicity by contaminant mixtures. A fast *in vitro* cellular efflux pump inhibition assay (CEPIA) was established evaluating first the effects of contaminants commonly found in the environment such as PFOS and BPA (Chapter 4). Next, an *in vivo* CEPIA assay was established using the juvenile *D. magna* model aquatic organism

and the potential of the MXR modulation by Ag NPs and ionic Ag was quantified *in vitro* and *in vivo* (Chapter 5).

### ***In vitro* co-culture model as a more realistic model for the gastrointestinal epithelium**

Due to the incorporation of Ag NPs in water filters, personal health care products and food supplements and food preservation (Wijnhoven et al. 2009), ingestion is expected to be a major uptake route. Therefore, the gastrointestinal tract could be a target organ for Ag NP exposure. Currently, most *in vitro* models concern gastrointestinal epithelial cell lines, but *in vivo* a mucus layer protects the underlying cells by trapping contaminants and particles preventing them to reach the epithelium. Therefore a co-culture model mimicking the gastrointestinal epithelium incorporating the mucus producing cells mimics more closely the *in vivo* situation and provides a more realistic Ag NP exposure. A co-culture model of Caco-2/TC7: HT29-MTX cells at a seeding ratio of 90:10 was successfully established incorporating a mucus layer. This ratio reflects the proportion of absorptive and goblet cells present in a healthy intestine (Walter et al. 1996). The mucus layer was formed *in vitro* and covered the monolayer of the differentiated cells (Chapter 2). Indeed the co-culture proved to be less sensitive to H<sub>2</sub>O<sub>2</sub>, a model inducer of oxidative stress. Furthermore, the IL-8 levels as a marker for inflammation were lower in the co-culture compared to the respective Caco-2/TC7 monocultures upon AgNO<sub>3</sub> exposure. As was shown earlier for ions, the mucus layer serves as a barrier (Pontier et al. 2001) and has reactive oxygen species (ROS)-scavenging properties and low ROS levels result in increased mucus thickness (Brownlee et al. 2007). The use of Caco-2 cells alone may lead to overestimation of effects since the protective barrier effect of the mucus *in vivo* is not taken into account. In addition, it is difficult to compare the results from different studies, especially when non-differentiated Caco-2 cells are used (Gerloff et al. 2009) because the differentiation has a strong impact on the potency of the NPs, with non-differentiated cells being more sensitive to NP exposure compared to differentiated cells (Gerloff et al. 2013, own unpublished results).

What is not yet included in the *in vitro* study, are the big shifts in pH in the gastrointestinal tract ranging from acidic to basic conditions that may alter the solubility and surface properties of the NPs. In addition, the intestinal fluid is comprised of a complex mixture of bile salts, ions, lipids, enzymes (Le Ferrec et al. 2001) and a rich bacterial micro flora. All these factors will seriously interact with the NPs and modify their properties (Hoet et al. 2004).

Unless the effects of these conditions altering NP characteristics and their interaction with cells are taken into account *in vitro* as well, the result obtained will poorly predict the effects of NPs *in vivo*.

### **NP size and synthesis method influence uptake, toxicity and dissolution**

The NP size, synthesis method and subsequent biomolecules present at the NP surface were found to be critical factors controlling uptake, dissolution and effects both *in vitro* and *in vivo* in daphnids (Chapters 2, 3 &5). A size dependent increase in IL-8 release was observed with Ag 20 and 200 nm NPs, although cellular metabolic activity and ROS formation were not affected in mono- or co-culture. The Ag NPs 20 nm induced a 4 times higher response than the Ag 200 nm (Chapter 2). Size-dependent effects (10-75 nm) were previously reported for Ag NPs in BEAS-2B lung cells (Gliga et al. 2014) and size dependent inflammatory markers were released from macrophages for uncoated Ag NPs, with Ag 20 nm NPs showing the highest induction (Park et al. 2011). In the co-culture model, Ag was detected in cells upon exposure to both Ag NPs 20 and 200 nm and AgNO<sub>3</sub> using secondary ion mass spectrometry (NanoSIMS50), a detection technique of high sensitivity and resolution. Ag 20 nm was accumulated in areas with high S content, probably in late endosomes or lysosomes while both Ag 200 nm and AgNO<sub>3</sub> were more homogeneously distributed within the cells. This suggests different uptake mechanisms depending on particle size as well as ionic form that can be related to the observed differences in IL-8 release. Ag NPs agglomerates have been previously reported to be localized in structures resembling endosomes or lysosomes (Kim et al. 2009) which is in accordance with our findings.

In the battery of bioassays using the model aquatic organisms *V. fischeri*, *D. subspicatus* and *D. magna* that are representatives of different trophic levels, the same order of toxicity was observed for all organisms with the biologically synthesized Ag NPs being more toxic than the conventional bare Ag NPs (Chapter 3). A size-dependence effect was observed for the bare Ag NPs where Ag 20 nm showing higher potency than Ag 200 nm. Ag NPs 20, 200 and 23 nm were found in the gut lumen of exposed daphnids, where they were attached to food debris (Chapter 3). Strikingly, Ag 23 nm NPs were found in what seems to be developing oocytes, indicating that Ag NPs can pass the gastrointestinal barrier (GIT) barrier and translocate to other tissues. An internalization and translocation of different NPs has been previously reported also for 20 and 1000 nm polystyrene NPs that were present in oil storage droplets in daphnids (Rosenkranz

et al. 2009) and 12 nm quantum dots localized in the brood chamber at high levels (Feswick et al. 2013). Although not tested within this thesis, potential consequences for fecundity cannot be excluded. In an earlier study, Zhao and Wang reported that chronic exposure of daphnids to Ag NPs led to decreased number of neonates and body length (Zhao and Wang 2011), which could be related to our finding of Ag localization in the developing oocytes. Ag ions have been previously shown to decrease the egg production rate in small crustaceans and it was concluded that the Ag accumulation via the food affects copepod reproduction via the observed reduced vitellogen levels in the ovary (Hook and Fisher 2001). Although the marine bacteria *V. fischeri* inhibition of bioluminescence assay requires NaCl as a medium in which the NPs agglomerated, still toxicity was observed and with the same size dependency as in the other assays. The effect concentrations were much higher than those in the daphnids' test (Chapter 3). Interspecies differences were observed for the organisms of different trophic levels. *D. magna* was the most sensitive, about 30 times and 400 times more sensitive than the algae *D. subspicatus* and the bacteria *V. fischeri*, respectively (Chapter 3). Interspecies differences have been previously reported and the contribution of Ag ions to toxicity was dependent on the trophic level of the organism and the exposure medium used. The highest contribution of Ag ions to effects was found for algae followed by small crustaceans and fish larvae (Wang et al. 2012). The relatively high sensitivity of *D. magna* may result from the fact that they are filter-feeders that ingest suspended material depending on size as well as they show a drinking behavior making both gills and gut being target organs. Additionally, at high exposure concentrations (>10 mg/L) NPs can adhere to the exoskeleton that can impede their locomotion and feeding efficiency (Gaiser et al. 2012).

The integration of a proteomic approach revealed different patterns in expression of proteins in cells in co-culture exposed to Ag 20, 200 nm and AgNO<sub>3</sub> (Chapter 2). Ag 20 nm led to dysregulation of proteins related to tight junction regulation and maintenance of epithelial and mucosal integrity that could lead to increased epithelial permeability. Interestingly, the trans-epithelial resistance (measure of epithelial integrity) remained unaltered. In accordance to our results, a disruption of the microvilli organization has been previously observed in TiO<sub>2</sub> NPs-exposed Caco-2 cells despite the absence of cytotoxicity and epithelial integrity disruption (Koeneman et al. 2010). Moreover, Ag 20 nm NPs altered the expression of proteins involved in xenobiotic metabolism which could lead to compromised detoxification processes. The proteomic approach clearly showed size-dependent effects as well as particle-dependent effects

as different Ag NPs did not cluster together in a principal component analysis (PCA) nor did they cluster with the effects of AgNO<sub>3</sub> used as a source of silver ions. Previous studies using a proteomic approach showed that smaller Ag NPs induced greater changes in the proteome of the colon cancer LoVo cells than Ag NPs larger than 100 nm. The finding of this thesis that NPs and ions affect different sets of proteins is in accordance with earlier studies with Ag NPs (Verano-Braga et al. 2014). Overall, the proteomic approach was valuable in detecting subtle changes and differences between different Ag particle sizes as well as ion related effects.

### **Ag NP synthesis method and surface effects**

The Ag NP synthesis method proved to be an important parameter in determining toxicity in our study. The Ag NPs synthesized by two different plant leaf extracts, *A. indica* (Ag 27 nm) and *O. sanctum* (Ag 23 nm) were the most potent ones (Chapter 3, 5). It has been also reported previously that biologically synthesized Ag NPs (using a microorganism) were more toxic than conventionally synthesized NPs (Suresh et al. 2012) which is in accordance with our study. Although the functional groups present on the surface of the biologically synthesized Ag NPs (Ag 23 and 27 nm) were similar, an additional peak was observed on the Ag 27 nm NPs in the Fourier Transform Infrared Spectroscopy (FTIR) measurements. This indicates that different biomolecules are present on the two biologically-synthesized Ag NPs that could lead to different uptake potential and interaction with biological sites. NPs with cationic sites were transported more efficiently than the ones with anionic sites (des Rieux et al. 2005) and positive polystyrene NPs were taken up to a higher extent than negative ones also through different uptake mechanisms by macrophages (Bhattacharjee et al. 2013a). The effect of the surface coating was also previously shown where humic acid-coated Ag NPs were more toxic than citrated-coated although they were both of comparable size. The humic acid-coated Ag NPs though, showed a higher uptake rate with slow elimination in the marine polychaete *Platynereis dumerilii* compared to the citrate coated ones and AgNO<sub>3</sub> (García-Alonso et al. 2014).

In the daphnids' and DMEM media the Ag NPs 20, 23 and 27 nm were found to have comparable sizes (Ag NPs 23 nm had only a slightly smaller size) indicating that the substantial differences in toxicity cannot be attributed to size differences (Chapter 5). The nanoparticle tracking analysis (NTA), a technique that analyses NPs on a particle by particle basis (Hole et al. 2013), was very useful for direct and real time visualization of the NPs in the different media (Chapter 5). Due to the visualization features and tracking of individual particles in motion,

NTA can detect different particle subpopulations that makes it a suitable technique for less stable dispersions that tend to aggregate. NTA was more suitable for our samples compared to the dynamic light scattering technique (DLS) (Chapter 3), technique that measures the scattered intensity of particles under motion, due to the presence of small aggregates that can have an impact on the accuracy of the measurements in the case of DLS due to its bias towards larger particles (Filipe et al. 2010) which highlights the need to use complementary sizing techniques.

### **Potential mechanism for indirect effects: interference with MXR mechanism**

The multi xenobiotic resistance is the first line of defense that a chemical encounters before entering the cells and it is present in all organisms studied so far (Bard 2000; Kurelec 1992). Therefore it is important to know whether Ag NPs also interact with the MXR efflux transporters, important members of which are the P-glycoprotein and multidrug resistance associated proteins (MRPs), as they would occur in combination with chemicals present in the environment and could enhance the toxicity of MXR transporter substrates. A fast *in vitro* cellular efflux pump inhibition assay (CEPIA) using calcein-AM as a substrate was optimized for the evaluation of modulation of efflux pumps by common environmental contaminants and Ag NPs with the use of the P-gp over-expressing canine kidney cell line (MDCKII-MDR1) and the parental MDCKII (MDCKII-WT) for comparison (Chapter 4). The assay revealed the MXR modulation by several different classes of contaminants such as PFOCs and BPA, confirming the broad substrate specificity of the MXR transporters.

For *in vivo* validation of the *in vitro* results, a cellular efflux pump inhibition assay was established with juveniles of *D. magna* (Chapter 5). MXR-related transporters were present in the juvenile and still transparent daphnids, and were modulated by both BPA and PFOS too confirming the *in vitro* results. Interestingly, both AgNO<sub>3</sub> as well as Ag NPs 23 nm interfered with the cellular efflux pumps both *in vitro* and *in vivo*. Ag NPs 23 nm were more potent and induced a higher response compared to AgNO<sub>3</sub>. Ag 27 nm NPs only inhibited MXR activity in daphnids suggesting that other efflux transporters in addition to P-gp are present in daphnids contributing to MXR. It has been previously shown that the transport of positively and negatively charged polystyrene NPs is mediated by P-gp and MRP1, respectively in Caco-2 cells which could explain the interference of Ag 27 nm in daphnids that could be transported by MRP-like transporters in daphnids (Bhattacharjee et al. 2013b).

Fluorescence microscopy with exposed daphnids showed that depending on the xenobiotics exposed to, the model MXR transporter substrate calcein accumulated in different parts of the daphnids' body. For example, calcein accumulated most in the filter setae of the thoracic appendages where the gills are located upon AgNO<sub>3</sub> exposure while Ag 23 and 27 nm NPs led to increased calcein fluorescence in the intestinal ceca and shell gland, the organ responsible for excretion. These results indicate that the interaction of Ag NPs with the daphnids depends on the size, ionic or particle form and surface properties. The presence of different functional groups, in the case of Ag 23 and 27 nm (plant leaves used for synthesis), could affect the recognition of the NPs by the transporters and specificity. The efficiency of particle retention has been shown to depend on the size of the distance between the filtering setae as well as on the particle surface and charge and surface attractions of e.g. filtering setae with particles (Gerritsen et al. 1988). *D. magna* proved to be a suitable *in vivo* organism for studying the interference of contaminants and Ag NPs with the MXR mechanism. It is a very sensitive organism, a filter-feeder that accumulates particles directly from the water column and its small size and transparency allows tracking and localization of fluorophores.

The compounds that interact with P-gp generally are moderately hydrophobic and have a molecular mass of about 391-490 Da (Bain and LeBlanc 1996) and a hydrogen bonding potential (Bain et al. 1997). For NPs the surface properties (e.g. presence of -NH<sub>2</sub> or -COOH groups), charge, size and dissolution potential seem to be appropriate and therefore these characteristics should be taken into account for quantitative structure-activity relationship (QSAR) studies for MXR inhibition. The interference of Ag NPs with MXR could have implications for ecotoxicology as it may enhance internal concentrations of other chemicals that exist in the environment as well when these toxic substances would normally be extruded.

### **Soluble Ag contribution to effects**

The release of Ag ions from Ag NPs is size, synthesis method and media dependent (Chapters 2, 3, 5). In the DMEM medium the dissolved Ag measured for bare Ag particles was below the limit of detection of our ICP-MS method (0.25 µg/L) which is in accordance with previous studies using uncoated particles (Gliga et al. 2014; Kruszewski et al. 2013). The highest release was observed for Ag 23 nm in the daphnids' medium (the mineral volvic water) while the lowest Ag content was found for the high NaCl medium used in the *V. fischeri* bioluminescence inhibition assay. The Ag release was a function of NP size with smaller sized

NPs releasing higher amounts of Ag in the media. This is in accordance with studies showing that smaller-sized Ag NPs led to higher levels of dissolved Ag (Gluga et al. 2014; Ma et al. 2012; Sotiriou and Pratsinis 2010; Yang et al. 2012) and that this release was also dependent on the surface coating (Newton et al. 2013; Zhao and Wang 2012a, 2012b).

Interestingly Ag NPs 23 nm were always more potent and more efficient in modulating the MXR activity *in vitro* compared to AgNO<sub>3</sub> and Ag NP 27 nm, while the levels of dissolved Ag in the media were comparable for AgNO<sub>3</sub> and Ag NPs 23 nm while for Ag 200 nm they were below the limit of detection (Chapter 5). This suggests that the differences observed in MXR inhibition cannot be explained by the differences in Ag ion levels. Previous studies reported that the Ag ions levels were not responsible for differences in toxicity between different Ag NPs (Suresh et al. 2012). Also Ag NPs were always more toxic compared to AgNO<sub>3</sub> at the same total Ag concentration (García-Alonso et al. 2014; Yin et al. 2011). Furthermore, different gene expression profiles were observed for AgNO<sub>3</sub> and Ag NPs-exposed *D. magna* (Poynton et al. 2012) and hepatocytes (Kim et al. 2009). These studies are in support of our findings of the proteomic study.

Although the method of ultrafiltration used in this thesis may underestimate the Ag concentration due to potential binding to the filtration membranes, this effect would be the same for all exposures. A recent study using a similar method but applied to NaHCO<sub>3</sub> solution recovered 100% of the AgNO<sub>3</sub> (Ma et al. 2012). This suggests that the small recovery of 1% for AgNO<sub>3</sub> in the cell culture media in our study may be due to complexation of Ag with components of the more complex media we used making the Ag hardly available for analysis with this method. A more systematic study of the Ag dissolution and Ag speciation in different media and the use of different techniques are needed for an accurate quantification and understanding of the contribution of different Ag species and a potential Trojan horse mechanism. For this, reference/standard NPs with full physical and biological characterization could be highly valuable for comparison also within studies.

The cells and organisms are exposed to the Ag NPs and ions simultaneously that both contribute to the overall effect but are taken up *via* different mechanisms and at a different rate. Zhao and Wang previously reported different uptake rates for Ag from Ag NPs and Ag ions in *D. magna* suggesting different mechanisms of uptake. For example, ions could be diffused through the gills and ion channels while Ag NPs are mostly ingested (Zhao and Wang 2012a).

Also in their study Ag from Ag NPs had a higher retention time and slower depuration rate compared to Ag from AgNO<sub>3</sub> (Zhao and Wang 2010). The Ag content in daphnids exposed to Ag 23 nm for 24 hrs was 41% of the total Ag-dosed in contrast to only 0.17-0.43% for AgNO<sub>3</sub> and the other NPs. This suggests that Ag NPs 23 nm are more readily taken up and also release ions within the cell or provide a carrier for Ag ions that are already bound on the NP surface. This efficient uptake is probably related to the small enough size in combination with the above described surface properties.

These results support the idea that there is indeed a NP effect and that the dissolution and the presence of soluble Ag alone cannot explain the differences in effects observed. It seems that for the chemically synthesized Ag NPs with only a low degree of dissolution, the size is a major determinant for toxicity. For the biogenic Ag NPs, on the other hand, both the high release of Ag ions, and the surface properties favor high uptake, strong interaction with biological sites and thus its relatively great toxicity.

### **Expected effects in the field/ *in vivo***

The concentrations at which observed effects were found in the *in vitro* co-culture model are high (e.g. above 20 mg/L) and at levels that are unlikely that humans will be exposed to through ingestion. Given the fact that complexation with the food matrix will render the NPs less bioavailable posing a low threat for intestinal health assuming absence of disease. The amount of Ag (as total Ag) predicted in surface water due to Ag-containing plastics and textiles is 40 and 140 ng/L for a minimum and intermediate scenario (Blaser et al. 2008) which is only slightly lower than the EC<sub>50s</sub> for AgNO<sub>3</sub> and Ag 23 nm NPs found in our study. The organisms in the environment, however, will encounter NPs not in their pristine form but rather in complexes with suspended organic matter, debris etc. that can act as chelators of metal ions (Collin et al. 2014) leading to even lower bioavailability that suggests that aquatic organisms are not likely to be exposed to concentrations that could pose a hazard. Previous studies have shown a decrease in toxicity and interaction of Ag NP with aquatic organisms in the presence of dissolved organic carbon (Bone et al. 2012; Glenn and Klaine 2013). For risk assessment the real exposure should be taken into account, for this thesis however, the focus was on studying mechanisms and understand the biological activity. Therefore it was chosen to use well-defined conditions as a worst case situation.

### Concluding remarks

A design of tiered approach for a testing system that gives an overview of an overall toxicity is highly valuable for emerging contaminants such as Ag NPs that are being continuously synthesized with a wide range of sizes, surface properties etc. First, a battery of bioassays and endpoints should be applied using organisms such as *V. fischeri* that are fast and inexpensive, followed by algae and daphnids' bioassays can provide a good initial indication of the potential toxicity of new materials and determine values for regulatory purposes. That could also lead to the determination of sub-lethal concentrations for the study of more relevant mechanistic endpoints at concentrations that probably reflect better human and environmental exposure. Subsequently, target sites/tissues and organisms expected for Ag NPs exposure and accumulation as well as organisms of concern can be identified and studied in respect to uptake and fate in the cell and organism. An integration of a test system using “omic” tools such as proteomics would then lead towards an identification of unknown and unanticipated mechanisms of action.

This integrated approach revealed that the size and the synthesis method are the factors affecting most the uptake and toxicity in both cells *in vitro* as well as *in vivo* in daphnids and dissolution in the different media with the biologically synthesized Ag NPs being more potent compared to the conventional Ag NPs. The gastrointestinal tract is expected to be a target site for Ag NPs exposure and a co-culture of Caco-2-TC7 and HT29-MTX cells optimized and employed in the current study represents a more realistic model compared to Caco-2 monocultures. The mucus layer provides an additional protective barrier and its absence can lead to overestimation of effects in *in vitro* studies. Ag was detected both in the cells in co-culture, in the gut of daphnids' as well as specific areas, seemingly developing oocytes, indicating a potential translocation of Ag NPs that could have consequences for fecundity. An *in vitro* and *in vivo* assay using *D. magna* as a model organism were successfully established to study the interference of Ag NPs and Ag ions with the MXR efflux transporters that were found to be modulated by Ag at low concentrations (0.18 µg/L), that are slightly lower compared to the predicted environmental concentrations.

The extent to which the Ag ions contribute to the effects of Ag NPs depends on the size and surface properties of the Ag NPs. For the conventional, uncoated Ag NPs, the Ag release is minimal and the size is the determining factor while for biologically synthesized particles the biomolecules present due to the synthesis method and Ag release affect most the uptake and effects. The simultaneous presence of Ag ions and NPs releasing ions can lead to an

exacerbation of the effects. The proteomic approach was successfully applied and it proved to be a useful technique in discerning subtle cellular changes in response to Ag NP exposure that would otherwise be unnoticed. Ag NPs 20 nm regulated different sets of proteins with a distinct pattern of cellular responses compared to Ag 200 nm and AgNO<sub>3</sub>, suggesting a different mode of action with effects being particle- and size-dependent.

These results obtained during this thesis are promising for future toxicity testing of new materials using lower animals and more realistic *in vitro* models leading to more meaningful results and more accurate assessment of Ag NP hazards.

### Future perspectives

The knowledge acquired from *in vitro* systems and single species assays contributes to a better understanding of mechanisms of action. Despite the fact that the actual NP concentrations at which humans and organisms are exposed to are unknown, exposure experiments that contribute to more realistic (eco)toxicological studies and the integration of realistic conditions in bioassays that could be found in the environment and *in vivo* are needed in NP studies. Therefore, future research efforts could involve the following aspects:

1. Incorporation of more realistic exposure scenarios with *D. magna* in the experimental system with the use e.g. of natural stream water/ addition of natural organic matter and study the impact on NP uptake and toxicity at realistic, lower concentrations that are expected to be reached in the environment.
2. Study trophic transfer from algae to daphnids (faster/ slower uptake and depuration?).
3. Assess the effects on reproduction and potential impact on vitellogenesis.
4. Study uptake mechanisms with Ag NPs having different surface functional groups.
5. Synthesis of Ag NPs of the same size with the surface charge or surface functionalization being the only factor (e.g. COOH groups or NH<sub>2</sub> groups) and evaluate differences in uptake, toxicity, dissolution and MXR interference *in vitro* and *in vivo* and comparison with reference NPs.
6. Study the involvement of other efflux transporters such as MRPs in the efflux of Ag NPs and ions *in vitro* and *in vivo*.
7. Investigate the combined ecotoxic effects of Ag NPs or ions with common environmental contaminants that are MXR substrates or inhibitors such as PFOS and BPA at environmentally relevant concentrations.

## References

- Bain LJ, LeBlanc GA. 1996. Interaction of structurally diverse pesticides with the human MDR1 gene product P-glycoprotein. *Toxicol. Appl. Pharmacol.* 141:288–98.
- Bain LJ, McLachlan JB, LeBlanc GA. 1997. Structure-activity relationships for xenobiotic transport substrates and inhibitory ligands of P-glycoprotein. *Environ. Health Perspect.* 105: 812–8.
- Bard S. 2000. Multixenobiotic resistance as a cellular defense mechanism in aquatic organisms. *Aquat. Toxicol.* 48: 357–389.
- Bhattacharjee S, Ershov D, Gucht J Van Der, Alink GM, Rietjens IMCM, Zuilhof H, et al. 2013a. Surface charge-specific cytotoxicity and cellular uptake of tri-block copolymer nanoparticles. *Nanotoxicology* 7:71–84.
- Bhattacharjee S, Opstal EJ, Alink GM, Marcelis ATM, Zuilhof H, Rietjens IMCM. 2013b. Surface charge-specific interactions between polymer nanoparticles and ABC transporters in Caco-2 cells. *J. Nanoparticle Res.* 15:1695.
- Blaser SA, Scherlinger M, Macleod M, Hungerbühler K. 2008. Estimation of cumulative aquatic exposure and risk due to silver: contribution of nano-functionalized plastics and textiles. *Sci. Total Environ.* 390:396–409.
- Bone AJ, Colman BP, Gondikas AP, Newton KM, Harrold KH, Cory RM, et al. 2012. Biotic and abiotic interactions in aquatic microcosms determine fate and toxicity of Ag nanoparticles: part 2-toxicity and Ag speciation. *Environ. Sci. Technol.* 46:6925–33.
- Brownlee IA, Knight J, Dettmar PW, Pearson JP. 2007. Action of reactive oxygen species on colonic mucus secretions. *Free Radic. Biol. Med.* 43:800–8.
- Collin B, Oostveen E, Tsyusko O V, Unrine JM. 2014. Influence of natural organic matter and surface charge on the toxicity and bioaccumulation of functionalized ceria nanoparticles in *Caenorhabditis elegans*. *Environ. Sci. Technol.* 48:1280–9.
- Des Rieux A, Ragnarsson EGE, Gullberg E, Pr eat V, Schneider Y-J, Artursson P. 2005. Transport of nanoparticles across an *in vitro* model of the human intestinal follicle associated epithelium. *Eur. J. Pharm. Sci.* 25:455–65.
- Feswick A, Griffitt RJ, Siebein K, Barber DS. 2013. Uptake, retention and internalization of quantum dots in *Daphnia* is influenced by particle surface functionalization. *Aquat. Toxicol.* 130-131:210–218.
- Filipe V, Hawe A, Jiskoot W. 2010. Critical evaluation of Nanoparticle Tracking Analysis (NTA) by NanoSight for the measurement of nanoparticles and protein aggregates. *Pharm. Res.* 27:796–810.
- Gaiser BK, Fernandes TF, Jepson MA, Lead JR, Tyler CR, Baalousha M, et al. 2012. Interspecies comparisons on the uptake and toxicity of silver and cerium dioxide nanoparticles. *Environ. Toxicol. Chem.* 31:144–54.
- Garc a-Alonso J, Rodr guez-Sanchez N, Misra SK, Valsami-Jones E, Croteau M-N, Luoma SN, et al. 2014. Toxicity and accumulation of silver nanoparticles during development of the marine polychaete *Platynereis dumerilii*. *Sci. Total Environ.* 476-477:688–95.
- Gerloff K, Albrecht C, Boots AW, F rster I, Schins RPF. 2009. Cytotoxicity and oxidative DNA damage by nanoparticles in human intestinal Caco-2 cells. *Nanotoxicology* 3:355–364.
- Gerloff K, Pereira DIA, Faria N, Boots AW, Kolling J, F rster I, et al. 2013. Influence of simulated gastrointestinal conditions on particle-induced cytotoxicity and interleukin-8 regulation in differentiated and undifferentiated Caco-2 cells. *Nanotoxicology* 7:353–366.
- Gerritsen J, Porter KG, Rudi Strickler J. 1988. Not by sieving alone: observations of suspension feeding in *Daphnia*. *Bull. Mar. Sci.* 43: 366–376.
- Glenn JB, Klaine SJ. 2013. Abiotic and biotic factors that influence the bioavailability of gold nanoparticles to aquatic macrophytes. *Environ. Sci. Technol.* 47:10223–30.

- Gluga AR, Skoglund S, Wallinder IO, Fadeel B, Karlsson HL. 2014. Size-dependent cytotoxicity of silver nanoparticles in human lung cells: the role of cellular uptake, agglomeration and Ag release. *Part. Fibre Toxicol.* 11:11.
- Hoet PH, Brüske-Hohlfeld I, Salata OV. 2004. Nanoparticles - known and unknown health risks. *J. Nanobiotechnology* 2:12.
- Hole P, Sillence K, Hannell C, Maguire CM, Roesslein M, Suarez G, et al. 2013. Interlaboratory comparison of size measurements on nanoparticles using nanoparticle tracking analysis (NTA). *J. Nanopart. Res.* 15:2101.
- Hook SE, Fisher NS. 2001. Sublethal effects of silver in zooplankton: importance of exposure pathways and implications for toxicity testing. *Environ. Toxicol. Chem.* 20: 568–74.
- Kim S, Eun Choi J, Choi J, Chung K, Park K, Yi J, et al. 2009. Oxidative stress-dependent toxicity of silver nanoparticles in human hepatoma cells. *Toxicol. Vitro.* 23:1076–1084.
- Koeneman BA, Zhang Y, Westerhoff P, Chen Y, Crittenden JC, Capco DG. 2010. Toxicity and cellular responses of intestinal cells exposed to titanium dioxide. *Cell Biol. Toxicol.* 26:225–38.
- Kruszewski M, Grądzka I, Bartłomiejczyk T, Chwastowska J, Sommer S, Grzelak A, et al. 2013. Oxidative DNA damage corresponds to the long term survival of human cells treated with silver nanoparticles. *Toxicol. Lett.* 219:151–9.
- Kurelec B. 1992. The multixenobiotic resistance mechanism in aquatic organisms. *Crit. Rev. Toxicol.* 22:23–43.
- Le Ferrec E, Chesne C, Artusson P, Brayden D, Fabre G, Gires P, et al. 2001. *In vitro* models of the intestinal barrier. *ATLA* 29: 649–668.
- Ma R, Levard C, Marinakos SM, Cheng Y, Liu J, Michel FM, et al. 2012. Size-controlled dissolution of organic-coated silver nanoparticles. *Environ. Sci. Technol.* 46:752–9.
- Newton KM, Puppala HL, Kitchens CL, Colvin VL, Klaine SJ. 2013. Silver nanoparticle toxicity to *Daphnia magna* is a function of dissolved silver concentration. *Environ. Toxicol. Chem.* 32:2356–64.
- Park MVDZ, Neigh AM, Vermeulen JP, de la Fonteyne LJJ, Verharen HW, Briedé JJ, et al. 2011. The effect of particle size on the cytotoxicity, inflammation, developmental toxicity and genotoxicity of silver nanoparticles. *Biomaterials* 32:9810–9817.
- Pontier C, Pachot J, Botham R, Lenfant B, Arnaud P. 2001. HT29-MTX and Caco-2/TC7 monolayers as predictive models for human intestinal absorption: role of the mucus layer. *J. Pharm. Sci.* 90: 1608–19.
- Poynton H, Lazorchak J, Impellitteri CA, Blalock BJ, Rogers K, Allen HJ, et al. 2012. Toxicogenomic responses of nanotoxicity in *Daphnia magna* exposed to silver nitrate and coated silver nanoparticles. *Environ. Sci. Technol.* 46: 6288–6296.
- Rosenkranz P, Chaudhry Q, Stone V, Fernandes TF. 2009. A comparison of nanoparticle and fine particle uptake by *Daphnia magna*. *Environ. Toxicol. Chem.* 28:2142–9.
- Sotiriou GA, Pratsinis SE. 2010. Antibacterial activity of nanosilver ions and particles. *Environ. Sci. Technol.* 44:5649–54.
- Suresh AK, Pelletier DA, Wang W, Morrell-Falvey JL, Gu B, Doktycz MJ. 2012. Cytotoxicity induced by engineered silver nanocrystallites is dependent on surface coatings and cell types. *Langmuir* 28:2727–2735.
- Verano-Braga T, Miethling-Graff R, Wojdyla K, Rogowska-Wrzesinska A, Brewer JR, Erdmann H, et al. 2014. Insights into the cellular response triggered by silver nanoparticles using quantitative proteomics. *ACS Nano* 8: 2161–2175.
- Walter E, Janich S, Roessler BJ, Hilfinger JM, Amidon GL. 1996. HT29-MTX/Caco-2 cocultures as an *in vitro* model for the intestinal epithelium: *in vitro-in vivo* correlation with permeability data from rats and humans. *J. Pharm. Sci.* 85:1070–6.

- Wang Z, Chen J, Li X, Shao J, Peijnenburg WJGM. 2012. Aquatic toxicity of nanosilver colloids to different trophic organisms: contributions of particles and free silver ion. *Environ. Toxicol. Chem.* 31:2408–13.
- Wijnhoven SWP, Peijnenburg WJGM, Herberts CA, Hagens WI, Oomen AG, Heugens EHW, et al. 2009. Nanosilver a review of available data and knowledge gaps in human and environmental risk assessment. *Nanotoxicology* 3:109–138.
- Yang X, Gondikas AP, Marinakos SM, Auffan M, Liu J, Hsu-Kim H, et al. 2012. Mechanism of silver nanoparticle toxicity is dependent on dissolved silver and surface coating in *Caenorhabditis elegans*. *Environ. Sci. Technol.* 46:1119–27.
- Yin L, Cheng Y, Espinasse B, Colman BP, Auffan M, Wiesner M, et al. 2011. More than the ions: the effects of silver nanoparticles on *Lolium multiflorum*. *Environ. Sci. Technol.* 45:2360–7.
- Zhao C-M, Wang W. 2010. Biokinetic uptake and efflux of silver nanoparticles in *Daphnia magna*. *Environ. Sci. Technol.* 44: 7699–7704.
- Zhao C-M, Wang W-X. 2011. Comparison of acute and chronic toxicity of silver nanoparticles and silver nitrate to *Daphnia magna*. *Environ. Toxicol. Chem.* 30:885–892.
- Zhao C-M, Wang W-X. 2012a. Importance of surface coatings and soluble silver in silver nanoparticles toxicity to *Daphnia magna*. *Nanotoxicology* 6:361–370.
- Zhao C-M, Wang W-X. 2012b. Size-dependent uptake of silver nanoparticles in *Daphnia magna*. *Environ. Sci. Technol.* 46:11345–51.

# Chapter 7

Summary



This thesis aims at the assessment of potential hazards of silver nanoparticles (Ag NPs) in comparison to Ag ions and identification of some key factors that determine the toxicity of Ag NPs for aquatic organisms and intestinal toxicity.

In **Chapter 1** background information is presented on Ag NPs, their increasing use and the environmental and human health concerns raised. Due to their ubiquitous incorporation in personal care products, food supplements and use in food preservation, the characterization of potential risk for humans and aquatic organisms is essential.

Ingestion is an important uptake route for humans. Therefore relevant and realistic intestinal *in vitro* models are needed in order to better evaluate mechanisms of Ag NP uptake and potential intestinal toxicity. For aquatic organisms the gut and the gills are major sites for first interactions with Ag NPs. A battery of bioassays representing organisms from different trophic levels can be used for fast, inexpensive screening of the continuous development of NPs with different sizes, surface modifications etc. Considering the wide range of NPs properties, new biological activities and mechanisms of action are to be anticipated. One of the challenges is to identify subtle mechanisms that are influenced by Ag NPs, and 'omic' tools such as proteomics could be useful to identify slight changes in cellular functions and describe modes of action. Among the mechanisms that could be affected by NPs is the multi xenobiotic efflux transporters (MXR), a first line defense mechanism for a broad range of substrates.

**Chapter 2** describes the establishment of a Caco-2/TC7:HT29-MTX intestinal co-culture model with mucus secretion. The mucus layer constitutes an important protective barrier to exogenous agents *in vivo* and may strongly reduce particle uptake. The effects of Ag NPs (20 and 200 nm) as well as AgNO<sub>3</sub> were compared as a source of ionic silver. Both uptake, intracellular localization and toxic and inflammatory potential were determined. Both Ag 20 and 200 nm NPs were taken up by the cells and Ag NPs 20 nm were mainly localized in organelles with high sulfur content as was shown by a probe with high lateral resolution (NanoSIMS50) while for Ag 200 nm a more diffused pattern was observed in the cell. A dose- and size-dependent increase in Interleukin-8 (IL-8) release was observed with a lack of cytotoxicity and oxidative stress. In a proteomic study sixty one differentially abundant proteins were identified. They mostly involved cytoskeleton arrangement and cell cycle, oxidative stress, apoptosis, metabolism/detoxification and stress. Ag NPs 20 nm also altered the expression of proteins involved in the maintenance of intestinal barrier and mucosal integrity as well as proteins that play an important role in xenobiotic metabolism. The low level of overlap between differentially abundant proteins observed in both Ag 20 nm NPs and

AgNO<sub>3</sub> treated co-culture suggests size- and particle-dependent responses that cannot only be attributed to soluble Ag.

The hazard of Ag NPs for aquatic organisms is studied in **Chapter 3**. The effects of Ag particles synthesized by a conventional (Ag 20, 200 nm) and biological method (*Ocinum sanctum* and *Azadirachta indica* plant leaf extracts-synthesized, Ag NPs 23 and 27 nm, respectively) in the bacterium *Vibrio fischeri*, the algae *Desmodesmus subspicatus* and the crustacean *Daphnia magna*. Ag particles exerted toxic effects in all organisms studied with Ag particles 23 nm being the most potent followed by Ag 27, 20 and 200 nm. The relative potency was the same in all organisms tested. Although soluble Ag ions were released in all media, the differences between the tested Ag NP cannot be explained solely based on soluble Ag. Secondary ion mass spectrometry (NanoSIMS50) analysis performed with *D. magna* showed that apart from their localization in the gut lumen, Ag 200 nm and Ag NPs 23 nm had passed the epithelial barrier as well. Ag NPs 23 nm was localized in specific areas, most probably in developing oocytes which could explain fecundity effects reported by others. This study supports the hypothesis that size, method of synthesis as well as surface chemistry affects the uptake, fate and toxic effects of Ag NPs.

**Chapters 4 and 5** focus on the interaction of contaminants and Ag NPs with the multi xenobiotic resistance mechanism (MXR). Across different species, cellular efflux pumps such as P-glycoprotein (P-gp) serve as a first line of defense by transporting toxic xenobiotics out of the cell. This mechanism is also active in aquatic organisms such as mussels, fish, and their larvae. This thesis reveals that this important protection mechanism against a variety of xenobiotics was inhibited by Ag NP, which could result in either higher or lower internal concentrations of toxic or endogenous compounds in cells. **Chapter 4** aimed at the quantification of the inhibition of the P-gp efflux pumps by several ubiquitous aquatic contaminants. The calcein-acetoxymethyl ester (calcein-AM) assay commonly used in pharmacological research was established with P-gp-overexpressing Madin-Darby canine kidney cells (MDCKII-MDR1) in a 96-well plate, avoiding extra washing, centrifugation, and lysis steps. This calcein-AM-based P-gp cellular efflux pump inhibition assay (CEPIA) was used to study the inhibition by commonly occurring environmental contaminants. Among others, the compounds pentachlorophenol (PCP), perfluorooctane sulfonate (PFOS), and perfluorooctanoate (PFOA) strongly inhibited the P-gp-mediated efflux of calcein-AM while the chlorinated alkanes did not seem to interact with the transporter. The fact that common

pollutants can be potent modulators of the efflux transporters is a motive to further study whether this increases the toxicity of other contaminants present in the same matrices.

Chemicals occur in the environment in mixtures and Ag NPs are one class of emerging contaminants expected to be found in the environment. One of the characteristics of the MXR efflux transporters is the lack of substrate specificity that makes them vulnerable to modulation. **Chapter 5** investigates the interaction of silver nanoparticles (Ag NPs, 20-200 nm) and Ag ions ( $\text{AgNO}_3$ ) with the MXR efflux transporters using the MDCKII and MDCKII-MDR1 cells and calcein-AM as a substrate in the previously optimized CEPIA assay. For *in vivo* validation of the *in vitro* results an *in vivo* CEPIA assay was established with *D. magna* juveniles as a model organism and the modulation of MXR activity was studied with the model P-gp and MRP1 inhibitors verapamil-HCl and MK571, respectively. Perfluorooctane sulfonate (PFOS) and bisphenol A (BPA) also inhibited the efflux of calcein from daphnids. Small-sized Ag NPs and  $\text{AgNO}_3$  inhibited the MXR activity in daphnids and MDCKII-MDR1, but *abcb1* gene expression remained unchanged. Both Ag NPs and dissolved ions contributed to the effects. This study provided for the first time evidence for interference of Ag NPs and  $\text{AgNO}_3$  with the MXR activity both *in vitro* and *in vivo* and the MXR activity modulation should be taken into account when Ag NP toxicity is assessed.

**Chapter 6** discusses the relevance of the established *in vitro* model for the gastrointestinal epithelium as well as the *in vitro* and *in vivo* bioassays for interference of contaminants and Ag NPs with the MXR efflux transporters. More complex *in vitro* models with incorporation of more cell lines are important in order to obtain more meaningful results. Ag NP dissolution was identified as a critical factor governing toxicity and it depends on the size and nature of the NPs. Due to the novel properties of NPs also novel mechanisms of action should be considered at concentrations that are likely to occur in the environment and reach humans. The application of a proteomic approach is discussed as a suitable tool to detect subtle changes at a cellular level at low concentrations, identify modes of action and discern NP and size effects. The multixenobiotic resistance mechanism is proposed as a relevant mechanism and the implications of its modulation by Ag NPs and the released ions are discussed. *D. magna* was proven to be a suitable *in vivo* model for studying the MXR mechanism due to the small body size and its transparency. A tiered approach using a battery of standard bioassays with model aquatic organisms, followed by determination of sub-lethal concentrations for mechanistic endpoints, identification of target organisms and tissues for Ag NP exposure and the integration of 'omic' tools is a step forward towards better understanding and prediction of

the toxic potential of new materials such as NPs. Implications for the *in vivo* and field conditions are discussed and aspects for more realistic (eco)toxicological studies and further research are provided.

# Chapter 8

Nederlandse samenvatting



Het doel van dit proefschrift is het evalueren van mogelijke nadelige effecten van zilver nano-deeltjes (Ag NPs) in vergelijking met die van zilver (Ag)-ionen, en de identificatie van belangrijke factoren die de toxiciteit van Ag NPs voor aquatische organismen bepalen.

In **hoofdstuk 1** wordt achtergrond informatie gegeven over Ag NPs, het toenemende gebruik ervan en eventuele nadelige effecten op aquatische organismen. Omdat Ag NPs veelvuldig verwerkt worden in verzorgingsproducten, voedingssupplementen en conserveermiddelen is het schetsen van de mogelijke risico's voor de gezondheid van de mens ook essentieel.

Voor mensen is inname via de mond de belangrijkste opname route van Ag NPs. Om het mechanisme van Ag NP opname en de mogelijke toxiciteit te evalueren zijn relevante en realistische intestinale *in vitro* modellen nodig. Voor aquatische organismen zijn de darmen en kieuwen de belangrijkste plaatsen voor het eerste contact met Ag NPs. Een heel scala aan '*in vivo* bioassays' (testen met organismen) is beschikbaar. Organismen die verschillende functies in de voedselketen, 'trofische' niveaus vertegenwoordigen kunnen gebruikt worden voor snelle, goedkope screening van van NPs van verschillende grootte, oppervlakte eigenschappen, enz. Gezien de grote diversiteit aan eigenschappen van NPs zijn uiteenlopende biologische effecten en mechanismen te verwachten. Een van de uitdagingen is het identificeren van subtiele effecten die worden veroorzaakt door Ag NPs. Vooral zogenoemde 'omic' tools, zoals proteomics, zijn geschikt om kleine veranderingen in cellen en hun functioneren te beschrijven. Een belangrijk mechanisme dat kan worden beïnvloed door NPs is de cellulaire efflux pomp werking om giftige stoffen uit de cel te verwijderen. De multi xenobiotische efflux transporters (MXR) zijn een eerste afweermechanisme voor een breed scala aan substraten.

**Hoofdstuk 2** bespreekt de ontwikkeling van een Caco-2/TC7:HT29-MTX intestinale co-cultuur met darmslijm secretie. De slijmlaag vormt een belangrijke beschermende barrière voor lichaamsvreemde stoffen *in vivo*, die mogelijk ook de opname van NPs sterk reduceert. De opname en effecten van Ag NPs (20 en 200 nm) en van dezelfde hoeveelheid zilver als alleen zilver ionen (AgNO<sub>3</sub>) zijn vergeleken. Zowel opname, intracellulaire lokalisatie, toxische effecten en ontstekingsreactie zijn vastgesteld in cellen met en zonder slijmlaag. Zowel Ag 20 als 200 nm NPs werden door de cel opgenomen. Ag NP 20 nm was voornamelijk te vinden in de organellen met een hoog zwavelgehalte, zoals aangetoond in een meetinstrument met zeer hoge laterale resolutie (NanoSIMS50). De Ag NPs 200 nm waren in de cel in een meer diffuus patroon zichtbaar. Een dosis- en grootte afhankelijke stijging van Interleukine-8 (IL-8) afgifte werd waargenomen zonder dat er cel toxiciteit of oxidatieve stress optrad. In de proteomics

studie werden eenenzestig algemeen voorkomende eiwitten geïdentificeerd die differentieel tot expressie gebracht waren. Hierbij waren meestal eiwitten betrokken die een rol spelen in de opbouw van het cytoskelet en de cel cyclus, bij oxidatieve stress, apoptose, metabolisme/detoxificatie en algemene cellulaire stress. Ag NPs 20 nm veranderden ook de samenstelling van eiwitten die betrokken zijn bij het onderhoud van de darmbarrière en de slijmlaag evenals eiwitten die een belangrijke rol spelen in het afbraakmetabolisme van milieuvreemde stoffen. De geringe overlap tussen differentieel tot expressie gebrachte algemeen voorkomende eiwitten die zowel in Ag 20 nm NPs als in AgNO<sub>3</sub> behandelde co-cultuur voorkomen, suggereert een grootte- en deeltjes afhankelijke reactie die niet alleen kan worden toegeschreven aan oplosbaar Ag.

Het risico van Ag NPs voor aquatische organismen wordt in **hoofdstuk 3** bestudeerd. De effecten worden vergeleken van Ag deeltjes gesynthetiseerd via een conventionele (Ag 20, 200 nm) en een biologische methode (*Ocinum sanctum* en *Azadirachta indica* plant bladerextracten gesynthetiseerde, Ag NPs 23 en 27 nm). Testorganismen zijn de bacterie *Vibrio fischeri*, de alg *Desmodesmus subspicatus* en de kreeftachtige *Daphnia magna*. Ag 23 deeltjes waren het sterkst toxisch voor alle organismen, gevolgd door Ag 27, 20 en 200 nm. De relatieve giftigheid was hetzelfde in alle geteste organismen. In alle media zijn vergelijkbare hoeveelheden zilver als oplosbare Ag ionen getest, en hieruit bleek dat de verschillende effecten van Ag NP niet alleen te verklaren zijn met oplosbaar Ag. Gedetailleerde lokalisatie van de NPs met NanoSIMS50 apparatuur liet zien dat in *D. magna* Ag NPs 200 nm en Ag NPs 23 nm in de darmvlokken aanwezig waren en ook de epitheel barrière waren gepasseerd. Ag NPs 23 nm waren in specifieke gebieden gelokaliseerd, hoogstwaarschijnlijk in ontwikkelende oöcyten. Dit zou mogelijk de eerder gerapporteerde vruchtbaarheidseffecten kunnen verklaren. Het in dit hoofdstuk beschreven onderzoek ondersteunt de hypothese dat de grootte, de methode van synthese, evenals de oppervlaktechemie invloed heeft op de opname, de lokalisatie en het toxische effect van Ag NPs.

**Hoofdstuk 4** en **5** zijn gewijd aan de interactie van Ag NPs en giftige stoffen met het eerder genoemde MXR mechanisme. Bij alle soorten organismen fungeren cellulaire efflux pompen zoals P-glycoproteïne (P-gp) als een eerste afweer mechanisme tegen giftige stoffen door deze uit de cel weg te pompen. Dit mechanisme is ook zeer actief in aquatische organismen zoals mosselen, vis, en hun larven. Het onderzoek beschreven in deze hoofdstukken toont dat dit belangrijke ontgiftings mechanisme, dat een scala aan ongewenste stoffen verwijdert, wordt geremd door Ag NPs. Dit zou een hogere of lagere interne

concentratie aan toxische of lichaamseigen nuttige stoffen in cellen tot gevolg kunnen hebben. Het doel van **hoofdstuk 4** is de remming van de P-gp efflux pomp in cellen door verschillende algemeen voorkomende aquatische verontreinigingen te kwantificeren. De gebruikte zogenoemde calcein-AM test, die gebruik maakt van ophoping in de cel van een fluorescerende stof bij remming van de efflux pomp werking, is een variant op de test die ontwikkeld is in farmacologisch onderzoek met speciale niercellen van een hond die extra veel P-gp activiteit hebben (MDCKII-MDR1 cellen). Deze test kan in een 96-wellsplaat worden uitgevoerd, waarbij nu extra handelingen zoals wassen, centrifugeren en oplossen van de cellen overbodig gemaakt zijn. Deze zogenoemde calcein-AM-gebaseerde CEPIA (efflux pump inhibition assay) is gebruikt om de remming van het P-gp mechanisme door veel voorkomende milieuverontreinigende stoffen te bestuderen. Voorbeelden van stoffen die sterk remmen zijn pentachloorfenol (PCP), perfluorooctane sulfonaat (PFOS), en perfluoro octanoaat (PFOA), en het kan niet uitgesloten worden dat deze stoffen de giftigheid van vele andere stoffen in het milieu, die normaal de cel uit gepompt worden, doen toenemen.

Omdat Ag NPs in het milieu ook met andere stoffen samen voor kunnen komen, is het van belang om ook te weten of Ag NPs deze algemene eerstelijns verdediging tegen vele soorten toxische stoffen beïnvloeden. **Hoofdstuk 5** beschrijft het onderzoek naar de interactie van Ag NPs, 20-200 nm en Ag ionen ( $\text{AgNO}_3$ ) met de MRX efflux transporter. Hiervoor worden de MDCKII en de MDCKII-MDR1 cellen gebruikt en calcein-AM als substraat zoals in de in hoofdstuk 4 geoptimaliseerde CEPIA. Voor de *in vivo* validatie van de *in vitro* resultaten, is bovendien een *in vivo* CEPIA ontwikkeld met onvolwassen *D. magna* als modelorganisme. Als standaard remmers in de CEPIA zijn verapamil-HCl en MK571 gebruikt. De kleinste Ag NPs en  $\text{AgNO}_3$  remden de MXR activiteit in de watervlooien, terwijl de gen expressie van het MDCKII-MDR1, *abcb1* gen onveranderd bleef. Ook de opgeloste Ag ionen droegen bij aan de effecten. Verder zijn als positieve controle de stoffen PFOS en bisphenol A (BPA) getest, en deze remden inderdaad ook de uitscheiding van het fluorescente calcein-AM uit de watervlooien. Dit onderzoek toont voor het eerst dat Ag NPs en  $\text{AgNO}_3$  zowel *in vitro* als *in vivo* de MXR activiteit remt. Deze modulatie van MXR activiteit zou in acht moeten worden genomen wanneer men de Ag NP toxiciteit evalueert.

**Hoofdstuk 6** bespreekt het belang van het ontwikkelde meer realistische *in vitro* model voor darmcellen met slijmlaag. Ook het belang van het testen van de *in vitro* en *in vivo* interferentie van Ag NPs met de MXR efflux transporters wordt besproken. De rol van vrijgekomen Ag van de Ag NP in het ontwikkelen van toxiciteit wordt besproken, evenals hoe

deze afhangt van de grootte en aard van het NP. Gezien de nieuwe ontwikkelingen in eigenschappen van NPs zouden ook de geïntroduceerde mechanismen in acht moeten worden genomen bij de risicoschatting van NPs die in het milieu terecht kunnen komen en ook mensen kunnen bereiken. De toepassing van proteomics wordt besproken als een geschikte methode om subtiele veranderingen op het spoor te komen die al kunnen optreden bij lage concentraties. Met proteomics kunnen werkingsmechanismen op cellulair niveau worden gedetecteerd en geïdentificeerd, en de mate van effect veroorzaakt door verschillende NPs onderscheiden. De modulatie door Ag NPs van het MXR mechanisme en de mogelijke implicaties hiervan worden besproken. De *in vivo* CEPIA met jonge *D. magna* blijkt een bruikbaar *in vivo* model om het MXR mechanisme te bestuderen, vanwege hun geringe afmeting en grote mate van doorzichtigheid. Besproken wordt hoe in een gefaseerde test aanpak een scala aan *in vivo* bioassays met aquatische organismen, toegepast kan worden, gevolgd door het bepalen van meer mechanistische eindpunten. De lokalisatie van Ag NPs in weefsels van blootgestelde cellen en organismen aangevuld met van 'omic' methoden kunnen het inzicht vergroten in de werking en de belangrijkste risico's van nieuwe materialen zoals NPs. Mogelijke implicaties voor effecten onder veldomstandigheden worden besproken en aspecten voor realistischer (eco)toxicologisch vervolgonderzoek worden aangedragen.

# Appendix

Acknowledgements

About the author

List of publications

Conferences and proceedings

SENSE diploma



## Acknowledgements

Many people and several circumstances contributed to the completion of this research that would have otherwise been impossible. First of all I would like to thank Luxembourg and its people for being given the opportunity to work and spend five great years full of learning and new experiences in this interesting multicultural country. Merci villmols!

I am deeply thankful to the Centre de Recherche Public - Gabriel Lippmann, Lucien Hoffmann, the Fonds National de la Recherche Luxembourg and Wageningen University for making this research possible.

There are no words to express my gratitude to my supervisors Tinka and Arno. Thank you for giving me the opportunity to make this PhD and research possible. Your advice, ideas, skill and input helped me throughout this process despite the difficulties and frustration I faced along the way. Tinka - thank you for keeping my thoughts and ideas structured, leading me towards the right direction and your guidance. Arno - you have been not only a mentor but also a trusted friend. Thank you for always keeping your good spirits and finding solutions to all types of problems that arise, your optimism and enthusiasm and sharing with me both good and bad moments.

This research relied on the work and input of many different people of different expertise and only through this collaboration this work was made possible and fun. Esther, Jean-Nicolas, Patrick, Cédric, Johanna, Céline, Jenny, Sylvain, Tommaso, Sebastian K., Sébastien C.: thank you for all your help and the smooth and fruitful collaboration, you introduced me in new techniques and areas and I have learned so much while working with you. Merci à tous! Servane thank you for your valuable assistance in the lab and always finding the time to help me. Delphine and Sébastien B. thank you for your help with the *D. magna* maintenance and your advice. The input of Marcin Kruszewski (University of Information Technology and Management in Rzeszow, Poland), Yekkuni L. Balachandran (Bharathiar University, India), Erik Ropstad and Camilla Carlson (Norwegian School of Veterinary Science, Norway) has been very valuable and their help is gratefully acknowledged. Thank you Hans for your advice, feedback and willingness to help out whenever needed. Many thanks to the teams of NUTOX and ERIS, that I have had the pleasure to be a part of, and their members for the nice team atmosphere and fruitful discussions. Special thanks to my MSc students Laure and Kahina, working with you has also been a source of learning for me.

I have been very lucky to share an office with wonderful people and colleagues: Sylvain, Matias, Terence, Lisa, Hannah, Fred, Marc, Daniel, Jaouad, Christelle, Joelle, Alexandra, Christos, Sébastien thank you for creating such a wonderful atmosphere in this office that we shared for five years, all the laughs, interesting discussions and funny indiac sessions! You all made my office life easier and more fun. Tommaso - thank you for your friendship and continuous support.

Far away from home, the friends I have met throughout these years in Luxembourg became a big international family. They all made my life in Luxembourg so much funnier, they have been a source of learning and inspiration and made me so much richer as a person. Mauricio thank you for always being there for me, your advice and wonderful friendship. Fabian, Canan and Céline: your friendship is so valuable to me, thank you for being in my life, for all the chats, travels and your support especially in the last year that has been a period with many ups and downs. Cosette, Helena, Riccardo, Javi, Maria, Rakel, Olatz, Jean-Marc, Núria, Catalina, Dave, Alex, Lara, Noelline, Lisa, Hannah, Katya, Arindam, Laura, Jay, Bob, Mads, Aida, Rai, Fede, Ceci, Erika: thank you for your friendship and all the moments we shared such as the activities, trips, numerous concerts, countless night outs, dinners, games and picnics. Nataša, despite being a bit far away thank you for your friendship and support and being an important link to Wageningen. Christian, thank you for challenging me in many ways and your patience and support in the last period of the PhD completion. Sarah and Hanne: thank you for the all the gatherings, interesting discussions and advice in the video-making activity.

I am very grateful for my friends in Greece that have always been there for me over the years despite the distance: Nitsa, Rea, Dimitra, Thodori, Zoe, Poly and Ioanna ευχαριστώ που είστε πάντα δίπλα μου.

My special thanks to my family for their support and advice: Sokrati, Lemonia, Niko, Evangelia and Philippo. My parents Sokratis and Lemonia will always have a special place in my heart. You are always there for me, believing in me, continuously supporting me and pushing me to pursue my dreams. You taught me about courage, determination and that everything is possible. Ευχαριστώ για όλη την αγάπη, υπομονή και στήριξη όλα αυτά τα χρόνια που είμαι μακριά!

**About the author**

Anastasia Georgantzopoulou was born on the 20<sup>th</sup> June 1982 in the small city of Karditsa in central Greece. In 2000 after finishing high school she pursued her studies in the School of Agronomy in the Aristotle University of Thessaloniki in Greece. During her studies and her specialization in plant protection, there was an increasing interest on the issues of environmental pollution, the effects of pesticides and chemicals on environment and non-target organisms and there was soon a turn towards environmental sciences.

After completing the studies in 2005, she was granted a scholarship for postgraduate studies abroad in the field of Ecotoxicology from the State Scholarship Foundation of Greece (IKY). In 2006 she enrolled for the MSc program in “Environmental Sciences” specialization of environmental toxicology in Wageningen University in The Netherlands. She performed her major thesis in the Unit of Toxicology under the supervision of Prof. Tinka Murk and the internship in the National Research Centre for Environmental Toxicology (EnTox), University of Queensland, Brisbane in Australia under the supervision of Dr. Miroslava Macova and Prof. Jochen Mueller.

After completion of the MSc studies she got a position in 2009 as a research scientist at the Centre de Recherche Public - Gabriel Lippmann in Belvaux, Luxembourg. After 2 years she got admitted to the PhD program of Wageningen University under the supervision of Prof. Tinka Murk and Dr. Arno Gutleb. The research on the implications of silver nanoparticles on the environment was conducted in the Centre de Recherche Public - Gabriel Lippmann in Belvaux, Luxembourg.

**List of Publications**

**Georgantzopoulou, A.**, Serchi, T., Leclercq, C.C., Renaut, J., Shao, J., Lankoff, A., Kruszewski, M., Lentzen, E., Grysan, P., Audinot, J.-N., Contal, S., Ziebel, J., Guignard, C., Hoffmann, L., Murk, A.J., Gutleb, A.C. Effects of silver nanoparticles and ions on a co-culture model for the gastrointestinal epithelium. *Tox. Sci.* submitted.

**Georgantzopoulou, A.**, Cambier, S., Serchi, T., Lankoff, A., Kruszewski, M., Balachandran, Y.L., Grysan, P., Audinot, J.-N., Ziebel, J., Guignard, C., Gutleb, A.C., Murk, A.J. Inhibition of multixenobiotic resistance transporters (MXR) by silver nanoparticles and -ions *in vitro* and *in vivo*. *Environ. Sci. Technol.* submitted.

**Georgantzopoulou, A.**, Skoczyńska, E., van den Berg, J.H.J., Brand, W., Legay, S., Klein, S.G., Rietjens, I.M.C.M., Murk, A.J. 2014. P-gp efflux pump inhibition potential of common environmental contaminants determined *in vitro*. *Environ. Toxicol. Chem.* 33, 804-13.

**Georgantzopoulou, A.**, Balachandran, Y.L., Rosenkranz, P., Dusinska, M., Lankoff, A., Wojewodzka, M., Kruszewski, M., Guignard, C., Audinot, J.-N., Girija, S., Hoffmann, L., Gutleb, A.C. 2013. Ag nanoparticles: size- and surface-dependent effects on model aquatic organisms and uptake evaluation with NanoSIMS. *Nanotoxicology* 7, 1168–78.

Audinot, J.-N., **Georgantzopoulou, A.**, Piret, J.P., Gutleb, A.C., Dowsett, D., Migeon, H.N., Hoffmann, L. 2013. Identification and localization of nanoparticles in tissues by mass spectrometry. *Surf. Interface Anal.* 45, 230–233.

Kruszewski, M., Brzoska, K., Brunborg, G., Asare, N., Dobrzynska, M., Dusinska, M., Fjellsbø, L.M., **Georgantzopoulou, A.**, Gromadzka-Ostrowska, J., Gutleb, A.C., Lankoff, A., Magdolenová, Z., Pran, E.R., Rinna, A., Instanes, C., Sandberg, W.J., Schwarze, P., Stepkowski, T., Wojewódzka, M., Refsnes, M. 2011. Toxicity of silver nanomaterials in higher eukaryotes, In: *Advances in Molecular Toxicology*. Elsevier B.V., pp. 179–218.

**Conferences and proceedings**

**Georgantzopoulou, A.**, Serchi, T., Leclercq, C.C., Renaut, J., Kruszewski, M., Lankoff, A., Lentzen, E., Grysan, P., Audinot, J.-N., Ziebel, J., Guignard, C., Hoffmann, L., Gutleb, A.C. Effects of different-sized silver nanoparticles (Ag NPs) on an intestinal co-culture model. BelTox Annual Meeting, Louvain-La-Neuve, B, 6.12.2013. p. 29

Mehennaoui, K., **Georgantzopoulou, A.**, Felten, V., Serchi, T., Contal, S., Ziebel, J., Guignard, C., Balachandran, YL., Giambérini, L., Gutleb, A.C. Comparative study of the effects of silver

nanoparticles on physiological and behavioural responses of *Gammarus sp.* BelTox Annual Meeting, Louvain-La-Neuve, B, 6.12.2013. p. 38

**Georgantzopoulou, A.**, Balachandran, Y.L., Rosenkranz, P., Kruszewski, M., Lankoff, A., Lentzen, E., Grysan, P., Audinot, J.-N., Ziebel, J., Guignard, C., Hoffmann, L., Gutleb, A.C. Differences in uptake and toxicity of similar-sized Ag NPs in *Daphnia magna*. SENSE / MilieuChemTox symposium: Think BIG, Act NANO, Amsterdam, NL, 1.11.2013

**Georgantzopoulou, A.**, Kruszewski, M., Lankoff, A., Audinot, J.-N., Serchi, T., Leclercq, C.C., Renaut, J., Guignard, C., Hoffmann, L., Gutleb, A.C. Use of an intestinal co-culture model to study the effects of Ag nanoparticles. 3RD Young Environmental Scientists Meeting Krakow, Poland, 11-13.02.2013. p.108

**Georgantzopoulou, A.**, Dusinska, M., Kruszewski, M., Lankoff, A., Audinot, J.N., Hoffmann, L., Gutleb, A.C. Use of an intestinal co-culture model to study the effects of Ag and TiO<sub>2</sub> nanoparticles. Mucus protective role and size dependent effects. Society of Toxicology SOT2012, San Francisco, USA, 11.-15.3.2012

**Georgantzopoulou, A.**, Cuny, L., Balachandran, Y.L., Guignard, C., Audinot, J.-N., Hoffmann, L., Gutleb, A.C. Differences in effects of similar sized Ag NPs on an intestinal co-culture model: testing considerations and concerns. Reproductive toxicology from *in vitro* to human. BelTox Annual Meeting, Edegem, B, 3.12.2012. p. 28

**Georgantzopoulou, A.**, Dusinska, M., Kruszewski, M., Balachandran, Y.L., Audinot, J.-N., Hoffmann, L., Gutleb, A.C. Differences in uptake and toxicity of similar-sized Ag NPs in *Daphnia magna*. Trends in Metal Toxicity and Ecotoxicity, BelTox Annual Meeting, Mechelen, B, 8.12.2011

**Georgantzopoulou, A.**, Balachandran, Y.L., Rosenkranz, P., Dusinska, M., Lankoff, A., Kruszewski, M., Guignard, C., Audinot, J.-N., Hoffmann, L., Gutleb, A.C. Effects of similar sized Ag and TiO<sub>2</sub> NPs on model aquatic organisms. Frontiers in Environmental Health HENVI2011- Challenges for Water Safety. Luxembourg, 28.10.2011

Audinot, J.-N., **Georgantzopoulou, A.**, Piret, J.P., Gutleb, A.C., Dowsett, D. Identification and localization of nanoparticles in tissues by mass spectrometry. XVIII International Conference on Secondary Ion Mass Spectrometry, Riva del Garda, I, 18.-23.9.2011

**Georgantzopoulou, A.**, Balachandran, Y.L., Rosenkranz, P., Dusinska, M., Kruszewski, M., Lankoff, A., Audinot, J.-N., Hoffmann, L., Gutleb, A.C. Differences in uptake and toxicity of

similar-sized Ag NPs in *Daphnia magna*. International Conference on Biological Responses to Nanoscale Particles. Essen, Germany, 11-15.10.2011

**Georgantzopoulou, A.**, Dusinska, M., Kruszewski, M., Balachandran, Y.L., Audinot, J.-N., Hoffmann, L., Gutleb, A.C. Ag and TiO<sub>2</sub> nanoparticles: effects on model aquatic organisms. Building a Bridge from NanoImpactNet to Nanomedical Research. Lausanne, CH, 14.-17.2.2011. p. 102

**Georgantzopoulou, A.**, Dusinska, M., Kruszewski, M., Balachandran, Y.L., Audinot, J.-N., Hoffmann, L., Gutleb, A.C. Ag and TiO<sub>2</sub> nanoparticles: effects on model aquatic organisms. BelTox2010, Louvain-la-Neuve, B, 25.11.2010. S40

**Georgantzopoulou, A.**, Dusinska, M., Kruszewski, M., Balachandran, Y.L., Hoffmann, L., Gutleb, A.C. Ecotoxicological studies of TiO<sub>2</sub> and Ag nanoparticles. Nanotoxicology2010. Edinburgh, UK, 2.-4.6.2010

**Georgantzopoulou, A.**, Dusinska, M., Kruszewski, M., Hoffmann, L., Gutleb, A.C. Ecotoxicological studies of TiO<sub>2</sub> and Ag nanoparticles using *Daphnia magna* and *Vibrio fischeri* as model organisms. 2nd NanoImpactNet Conference: For a healthy environment in a future with nanotechnology. Lausanne, CH, 9.-12.3.2010



*Netherlands Research School for the  
Socio-Economic and Natural Sciences of the Environment*

# D I P L O M A

*For specialised PhD training*

The Netherlands Research School for the  
Socio-Economic and Natural Sciences of the Environment  
(SENSE) declares that

***Anastasia Georgantzopoulou***

born on 20 June 1982 in Karditsa, Greece

has successfully fulfilled all requirements of the  
Educational Programme of SENSE.

Wageningen, 6 February 2015

the Chairman of the SENSE board

Prof. dr. Huub Rijnaarts

the SENSE Director of Education

Dr. Ad van Dommelen

*The SENSE Research School has been accredited by the Royal Netherlands Academy of Arts and Sciences (KNAW)*



K O N I N K L I J K E N E D E R L A N D S E  
A K A D E M I E V A N W E T E N S C H A P P E N



The SENSE Research School declares that **Ms Anastasia Georgantzopoulou** has successfully fulfilled all requirements of the Educational PhD Programme of SENSE with a work load of 36 EC, including the following activities:

#### SENSE PhD Courses

- o Ecotoxicology (2006)
- o Environmental Research in Context (2013)
- o Research in Context Activity: Creation of animated research video 'Effects of silver nanoparticles on environment and health' (2014)

#### Other PhD and Advanced MSc Courses

- o General Toxicology, Wageningen University (2007)
- o Summer School 'Environmental effects of nanoparticles and nanomaterials', University of Birmingham, United Kingdom (2009)
- o First Nanosafety Autumn School 'Ecotoxicology of nanoparticles: from characterisation to risk assessment', University of Ca Foscari of Venice, Italy (2009)
- o Training School 'Handling protocols and standardisation of nanomaterials in toxicological research', European Network on the Health and Environmental Impact of Nanomaterials (NanoImpactNet) and Institute for Work and Health, Lausanne, Switzerland (2010)
- o NanoImpactNet Training School on risk assessment issues of nanomaterials in the aquatic and terrestrial environment, Leiden University, The Netherlands (2011)
- o Basic Embryology and Developmental Toxicity Testing, Society of Toxicology (SOT), United States (2012)
- o Genotoxicity & mutagenicity testing: a brief overview of the main tests, pitfalls and regulatory framework, Belgian Society of Toxicology (BelTox), Belgium (2012)

#### Management and Didactic Skills Training

- o Supervision of MSc student: thesis entitled 'Effects of silver nanoparticles on an in vitro cell culture model for the human intestinal epithelium'(2011-2012)
- o Supervision of Internship student: thesis entitled 'Effects of silver nanoparticles on freshwater organisms'(2013-2014)

#### Oral Presentations

- o *Effects of similar sized Ag and TiO<sub>2</sub> NPs on model aquatic organisms.* Frontiers in Environmental Health - Challenges for Water Safety - HENV12011 Conference, 28 October 2011, Luxembourg, Luxembourg
- o *Use of an intestinal co-culture model to study the effects of Ag and TiO<sub>2</sub> nanoparticles: Mucus protective role and size dependent effects.* Conference SOT2012, 11-15 March 2012, San Francisco, United States

SENSE Coordinator PhD Education

Dr. ing. Monique Gulickx

The research described in this thesis was financially supported by the Fonds National de la Recherche Luxembourg (FNR) within the projects NanEAU (FNR/08/SR/07) and NanEAUII (C10/SR/799842).

Cover designed by Eugenia Georgantzopoulou

Printed by GVO drukkers & vormgevers B.V., Ede, The Netherlands

